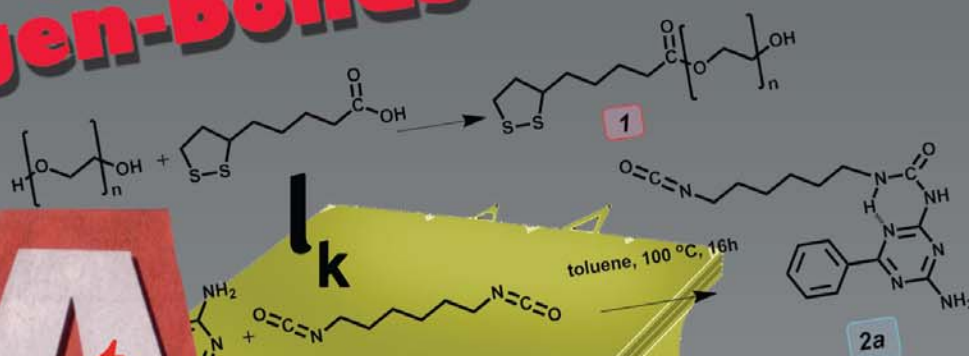


hydrogen-bonds



The collage features several key elements:

- Text:**
 - Dad** (large, dark letters)
 - UPy** (large, bold letters)
 - spring constant** (diagonal text)
 - AFM** (large, red letters)
 - SUPRAMOLECULAR POLYMERS** (diagonal text)
 - 2a** (small label in a blue box)
- Chemical Structures:**
 - A polymer chain with a repeating unit containing a hydroxyl group and a disulfide bridge.
 - A chemical structure of a triazine-based molecule (labeled 2a) with a phenyl group and a carbonyl group.
 - A chemical structure of a triazine-based molecule with a carbonyl group and a phenyl group.
- Diagram:**
 - A yellow paper with a diagram of a probe tip interacting with a sample. The tip is labeled **TIP** and the sample is labeled **SAMPLE**. The tip is shown with a **FRONT ATOM** and a **POINT** (labeled **p**). The diagram includes a scale bar for force in pN (25 to 200) and a label **sigma** (red).
- Mathematical Symbols:**
 - σ (red)
 - τ (red)
 - β (black)
 - t_D (red)
 - r^0 (black)
 - k (black)
 - x_β (black)

Anika Embrechts

Single Molecule Force Spectroscopy of self-complementary hydrogen-bonded supramolecular systems: *dimers, polymers and solvent effects*

Anika Embrechts

This research was financially supported by the Council for Chemical Sciences of the Netherlands Organization for Scientific Research, ECHOgrant 754021.

Members of the committee:

Chairman:	Prof. Dr. G. van der Steenhoven	University of Twente, The Netherlands
Promotor:	Prof. Dr. G. J. Vancso	University of Twente, The Netherlands
Assistant-promotor:	Prof. Dr. H. Schönherr	Universität Siegen, Germany
Members:	Prof. Dr. D. Anselmetti	Universität Bielefeld, Germany
	Prof. Dr. P. Hinterdorfer	Johannes Kepler Universität Linz, Austria
	Prof. Dr. R. P. Sijbesma	Technical University Eindhoven, The Netherlands
	Prof. Dr. V. Subramaniam	University of Twente, The Netherlands
	Dr. A. H. Velders	University of Twente, The Netherlands
	Dr. M. L. Bennink	University of Twente, The Netherlands

Single Molecule Force Spectroscopy of complementary hydrogen-bonded supramolecular systems: dimers, polymers and solvent effects.

A. Embrechts

PhD Thesis

University of Twente, Enschede, The Netherlands

© Anika Embrechts 2011

ISBN: 978-90-5335-400-1

No part of this work may be reproduced by print, photocopy or any other means without the permission of the publisher.

**SINGLE MOLECULE FORCE SPECTROSCOPY OF COMPLEMENTARY
HYDROGEN-BONDED SUPRAMOLECULAR SYSTEMS: DIMERS, POLYMERS
AND SOLVENT EFFECTS**

PROEFSCHRIFT

ter verkrijging van
de graad van doctor aan de Universiteit Twente,
op gezag van de rector magnificus,
prof. dr. H. Brinksma,
volgens besluit van het College voor Promoties
in het openbaar te verdedigen
op donderdag 19 mei 2011 om 16.45 uur

door

Anika Embrechts

geboren op 15 januari 1980
te Rotterdam

Dit proefschrift is goedgekeurd door:

Promotor: prof. dr. G. J. Vancso

Assistent-promotor: prof. dr. H. Schönherr

Table of Contents

CHAPTER 1

SUPRAMOLECULAR CHEMISTRY: TOP-DOWN VS. BOTTOM-UP

1.1 INTRODUCTION	2
1.2 THE ORIGIN OF SUPRAMOLECULAR CHEMISTRY	2
1.3 SUPRAMOLECULAR POLYMERS	5
1.4 THESIS WORK	7
REFERENCES AND NOTES	9

CHAPTER 2

SINGLE MOLECULE MECHANICS OF SUPRAMOLECULAR HYDROGEN-BONDED SYSTEMS

2.1 INTRODUCTION	16
2.2 ESSENTIAL FORCES IN NATURE	17
2.2.1 Covalent bonds (non metallic)	18
2.2.2 Ionic interactions	19
2.2.3 Dipole-dipole interactions	19
2.2.4 Coordinative bonds	20
2.2.5 Van der Waals interactions	20
2.2.6 Hydrogen-bonds	21
2.3 SUPRAMOLECULAR HYDROGEN-BONDED POLYMERS	27
2.4 SOLVENT EFFECTS ON A SINGLE MOLECULE LEVEL	29
2.5 SINGLE MOLECULE STUDIES	33
2.6 AFM-BASED SINGLE MOLECULE FORCE SPECTROSCOPY	35
2.7 AFM-BASED SMFS OF SUPRAMOLECULAR HYDROGEN-BONDS	39

2.8 CONCLUSION AND OUTLOOK	46
REFERENCES AND NOTES	47

CHAPTER 3

AFM-BASED SINGLE MOLECULE FORCE SPECTROSCOPY OF SUPRAMOLECULAR UREIDOPYRIMIDINONE DIMERS AND POLYMERS IN HEXADECANE

3.1 INTRODUCTION	58
3.2 RESULTS AND DISCUSSION	61
3.3 CONCLUSIONS	65
3.4 MATERIALS AND METHODS	65
APPENDIX	66
REFERENCES AND NOTES	68

CHAPTER 4

AFM-BASED SINGLE MOLECULE FORCE SPECTROSCOPY OF SUPRAMOLECULAR UREA-AMINOTRIAZINE-BASED DIMERS

4.1 INTRODUCTION	72
4.2 UAT-BASED DIMER CHARACTERIZATION IN BULK	73
4.3 SINGLE MOLECULE CHARACTERIZATION OF UAT-BASED DIMERS	78
4.4 DISCUSSION AND CONCLUSION	81
4.5 MATERIALS AND METHODS	83
APPENDIX	87
REFERENCES AND NOTES	94

CHAPTER 5

AFM-BASED SINGLE MOLECULE FORCE SPECTROSCOPY OF SUPRAMOLECULAR UREA-AMINOTRIAZINE-BASED POLYMERS

5.1 INTRODUCTION	100
5.2 RESULTS AND DISCUSSION	101
5.3 CONCLUSIONS	106
5.4 MATERIALS AND METHODS	106
REFERENCES AND NOTES	108

CHAPTER 6

AFM-BASED SMFS OF UPY DIMERS AND POLYMERS IN DIFFERENT SOLVENTS

6.1 INTRODUCTION	112
6.2 UPY DIMERS IN 2-PROPANOL AND 1-NONANOL	115
6.2.1 UPy dimers in 2-propanol	115
6.2.2 UPy dimers in 1-nonanol	125
6.2.3 Discussion and conclusion	128
6.3 SUPRAMOLECULAR UPY POLYMERS IN MIXED SOLVENTS	129
6.3.1 UPy polymers in a 50:50 mixture of 2-propanol and hexadecane	129
6.3.2 UPy polymers in a 80:20 mixture of 2-propanol and hexadecane	133
6.4 DISCUSSION AND CONCLUSION	134
6.5 MATERIALS AND METHODS	135
APPENDIX	136
REFERENCES	139

CHAPTER 7

OUTLOOK AND FUTURE EXPERIMENTS

7.1 OUTLOOK	144
--------------------	------------

REFERENCES	149
-------------------	------------

SUMMARY	153
----------------	------------

SAMENVATTING	157
---------------------	------------

ACKNOWLEDGEMENTS	161
-------------------------	------------

CURRICULUM VITAE	164
-------------------------	------------

PUBLICATIONS	165
---------------------	------------

CHAPTER 1

SUPRAMOLECULAR CHEMISTRY: TOP-DOWN VS. BOTTOM-UP

*Few scientists acquainted with the chemistry of
biological systems at the molecular level can avoid being inspired.*

– Donald Cram

*I am among those who think that science has great beauty.
A scientist in his laboratory is not only a technician:
he is also a child placed before natural phenomena
which impress him like a fairy tale.*

– Marie Curie

1.1 INTRODUCTION

Self-organization and self-assembly are intriguing phenomena in the world of chemistry, physics and especially biology. There are many accepted “definitions” of both phenomena^[1] in different fields of application and the terms are often used as synonyms as well. To avoid confusion, the term self-assembly will here solely be used and considered as the controlled formation of higher order architectures from small building blocks using weak interactions. Especially in the field of supramolecular chemistry, molecules are held together by (multiple of) these weak interactions such as hydrogen-bonds, dipole-dipole interactions or dispersion forces. The energy of these weak interactions between molecules and molecular structures is in the order of the thermal energy (kT) and so supramolecular systems are very dynamic: weak interactions are broken and formed within (a fraction of) seconds. The shallow energy barriers provide supramolecular systems with extraordinary properties compared to the more rigid covalently bonded systems.

1.2 THE ORIGIN OF SUPRAMOLECULAR CHEMISTRY

Initially research regarding self-assembly and supramolecular chemistry was dominated by the investigation of biological systems^[2,3] such as enzymes, proteins and viral capsids. Host-guest chemistry and the well-known lock-key principle were already described for enzymes in 1894 by Emil Fischer^[2]. Despite the fact that self-assembly of biological systems is still a major field of research, numerous interesting synthetic systems have emerged over the last decades, starting among others with the pioneering work of Nobel laureates Jean-Marie Lehn, Charles Pedersen and Donald Cram in their research “beyond the molecule” of *e.g.* crown ethers^[4,5] and cryptands^[5,6] (see also Figure 1- 1).

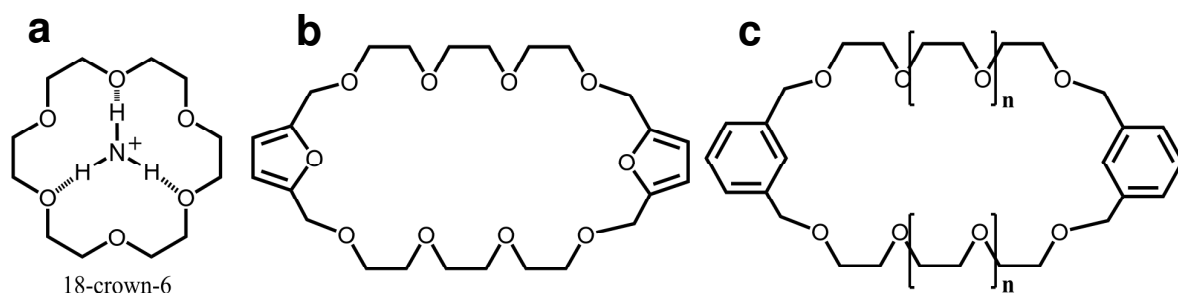


Figure 1- 1. (a) 18-crown-6^[6] receptor interacting with ammonium via hydrogen bonding; (b,c) novel crown ethers synthesized by Reinhoudt^[7] in 1975 based on the reaction of 2,5-bis(hydroxymethyl)furan and 1,3-bis(bromomethyl)benzene with poly ethylene glycolates/ditosylates.

Over the past decades detailed studies of crown ether receptors provided new insights into mechanisms for catalysis^[8] and chiral recognition^[9]. Other cyclic supramolecular receptors like cucurbiturils^[10], cyclodextrins^[11], rotaxanes and catenanes^[12] were studied as well and the reversible recognition of these cyclic receptors^[13] is nowadays applied in a variety of fields reaching from single molecule electronics^[12c,14], materials science^[15,16] to drug delivery^[17]. An overview of the wide range of applications of such bio-inspired materials is shown in Figure 1- 2.

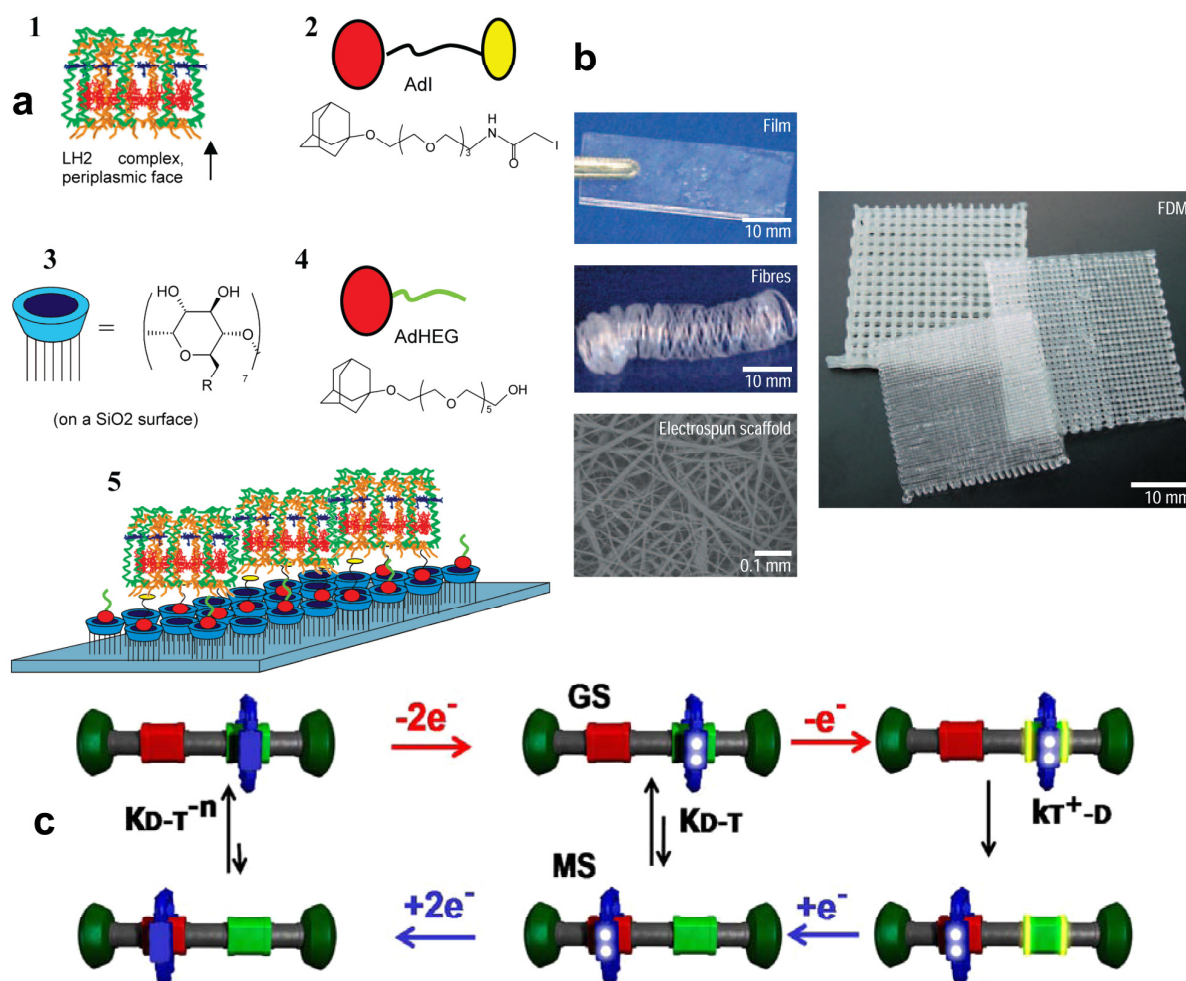


Figure 1- 2. Several applications based on supramolecular interactions: (a) light harvesting antenna (from *Rhodobacter sphaeroides*) deposited on a cyclodextrin molecular printboard (1-5)^[15d]; (b) supramolecular hydrogen-bonded polymers for biomedical applications^[16a]; (c) supramolecular electronic switches based on bistable [2]rotaxanes^[14b]. The green and red sites on the dumbbell components correspond to tetrathiafulvalene (TTF) and dioxynaphthyl (DNP) units, respectively. Using oxidation and reduction cycles the cyclobis(paraquat-p-phenylene)-ring (blue) can be moved from the green to the red site and vice versa. *Image adapted and compiled from refs. 14b, 15d and 16a.* Steuerman, D.W.; Tseng, H.-R.; Peters, A.J.; Flood, A.H.; Jeppesen, J.O. Nielsen, K.A.; Stoddart, J.F.; Heath, J.R. Molecular-Mechanical Switch-Based Solid-State Electrochromic Devices. *Angew. Chem. Int. Ed.* **2004**, *43*, 6486-6491. Copyright Wiley-VCH Verlag GmbH & Co. KGaA. Reproduced with permission.

As is also demonstrated in Figure 1- 2, nature provides us with inspiring sources of complex and energy efficient examples of self-assembling systems based on weak interactions. The 3D conformation of DNA^[18] and a wide variety of proteins are only two of the fascinating examples of nature's ability to utilize self-assembly and provide our human body with extraordinary functionalities. These examples have led to the development of compelling materials, such as hydrogen-bond-based (biocompatible) polymers with self-healing properties^[16,19]. Furthermore a novel class of bio-inspired catalysts was developed by Fréchet and co-workers which mimics the spatial confinement of reactive centres in a multistep cascade reaction^[20]. Without these confined synthetic pockets almost no enzymatic activity is observed. So a fundamental understanding of these processes on the single molecule level, where confinement effects can be probed, is essential to achieve a broader understanding on any level of biological processes.

Since the 3D geometry, and as a consequence enzymatic activity, of many biomolecules depends on supramolecular interactions it is highly interesting to study these molecular assemblies or "supermolecules" in more detail. Self-assembly of these macromolecules takes place due to an intricate balance of attractive and repulsive forces created by weak non-covalent interactions (such as van der Waals and Coulomb interactions, hydrophobic effects and hydrogen-bonds). The energy of these pairwise interactions is generally in the order of the thermal energy (kT) and so these self-assembled systems have very subtle equilibrium conditions. Small fluctuations in confined environmental conditions may subsequently cause large (non-linear) responses and hence the behaviour of these systems based on weak interactions is often hard to predict. Moreover, most systems can often be kinetically (or kinetically and thermodynamically) controlled^[21], so different (meta)stable equilibrium states can be present. The reversible characteristics and kinetic control open up possibilities to control molecular chirality^[22], which introduces additional complexity in the system.

Challenges in studying and understanding these biological processes often arise due to the complexity of the system and the need for simplified model systems still exists. Hence a complete understanding of these systems can only be obtained if they are studied on all levels of complexity: from single molecule to bulk. This becomes even more important now that recent studies using single molecule techniques have demonstrated that the information obtained in such single molecule experiments can be *significantly different* (see also Figure 1- 3) from that given by the ensemble-averaged studies^[23]. Using single molecule

techniques, slow fluctuations in the enzymatic dynamics of the oxidation of cholesterol^[24] could for instance be detected, which would otherwise have been hidden in ensemble averaged data. Hence, the observation of only ensemble averaged bulk properties may hide interesting phenomena, such as certain transition states^[25], electronic localization phenomena^[23a] or the influence of molecular aggregates in solution.

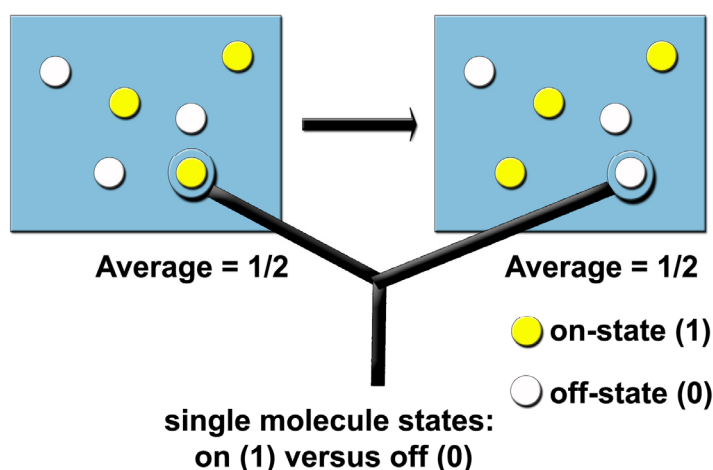


Figure 1- 3. Schematic overview of single molecule versus bulk ensemble experiments: although a bulk measurement would provide the same result for the situation on the left and right (3 on- and 3 off-states: average = $\frac{1}{2}$), a single molecule experiment would be able to detect the two different states (on- or off-state).

Emerging single molecule approaches^[26] will therefore contribute to a new level of understanding, since the immediate local environment is probed and small fluctuations can be observed. Using these single molecule techniques, energy efficient nanomachines and quantum computers, as for instance envisioned by Richard Feynman^[27], might no longer be science fiction in the near future.

For initial single molecules studies on supramolecular interactions, supramolecular polymers appear to be a good candidate, since limited complexity is present compared to biological systems. Furthermore materials science might benefit substantially from these single molecule studies since new self-healing materials – based on supramolecular (hydrogen-bond) interactions – might be developed using the knowledge that is obtained in studies of single molecule interactions in these synthetic supramolecular systems.

1.3 SUPRAMOLECULAR POLYMERS

Supramolecular polymers are macromolecules which consist of monomeric building blocks that are held together by non-covalent weak interactions. These weak interactions are often

(highly) directional and therefore contribute largely to the 3D structure these polymer chains adopt. Although there are several types of supramolecular polymers such as metallo-supramolecular^[28] and hydrogen-bonded polymers^[29], it is the latter class that resembles the hydrogen-bond building blocks of nature more closely. This close resemblance, and the fact that these polymers are also often used in materials science, makes hydrogen-bonded supramolecular polymers ideal candidates to study single molecule supramolecular interactions. The properties of hydrogen-bonded polymers strongly depend on the number of bonds and strength of the hydrogen-bonded arrays that are responsible for the reversible interaction between (polymer) segments. Nowadays a wide variety of hydrogen-bonded polymers is available including supramolecular block-copolymers^[30] and supramolecular polymer networks^[31]. A schematic overview of various arrangements of these polymers is presented in Figure 1- 4.

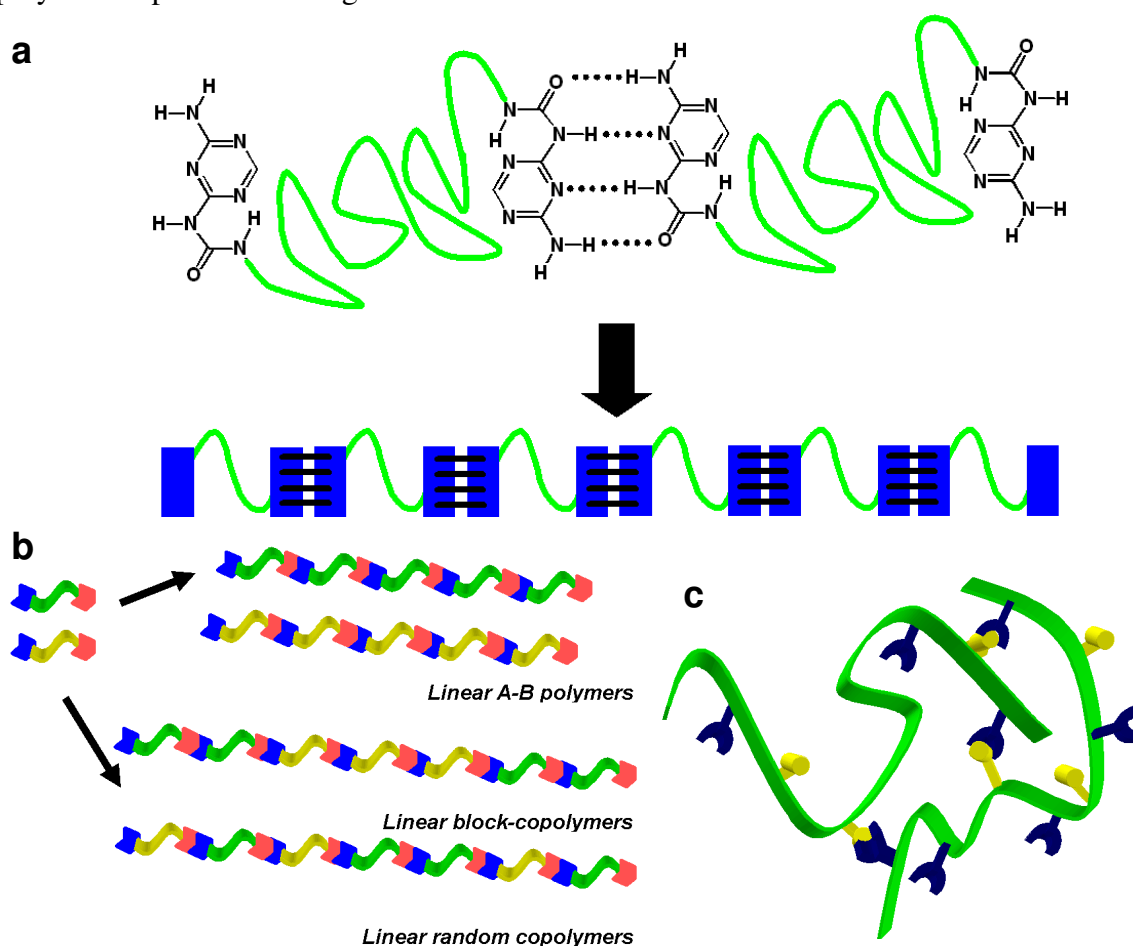


Figure 1- 4. Schematic overview of a variety of supramolecular hydrogen-bonded polymers: (a) formation of complementary A-A urea-aminotriazine-based supramolecular polymers; (b) via thermodynamic and kinetic control a variety of supramolecular polymers – with a broad range of properties – can be formed from only two different A-B monomers; (c) supramolecular polymer with multiple reactive side chains. A very dynamic entangled network can be formed if polymer chains form hydrogen-bonded crosslinks.

To be able to understand structure-property relationships and design and develop these materials, it is of vital importance to probe the contribution of the different molecular scale contributors to hydrogen-bond strength in solution. The hydrogen-bond strength of (supra)molecular complexes in different solvents is usually determined by measuring the concentration-dependent transition of dimers to monomers in the solvent of interest, *e.g.* with isothermal titration calorimetry (ITC) or nuclear magnetic resonance spectroscopy (NMR). Unfortunately these techniques rely on ensemble averaged bulk data which may hide interesting local environmental effects in close proximity of the bond. Since supramolecular hydrogen-bonded systems are nowadays used and further developed as building blocks *e.g.* for self-healing polymers^[19] and molecular motors^[32], single molecule measurements will provide new molecular level insight to support this development for future applications. Furthermore single molecule investigations are interesting from a fundamental point of view due to the disparity of theoretical calculations^[33] and bulk measurements of equilibrium dimerization constants K_{dim} observed in several of these systems^[34,35].

1.4 THESIS WORK

The work described in this thesis aims at a better understanding of the structure-property relationships of supramolecular assemblies – with a specific focus on hydrogen-bonded dimers and polymers – by combining ensemble averaged and single molecule techniques. Chapter 2 will give an overview of a variety of hydrogen-bonded supramolecular dimers and polymers. Furthermore solvent effects influencing the hydrogen-bond stability of these supramolecular assemblies will be discussed. Finally, an overview of single molecule techniques – with a special focus on Atomic Force Microscopy-based Single Molecule Force Spectroscopy (AFM-based SMFS) – is provided. Single molecule techniques have proven to provide a more detailed understanding of phenomena that occur on small length or time scales^[22,24], which can not be studied with conventional bulk analysis techniques. Thus, single molecule data obtained via AFM-based SMFS may shed light on the disparity of theoretical calculations^[33] and bulk measurements of equilibrium dimerization constants K_{dim} observed in several of these supramolecular hydrogen-bonded systems^[34,35].

Chapter 3 covers the synthesis and characterization of self-assembling supramolecular hydrogen-bonded ureidopyrimidinone (UPy) arrays in the bulk as well as at surfaces. In

particular AFM-based SMFS was used to investigate the energy landscape of the hydrogen-bonds of UPy-dimers and polymers in hexadecane. Exploiting the Kramers-Bell-Evans approach^[36-39], this technique directly yielded the equilibrium dimerization constant K_{dim} based on the measured bond strength values at different bond loading rates (stretching rates) of individual molecules. AFM-based SMFS provided quantitative estimates for the value of the equilibrium dimerization constant K_{dim} for (UPy)₂ in hexadecane. So AFM-based SMFS enables one to study hydrogen-bond stability where common methods like isothermal titration calorimetry (ITC), nuclear magnetic resonance (NMR) and even fluorescence microscopy tend to fail due their detection limit. In addition, this technique circumvents possible solubility and aggregation problems in various solvents and hence yields hydrogen-bond strength data of complementary quadruple hydrogen-bonded arrays also in these notoriously difficult situations. The formation and bond failure of supramolecular UPy-polymers was studied in Chapter 3 as well. The rupture force observed as a function of the number of linkers N was in quantitative agreement with the theory on uncooperative bond rupture for supramolecular linkages switched in series.

In Chapter 4 the study of a second quadruple hydrogen-bonded system is reported, which closely resembles the well-studied UPy hydrogen-bonded array. A urea-aminotriazine (UAT)-based quadruple hydrogen-bonded array was synthesized and characterized in bulk and at the surface. The close resemblance of this UAT moiety with the well-studied (UPy)₂ array provided the opportunity to investigate the influences of molecular structure, geometry and other contributions that might affect the hydrogen-bond strength. Using AFM-based SMFS measurements the value of the dimerization constant K_{dim} for UAT in hexadecane was determined and a structural comparison with the previously obtained data for K_{dim} of UPy in hexadecane is provided.

The AFM-based single molecule investigation of supramolecular hydrogen-bonded UAT-based polymers in hexadecane is discussed in Chapter 5. In line with the obtained data for UPy-based supramolecular polymers in Chapter 3 the observed rupture force was a function of the number of linkers N . A quantitative agreement with the theory on uncooperative bond rupture for supramolecular linkages switched in series could be demonstrated for a UAT-based supramolecular polymer as well.

Chapter 6 presents an overview of Upy dimers and polymers studied in polar solvents (2-propanol and 1-nonanol) and mixtures of polar and apolar solvents (2-propanol and hexadecane). The observed rupture forces, hint at a possible influence of molecular

aggregates, *c.q.* clusters of solvent molecules, on the hydrogen-bond strength of (UPy)₂ in 2-propanol, 1-nonanol and mixtures of 2-propanol and hexadecane. This observation stresses the need for single molecule measurements and bottom-up developments for supramolecular nanoscale applications. Like Purcell^[40] already demonstrated mathematically in 1976: downscaling of traditionally designed systems does not always provide the desired or expected function in nanoscale environments. In his work “Life at low Reynolds numbers” Purcell demonstrated among others that inertia no longer plays a role for micron-sized or even smaller particles, and so this phenomenon has to be taken into account for top-down design. Hence when (supramolecular) self-assembled nanostructures are designed and developed, like for instance molecular motors, it is important to consider the effects that play a role at similar length scales, such as the possible existence of molecular aggregates and their influence on the designed (nano)structures.

Chapter 7 provides an outlook on future developments, which may create opportunities to enhance our understanding of the key contributors to hydrogen-bond stability and their influence on the stability and function of higher architectures or even bulk materials. Furthermore the feasibility of AFM-based SMFS as a tool for (single molecule) bond strength analysis is discussed. Ultimately this work contributes to a better understanding of the structure-property relationships that determine the bond strength and resulting bulk properties of these supramolecular systems.

REFERENCES AND NOTES

1. *Self-organization can be interpreted as any process which creates more order and hence an increase in complexity can be used as a measure for self-organization. Self-assembly can also be defined as ‘the process whereby components spontaneously organise into more complex objects’. However these definitions are rather vague and can be applied to a wide range of different processes ranging from solar systems to self-assembled monolayers. In biology self-organization and self-assembly are sometimes considered as different processes as is discussed in the following article:* John, K.; Bär, M. *Phys. Rev. Lett.* **2005**, 95, 198101.
2. Fischer, E. *Ber. Dtsch. Chem. Ges.* **1894**, 27, 2985-2993.

3. (a) Keates, R.A.B.; Hall R.H. *Nature* **1975**, 257, 418-421; (b) Bates, D.L.; Danson, M.J.; Hale, G.; Hooper, E.A.; Perham, R.M. *Nature* **1977**, 268, 313-316; (c) Wagner, G.W.; Bancroft, J.B. *Virology* **1968**, 34, 748-756.
4. (a) Dietrich, B.; Lehn, J.M.; Sauvage, J.P. *Tetrahedron. Lett.* **1969**, 34, 2885-2889; (b) Dietrich, B.; Lehn, J.M.; Sauvage, J.P. *Tetrahedron. Lett.* **1969**, 34, 2889-2892; (c) Lehn, J.M.; Sauvage, J.P. *J. Am. Chem. Soc.* **1975**, 97, 6700-6707.
5. (a) Cram, D.J.; Cram, J.M. *Science* **1974**, 183, 803-809; (b) Cram, D.J.; Cram, J.M. *Acc. Chem. Res.* **1978**, 11, 8-14.
6. Pedersen, C.J. *J. Am. Chem. Soc.* **1967**, 89, 7017.
7. Reinhoudt, D.N.; Gray, R.T. *Tetrahedron Lett.* **1975**, 75, 2105-2108.
8. (a) Lehn, J.M. *Pure & Appl. Chem.* **1979**, 51, 979-997; (b) Verboom, W.; Rudkevich, D.M.; Reinhoudt, D.N. *Pure & Appl. Chem.* **1994**, 66, 679-686; (c) Mateos-Timoneda, M.A.; Crego-Calama, M.; Reinhoudt, D.N. *Chem. Soc. Rev.* **2004**, 33, 363-372.
9. (a) Kuhn, R.; Erni, F. *Anal. Chem.* **1992**, 62, 2815-2820; (b) Hamada, T.; Manabe, K.; Ishikawa, S.; Nagayama, S.; Shiro, M.; Kobayashi, S. *J. Am. Chem. Soc.* **2003**, 125, 2989-2996; (c) Wenzel, T.J.; Bourne, C.E.; Clark, R.L. *Tetrahedron* **2009**, 20, 2052-2060.
10. (a) Mock, W.L.; Shih, N.H. *J. Org. Chem.* **1986**, 51, 4440-4446; (b) Lee, J.W.; Selvapalam, S.N.; Kim, H.-J.; Kim, K. *Acc. Chem. Res.* **2003**, 36, 621-630.
11. (a) Villiers, A. *Compt. Rend. Acad. Sci.* **1891**, 112, 536; (b) Sängner, W. *Angew. Chem. Int. Ed. Engl.* **1980**, 19, 344-362; (c) Szejtli, J. *Pure Appl. Chem.* **2004**, 76, 1825-1845; (d) Xie, Y.; Menual, S.; Joly, J.-P.; Coucot, B.; Elysée, J.; Ghermani, N.-E.; Marsura, A. *Tetrahedron* **2007**, 63, 1706-1714; (e) Xie, Y.; Wang, X.; Han, X.; Xue, X.; Ji, W.; Qi, Z. Liu, J.; Zhao, B.; Ozaki, Y. *Analyst* **2010**, 135, 1389-1394.
12. (a) Schill, G.; Zurcher, C. *Naturwissenschaften* **1971**, 58, 40-45; (b) Anelli, P.L.; Ashton, P.R.; Ballardini R.; Balzani, V.; Delgado, M.; Gandolfi, M.T.; Goodnow, T.T.; Kaifer, A.E.; Philp, P. Pietraszkiewicz M.; Prodi, L.; Reddington, M.V.; Slawin, A.M.Z.; Spencer, N.; Stoddart, J.F.; Vicent, C.; Williams, D.J. *J. Am. Chem. Soc.* **1992**, 114, 193-218; (c) Collier C.P.; Wong, E.W.; Belohradsky, M.; Raymo, F.M.; Stoddart, J.F.; Kuekes, P.J.; Williams, R.S.; Heath, J.R. *Science* **1999**, 285, 391-394; (d) Kay, A.R.; Leigh, D.A.; Zerbetto, F. *Angew. Chem. Int. Ed.* **2007**, 46, 72-191; (e) Beyler, M.; Heitz, V.; Sauvage, J.P. *J. Am. Chem. Soc.* **2010**, 132, 4409-4417.
13. (a) Miyaji, H.; Kim, D.-S.; Chang, B.-Y.; Park, E.; Park, S.-M.; Ahn, K.H.; *Chem. Commun.* **2008**, 6, 753-755; (b) Meyer, E.A.; Castellano, R.K.; Diederich, F. *Angew.*

- Chem Int. Ed.* **2003**, *42*, 1210-1250; (c) Mortimer, R.J.; Weightman, J.S.; Willner, I.; Pardo-Yissar, V.; Katz, E.; Ranjit, K.T. **2001**, *497*, 172-177; (d) Seel, C.; Vögtle, F. *Angew. Chem. Int. Ed.* **1992**, *31*, 528-549.
14. (a) Heath, J.R. *Pure & Appl. Chem.* **2000**, *72*, 11-20; (b) Steuerman, D.W.; Tseng, H.-R.; Peters, A.J.; Flood, A.H.; Jeppesen, J.O.; Nielsen, K.A.; Stoddart, J.F.; Heath, J.R. *Angew. Chem. Int. Ed.* **2004**, *43*, 6486-6491; (c) Dichtel, W.R.; Heath, J.R.; Stoddart, J.F. *Phil. Trans. R. Soc. A* **2007**, *365*, 1607-1625.
15. (a) Michels, J.J.; Huskens, J.; Reinhoudt, D.N. *J. Am. Chem. Soc.* **2002**, *124*, 2056-2064; (b) Ludden, M.J.W.; Li, X.; Greve, J.; Van Amerongen, A.; Escalante, M.; Subramaniam, V.; Reinhoudt, D.N.; Huskens, J. *J. Am. Chem. Soc.* **2008**, *130*, 6964-6973; (c) Dorokhin, D.; Hsu, S.H.; Tomczak, N.; Reinhoudt, D.N.; Huskens, J.; Velders, A.H.; Vancso, G.J. *ACS Nano* **2009**, *4*, 137-142; (d) Escalante, M.; Lenferink, A.; Zhao, Y.; Tas, N.; Huskens, J.; Hunter, C.N.; Subramaniam, V.; Otto, C. *Nano Lett.* **2010**, *10*, 1450-1457.
16. (a) Dankers, P.Y.W.; Harmsen, M.C.; Brouwer, L.A.; Van Luyn, M.J.A.; Meijer, E.W. *Nat. Mat.* **2005**, *4*, 568-574; (b) Botterhuis, N.E.; Van Beek, D.J.M.; Van Gemert, G.M.L.; Bosman, A.W.; Sijbesma, R.P. *J. Polym. Sci. A1* **2008**, *46*, 3877-3885; (c) De Greef, T.F.A.; Meijer, E.W. *Nature* **2008**, *453*, 171-173.
17. (a) Patel, S.K.; Lavasanifar, A.; Choi, P. *Biomaterials* **2010**, *31*, 1780-1786; (b) Van de Manakker, F.; Vermonden, T.; Van Nostrum, C.F.; Hennink, W.E. *Biomacromolecules* **2009**, *10*, 3157-3175; (c) Kharlampieva, E.; Kozlovskaya, V.; Sukhishvili, S. *Adv. Mat.* **2009**, *21*, 3053-3065.
18. Watson, J.D.; Crick, F.H.C. *Nature* **1953**, *171*, 737-738.
19. (a) Folmer, B.J.B.; Sijbesma, R.P.; Versteegen, R.M.; Van der Rijt, J.A.J.; Meijer, E.W. *Adv. Mater.* **2000**, *12*, 874-878; (b) Montarnal, D.; Tournilhac, F.; Hidalgo, M.; Couturier, J.-L.; Leibler, L. *J. Am. Chem. Soc.* **2009**, *131*, 7966-7968.
20. (a) Chi, Y.C.; Scroggins, S.T.; Fréchet, J.M.J. *J. Am. Chem. Soc.* **2008**, *130*, 6322-6323; (b) Helms, B.; Guillaudeau, S.J. Xie, Y, McMurdo, M.; Hawker, C.J.; Fréchet, J.M.J. *Angew. Chem Int. Ed.* **2005**, *44*, 6384-6387; (c) Hecht, S.; Fréchet, J.M.J. *Angew. Chem Int. Ed.* **2001**, *40*, 74-91.
21. (a) Kidd, T.J.; Leigh, D.A.; Wilson, A.J. *J. Am. Chem. Soc.* **1999**, *121*, 1599-1600; (b) Hasenknopf, B.; Lehn, J.-M.; Boumediene, N.; Leize, E.; Van Dorsselaer, A. *Angew. Chem. Int. Ed.* **1998**, *37*, 3265-3268; (c) Gillard, R.E.; Raymo, F.M.; Stoddart, J.F. *Chem Eur. J.* **1997**, *3*, 1933-1940.

22. (a) Smulders, M.M.J.; Filot, I.A.W.; Leenders, J.M.A.; Van der Schoot, P.; Palmans, A.R.A.; Schenning, A.P.H.J.; Meijer, E.W. *J. Am. Chem. Soc.* **2010**, *132*, 611-619; (b) Wilson, A.J.; Masuda, M.; Sijbesma, R.P.; Meijer, E.W. *Angew. Chem. Int. Ed.* **2005**, *44*, 2275-2279; (c) Hirschberg, J.H.K.K.; Brunsveld, L.; Ramzo, A.; Vekemans, J.A.J.M.; Sijbesma, R.P.; Meijer, E.W. *Nature* **2000**, *407*, 167-170; (d) Rivera, J.M.; Martin, T.; Rebek, J. *Science* **1998**, *279*, 1021-1023.
23. (a) Schindler, F.; Lupton, J.M. *Nanolett.* **2010**, *10*, 2683-2689; (b) Kol'chenko, M.A.; Nicolet, A.A.L.; Galouzis, M.D.; Hofmann, C.; Kozankiewicz, B.; Orrit, M. *New J. Phys.* **2009**, *11*, 023037; (c) He, Y.; Burov, S.; Metzler, R.; Barkai, E. *Phys. Rev. Lett.* **2008**, *101*, 058101; (d) Cecconi, C.; Shank, E.A.; Bustamante, C.; Marqusee, S. *Science* **2005**, *309*, 2057-2060.
24. Lu, P.H.; Xun L.; Xie, X.S. *Science* **1998**, *282*, 1877-1882.
25. Dietz, H.; Rief, M. *Proc. Natl. Acad. Sci. U.S.A.* **2004**, *101*, 16192-16197.
26. (a) Cornish, P.V.; Ha, T. *ACS Chem. Biol.* **2007**, *2*, 53-61; (b) Ritort, F. *J. Phys.: Condens. Matter* **2006**, *18*, R531-R583; (c) Gimzewski, J.K.; Joachim, C. *Science* **1999**, *283*, 1683-1688; (d) Mehta, A.D.; Rief M.; Spudich, J.A.; Smith, D.A.; Simmons, R.M. *Science* **1999**, *283*, 1689-1695.
27. in Richard Feynman's visionary lecture during the annual meeting of the American Physical Society in 1959: "There is plenty of room at the bottom".
28. (a) Schwarz, G.; Sievers, T.K.; Bodenthin, Y.; Hasslauer, I.; Geue, T.; Koetz, J.; Kurth, D.G. *J. Mater. Chem.* **2010**, *20*, 4142-4148; (b) Moughton, A.O.; O'Reilly, R.K. *Macromol. Rapid Commun.* **2010**, *31*, 37-52; (c) Chiper, M.; Hoogenboom, R.; Schubert, U.S. *Macromol. Rapid Commun.* **2009**, *30*, 565-578; (d) Oh, M.; Carpenter, G.B.; Sweigart, D.A. *Organometallics* **2003**, *22*, 2364-2366; (e) Loeb, S.J.; Shimizu, G.K.H. *J. Chem. Soc.* **1993**, *18*, 1395-1397.
29. (a) Besenius, P.; Portale, G.; Bomans, P.H.H.; Janssen, H.M.; Palmans, A.R.A.; Meijer, E.W.; *Proc. Natl. Acad. Sci. U.S.A.* **2010**, *107*, 1788-17893; (b) De Greef, T.F.A.; Meijer, E.W. *Nature* **2008**, *453*, 171-173; (c) Bouteiller, L. *Adv. Polym. Sci.* **2007**, *207*, 79-112; (d) Park, T.; Zimmerman, S.C. *J. Am. Chem. Soc.* **2006**, *128*, 14236-14237; (e) Lehn, J.-M. *Polym. Int.* **2002**, *51*, 825-839; (f) Brunsveld, L.; Folmer, B.J.B.; Meijer, E.W.; Sijbesma, R.P. *Chem. Rev.* **2001**, *101*, 4071-4097.
30. (a) Ruiz de Luzuriaga, A.; Garcia, I.; Mercerreyes, D.; Etxeberria, A.; Pomposo, J.A. *Polymer* **2010**, *51*, 1355-1362; (b) Park, T.; Zimmerman, S.C. *J. Am. Chem. Soc.* **2006**,

- 128, 13986-13987; (c) Binder, W.H.; Bernstoff, S.; Kluger, C.; Petraru L.; Kunz, M.J. *Adv. Mater.* **2005**, *17*, 2824-2828; (d) Ten Cate, A.T.; Van Beek, D.J.M.; Spiering, A.J.H.; Dankers, P.Y.W.; Sijbesma, R.P.; Meijer E.W. *Polymer Preprints* **2003**, *44*, 618-619; (e) Zhang, P.; Moore, J.F. *J. Polym. Sci. A1* **2000**, *38*, 207-219.
31. (a) Binder, W.H.; Zirbs, R. *Adv. Polym. Sci.* **2007**, *207*, 1-78; (b) Lange, R.F.M.; Van Gurp, M.; Meijer, E.W. *J. Polym. Sci. A1* **1999**, *37*, 3657-3670.
32. Leigh, D.A.; Wong, J.K.Y.; Dehez, F.; Zerbetto, F. *Nature* **2003**, *424*, 174-179.
33. Sartorius, J.; Schneider, H.-J. *Chem. Eur. J.* **1996**, *2*, 1446-1452.
34. Ligthart, G.B.W.L.; Guo, D.; Spek, A.L.; Kooijman, H.; Zuilhof, H.; Sijbesma, R.P. *J. Org. Chem.* **2008**, *73*, 111-117.
35. (a) De Greef, T.F.A.; Nieuwenhuizen, M.M.L.; Sijbesma, R.P.; Meijer, E.W. *J. Org. Chem.* **2010**, *75*, 598-610; (b) De Greef, T.F.A.; Nieuwenhuizen, M.M.L.; Stals, P.J.M.; Fitié, C.F.C.; Palmans, A.R.A.; Sijbesma, R.P.; Meijer, E.W. *Chem. Commun.* **2008**, 4306-4308.
36. Kramers, H.A. *Physica* **1940**, *7*, 284-304.
37. Hänggi, P.; Talkner, P.; Borkovec, M. *Rev. Mod. Phys.* **1990**, *62*, 251-341.
38. Bell, G.I. *Science* **1978**, *200*, 618-627.
39. Evans, E. *Annu. Rev. Biophys. Biomol. Struct.* **2001**, *30*, 105-128.
40. Purcell, E.M. *Am. J. Phys.* **1976**, *45*, 3-11.



CHAPTER 2

SINGLE MOLECULE MECHANICS OF SUPRAMOLECULAR HYDROGEN-BONDED SYSTEMS

Ludwig Boltzmann, who spent much of his life studying statistical mechanics, died in 1906, by his own hand. Paul Ehrenfest, carrying on the work, died similarly in 1933. Now it is our turn to study statistical mechanics. Perhaps it will be wise to approach the subject cautiously.

– David Goodstein

2.1 INTRODUCTION

Research in the past decades has shown that nature's complex, versatile and efficient interactions can be attributed to the fact that reversible bonds can be formed and broken. Often several of these non-covalent bonds are formed and secondary, tertiary and quaternary 3D structures are created in proteins. Specific secondary structures like, α -helices, β -sheets and β -turns^[1] in proteins are held together by a large number of non-covalent hydrogen-bonds as is demonstrated in Figure 2- 1. The Green Fluorescent Protein (GFP)^[2] for instance - which is nowadays an essential part of the biological labeling toolkit - owes its fluorescence emission to a specific conformation that is held together by highly directional hydrogen-bonds (see Figure 2- 1c and Figure 2- 2). In 2008 Osamu Shimomura, Martin Chalfie and Roger Tsien were awarded the Nobel Prize for Chemistry for their contribution in identifying these proteins as well as their use as a tool to study cellular processes.

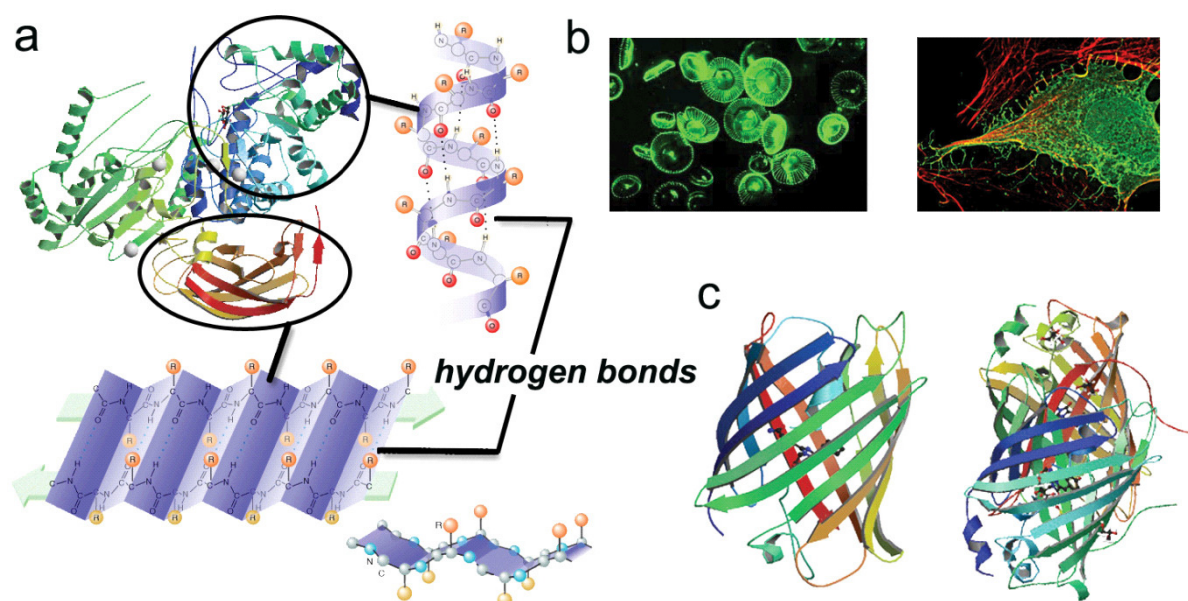


Figure 2- 1. (a) Schematic representation of α -helix and β -sheet formation via hydrogen-bonding in the protein^[3] β -glucosidase^[4]; (b) Green Fluorescent Proteins (GFPs) naturally occur in bioluminescent jelly fish, sea anemone and corals (left). However nowadays they are also used as a tool for biological (cell) labelling (right)^[5]; (c) a schematical representation of the 3D structure of a member of the GFP-like proteins (left), namely monomeric Azami-Green (mAG, 27% identical amino-acid sequence to avGFP), which naturally occurs in coral and displays green fluorescence emission^[6]. By contrast, the slightly different chemical structure of aceGFP only shows fluorescence emission when UV-irradiation is used (right)^[7]. *Image was adapted and compiled from refs. 3-7.*

Minor changes in the amino acid order of these proteins influence the hydrogen-bond interactions and the fluorescence emission as well^[3,4].

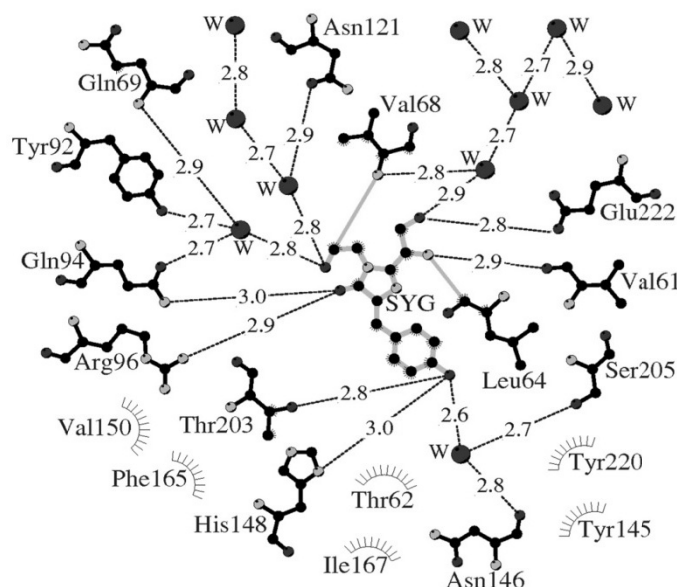


Figure 2- 2. A schematic drawing which stresses the importance of water and hydrogen-bonds for the 3D conformation of the GFP protein and the direct surrounding of the chromophore of aceGFP. Water is displayed as dots; hydrogen-bonds ($< 3.3 \text{ \AA}$) are displayed as lines and Van der Waals forces ($< 3.9 \text{ \AA}$) as grey "eye-lashes". This figure was produced using **LIGPLOT/HBPLUS**. Image was adapted from ref. 7.

As can be seen in Figure 2- 2, inter- and intramolecular forces play a major role in the conformation of proteins. Moreover small deviations in the sequence of the amino acids or the absence of water and hydrogen-bonds can completely alter the structure, properties and function of the system. To understand the influence of different forces on the structure and properties of these assemblies, an overview of the different forces (so called bond-types) that are essential in nature is presented below. Subsequently, this chapter will focus on non-covalent supramolecular interactions and hydrogen-bonded systems in more detail.

2.2 ESSENTIAL FORCES IN NATURE^[8]

In the gas phase four main contributions can be discerned that determine intermolecular interactions: electrostatic interactions between the distributed charges; repulsive interactions between the electron clouds at close approach; induction interactions between permanent dipoles and induced charges and dispersion interactions between induced dipoles. According to the Hellman-Feynman theorem^[9] all intermolecular forces are fundamentally electrostatic

interactions. A schematic overview of bond types and their accompanying strength is presented in Table 2- 1.

<i>Bond type</i>	<i>Bond energy [kT]</i>	<i>Bond energy [kJ/mol]</i>	<i>Range of action (dep. on r)*</i>	<i>Characteristics</i>
Covalent	100-300	200-800	Short range: 0.1-0.2 nm	highly directional
Ionic	100-300 and above	200-800 ^{&} and above	Long range [#] (1/r)	influenced by dielectric permittivity of solvent
Hydrogen-bond	5-10	10-40	Short range (1/r ²)	moderately directional
Dipole-dipole	0.5-2	1-5	Short range: 0.1 nm (1/r ³)	bond strength depends on angle between dipole moments
Van der Waals	~1	~3	Short range (1/r ⁶)	acts between all atoms and molecules

Table 2- 1. Various bond types and their characteristic bond strengths (or bond energies): the dependence of the bond energy on the radius between species (atoms and/or ions) provides a measure for the range of action of the force; [&]lattice energies of 4000 kJ/mol have even been reported (MgO); [#]for isolated NaCl ions it can be calculated that for a separation r larger than 50 nm the Coulomb energy will drop below kT , hence they are classified as long range interactions. *Data was taken from ref. 8.*

2.2.1 Covalent bonds (non metallic)

Covalent bonds are formed when binding electrons from the outer electron shell are shared between atoms and the discrete nature of the individual atoms is lost. Covalent forces are therefore defined as the forces that bind these atoms together. Based on the valency of the atoms involved, the covalent bonds determine the way the individual atoms will arrange in molecules or crystal lattices. So covalent bonds are directional and the formation of covalent bonds leads to distinct bond angles. Especially when double or triple bonds are formed, the

flexibility and rotational freedom of the molecule may be limited to a large extent. Covalent forces have an action radius on the order of the interatomic separation (0.1-0.2 nm) and the bond strength or bond energy lies mainly in the range of 100-300 kT (product of Boltzmann constant k and temperature T : at 298 K, $kT = 2.5 \text{ kJ/mol}$).

2.2.2 Ionic interactions

A large difference in electronegativity of atoms can cause the transfer of one or more electrons upon which ionic species are formed. The ionic (electrostatic) interaction of the - now charged – atoms is similar or even stronger than covalent forces and is defined by the Coulomb force:

$$F(r) = \frac{Q_1 \cdot Q_2}{4\pi\epsilon_0\epsilon r^2} = \frac{z_1 \cdot z_2 \cdot e^2}{4\pi\epsilon_0\epsilon r^2} \quad (\text{and } W(r) = \int_{\infty}^r F(r) = \frac{z_1 \cdot z_2 \cdot e^2}{4\pi\epsilon_0\epsilon r}) \quad \text{Equation 2-1}$$

with $F(r)$ the radius-dependent force, Q_1 and Q_2 the charges of the ions (or z_1 and z_2 the ionic valencies) and ϵ_0 the dielectric permittivity of vacuum, ϵ the dielectric permittivity of the medium, e the elementary electron charge and $W(r)$ the radius-dependent potential energy.

Characteristic for Coulomb forces are the high bond strength, the long range working distance and the disadvantageous influence of charge screening on the ionic bond strength in media with high dielectric constants such as water.

2.2.3 Dipole-dipole interactions

An inhomogeneous electron distribution (and so a difference in electronegativity) which is not sufficient to provoke electron transfer can still cause attractive and repulsive interactions between molecules with a so called dipole moment. The strength of this dipole-dipole interaction depends on the apparent dipole moment as well as the orientation and is obviously not as strong as ionic interactions. In comparison, the maximum attractive energy of two point dipoles which are perfectly aligned and oriented relative to each other at a distance r , is defined as:

$$W(r) = \frac{-2\mu_1 \cdot \mu_2}{4\pi\epsilon_0\epsilon r^3} \quad \begin{array}{c} \text{+} \quad \text{---} \quad \text{---} \quad \text{---} \quad \text{+} \\ \text{---} \quad \text{---} \quad \text{---} \quad \text{---} \quad \text{---} \end{array} \quad \text{Equation 2-2}$$

with μ_1 and μ_2 the electric dipole moments.

As can be directly observed from the two equations for ionic and dipole-dipole interactions, the energy of dipole-dipole forces have a $1/r^3$ dependency compared to a $1/r$ dependency for ionic interactions. As a consequence the range of action of these dipole-dipole interactions is considerably smaller than ionic interactions and so no long-range alignment of these polar molecules has been observed in liquid environment.

2.2.4 Coordinative bonds

Coordinative bonds are well known in nature, and have delicately tunable bond strengths which lie in between the stronger covalent bonds and the weaker dipole-dipole interactions. Examples can be found in the iron-complexes (heme groups) in metalloproteins like hemoglobin which are able to bind oxygen in our red blood cells, as well serve as anti-oxidants and iron-regulators in the body. Coordinative bonds are formed when at least one electron pair of a ligand is donated to a central atom or ion. The strength of these bonds, and hence the life-time, can be fine-tuned using a specific ligand and central atoms/ions.

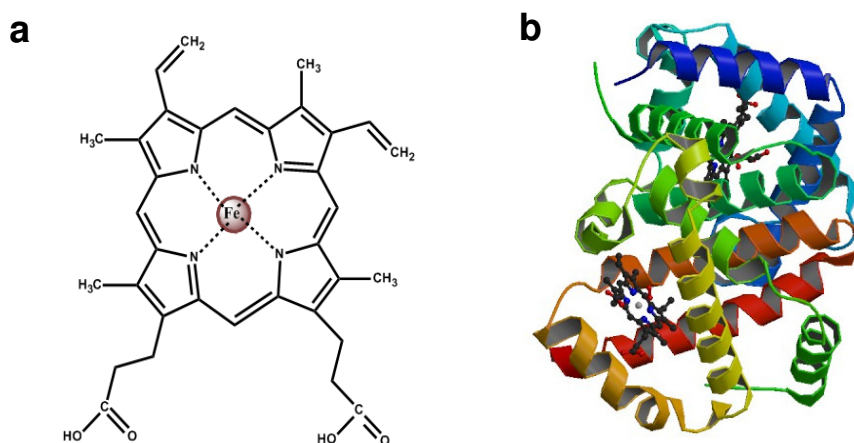


Figure 2- 3. (a) Coordinative bonds of a heme group which is formed due to the interaction of an electron pair of a double unoccupied orbital of nitrogen (N) and iron (Fe²⁺). In biology these heme groups, in for instance hemoglobin, bind large amounts of oxygen; (b) schematic ribbon structure of the metalloprotein hemoglobin. Heme groups can be clearly witnessed in between the α -helices of the protein.

2.2.5 Van der Waals interactions

Van der Waals interactions are omnipresent, belong to the group of weak interactions and act between all molecules and atoms. Three contributions to the Van der Waals force can be discerned:

- Keesom forces: forces acting between rotating permanent dipoles (Boltzmann averaged)
- Debye forces: forces acting between a permanent dipole and the accompanying induced dipole
- London dispersion forces: forces acting between two induced dipoles

From the three contributions mentioned above only the London dispersion forces are always present and act also between neutral atoms and molecules without any permanent dipole moment. The origin of dispersion forces can be found in quantum mechanics, however the resulting interaction is mainly electrostatic in nature. The dispersion force results basically from the fact that a finite dipole moments can exist (even for a nonpolar molecule) due to the position of the orbiting electrons. This dipole moment polarizes all nearby neutral atoms by its electric field, which creates an attractive force between the two atoms. The London dispersion forces are often considered as the most important contribution to the total Van der Waals force and are known to affect: the properties of gases, liquids and thin films, surface tension, wetting behavior, (physical) adsorption and adhesion. Debye and Keesom forces are only observed in case permanent dipoles are present and are – just like dispersion forces between neutral atoms - rather short-range interactions. Debye (or induction) forces are found when polar and nonpolar molecules interact, whereas Keesom (or orientation) forces are observed when polar molecules interact. The interaction energy of all Van der Waals forces varies with the inverse sixth power of the distance.

2.2.6 Hydrogen-bonds

Hydrogen-bonds are clearly electrostatic in nature. The exceptionally high melting and boiling point of a low molar mass liquid like water demonstrates that additive hydrogen-bond interactions can approach quasi-covalent bond strengths. Hydrogen-bonds, generally denoted as $Y \cdots H-X$, can be formed between electronegative atoms ($Y=N, O, F$) and hydrogen atoms which are covalently attached to electronegative atoms ($X-H$). Intermolecular distances therefore show a quasi-covalent character and are often much smaller than the sum of the Van der Waals radii (for ice $O-H_{\text{intra}} = 0.10$ nm, $O \cdots H = 0.176$ nm and $r_{\text{vdW}} = 0.26$ nm). Depending on the X and Y atoms involved and the geometry, the strength of these hydrogen-bonds lies between 10-40 kJ/mol (5-10 kT). Thus these bonds are typically much stronger than Van der

Waals interactions (~ 1 kT), but weaker than covalent, metallic or ionic bonds (~ 100 - 300 kT). Furthermore the bond length depends on the acidity of the X-H group and on the basicity of Y, however to a lesser extent^[10]. The dependence of acidity on the bond length was demonstrated by Desiraju for substituted chloroalkyls, by studying the influence of the number of electron-withdrawing Cl atoms of the chloroalkyl on the hydrogen-bond length^[11]. Furthermore a clear correlation between the bond length and the pK_a of different hydrogen-bond pairs in dimethyl sulfoxide (DMSO)^[12] was demonstrated. The influence of electronic effects and steric hinderence was observed as well.

Cooperative interactions^[13] play a major role in hydrogen-bonded systems, especially in biology. A single hydrogen-bond between a hydrogen donor (D) and acceptor (A) itself may not be very strong, but it is the combination of multiple hydrogen-bonds and other interactions such as π - π stacking that can create a very stable complex even in highly competing polar solvents like ethanol and water. In apolar solvents hydrogen-bond strengths close or equal to that of covalent interactions were observed. Hydrogen-bonding also depends on polarization and charge mobility^[14]. Since the strongest dipole-dipole interactions are obtained when dipole moments are aligned often linear and planar hydrogen-bonded structures are observed (see also paragraph 2.2.3).

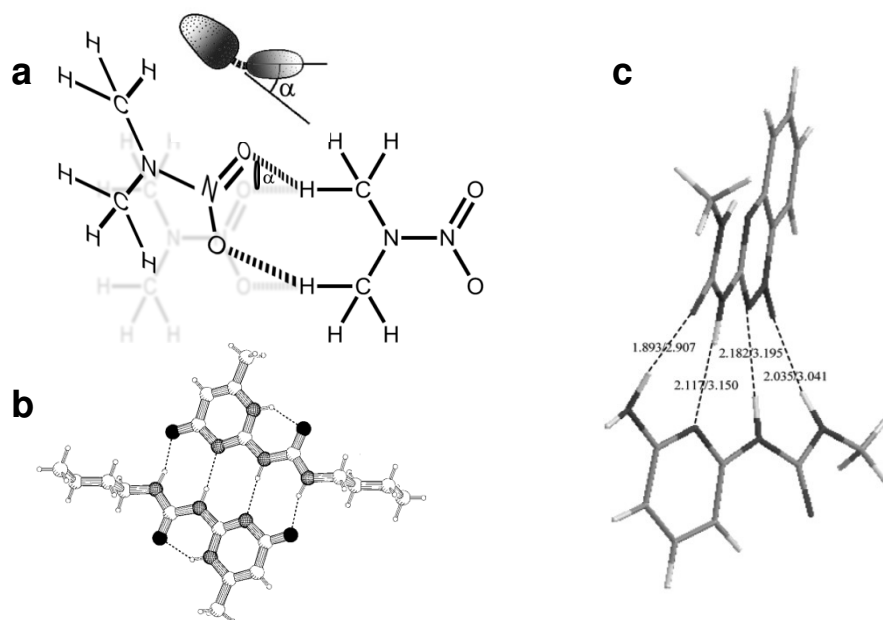


Figure 2- 4. (a) Deformation of a planar hydrogen-bond angle: the hydrogen-bond angle is zero degrees if a planar structure is formed. In case bending in or out of plane is necessary to form the hydrogen-bond, a tilt angle α is introduced^[8]; (b) linear arrangement of hydrogen-bonds in a ureidopyrimidinone (UPy) hydrogen-bonded array: planar conformation^[15]; (c) a non-planar hydrogen-bonded complex: a tilt angle of 28.5 degrees between the two π planes was observed^[16]. Image was adapted and compiled from refs. 8, 15 and 16.

Hence hydrogen-bonds are moderately directional, although some hydrogen-bond angles of 20° or more were observed. This favorable linear arrangement of hydrogen-bonds is demonstrated in Figure 2-4 until 2-6 for several hydrogen-bonded systems. This directionality also explains the larger influence of hydrogen-bonds on the geometry of proteins (Figure 2-2), DNA (Figure 2-6) and lipids.

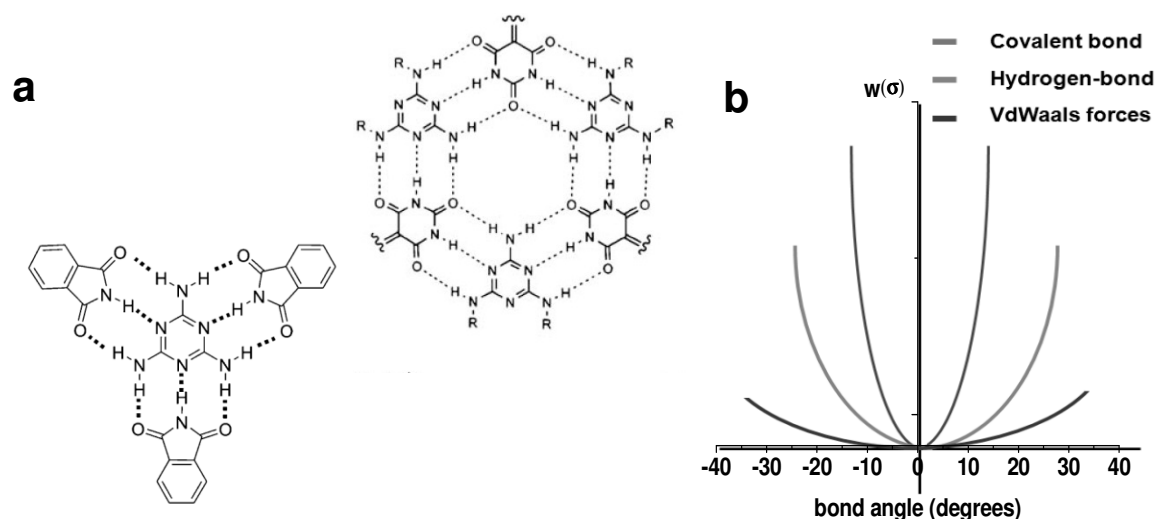


Figure 2- 5. (a) Two different hydrogen-bonded systems. The preferential formation of linear hydrogen-bonded arrays can be clearly discerned; (b) different bonds types display high (covalent bonds), moderate (hydrogen-bonds) or only weak directionality^[8] due to the bond angle-dependent potential energy $w(\sigma)$. *Image (right) was adapted from ref. 8.*

Different types of DNA can be discerned with different dimensions and base pair tilt angle to the helical axis, so called A-DNA, B-DNA and Z-DNA. Their geometry strongly depends on the interaction with the water molecules in the grooves. The phosphate groups in the A-helix bind fewer H_2O molecules and hence the A-form is more favorable in cases of dehydration. More strikingly Z-DNA (with zigzagging phosphate backbone) is a left-handed double helix, whereas A-DNA and B-DNA are right-handed helices. The different conformations again demonstrate the versatile and flexible characteristics of DNA, based on directionality of the same hydrogen-bonded base pair scheme.

Since water molecules compete with the formation of hydrogen-bonds of the molecule itself, often hydrophobic pockets^[13a] are created in nature which do not allow water to penetrate. However the reversible character of all the hydrogen-bonds involved easily allows for various other 3D conformations when this becomes necessary for other functionalities of the protein such as signaling. The highly complex hydrogen-bond interactions of proteins, DNA or RNA

can be modeled using synthetic analogs such as supramolecular polymers: macromolecules which consist of monomeric buildings blocks that are held together by non-covalent weak interactions such as hydrogen-bonds.

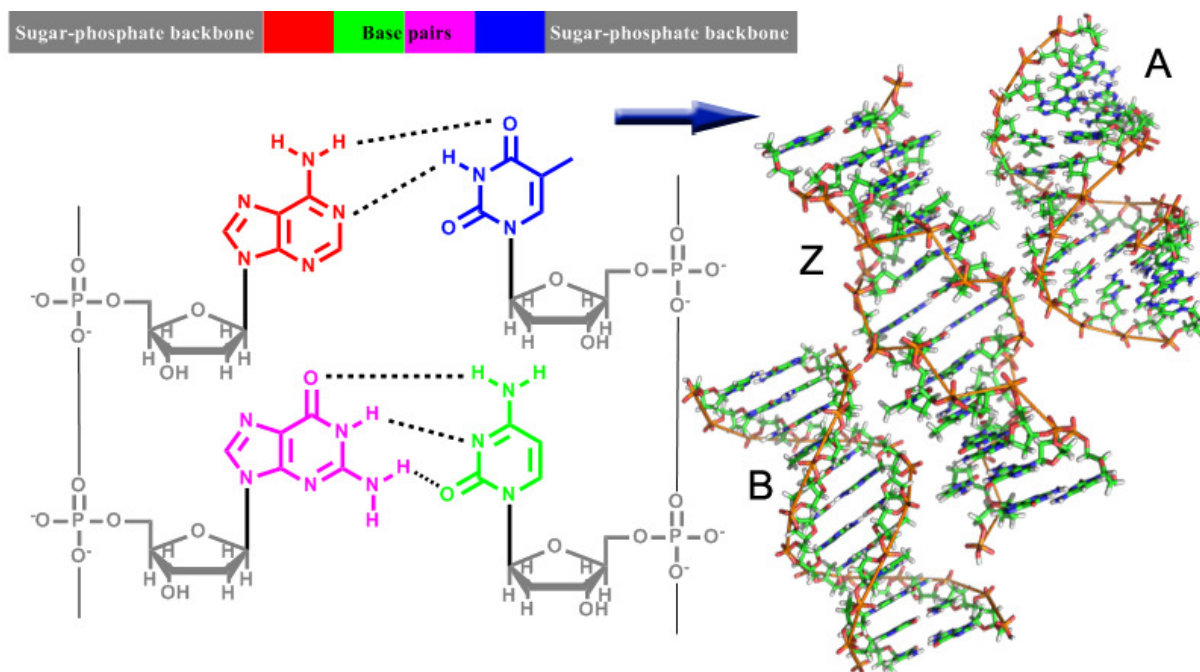


Figure 2- 6. Chemical structure of DNA which forms the well-known DNA double helix via hydrogen-bonding (either A-DNA, B-DNA and Z-DNA can be formed (represented in ball-stick models)): adenine-thymine and guanine-cytosine form two and three hydrogen-bonds per base pair respectively. *Image was adapted from http://images.wikia.com/psychology/images/b/b1/A-DNA,_B-DNA_and_Z-DNA.png.*

Detailed knowledge of intermolecular and intramolecular hydrogen-bonds would in turn enable us to design novel supramolecular hydrogen-bonded polymers^[17b-e] which were already briefly discussed in Chapter 1. These hydrogen-bonded polymers can be exceptionally stable even in polar solvents^[13b,18]. Due to the reversible interactions these polymers display special properties (see also Figure 2- 7) and can be used as self-healing materials^[17]. As was demonstrated by Sijbesma, Meijer and co-workers^[19] and more recently by Leibler and co-workers^[20], a new and exciting class of polymer materials can be ingeniously designed utilizing supramolecular hydrogen-bonding building blocks such as for instance widely available urea moieties. Furthermore recent studies have demonstrated chiral control and amplification based on benzene-1,3,5-tricarboxamide hydrogen-bonded polymers^[21]. Chiral control is frequently observed in nature, but complete synthetic control is hard to achieve. The effectiveness of certain drugs and medicines greatly relies on enantiopure materials. Therefore

studying chiral recognition and control based on hydrogen-bond interactions may lead to synthetic routes to synthesize 100% enantiopure medicines and drugs.

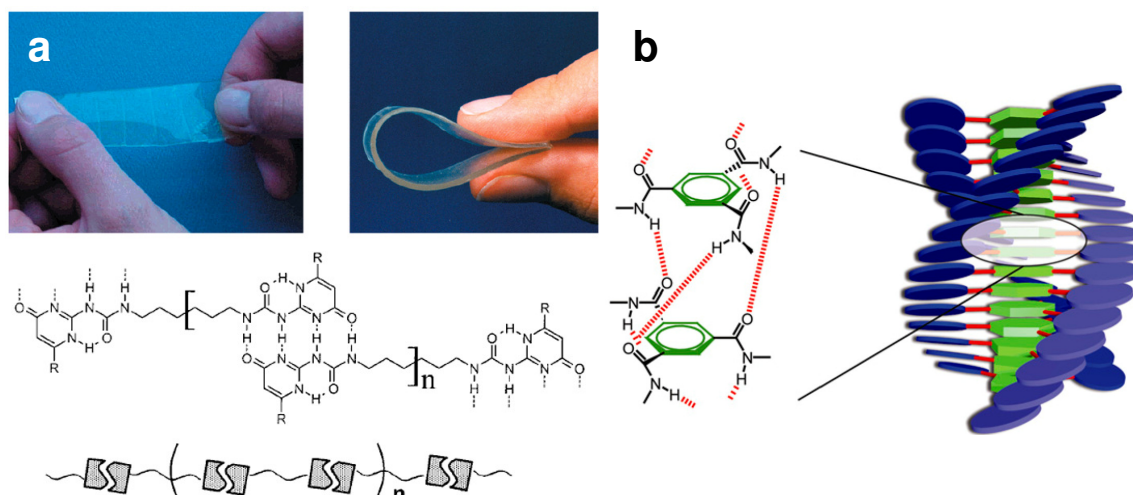


Figure 2- 7. (a) Examples of designed supramolecular polymers based on ureidopyrimidone units^[19]. Polymers are held together by bifunctional monomer units. Depending on the linker in between the hydrogen-bond units polymers, different properties can be obtained; (b) benzene-1,3,5-carboxamide self-assembles into triple hydrogen-bonded helices in water. By introducing hydrophobic chiral amino acid substituents in the outer shell the handedness and stability of the helix can be controlled^[18]. *Image was adapted and compiled from refs. 18 and 19.*

Based on solvent polarity the material properties of supramolecular benzene-1,3,5-tricarboxamide supramolecular polymers can be fine-tuned as well: supramolecular nanorods will be stabilized by apolar solvents and hence increase material strength.

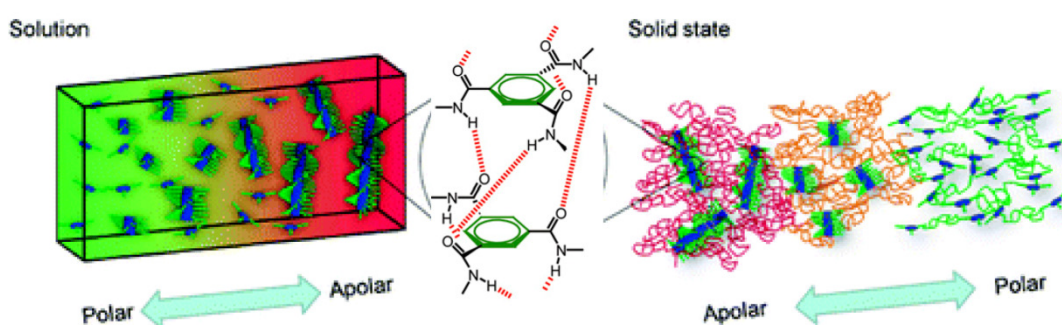


Figure 2- 8. Solvent polarity controlled supramolecular nanorod formation of benzene-1,3,5-carboxamide supramolecular polymers^[22]. *Image was adapted from ref. 22.*

A theoretical approach on the bond strength of these hydrogen-bonded arrays in chloroform was introduced by Sartorius and Schneider^[23], based on primary and secondary interactions.

Primary interactions can be defined as the hydrogen-bond interaction itself, whereas secondary interactions are defined as the repulsive or attractive interactions between neighboring hydrogen-bond donors and acceptors, as is displayed in Figure 2- 9.

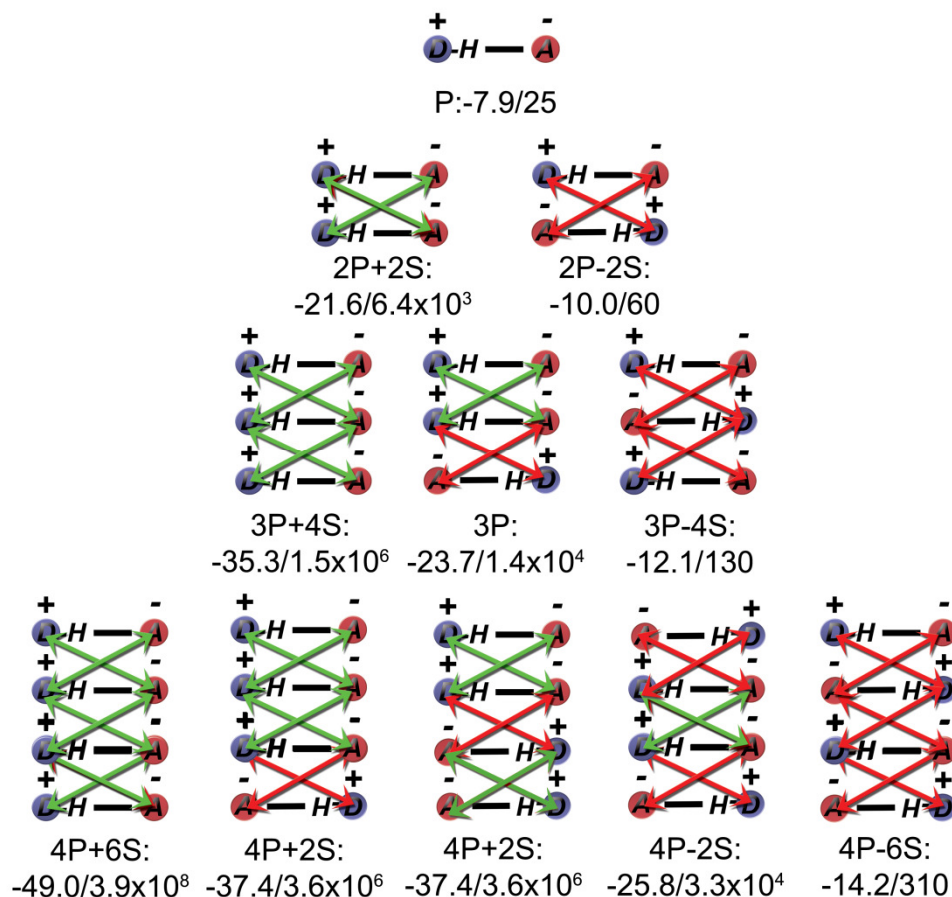


Figure 2- 9. Schematic representation of different hydrogen-bonded arrays and their primary (P) and secondary (S) hydrogen-bond interactions with predicted values for free energy of binding ΔG (kJ/mol) and the binding constant K (M^{-1}) in chloroform ($\Delta G/K$). P=primary interaction ($\Delta G_p = 7.9$ kJ/mol); S=secondary interaction, either repulsive or attractive ($\Delta G_s = 2.9$ kJ/mol). Image was adapted from ref. 23.

According to this approach hydrogen-bond strength is based on additive interactions: a primary hydrogen-bond contributes -7.9 kJ/mol to the free energy of binding $\Delta G_{binding}$ whereas a secondary hydrogen-bond contributes 2.9 kJ/mol to $\Delta G_{binding}$ (either positive (repulsive) or negative (attractive)). Although this additive scheme can be used to predict a certain range of dimer hydrogen-bond strength, various experimental approaches^[24,15] have demonstrated that also large deviations can be found. Furthermore the existence and influences of cooperative effects^[13] in these supramolecular systems are still under debate and are unaccounted for in this model.

2.3 SUPRAMOLECULAR HYDROGEN-BONDED POLYMERS

Although many supramolecular polymers are hydrogen-bonded polymers, supramolecular polymers (aggregates) can also consist of (metal-)coordinating building blocks, such as cyclodextrins^[25] or porphyrins^[26]. The metal-coordination polymers are based on metals such as ruthenium(II), cobalt(II), copper(II), iron(II), cadmium(II) and zinc(II)^[27]. This type of supramolecular polymer is however not discussed in more detailed, since a specific focus on hydrogen-bond interactions was chosen. A great variety of hydrogen-bonded polymers have been designed and synthesized over the past decades. Besides the supramolecular polymers that were already discussed previously the triple hydrogen-bonded liquid crystalline polymers designed by Lehn^[28] and the hydrogen-bonded calixarene-based supramolecular polymers by Rebek^[29] must be mentioned as well for their specific properties (see also Figure 2- 10).

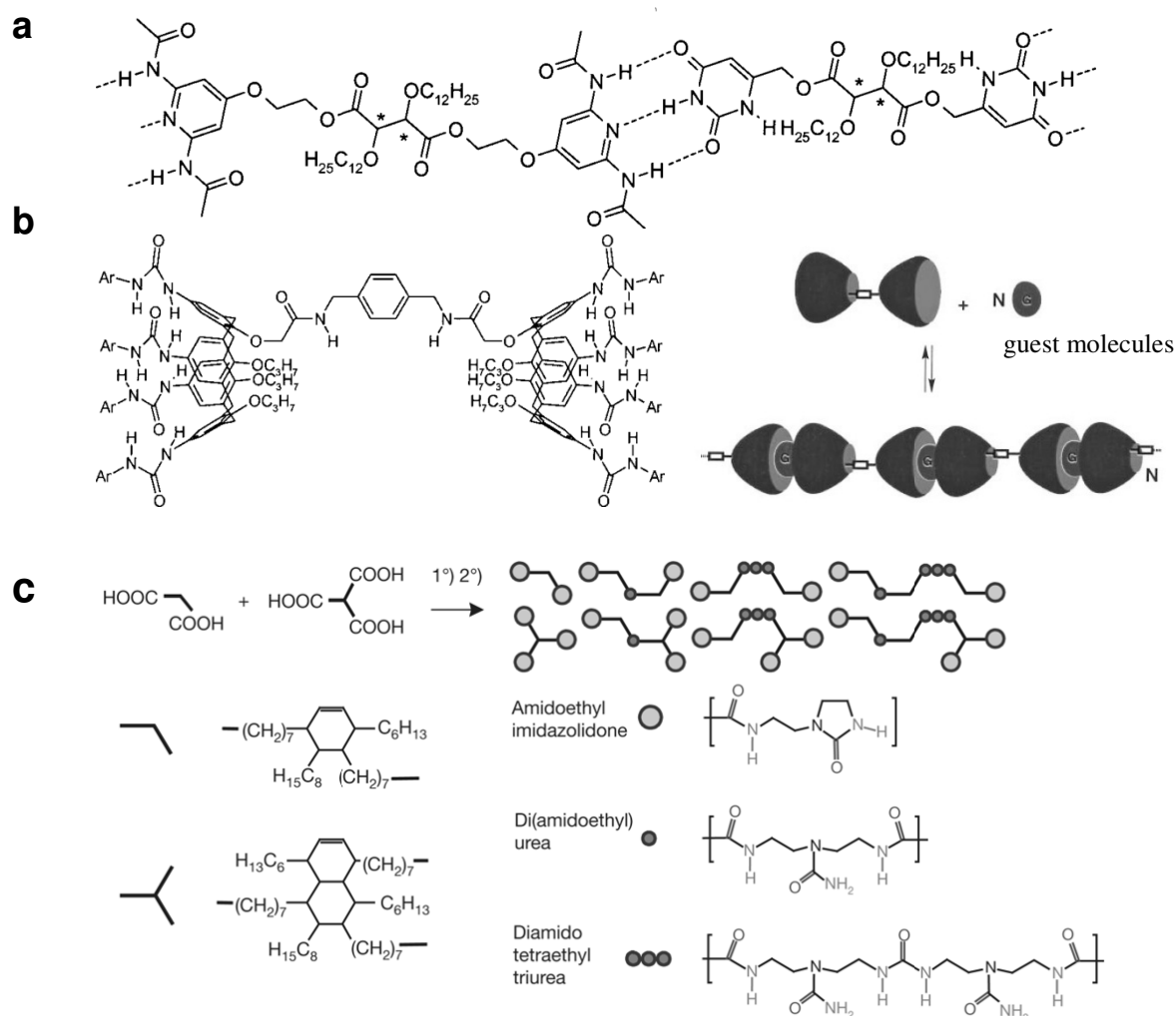


Figure 2- 10. Hydrogen-bonded supramolecular polymers which display specific properties: (a) triple hydrogen-bonded liquid crystalline polymers designed by Lehn^[28]; (b) hydrogen-bonded calixarene supramolecular polymers by Rebek^[29]; (c) urea-based self-healing supramolecular polymers by Leibler^[20]. *Image was adapted and compiled from refs. 20, 28 and 29.*

Already more than twenty years ago, Lehn and co-workers created liquid crystalline polymers from solid starting materials with triple hydrogen-bond functionalities. In this process fibers with long triple helix-based structures were formed based on molecular recognition^[28]. More recently Rebek and co-workers^[29] synthesized a calixarene-based supramolecular polymer and discussed its use as a “programmable” polymer, where the preferential association can be used as a binary code. Finally Leibler and co-workers^[20] recently demonstrated the fabrication of a self-healing polymer which is able to maintain its strength to a significant degree after the materials is cut and stored away separately for almost a day. These materials can be of use in many applications ranging from children’s toys to adjustable O-rings.

The properties of hydrogen-bonded polymers strongly depend on the number of bonds (see Figure 2- 9), the strength and the bonding environment of the hydrogen-bonded arrays that forms the reversible interaction between polymer segments. The bond strength depends on the dipole moment (O^-H^+ , N^-H^+ and F^-H^+), the geometry (*c.q.* hydrogen-bond angle), stability of tautomers and/or substituents of the hydrogen-bond. Furthermore Figure 2- 8 already demonstrates the distinct influence of solvent polarity on the hydrogen-bond strength. Polar solvents tend to destabilize hydrogen-bond interactions since the dipole interactions of the solvent compete with those of the solute. To be able to understand structure-property relationships and design these materials, it is of vital importance to identify the key molecular contributors to hydrogen-bond strength in solution. Previous studies by Sijbesma and Meijer^[15] already indicated that these contributions are insufficiently covered by currently available models^[22], which are based on primary and secondary hydrogen-bond interactions. Furthermore these models assume that bond energy per hydrogen-bond interaction is additive, which is clearly not the case if cooperativity plays a role^[13]. Generally positive cooperativity is observed where multiple interactions stabilize the system. This is for instance demonstrated for the stacking of UPy dimers. Based on 2D nuclear magnetic resonance (NMR; in CHCl_3) the cooperative stacking of UPy hydrogen-bond dimers was found to introduce a difference in the lifetime from 80 ms to 1600 ms for each individual unit in the duplex^[32]. So cooperative effects may influence the bond life time over orders of magnitudes.

The bulk (hydrogen-)bond strength of materials in different solvents is generally studied using the concentration-dependent transition of dimers to monomers in the solvent of interest, which can among others be determined by isothermal titration calorimetry^[30] (ITC) or nuclear magnetic resonance^[15,31,33] (NMR) spectroscopy. These techniques are very convenient to

study hydrogen-bonded arrays with low hydrogen-bond strengths. However, accurate analysis of arrays with high dimerization constants in (relatively) non-polar solvents (*e.g.* chloroform, toluene and hexadecane) becomes far more complicated because of the inherent limits of detection. This has been demonstrated by the Meijer-group in their effort to determine accurate values for the dimer binding constant of UPy (ureidopyrimidinone, DDAA-array) in chloroform. Ultimately, fluorescence spectroscopy techniques provided the necessary accuracy^[32]. Although feasible, such studies require a suitable fluorescent label that does not display any crosstalk with the hydrogen-bonded array. Furthermore the solubility of the labeled and unlabeled hydrogen-bonded arrays should be similar in the solvent used. Thus, although fluorescent spectroscopy was used for the analysis of strong binding (UPy)₂ complexes by Meijer et al.^[33], the requirements mentioned above can seriously hamper the applicability.

The methods described above provide bulk ensemble averaged data and hence the direct (solvent) environment of a single hydrogen-bonded array can not be probed, but a general understanding of a bulk “hydrogen-bonded array-solvent” system is provided. These methods can however not be used to study the influence of local solvent-ligand/receptor interactions. Exactly these local solvent-hydrogen-bonded array interactions receive growing attention since these hydrogen-bonded arrays are currently used as building blocks for single molecule motors^[37]. Leigh and co-workers^[37] demonstrated that the rate of rotation for their single molecule rotary motors could be controlled by a change in solvent polarity. When methanol or DMSO were added to the single molecule rotary motors in bulk, the ground state interactions were weakened substantially, which resulted in an increased rate of rotation. On a single molecule level a small solvent “contamination” or the presence of a mixed solvent could create a specific distribution of single molecule rotary velocities states. This demonstrates the necessity of studying solvent effects on hydrogen-bonded arrays especially on a single molecule level if the unconvoluted values are to be determined.

2.4 SOLVENT EFFECTS ON A SINGLE MOLECULE LEVEL

As was previously discussed, the polarity of the solvent plays a major role in the bond strength of hydrogen-bonded arrays. This is directly related to the influence of competitive dispersion interactions between the solvent and the solute molecules. The association constant (K_{eq}/K_{dim}) – which is a measure for the free energy of binding ΔG (*c.q.* bond strength) – of

hydrogen-bonded species has been studied for a large number of species in solvents as well as in the gas phase. The affinity or equilibrium constant K_{eq} is governed by the kinetic rate constants, k_{on} and k_{off} : $K_{eq} = k_{on}/k_{off}$. In equilibrium, k_{off} is the rate of complex dissociation, whereas, k_{on} corresponds to the rate of complex formation. From the value of k_{off} , the bond lifetime of the complex in equilibrium can be determined: $t_{off}(0) = k_{off}^{-1}$.

Many approaches focused on deriving structural constants for hydrogen-bond strength of a certain range of species. However, Abrahams and Platts^[34] demonstrated that – for small and simple molecules – hydrogen-bond interactions between two functional groups can be approximated by a simple and straightforward relationship. The only parameters involved are the solvent-dependent constants c_1 and c_2 , the functional group constant for the hydrogen-bond donor α_2^H and the hydrogen-bond acceptor β_2^H :

$$\log K = c_1 \alpha_2^H \beta_2^H + c_2 \quad \text{Equation 2-3}$$

The solvent-dependent constant c_1 accounts for the main contribution of the solvent, whereas the constant c_2 represents the adverse effect when a non-covalent complex of two species is formed in solution ($\sim +5\text{kJ/mol}$). Since the molecular motion of the solute species is only slightly restricted here, this effect is rather small (compared to for instance covalent bond formation in solution)^[35].

Based on the competition depicted in Figure 2- 11 between solvent-solute, solute-solute and solvent-solvent an estimate for the free energy of binding of the hydrogen-bond interaction in any solvent can be obtained using the hydrogen-bond donor and acceptor constants for the solute (α and β) and the hydrogen-bond donor and acceptor constant for the solvent (α_s and β_s)^[36].

This approach leads to a general profile for the hydrogen-bond interactions between two neutral functional groups in any solution. The general profile in Figure 2- 11 provides a schematic of the solvents effects that will play a role in reversible hydrogen-bond interactions. In the two regimes where solvent-solute interactions dominate, hydrogen-bond interactions between the functional groups are less favorable. In the third regime solute-solute interactions dominate and hence hydrogen-bonding is favorable.

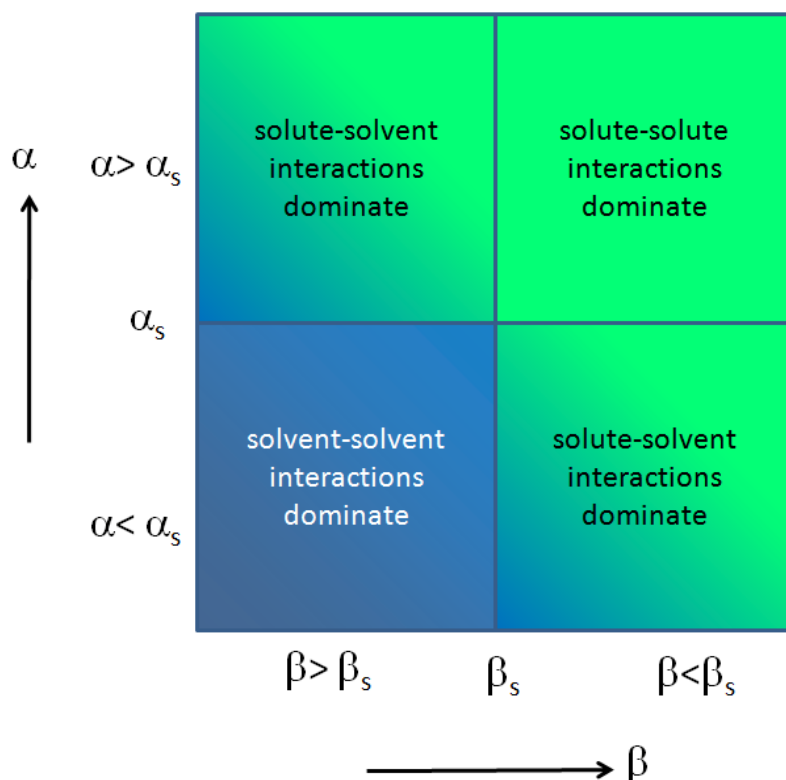


Figure 2- 11. General scheme for the hydrogen-bond interaction of two neutral functional groups in any solvent. Based on the competition between solvent-solute, solute-solute and solvent-solvent an estimate for the free energy of binding of the hydrogen-bond interaction in any solvent can be obtained using the hydrogen-bond donor and acceptor constants for the solute (α and β) and the hydrogen-bond donor and acceptor constant for the solvent (α_s and β_s). Image was adapted from ref. 36.

However also in the fourth regime, the so-called solvophobic zone where solvent-solvent interactions dominate, hydrogen-bonding is favorable between solute molecules since this enhances the solvent-solvent interactions. The general profile in Figure 2- 12 demonstrates why dimethylsulfoxide (DMSO) is one of the best solvents for hydrogen-bonding species: almost all solvent-solute interactions are favorable.

The analysis above however assumes that all solute-solvent complexes can be formed in solution or 100 % solvent-solvent and 100% solute-solute interactions can be achieved. This is generally not the case and a Boltzmann weighted average of the solvent and solute interactions would represent the distribution more accurately.

In mixed solvents of highly polar and apolar components, like mixtures of water and hydrocarbons for instance, even dramatic effects of the solvophobic regime may be observed: water is known to form cages around the hydrophobic hydrocarbons to minimize interactions and still form an optimal number of intermolecular hydrogen-bonds (see Figure 2- 13).

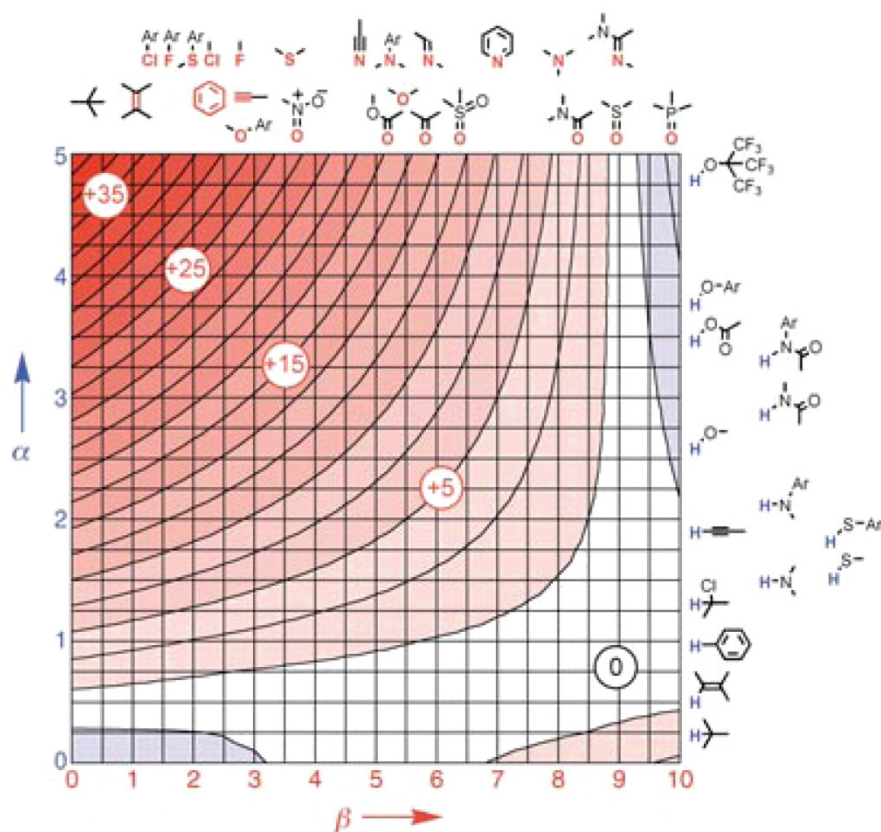


Figure 2- 12. General profile for a wide variety of hydrogen-bond interactions in DMSO (red areas represent an unfavorable solute-solute interaction (free energy of binding, $\Delta G_{H-bond} > 0$) whereas blue represents favorable hydrogen-bond interactions ($\Delta G_{H-bond} < 0$). At the zero cross-over point $\alpha = \alpha_s$ and $\beta = \beta_s$. The solute-solvent interactions in the top-left corner of the profile dominate and hence DMSO is one of the best solvents to disrupt hydrogen-bond interactions. *Image was adapted from ref. 36.*

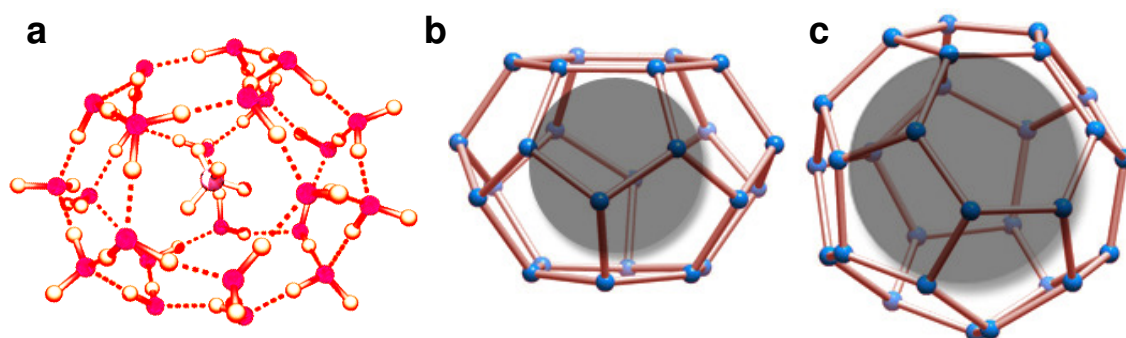


Figure 2- 13. Schematic representation of water cages around hydrophobic solute molecules in the gas phase: methane (a), longer alkanes (b,c: alkanes in black, oxygen atoms in blue, hydrogen atoms not shown). Depending on the size of the alkane larger clathrate cages are formed. *Image was adapted from ref. 8.*

The fact that water forms cages around hydrophobic molecules demonstrates that, although solvent-solute interactions can be minimized, solvent-solute interactions can only be limited to some extent: in any solute-solvent system a solvation shell is unavoidable. It is exactly this solvation shell that will influence the hydrogen-bond strength of the hydrogen-bonded moieties on a single molecule level and hence influence the properties of the single molecule species. To study the effect of these solvent molecules in close proximity of the hydrogen-bonded array and obtain more insight into structure property-relationships, single molecule techniques become crucial.

2.5 SINGLE MOLECULE STUDIES

Nowadays single molecule techniques^[38,39] can be used to study systems in which spatial and temporal averaging is likely to play an important role and important properties might be hidden in ensemble averaged data. Spatial resolution for single molecule manipulation can either be obtained via mechanical transducers such as cantilevers^[40] or microneedles^[41] or via external field manipulators such as optical^[42]/magnetic tweezers^[43] and flow fields using microscopic beads. In the former case spatial resolution is obtained through beam deflection of a bendable beam/probe whereas in the latter case bead displacement is monitored. Furthermore the probe that is used must be designed to generate and detect minute forces in a range from piconewtons to nanonewtons (10^{-12} - 10^{-9} N) to be able to manipulate and measure forces on a single molecule level. A clear overview of these techniques, their range of application and the main (dis)advantages is among others provided by Bustamante et al.^[44] and Gaub and co-workers^[45].

Many biophysical processes and interactions could be observed in real-time using these single molecule manipulation techniques such as DNA mechanics^[46], protein folding^[38c,47], binding potentials of host-guest interactions^[38b,48], mechanical work of motor proteins^[41d,49], but also elastic behavior of (synthetic) macromolecules^[50,51] became feasible. Especially Atomic Force Microscopy (AFM)-based force spectroscopy and related techniques, such as force-clamp spectroscopy^[52] have matured over the past decades. These fast developments in AFM-related techniques mainly occur since the force sensitivity of AFM can be conveniently combined with topographical imaging due to the high spatial resolution. This high spatial resolution led to the development of molecular recognition imaging^[53] as well as single-molecule recognition patterning^[54]. Furthermore an experimental approach to study intermolecular

forces and bond energies between ligand-receptor pairs^[55] using AFM was introduced in parallel by Gaub and co-workers and Lee and co-workers. The underlying theoretical framework for these measurements was previously described by Bell^[56] and later by Evans and Ritchie^[57] using the biomembrane force probe (BFP) to study antibody-receptor interaction of red blood cells as well as (strept)avidin and biotin interactions. More recently the binding thermodynamics of cosolute molecules surrounding a single polymer chain was reported^[58]. An overview of the variety of possible phenomena and parameters that can be studied using AFM-based techniques was discussed by Gianotti and Vancso^[59a] as well as Zhang and co-workers^[59b] and is schematically displayed in Figure 2- 14.

AFM-based Single Molecule Force Spectroscopy (AFM-based SMFS) therefore seems a suitable candidate to obtain insight in supramolecular (biological) interactions by studying structure-property relationships of supramolecular polymers on a single molecule level. That is why the next paragraph will zoom in on the principles of AFM-based SMFS^[50e,60] and its use to study the energy landscape of supramolecular bonds.

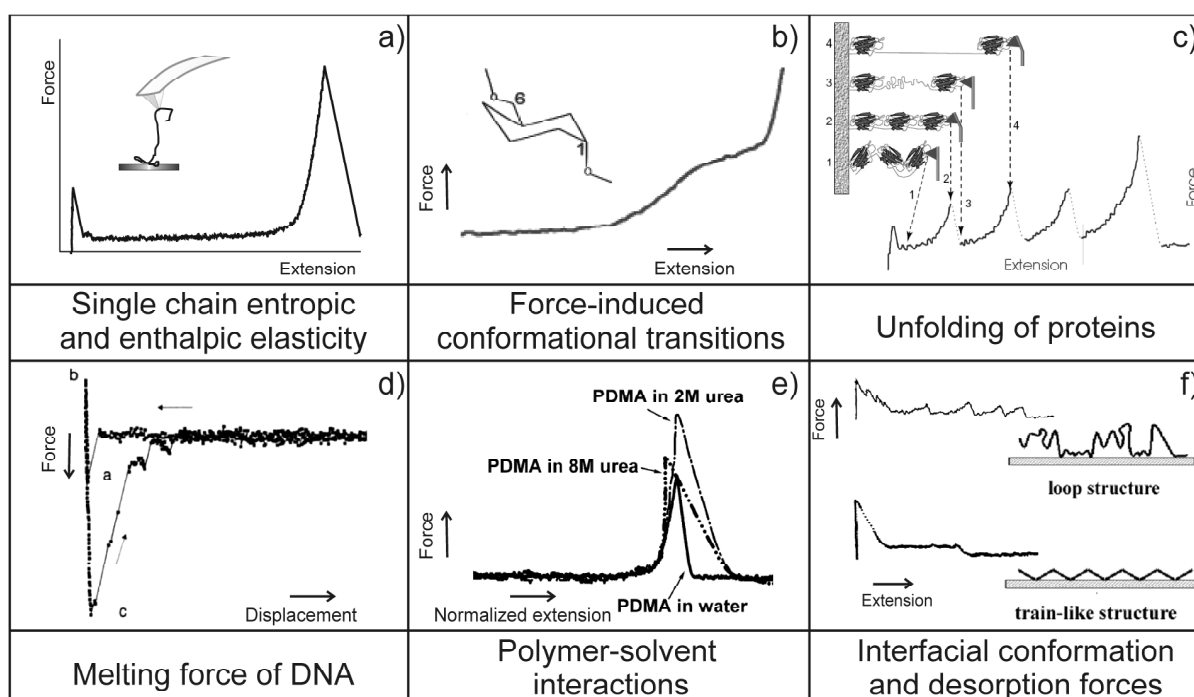


Figure 2- 14. Overview of different AFM-based SMFS experiments. Different phenomena and properties are studied such as (a) single chain entropic and enthalpic elasticity of macromolecules using various statistical mechanics approaches; (b) force-induced conformational transition of for instance the chair-boat transition of polysugars; (c) force induced unfolding of proteins; (d) melting force and hysteresis of DNA; (e) elasticity behaviour of macromolecules with varying polymer-solvent interaction; (f) interfacial conformation and desorption forces of macromolecules. *Image was adapted from ref. 59a.*

2.6 AFM-BASED SINGLE MOLECULE FORCE SPECTROSCOPY

An AFM-based SMFS sample-scanning setup, which is displayed in Figure 2- 15, is based on a piezo-driven AFM which is able to position the sample with (sub-)nanometer precision in X, Y and Z-direction.

An AFM-probe is then used to detect and apply minute forces which are monitored via the optical beam method where laser light is deflected from the cantilever and collected at the photodetector. During a force spectroscopy experiment the AFM-tip – which has a radius which ranges from a few to tens of nanometers – is used to pick-up single molecules, or the AFM-tip is chemically modified^[61] with the molecule of interest. If the AFM-tip is not chemically modified, a modified surface is used, which contains chemically or physically adsorbed molecules with large intermolecular spacing. In Figure 2- 15 the piezo-scanner displacement in a typical force spectroscopy cycle is demonstrated and the accompanying deflection vs. piezo-position curve is obtained. Since the spring constant and the deflection sensitivity can be calibrated and the deflection is known, this data can easily be converted to a force-distance or force-extension curve.

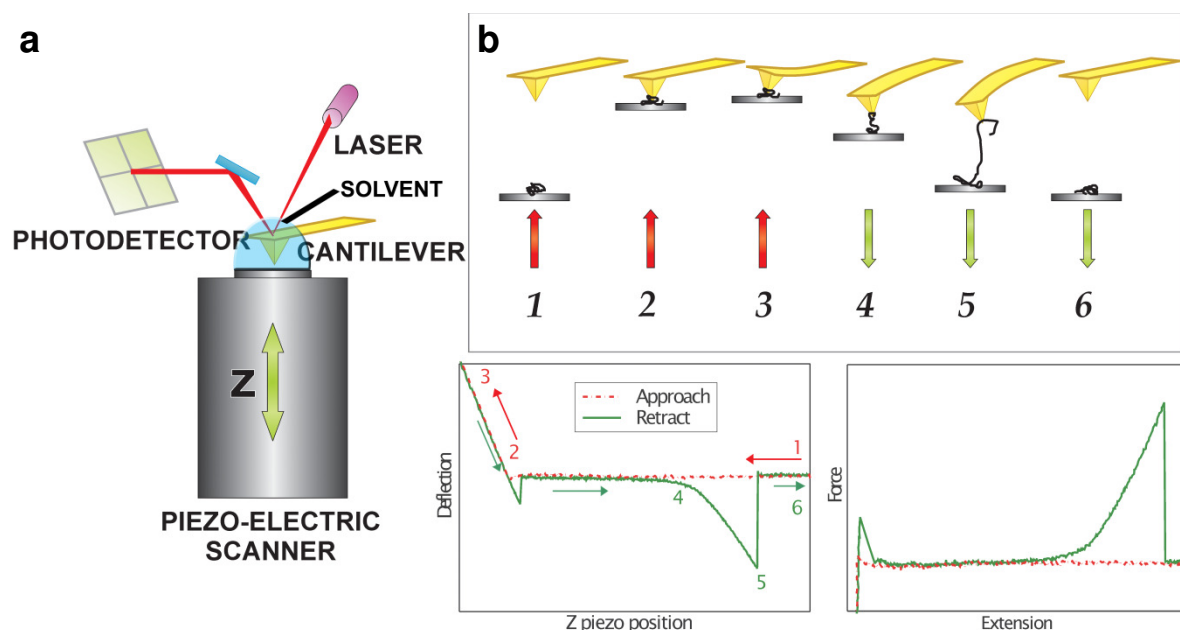


Figure 2- 15. (a) Schematic overview of an AFM-setup where a pieze-electric sample scanner and a sharp AFM-probe are used to study the tip-sample interaction via optical beam detection; (b) overview of a single molecule deflection-displacement curve which can be converted to a force-extension curve. *Image was adapted from ref. 59a.*

In a deflection vs. piezo-position curve the cantilever deflection z_c versus the piezo-position z_p is determined. The transformation to a force-distance curve can be achieved by converting z_c

and z_p into force and distance respectively^[60b,62]. Using cantilever calibration methods (see below), the force F is obtained by multiplying the cantilever deflection by its spring constant k_{spring} .

$$F = k_{spring} \cdot z_c \quad \text{Equation 2-4}$$

The tip-sample separation (or distance) D is determined by adding the deflection to the piezo position:

$$D = z_p + z_c \quad \text{Equation 2-5}$$

To be able to correctly convert the deflection vs. piezo-position curve into a force-distance curve, the zero position of the piezo has to be determined. In case of a calibration measurement on a hard surface, where the contact and non-contact regime are rather straightforward to detect (see Figure 2- 16), the zero position of the piezo can easily be detected. This becomes more complicated when repulsive and/or attractive forces start to interfere. Therefore the conversion to force-distance curves is nowadays often implemented in the software of commercial AFMs.

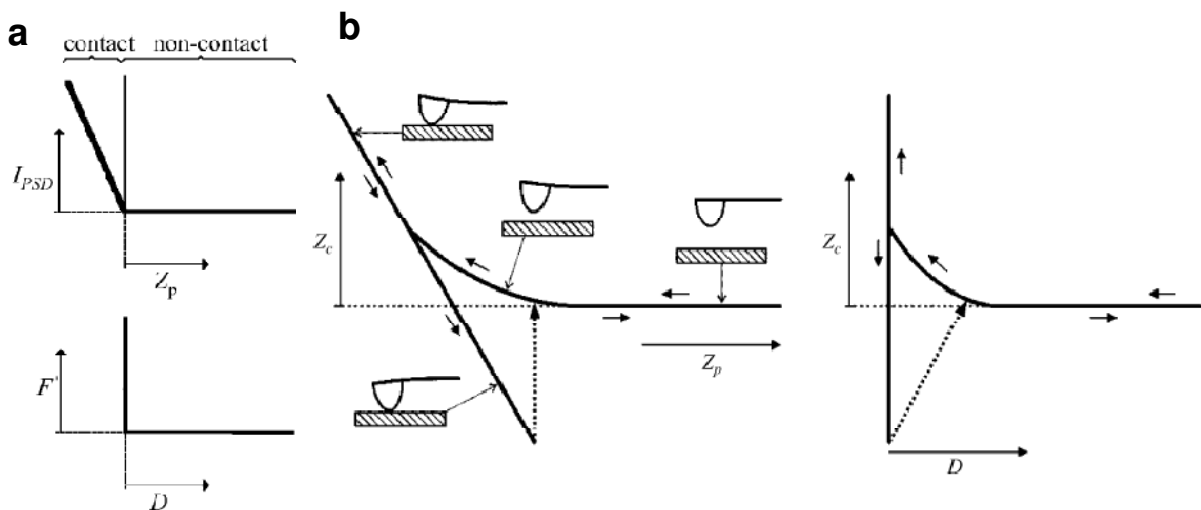


Figure 2- 16. Conversion of a deflection vs. piezo-position curve to the corresponding force-distance curve (see also Equation 2-4 and 2-5): (a) simplified hard-substrate case; (b) more challenging case with attractive and repulsive forces. *Image was adapted from ref. 60b.*

Furthermore the force-distance curve is often converted to the positive force quadrant in case the elasticity of polymers is studied, since this simplifies the use of statistical dynamics models of polymers (see also Figure 2- 15b). In that case the conversion to force by Hooke's law to the positive force quadrant is achieved by:

$$F = -k_{spring} \cdot z_c \quad \text{Equation 2-6}$$

Spring constants can be determined using several methods such as theoretical^[63], static loading^[64], and vibrational^[65] approaches as well as thermal oscillation methods^[66]. The advantages and disadvantages of these methods are thoroughly discussed by Bhushan^[67a] and Hodges^[67b]. Each of these approaches relies either on valid assumption of boundary conditions or on a precise experimental approach and hence errors can be introduced rapidly^[68]. However extensive progress has been made over the past two decades in understanding the principles behind spring constant calibration which has reduced errors significantly as is for instance discussed by Ohler^[69]. Using the Sader or thermal tune method (either using optical beam or laser Doppler vibrometry) the spring constants can be determined within ~5% error margin^[69a].

Single molecule events can be discerned by the presence of only one rupture event, however this does not exclude a rupture event where multiple chains are broken simultaneously^[70]. Therefore statistical mechanics approaches for polymer chains can be used to ascertain that only a single polymer chain is stretched. The elasticity of the single molecule rupture event is fitted to models, such as the worm-like chain^[73] (WLC) and freely-jointed chain^[74] (FJC) model - using a fast converging non-linear least-square fit, based on the Marquardt-Levenberg algorithm^[72] - and compared with available data for the supramolecular polymer (linker) under investigation (see Figure 2- 17). Hence a “master-plot” with an overlay of all single molecule rupture events can be created. Various models exist to describe the entropic and elastic behavior of a single molecule polymer chain. The WLC and FJC model are probably the best well-known models, however also modifications exist like for instance the modified Marko-Siggia WLC^[75], Odijk-WLC^[76] and extended-FJC^[77]. The WLC model assumes that a polymer chain is a string with a constant bending elasticity and therefore the molecule can be defined by its persistence length l_p ^[72c]. The polymer chain is assumed linear below the persistence length and the extension is limited to the contour length L_c of the polymer. The advantage of the WLC model is that both entropic and enthalpic contributions are taken into

account, but unfortunately the model can only be used accurately for small extensions and low stress.

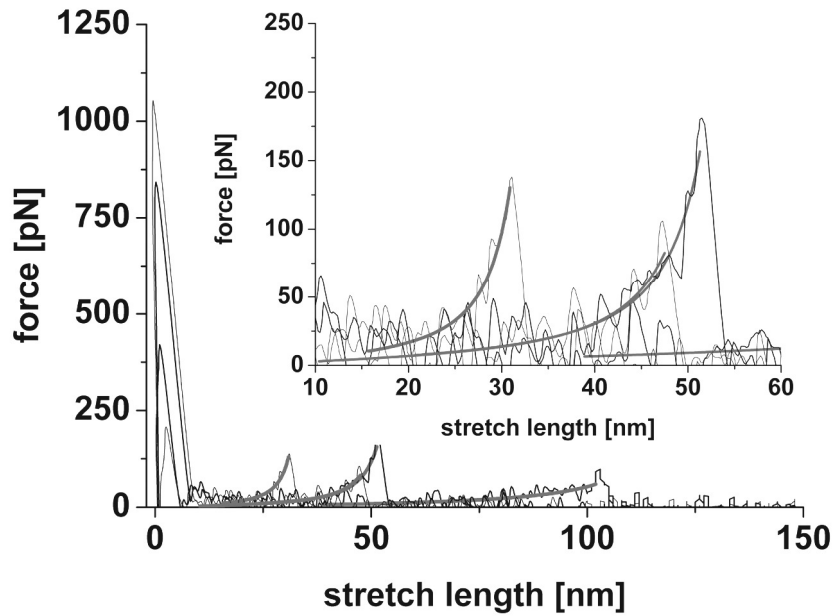


Figure 2- 17. Fit of force-extension curves to the worm-like chain model for polyethylene glycol chain linked hydrogen-bonded polymers in hexadecane: $r = (108.3 \pm 45.5) \times 10^3$ pN/s, RT. Inset: zoom of force-extension curves. Solid lines represent fits using the wormlike chain (WLC) model. A persistence length of $l_p = 3.63 \pm 0.40$ Å was determined.

Faithful reproduction of force-extension behaviour of various macromolecules such as DNA^[73b,78], proteins^[79] and polymers such as polystyrene (PS)^[80], poly(methacrylic acid) (PMAA)^[81], polydimethylsiloxane (PDMS)^[82] and poly(N-isopropylacrylamide) (PNIPAAm)^[83] was demonstrated using the WLC model. However recent literature^[84] has demonstrated that closer agreement between force-extension and fitted data can be obtained by adding an additional term for the enthalpic contributions included in extended WLC models such as the Odijk WLC^[76], and modified Marko-Siggia WLC^[75].

The FJC model^[74] (see Figure 2- 18) describes the polymer chain as a number of rigid orientation-independent Kuhn segments (with segment lengths l_K) connected via flexible joints. Full extension of the macromolecular chain is reached at $N \cdot l_K$ and long-range interactions are not taken into account. Due to this definition and the boundary conditions, this model is able to describe force-extensions curves for small forces and stretch lengths. If the applied forces are high enough to cause bond deformation and not only entropic but also

enthalpic effects are concerned, the modified or extended FJC models^[77] can be applied. The segment elasticity K_s is introduced and the molecule is described as if it consists of n separate springs. The standard FJC model was applied to describe force-extension behaviour of several macromolecules such as DNA^[85], PMAA^[81,86] and PDMS^[82b] in reasonable agreement with experimental data.

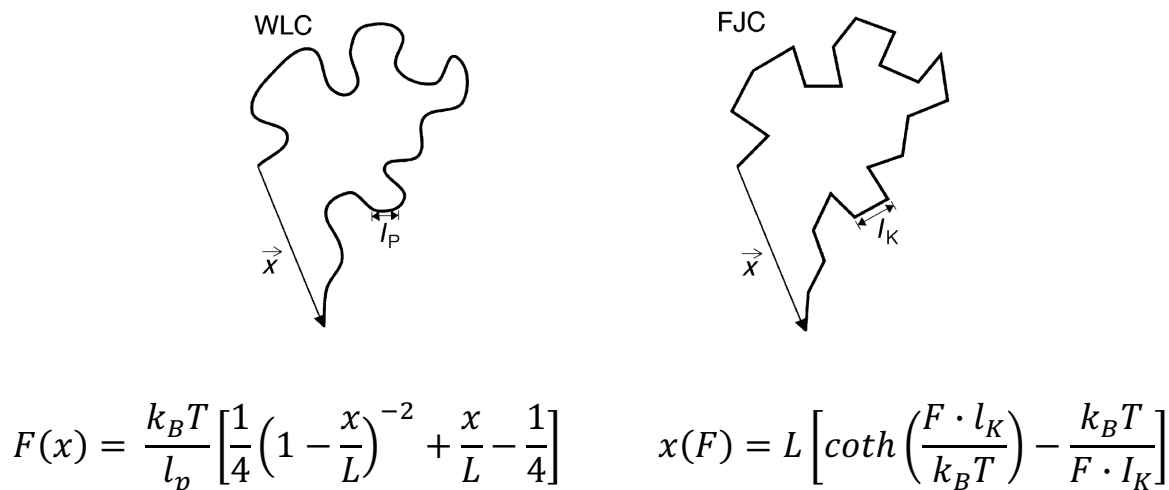


Figure 2- 18. Schematic representation of the WLC and FJC polymer models: in the WLC model the polymer chain is defined by its persistence length l_p , whereas in the FJC model the polymer chain is defined by its Kuhn segment length l_K . Force-extension behaviour is defined by: the polymer length L , temperature T and their characteristic persistence or Kuhn segment length l_p or l_K respectively. *For the FJC model no exact solution of the force-extension fit is available since no inverse exists for $x(F)$ and the fit parameters can only be obtained numerically.*

In accordance with the developments in WLC fitting, extended and modified FJC models^[77] have been developed and applied in recent literature to obtain a better agreement between experimental data and the applied model^[87]. Using models such as the modified FJC model, a discrete persistence chain model^[89] or even a Ashkin-Teller-like model^[90] the elastic behaviour of a wide variety of macromolecules^[50,91] can nowadays be successfully described.

2.7 AFM-BASED SMFS OF SUPRAMOLECULAR HYDROGEN-BONDS

As mentioned before, ligand-receptor interactions have been studied using various (single molecule) approaches to determine the energy landscape along the unbinding axis^[54-56]. Dynamic force spectroscopy was for instance used to study the unbinding forces, energy barriers and natural bond lifetimes of biotin-(strept)avidin systems^[71c]. The energy difference

between bound and unbound state determines the quantities of bound complex [AB] and the free ligands and receptors [A] and [B] in solution. In equilibrium, k_{off} is the rate of complex dissociation, whereas, k_{on} corresponds to the rate of complex formation. The affinity or equilibrium constant $K_D = K_{eq}$ is governed by the kinetic rate constants, k_{on} and k_{off} : $K_{eq} = k_{\text{on}}/k_{\text{off}}$. From the value of k_{off} , the bond lifetime of the complex in equilibrium can be determined: $t_{\text{off}}(0) = k_{\text{off}}^{-1}$. Natural bond lifetimes of these ligand-receptor interactions can vary from months (biotin-avidin) to microseconds depending on the bond strength (see Table 2- 2). Hydrogen-bonded arrays can also be regarded as ligand-receptor interactions and hence, dynamic force spectroscopy (DFS) enables us to study the bond strength, natural bond lifetime and energy barriers of hydrogen-bonded dimers and polymers. DFS provides a method to probe the inner world of molecular interactions as discussed extensively by Evans^[55a,92,96]. By using different loading rates to study the dissociation of complex biological interactions certain energy barriers may be exposed and suppressed which can not be studied using conventional equilibrium approaches.

Ligand	Receptor	Force [pN]	Bond lifetime	Bond energy [kT]	Bond affinity (K_D [M])
Biotin	Avidin ^[55a,92]	160 ± 20 (1 Hz) 170 ± 19 (200 nN/s) 326 ± 33 (800 nN/s)	months	35	10 ¹⁵
Human Serum Albumin (HSA)	Anti-HSA ^[71c]	244 ± 22 (not given)	1500 seconds	-	10 ⁸
Fibrinogen	RGD ^[93]	93 (0.1-1000 nN/s)	milliseconds	14.8	-
Antibody	Antigen ^[94]	35-165 (not given)	micro-milliseconds - hours	8-25	10 ² – 10 ⁸

Table 2- 2. Natural bond lifetime distributions for several biological ligand-receptor interactions. *The antibody-antigen data provides a general indication, specific ligand-receptor interactions may vary in bond strength over a broad range. Data was based on refs. 55a, 71c, 92-94.*

Even a whole cascade of activation barriers can be revealed. Furthermore single molecule hydrogen-bonded dimers and polymers can also be studied in organic solvents using this approach whereas traditional ligand-receptor interactions are often studied under biological conditions (H₂O, pH~7).

If a force is applied, and the system is moved from equilibrium, the bond lifetime of a ligand-receptor bond is significantly reduced due to the reduction of the activation energy barrier:

$$t_{off}(f) = t_D \cdot e^{(E_b - x_\beta \cdot f) / kT} \quad \text{Equation 2-5}$$

where $t_{off}(f)$ is the bond life time under the applied load, t_D is the diffusion relation time and x_β is the characteristic length in the direction of the force and E_b is the energy of the ligand-receptor interaction under load.

Far-from-equilibrium measurements can be achieved when the experimental conditions are chosen as such that the chance of rebinding approaches zero (and hence $S_a(t) \cdot k_{on} \rightarrow 0$, where $S_a(t)$ is the likeliness of association and k_{on} is the kinetic on-rate). In that case the ligand and receptor molecules move much faster away from each other than diffusive processes can bring them together due to the elastic linker. Therefore the frequency of unbinding becomes a direct function of the applied force over time (first order (Markov) process with time-dependent rate constant) far-from-equilibrium. The most probable rupture force f^* is then defined as:

$$f^* = f_\beta \cdot \ln\left(\frac{r_f}{r_f^0}\right) \quad \text{Equation 2-7}$$

$$\frac{\Delta E_b}{k_B T} = -\ln(r_f^0) + \ln(f_\beta) - \ln(t_D) \quad \text{Equation 2-6}$$

where $f_\beta (= k_B T / x_\beta)$ is the thermal scale force and $r_f^0 (= f_\beta / t_{off}(0))$ is the loading rate at zero force and ΔE is the energy difference between bound and transition state (see Figure 2- 19).

For strong binding complexes with a very sharp energy potential the free energy of binding ΔG for a ligand-receptor or hydrogen-bonded array can be determined via Equation 2-8, since ΔG can be estimated based on the energy difference between bound and transition state ΔE_b ^[97]:

$$\frac{\Delta G}{k_B T} = -\ln(r_f^0) + \ln(f_\beta) - \ln(t_D) \quad \text{Equation 2-8}$$

$$\Delta G = -RT \ln K_{eq}$$

$$\text{Equation 2-9}$$

The equilibrium binding constant K_{eq} is then determined via equation 2-9. For a single sharp energy barrier this thermal scale force f_β defines Δf due to the thermally activated kinetics. As can be observed in Figure 2- 19 the slope of the f vs. $\log(r_f)$ -plot provides f_β and the cross-section of the x-axis is the extrapolated loading rate at zero force r_f^0 (directed by f_β and t_D).

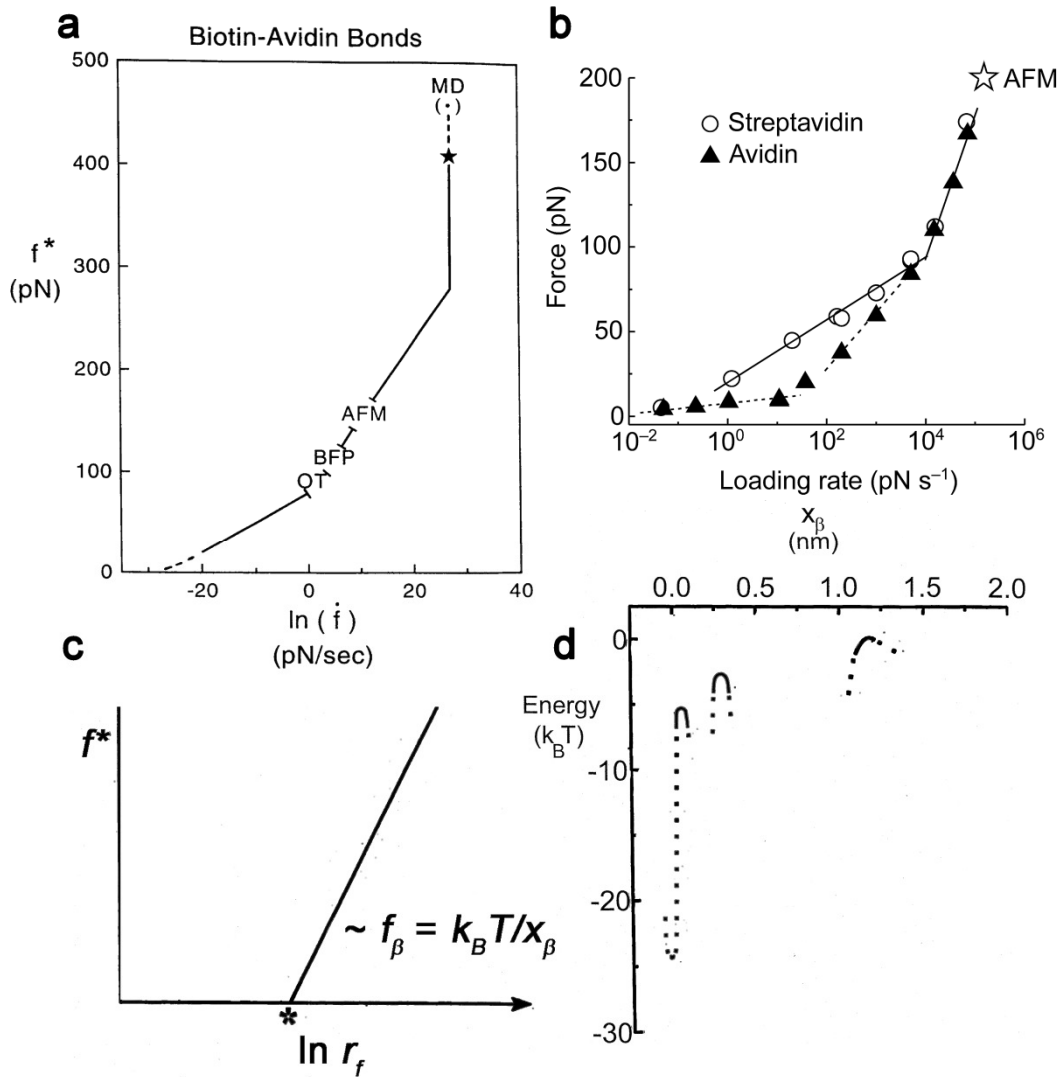


Figure 2- 19. (a) Theoretical loading rate-dependent most probable rupture force f^* of biotin-avidin bonds probed over 12 orders of magnitude using different techniques; AFM for fastest loading rates $\sim 10^4$ - 10^5 pN/s; Biomembrane Force Probe (BFP) for intermediate loading rates ~ 10 - 10^3 pN/s and optical techniques for the slowest loading rates ~ 1 - 10 pN/s; (b) theoretical logarithmic dependence of the most probable rupture force f^* on the applied loading rate r_f in far-from-equilibrium conditions; (c) rupture force versus logarithm of the loading rate for streptavidin- and avidin-biotin dissociation^[55a,98]; (d) overview of the different energy barriers and corresponding characteristic lengths of the transition state x_β , that were determined for biotin-streptavidin interactions. Image was adapted and compiled from refs. 55a, 92, 97 and 99.

If a statistically significant number of single molecule events is collected for several loading rates and accumulated in histograms, the most probable rupture force f^* (for each loading rate) as well as the bond strength and bond lifetime can be directly determined. Under certain conditions (high loading rates, very flexible polymer linker and a significant number of single molecule events) the value of f^* can be determined using Gaussian fitting. In other cases Monte Carlo approaches, using the persistence length and contour length of the polymer linker as additional inputs^[55a,79c,92,98], will provide a more accurate value for f^* .

Evans and co-workers^[98a] used a biomembrane force probe (BFP) with functionalized glass microbeads to study ligand-receptor interactions in aqueous media (see Figure 2- 20). The beads were decorated with hetero bifunctional poly (ethylene glycol) (PEG)-chains to prevent non-specific adhesion. Dilute concentrations of the ligand and receptor pair were used to create the desirable end-functionalized microbeads. At higher loading rates the flexible PEG-linker reduces the likeliness of rebinding after a rupture event to almost zero. Using microbeads, the surface functionalization has to be controlled extremely well to be able to study true single molecule interactions, due to the small curvature.

When functionalized AFM-probes are used as force sensors – with a tip radius in the order of a few to tens of nanometers – the probability of detecting single molecule interactions using very dilute solutions for the final end-functionalization will be significantly improved. Therefore single molecule ligand-receptor interactions are nowadays often studied by AFM-based force spectroscopy, although (slightly) different loading rate regimes can be probed with the different techniques (see Figure 2- 19).

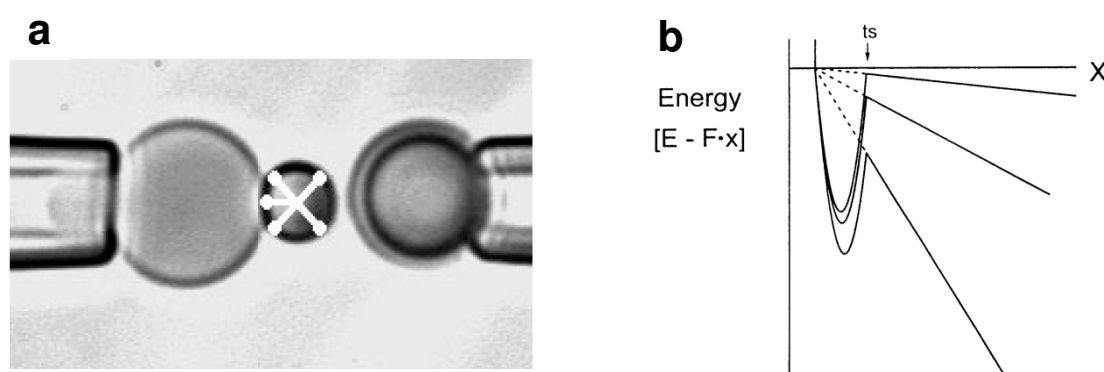


Figure 2- 20. (a) The biomembrane force probe used to study biotin-(strept)avidin and carbohydrate-L selectin receptor-ligand interactions; (b) schematical representation of the reduced transition state energy barrier induced by an applied external force. *Image was adapted and compiled from refs. 55a, 92 and 97.*

The success rate of observing a single molecule event via AFM-based SMFS depends on the surface density on the AFM-probe or sample surface. So a delicate balance has to be found which guarantees a majority of single molecule events. Based on an estimate of Evans^[99] a ~95% confidence level for single molecule detection is achieved if 1 out of 10 force curves results in a specific interaction.

Not only supramolecular dimers but also supramolecular polymers can be studied using AFM-based SMFS. Evans and Williams^[96,100] analysed and described the effect of several geometries of multiple ligand-receptor interactions. In the case of multiple bonds in parallel, the force is partitioned among all the existing bonds whereas for a sheared zipper geometry the force is applied on the first bond and once this bond fails the force propagates to the next bond (see also Figure 2- 21). For multiple bonds in series the force is experienced fully by each bond.

Cooperative failure in short DNA duplexes connected by PEG-linkers was for instance successfully studied using AFM-based force microscopy^[101]. In that case the energy barrier that has to be overcome is given by the sum of individual barrier energies and the energy barrier can be considered as one single macro-bond. As a consequence, the rate of unbinding for parallel cooperative bonds far-from equilibrium does not increase as much with force as for cooperative bonds in series.

If cooperativity does not play a role and bonds are linked in series, each bond experiences the same force and any random rupture event leads to complete failure. As a result the rate of uncooperative failure for N bonds in series is N times faster in far-from equilibrium conditions than the rate for a single bond. Therefore the most probable rupture force f^* decreases with increasing N :

$$f^* = f_\beta [\ln(r_f) - \ln(N)] \quad \text{Equation 2-10}$$

On the other hand the unbinding force for N identical bonds in parallel, is not reduced by $\ln(N)$ for each additional bond, but exactly a factor of N larger compared to a single bond subjected to the same load:

$$f^* \approx N \cdot f_\beta \left[\ln(r_f) - \ln\left(\frac{f^*}{f_\beta}\right) \right] \quad \text{Equation 2-11}$$

Finally some uncooperative failure can be modelled as zipper-like failure. This was for instance demonstrated by DFS of native Ig titin domains by AFM and optical tweezers^[102]. In case of N identical bonds the force that has to be applied for complete failure of the zipper is given by:

$$f^* = f_\beta [\ln(r_f) + \ln(N)]$$

Equation 2-12

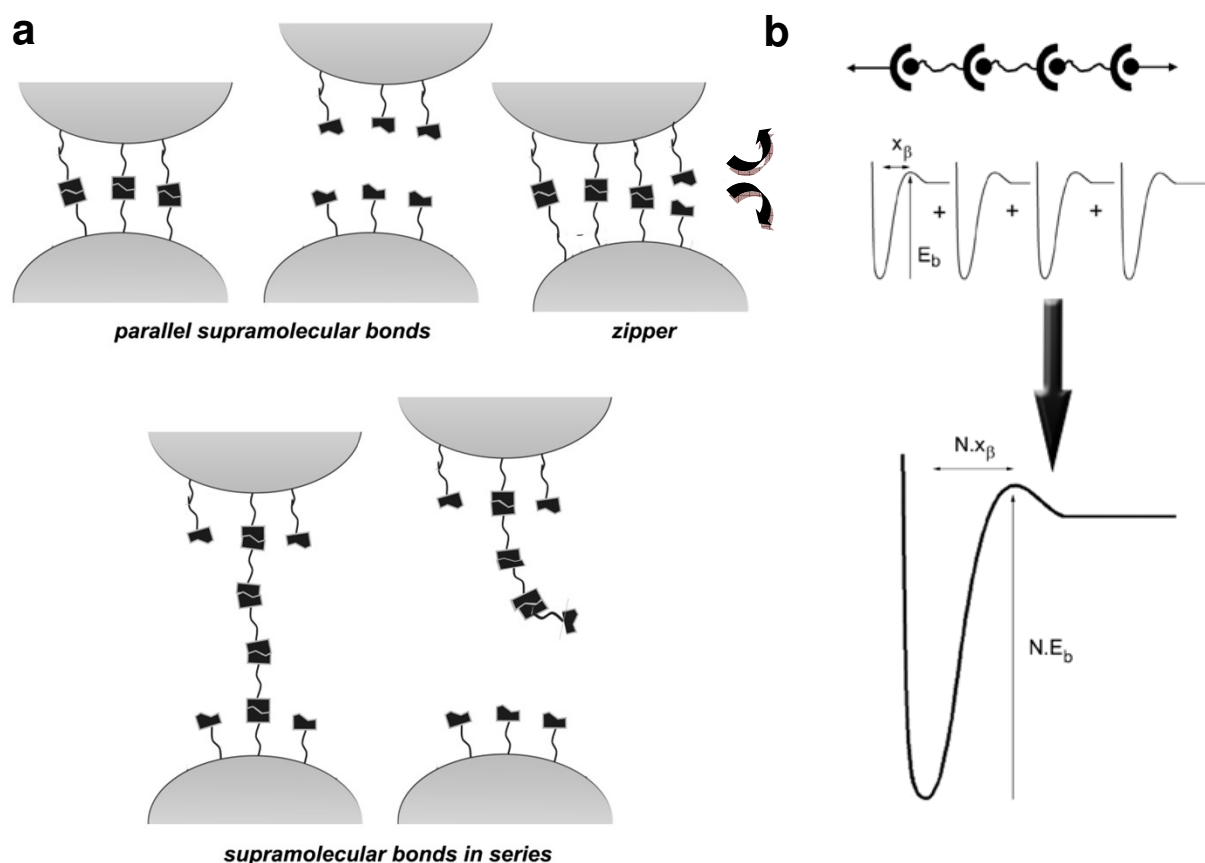


Figure 2- 21. (a) Different geometries of multiple supramolecular bond interactions. Depending on the geometry and cooperative effects there is a distinct dependence of the rupture force and the number of (supramolecular) linkers N ; (b) for cooperative ligand-receptor interactions acting in parallel and in series all bonds can be considered as a single macro-bond. Image was adapted and compiled from ref. 100.

Some final remarks must be made regarding the use of force spectroscopy to study energy barriers and bond strength of ligand-receptor interactions. Using force spectroscopy, the energy landscape that is probed is selected by the applied force - and especially the direction of the force. In case of a reversible interaction that is not manipulated by force, the 3D energy landscape is not distorted and hence other energy pathways might be probed. Furthermore it is

known from DFS studies of ligand-receptor pairs, that the bond lifetime $t_{\text{off}}(0)$ that is determined using Evans-based analysis not necessarily corresponds to data obtained in bulk equilibrium studies. For biological ligand-receptor interactions, such as the carbohydrate-L selectin bond between white blood cells and blood vessel walls, the influence of the lipid and protein conformation in close proximity of the ligand-receptor interaction is still probed in bulk equilibrium conditions.

However at the single molecule level these effects may be highly reduced since the isolated ligand-receptor interaction is studied. Hence, the differences in bond lifetimes that are obtained by both techniques may provide interesting insight into the bonding environment (solvent effect, influence of neighbouring molecules, etc.) of the ligand-receptor interaction itself. Since complexity is reduced significantly in supramolecular dimers and polymers in comparison to various biological systems, it is expected that the measured single molecule data will correlate more closely to data obtained via bulk analysis of the hydrogen-bonded species.

2.8 CONCLUSION AND OUTLOOK

Here we described a different approach to study hydrogen-bonded arrays with high binding constants, namely AFM-based SMFS. This technique can directly yield the bond strength values under different bond loading rates (stretching rates) conditions for single molecules. Using this technique it is now possible to study the hydrogen-bond strength of complementary quadruple hydrogen-bonded arrays in a highly apolar solvent (hexadecane) due to the loading rate-dependent energy landscape of the bond^[51]. Since AFM-based SMFS is performed at very low concentrations ($\sim\mu\text{M}$ and nM) and at far-from equilibrium conditions, solubility issues are circumvented. In addition, not only ensemble averaged bulk data, but also single molecule data can be obtained. Hence the immediate surrounding and inner world of these reversible interactions can be probed which might also reveal the influence of molecular aggregates, *c.q.* molecular solvent clusters. Insight into the influence of the immediate solvent surrounding of single molecule interactions could be of major interest for future design and development of molecular machines, such as the catenanes^[34].

REFERENCES AND NOTES

1. Stryer, L. *Biochemistry* 4th ed. **1995**, W.H. Freeman and Company, New York.
2. (a) Chalfie, M.; Tu, Y.; Euskirchen, G.; Ward, W.W.; Prasher, D.C. *Science* **1994**, 263, 802-805; (b) Moerner, W.E.; Orrit, M. *Science* **1999**, 283, 1670-1676; (c) Lippencott-Schwartz, J.; Snapp, E.; Kenworthy, A. *Nat. Rev.* **2001**, 2, 445-456; (d) Tozzini, V. *Accounts Chem. Res.* **2010**, 4, 220-230.
3. Lodish, H.; Baltimore, D.; Berk, A.; Zipursky, S.L.; Matsudaira, P.; Darnell, J. *Molecular Cell Biology* 3rd ed. **1995**, Scientific American Books, New York.
4. Pozzo, T.; Linares Pasten, J.; Karlsson, E.N.; Logan, D.T. *J. Mol. Biol.* **2010**, 397, 724-739.
5. Matthews, C.A.; Shaw, J.E.; Hooper, J.A.; Young, I.G.; Crouch, M.F.; Campbell, H.D. *J. Neurochem.* **2007**, 100, 693-707.
6. Ebisawa, T.; Yamamura, A.; Kameda, Y.; Hayakawa, K.; Nagata, K.; Tanokura, M. *Acta Cryst.* **2010**, 66, 485-489
7. Pletneva, N.V.; Pletnev, V.Z.; Lukyanov, K.A.; Gurskaya, N.G.; Goryacheva, E.A.; Martynov, V.I.; Wlodawer, A.; Dauter, Z.; Pletnev, S. *J. Biol. Chem.* **2010**, 285, 15978-15984.
8. Israelachvilli, J.N. *Intermolecular and surface forces*, 3rd ed. **2011**, Academic Press (Elsevier), San Diego, United States of America.
9. Feynman, R.P. *Phys. Rev.* **1939**, 56, 340-343.
10. Steiner, T. *J. Chem. Soc. Chem. Commun.* **1994**, 2341-2342.
11. Desiraju, G.R. *J. Chem. Soc. Chem. Commun.* **1989**, 179-180.
12. Pedireddi, V.R.; Desiraju, G.R. *J. Chem. Soc. Chem. Commun.* **1992**, 988-990.
13. (a) Muley, L.; Baum, B.; Smolinski, M.; Freindorf, M.; Heine, A.; Klebe, G.; Hangauer, D.G. *J. Med. Chem.* **2010**, 53, 2126-2135; (b) Hunter, C.A.; Anderson, H.L. *Angew. Chem. Int. Ed.* **2009**, 48, 7488-7499; (c) Hirschberg, J.H.K.K.; Brunsveld, L.; Ramzi, A.; Vekemans, J.A.J.M.; Sijbesma, R.P.; Meijer, E.W. *Nature* **2000**, 407, 167-170; (d) Jeffrey, G.A.; Saenger, W. *Hydrogen Bonding in Biological Structures*, Springer-Verlag, New York, **1991**.
14. (a) Xu, Z.; Mei, Y.; Dian, L.; Zhang, D. *Chem. Phys. Lett.* **2010**, 495, 151-154; (b) Pal, S.; Manna, A.K.; Pati, S.W. *J. Chem. Phys.* **2008**, 129, 204301; (c) Rablen, P.R.; Lockman, J.W.; Jorgensen, W.L. *J. Phys. Chem. A* **1998**, 102, 3782-3797; (d) Koch, U.;

- Popelier, P.L.A. *J. Phys. Chem.* **1995**, *99*, 9747-9754; (e) Carroll, M.T.; Bader, R.F.W. *Mol. Phys.* **1988**, *65*, 695-722.
15. (a) Beijer, F.H.; Kooijman, H.; Spek, A.L.; Sijbesma, R.P.; Meijer, E.W. *Angew. Chem. Int. Ed.* **1998**, *37*, 75-78; (b) Beijer, F.H.; Sijbesma, R.P.; Kooijman, H.; Spek, A.L.; Meijer, E.W. *J. Am. Chem. Soc.* **1998** *120*, 6761-6769.
16. Ligthart, G.B.W.L.; Guo, D.; Spek, A.L.; Kooijman, H.; Zuilhof, H.; Sijbesma, R.P. *J. Org. Chem.* **2008**, *73*, 111-117.
17. (a) Bergman, S.D.; Wudl, F. *J. Mater. Chem.* **2008**, *18*, 41-62; (b) Brunsveld, L.; Folmer, B.J.B.; Meijer, E.W.; Sijbesma, R.P. *Chem. Rev.* **2001**, *101*, 4071-4097; (c) Armstrong, G.; Buggy, M. *J. Mater. Sci.* **2005**, *40*, 547-559; (d) Lehn, J.M. *Polym. Int.* **2002**, *51*, 825-839; (e) Sijbesma, R.P.; Beijer, F.H.; Brunsveld, L.; Folmer, B.J.B.; Hirschberg, J.H.K.K.; Lange, R.F.M.; Lowe, J.K.L.; Meijer, E.W. *Science* **1997**, *278*, 1601-1604.
18. (a) Besenius, P.; Portale, G.; Bomans, P.H.H.; Janssen, H.M.; Palmans, A.R.A.; Meijer, E.W. *Proc. Natl. Acad. Soc. U.S.A.* **2010**, *107*, 17888-17893; (b) Smulders, M.M.J.; Schenning, A.P.H.J.; Meijer, E.W. *J. Am. Chem. Soc.* **2008**, *130*, 606-611.
19. (a) Brunsveld, L.; Folmer, B.J.B.; Meijer, E.W.; Sijbesma, R.P. *Chem. Rev.* **2001**, *101*, 4071-4097; (b) Folmer, B.J.B.; Sijbesma, R.P.; Versteegen, R.M.; Van der Rijt, J.A.J.; Meijer, E.W. *Adv. Mater.* **2000**, *12*, 874-878.
20. Montarnal, D.; Tournilhac, F.; Hidalgo, M.; Couturier, J.-L.; Leibler, L. *J. Am. Chem. Soc.* **2009**, *131*, 7966-7968.
21. (a) Smulders, M.M.J.; Filot, I.A.W.; Leenders, J.M.A.; Van der Schoot, P.; Palmans, A.R.A.; Schenning, A.P.H.J.; Meijer, E.W. *J. Am. Chem. Soc.* **2010**, *132*, 611-619; (b) Palmans, A.R.A.; Meijer, E.W. *Angew. Chem. Int. Ed.* **2007**, *46*, 8948-8968.
22. Mes, T.; Smulders, M.M.J.; Palmans, A.R.A.; Meijer, E.W. *Macromolecules* **2010**, *43*, 1981-1991.
23. Sartorius, J.; Schneider, H.-J. *Chem. Eur. J.* **1996**, *2*, 1446-1452.
24. Djurdjevic, S.; Leigh, D.A.; McNab, H.; Parsons, S.; Teobaldi, G.; Zerbetto, F. *J. Am. Chem. Soc.* **2007**, *129*, 476-477.
25. (a) Sandier, A.; Brown, W.; Mays, H. *Langmuir* **2000**, *16*, 1634-1642; (b) Li, G.; McGown, L.B.; *Science* **1994**, *264*, 249-251.
26. (a) Van Hameren, R.; Van Buul, A.M.; Castriciano, M.A.; Villari, V.; Micali, N.; Schön, P.; Speller, S.; Monsu Scolaro, L.; Rowan, A.E.; Elemans, J.A.A.W.; Nolte,

- R.J.M. *Nano Lett.* **2008**, *8*, 253-259; (b) De Witte, P.A.J.; Castriciano, M.; Cornelissen, J.J.L.M.; Monsu Scolaro, L.; Nolte, R.J.M.; Rowan, A.E.; *Chem. Eur. J.* **2003**, *9*, 1775-1781; (c) Michelsen, U.; Hunter, C.A. *Angew. Chem. Int. Ed.* **2000**, *29*, 764-767.
27. (a) Schwartz, G.; Sievers, T.K.; Bodenthin, Y.; Hasslauer, I.; Geue, T.; Koetz, J.; Kurth, D.G. *J. Mater. Chem.* **2010**, *20*, 4142-4148; (b) Ott, C.; Kranenburg, J.M.; Guerrero-Sanchez, C.; Hoepfener, S.; Wouters, D.; Schubert, U.S. *Macromolecules* **2009**, *42*, 2177-2183; (c) Beck, J.B.; Rowan, S.J. *J. Am. Chem. Soc.* **2003**, *125*, 13922-12923.
 28. (a) Lehn, J.-M. *Makromol. Chem. Macromol. Symp.* **1993**, *69*, 1-17; (b) Fouquey, C.; Lehn, J.-M.; Levelut, A.-M. *Adv. Mater.* **1990**, *2*, 254-257.
 29. (a) Castellano, R.K.; Nuckolls, C.; Eichhorn, S.H.; Wood, M.R.; Lovinger, A.J.; Rebek, J. Jr. *J. Am. Chem. Soc.* **1998**, *38*, 2603-2606; (b) Castellano, R.K.; Rudkevich, D.M.; Rebek, J. Jr. *Proc. Natl. Acad. Sci. U.S.A.* **1997**, *94*, 7132-7137.
 30. (a) Kuykendall, D.W.; Anderson, C.A.; Zimmerman, S.C. *Org. Lett.* **2009**, *11*, 61-64; (b) Kitova, E.N.; Bundle, D.R.; Klassen, J.S. *Angew. Chem. Int. Ed.* **2004**, *43*, 4183-4186; (c) Ward, W.H.J.; Holdgate, G.A. *Prog. Med. Chem.* **2001**, *38*, 309-376.
 31. (a) Schalley, C.A. *Analytical Methods in Supramolecular Chemistry*, Wiley-VCH Verlag, Weinheim, **2007**; (b) Rüdiger, V.; Schneider, H.-J. *Chem. Eur. J.* **2000**, *6*, 3771-3776; (c) Williams, D.H.; Maguire, A.J.; Tsuzuki, W.; Westwell, M.S. *Science* **1998**, *280*, 711-714.
 32. Folmer, B.J.B.; Sijbesma, R.P.; Kooijman, H.; Spek, A.H.; Meijer, E.W. *J. Am. Chem. Soc.* **1999**, *121*, 9001-9007.
 33. Söntjens, S.H.M.; Sijbesma, R.P.; Van Genderen, M.H.P.; Meijer, E.W. *J. Am. Chem. Soc.* **2000**, *122*, 7487-7493.
 34. Abrahams, M.H.; Platts, J.A. *J. Org. Chem.* **2001**, *66*, 3484-3491.
 35. (a) Bohm, H.-J. *J. Comput.-Aided Mol. Des.* **1994**, *8*, 243-256; (b) Page, M.I.; Jencks, W.P. *Proc. Natl. Acad. Sci. U.S.A.* **1971**, *68*, 1678-1683.
 36. Hunter, C.A. *Angew. Chem. Int. Ed.* **2004**, *43*, 5310-5324.
 37. (a) Leigh, D.A.; Wong, J.K.Y.; Dehez, F.; Zerbetto, F. *Nature* **2003**, *424*, 174-179; (b) Leigh, D.A.; Murphy, A. Smart, J.P. Deleuze, M.S.; Zerbetto, F. *J. Am. Chem. Soc.* **1998**, *120*, 6458-6467.
 38. (a) Veldhuis, G.; Segers-Nolten, I.; Ferlemann, E.; Subramaniam, V. *ChemBioChem* **2009**, *10*, 436-439; (b) Joo, C.; Balci, H.; Ishitsuka, Y.; Buranachai, C.; Ha, T. *Annu.*

- Rev. Biochem.* **2008**, 77, 51-76; (c) Moerner, W.E.; Orrit, M. *Science* **1999**, 283, 1670-1676; (d) Femino, A.M.; Fay, F.S.; Fogarty, K.; Singer, R.H. *Science* **1998**, 280, 585-590; (e) Funatsu, T.; Harada, Y.; Tokunaga, M.; Saito, K.; Yanagida, T. *Nature* **1995**, 374, 555-559.
39. (a) Yodh, J.G.; Schlierf, M.; Ha, T. *Q. Rev. Biophys.* **2010**, 43, 185-217; (b) Gump, H.; Stahl, S.W.; Strackharn, M.; Puchner, E.M.; Gaub, H.E. *Rev. Sci. Instrum.* **2009**, 80, 063704; (c) Tisler, J.; Balasubramanian, G.; Naydenov, B.; Koselov, R.; Grotz, B.; Reuter, R.; Boudou, J.-P.; Curmi, P.A.; Sennour, M.; Thorel, A.; Börsch, M.; Aulenbacher, K.; Erdmann, R.; Hemmer, P.R.; Jelezko, F.; Wrachtrup, J. *ACS Nano* **2009**, 3, 1959-1965; (d) Tarsa, B.P.; Brau, R.R.; Ferrer, J.M.; Freyzon, Y.; Matsudaira, P.; Lang, M.J. *Angew. Chem. Int. Ed.* **2007**, 46, 1999-2001; (e) Van Dijk, M.A.; Kapitein, L.C.; Van Mameren, J.; Schmidt, C.F.; Peterman, E.J.G. *J. Phys. Chem. B* **2004**, 108, 6479-6484; (f) Bianco, P.R.; Brewer, L.R.; Corzett, M.; Balhorn, R.; Yeh, Y.; Kowalczykowski, S.C.; Baskin, R.J. *Nature* **2001**, 409, 374-378; (g) Ha, T. *Single. Mol.* **2001**, 4, 283-284.
40. (a) Puchner, E.M.; Gaub, H.E. *Curr. Opin. Struct. Biol.* **2009**, 19, 605-614; (b) Hugel, T.; Seitz, M. *Macromol. Rapid. Commun.* **2001**, 22, 989-1016; (c) Zlatanova, J.; Lindsay, S.M.; Leuba, S.H. *Prog. Biophys. Mol. Biol.* **2000**, 74, 37-61; (d) Marszalek, P.E.; Lu, H.; Li, H.; Carrion-Vazquez, M.; Oberhauser, A.F.; Schulten, K.; Fernandez, J.M.; *Nature* **1999**, 402, 100-103; (e) Viani, M.B.; Schaffer, T.E.; Chand, A.; Rief, M.; Gaub, H.E.; Hansma, H.K. *J. Appl. Phys.* **1999**, 86, 2258-2262; (f) Binnig, G.; Quate, C.F.; Gerber, C. *Phys. Rev. Lett.* **1986**, 56, 930.
41. (a) Ayithey, P.N.; Walker, J.S.; Rice, J.J.; De Tombe, P.P. *Pflugers Arch.* **2009**, 457, 1415-1422; (b) Ruff, C.; Furch, M.; Brenner, B.; Manstein, D.J.; Meyhöfer, E. *Nat. Struct. Biol.* **2001**, 8, 226-229; (c) Kellermayer, M.S.Z.; Granzier, H.I.; *Biochem. Biophys. Res. Commun.* **1996**, 221, 491-497; (d) Kishino, A.; Yanagida, T. *Nature* **1988**, 334, 74-76.
42. (a) Gutiérrez-Medina, B.; Andreasson, J.O.L.; Greenleaf, W.J.; LaPorta, A.; Block, S.M. *Method. Enzymol.* **2010**, 475, 377-404; (b) Kellermayer M.S.Z.; Smith, S.B.; Granzier, H.I.; Bustamante, C. *Science* **1997**, 276, 1112-1116; (c) Ashkin A.; Schutze, K.; Dziedzic, J.M.; Euteneuer U.; Schliwa M. *Nature* **1990**, 348, 346-348; (d) Howard, J.; Hudspeth, A.J.; Vale, R.D. *Nature* **1989**, 342, 154-158.

43. (a) Manosas, M.; Meglio, A.; Spiering, M.M.; Ding, F.; Benkovic, S.J.; Barre, F.X.; Saleh O.A.; Alleman, J.F.; Bensimon, D.; Croquette, V. *Method. Enzymol.* **2010**, *475*, 297-320; (b) Celedon, A.; Nodelman, I.M.; Wildt, B.; Dewan, R.; Searson, P.; Wirtz, D.; Bowman, G.D.; Sun, S.X. *Nature Lett.* **2009**, *9*, 1720-1725; (c) Kim, K.; Saleh, O.A. *Nucleic Acids Res.* **2009**, *37*, e136; (d) Strick, T.R.; Croquette, V.; Bensimon, D. *Nature* **2000**, *404*, 901-904; (e) Smith, S.B.; Finzi, L.; Bustamante, C. *Science* **1992**, *258*, 1122-1126.
44. (a) Bustamante, C. *Annu. Rev. Biochem.* **2008**, *77*, 45-50; (b) Bustamante, C.; Macosko, J.C.; Wuite, G.J.L. *Nat. Rev. Mol. Cell Biol.* **2000**, *1*, 130-136.
45. Clausen-Schaumann, H.; Seitz, M.; Krautbauer, R. Gaub, H.E. *Curr. Opin. Chem. Biol.* **2000**, *4*, 524-530.
46. (a) Chaurasiya, K.R.; Paramanathan, T.; McCauley, M.J.; Williams, M.C. *Phys. Life Rev.* **2010**, *7*, 299-341; (b) Michaelis, J.; Muschielok, A.; Andrecka, J.; Kügel, W.; Moffitt, J.R. *Phys. Life Rev.* **2009**, *6*, 250-266; (c) Bustamante, C.; Bryant, Z.; Smith, S.B. *Nature* **2003**, *421*, 423-427; (d) Krautbauer, R.; Clausen-Schaumann, H.; Gaub, H.E. *Angew. Chem. Int. Ed.* **2000**, *39*, 3912-3915; (e) Lee, G.U.; Chrisey, L.A.; Colton, R.J. *Science* **1994**, *266*, 771-773.
47. (a) Jollymore, A.; Li, H. *J. Mol. Biol.* **2010**, *402*, 610-617; (b) Oberhauser, A.F.; Carrion-Vazquez, M. *J. Biol. Chem.* **2008**, *293*, 6617-6621; (c) Li, H.; Linke, W.A.; Oberhauser, A.F.; Carrion-Vazquez, M.; Kerkvliet, J.G.; Lu, H.; Marszalek, P.E.; Fernandez, J.M. *Nature* **2002**, *418*, 998-1002; (d) Rief, M.; Pascual, J.; Saraste, M.; Gaub, H.E. *J. Mol. Biol.* **1999**, *286*, 553-561; (e) Mitsui, K.; Hara, M.; Ikai, A. *FEBS Lett.* **1996**, *385*, 29-33.
48. (a) Anselmetti, D.; Bartels, F.W.; Becker, A.; Decker, B.; Eckel, R.; McIntosh, M.; Mattay, J.; Plattner, P.; Ros, R.; Schäfer, C.; Sewald, N. *Langmuir* **2008**, *24*, 1365-1370; (b) Zou, S.; Schönherr, H.; Vancso, G.J. in *Scanning probe microscopy beyond imaging: Manipulation of Molecules and Nanostructures* (Ed. Samori, P.) Wiley-VCH, Weinheim, **2006**, p. 315-353; (c) Eckel, R.; Ros, R.; Decker, B.; Mattay, J.; Anselmetti, D. *Angew. Chem. Int. Ed.* **2005**, *44*, 484-488; (d) Auletta, T.; De Jong, M.R.; Mulder, A.; Van Veggel, F.C.J.M.; Huskens, J.; Reinhoudt, D.N.; Zou, S.; Zapotoczny, S.; Schönherr, H.; Vancso, G.J. *J. Am. Chem. Soc.* **2004**, *126*, 1577-1584; (e) Schönherr, H.; Beulen, M.W.J.; Bügler, J.; Huskens, J.; Van Veggel, F.C.J.M.; Reinhoudt, D.N.; Vancso, G.J. *J. Am. Chem. Soc.* **2000**, *122*, 4963-4967.

49. (a) Chemla, Y.R. *Phys. Chem. Chem. Phys.* **2010**, *12*, 3080-3095; (b) Muneyuki, E.; Watanabe-Nakayama, T.; Suzuki, T.; Yoshida, M.; Nishizaka, T.; Noji, H. *Biophys. J.* **2007**, *92*, 1806-1812; (c) Verbrugge, S.; Kapitein, L.C.; Peterman, E.J.G. *Biophys. J.* **2007**, *92*, 2536-2545; (d) Keller, D.; Bustamante, C.; *Biophys. J.* **2000**, *78*, 541-556.
50. (a) Yu, Y.; Zhang, Y.; Jiang, Z.; Zhang, X. *Langmuir* **2009**, *25*, 10002-10006; (b) Fugmann, S.; Sokolov, I.M. *EPL* **2009**, *86*, 28001; (c) Zhang, X.; Liu, C. Shi, W. *Physical Properties of Polymers Handbook Chapter 30: Force Spectroscopy of Polymers: Beyond Single Chain Mechanics*; Springer, New York, **2007**; (d) Strick, T.R.; Dessinges, M.-N.; Charvin, G.; Dekker, N.H.; Alleman, J.-F.; Bensimon, D.; Croquette, V. *Rep. Prog. Phys.* **2003**, *66*, 1-45; (e) Janshoff, A.; Neitzert, M.; Oberdörfer, Y.; Fuchs, H. *Angew. Chem. Int. Ed.* **2000**, *39*, 3212-3237.
51. (a) Embrechts, A.; Schönherr, H.; Vancso, G.J. *J. Phys. Chem. B* **2008**, *112*, 7359-7362; (b) Zou, S.; Schönherr, H.; Vancso, G.J. *J. Am. Chem. Soc.* **2005**, *127*, 11230-11231; (c) Zou, S.; Schönherr, H.; Vancso, G.J. *Angew. Chem., Int. Ed.* **2005**, *44*, 956-959.
52. (a) Li, J.; Fernandez, J.M.; Berne, B.J. *Proc. Nat. Acad. Sci. U.S.A.* **2010**, *107*, 19284-19289; (b) Rama Koti Ainavarapu, S.; Wiita, A.P.; Dougan, L.; Uggerud, E.; Fernandez, J.M. *J. Am. Chem. Soc.* **2008**, *130*, 6479-6487; (c) Oberhauser, A.F.; Hansma, P.K.; Carrion-Vazques, M. Fernandez, J.M. *Proc. Nat. Acad. Sci. U.S.A.* **2001**, *98*, 468-472.
53. Kienberger, F.; Ebner, A.; Gruber, H.J.; Hinterdorfer, P. *Acc. Chem. Res.* **2006**, *39*, 26-36.
54. Cordes, T.; Strackharn, M.; Stahl, S.W.; Summeren, W.; Steinhauer, C.; Forthmann, C.; Puchner, E.M.; Vogelsang, J.; Gaub, H.E.; Tinnefeld, P. *Nano Lett.* **2010**, *10*, 645-651.
55. (a) Moy, V.T.; Florin, E.L.; Gaub, H.E. *Science* **1994**, *266*, 257-259; (b) Lee, G.U.; Kidwell, D.A.; Colton, R.J. *Langmuir* **1994**, *10*, 354-357.
56. Bell, G.I. *Science* **1978**, *200*, 618-627.
57. Evans, E.; Ritchie, K. in *Scanning Probe Microscopies and Molecular Materials* (Eds. Rabe, J.; Gaub, H.; Hansma, P.K.), **1994**, Kluwer Publ., Amsterdam.
58. Geisler, M.; Netz, R.R.; Hugel, T. *Angew. Chem. Int. Ed.* **2010**, *49*, 4730-4733.
59. (a) Gianotti, G.I.; Vancso, G.J. *ChemPhysChem* **2007**, *8*, 2290-2307; (b) Lui, C.J.; Shi, W.Q.; Cui, S.X.; Wang, Z.Q.; Zhang, X. *Curr. Opin. Solid State Mater. Sci.* **2005**, *9*, 140-148.

60. (a) Puchner, E.M.; Gaub, H.E. *Curr. Opin. Struc. Biol.* **2009**, *19*, 605-614; (b) Butt, H.-J.; Capella, B.; Kappl, M. *Surf. Sci. Rep.* **2005**, *59*, 1-152; (c) Zlatanova, J.; Lindsay, S.M.; Leuba, S.H. *Prog. Biophys. Mol. Biol.* **2000**, *74*, 37-61; (d) Ortiz, C.; Hadziioannou, G. *Macromolecules* **1999**, *32*, 780-787; (e) Bemis, J.E.; Akhremitchev, B.B.; Walker, G.C. *Langmuir* **1999**, *15*, 2799-2805.
61. (a) Drew, M.E.; Chworos, A.; Oroudjev, E.; Hansma, H.; Yamakoshi, Y. *Langmuir* **2010**, *26*, 7117-7125; (b) Ebner, A.; Wildling, L.; Zhu, R.; Rankl, C.; Haselgrübler, T.; Hinterdorfer, P.; Gruber, H.J. *Top. Curr. Chem.* **2008**, *285*, 29-76; (c) Seitz, M.; Friedsam C.; Jostl, W.; Hugel, T.; Gaub, H.E. *ChemPhysChem* **2003**, *4*, 986-990; (d) Grandbois, M. Beyer, M.; Rief, M.; Clausen-Schaumann, H.; Gaub, H.E. *Science* **1999**, *283*, 1727-1730; (e) Hinterdorfer, P.; Baumgartner, W.; Gruber, H.J.; Schilcher, K.; Schindler, H. *Proc. Natl. Acad. Sci. U.S.A.* **1996**, *93*, 3477-3481.
62. Cappella, B.; Baschieri, P.; Frediani, C.; Miccoli, P.; Ascoli, C. *IEEE Eng. Med. Biol.* **1997**, *16*, 58-65.
63. (a) Chen, B.-Y.; Yeh, M.-K.; Tai, N.-H. *Anal. Chem.* **2007**, *79*, 1333-1338; (b) Poggi, M.A.; McFarland, A.W.; Colton, J.S.; Bottomley, L.A. *Anal. Chem.* **2005**, *77*, 1192-1195; (c) Hazel, J.L.; Tsukruk, V.V. *Thin Solid Films* **1999**, *339*, 249-257; (d) Hazel, J.L.; Tsukruk, V.V. *J. Tribol.* **1998**, *120*, 814-819; (e) Neumeister, J.M.; Ducker, W.A. *Rev. Sci. Instrum.* **1994**, *65*, 2527-2531.
64. (a) Gates, R.S.; Reitsma, M.G.; *Rev. Sci. Instrum.* **2007**, *78*, 086101; (b) Holbery, J.D.; Eden, V.L.; Sarikaya, M.; Fischer, R.M. *Rev. Sci. Instrum.* **2000**, *71*, 3769-3776; (c) Gibson, C.T.; Watson, G.S.; Myhra, S. *Nanotechnology* **1996**, *7*, 259-262; (d) Senden, T.J.; Ducker, W.A. *Langmuir* **1994**, *10*, 1003-1004; (e) Butt, H.-J.; Siedle, P.; Seifert, K.; Seeger, T.; Fendler, K.; Bamberg, E.; Goldie, K.; Engel, A. *J. Microscopy* **1993**, *169*, 75-84.
65. (a) Golovko, D.S.; Haschke, T.; Weichert, W.; Bonaccorso, E. *Rev. Sci. Instrum.* **2007**, *78*, 043705; (b) Maeda, N.; Senden, T.J. *Langmuir* **2000**, *16*, 9282-9286; (c) Walters, D.A.; Cleveland, J.P.; Thomson, N.H.; Hansma, P.K.; Wendman, M.A.; Gurley, G.; Elings, V. *Rev. Sci. Instrum.* **1996**, *67*, 3583-3590; (d) Sader, J.E. *Rev. Sci. Instrum.* **1995**, *66*, 4583-4587; (e) Cleveland, J.P.; Manne, S.; Bocek, D.; Hansma, P.K. *Rev. Sci. Instrum.* **1993**, *64*, 403-405.
66. (a) Su, C.; Fischl, R.; Shi, J.; Belikov, S. *J. Nanosci. Nanotechno.* **2009**, *9*, 736-740; (b) Schäffer, T. *Nanotechnology* **2005**, *16*, 664-670; (c) Sader, J.E. *Appl. Phys.* **1998**, *84*,

- 64-76; (d) Butt, H.-J.; Jaschke, M. *Nanotechnology* **1995**, *6*, 1-7; (e) Hutter, J.L.; Bechhoefer, J. *Rev. Sci. Instrum.* **1993**, *64*, 1868-1873.
67. (a) Palacio, M.L.B.; Bhushan, B. *Crit. Rev. Solid State* **2010**, *35*, 73-104; (b) Hodges, C.S. *Adv. Colloid Interface Sci.* **2002**, *99*, 13-75.
68. (a) Pirzer, T.; Hugel, T. *Rev. Sci. Instrum.* **2009**, *80*, 035110; (b) Hutter, J.F. *Langmuir* **2005**, *21*, 2630-2632; (c) Proksch, R.; Schäffer, T.E.; Cleveland, J.P.; Callahan, R.C.; Viani, M.B. *Nanotechnology* **2004**, *15*, 1344-1350.
69. (a) Ohler, B.; *Rev. Sci. Instrum.* **2007**, *78*, 063701; (b) Ohler, B. Veeco Application Note AN94, Rev. A0 **2007**.
70. Ratto, T.V.; Rudd, R.E.; Langry, K.C.; Balhorn, R.L.; McElfresh, M.W. *Langmuir* **2006**, *22*, 1749-1757.
71. (a) Ray, C.; Guo, S.; Brown, J.; Li, N.; Akhremitchev, B.B. *Langmuir* **2010**, *26*, 11951-11957; (b) Friddle, R.W.; Podsiadlo, P.; Artyukhin, A.B.; Noy, A.; *J. Phys. Chem. C* **2008**, *112*, 4986-4990; (c) Hinterdorfer, P.; Baumgartner, W.; Gruber, H.J.; Schilcher, K.; Schindler, H. *Proc. Natl. Acad. Sci. U.S.A.* **1996**, *93*, 3477-3481;
72. (a) Press, W.H.; Teukosky, S.A.; Vetterling, W.T.; Flannery, B.P. *Numerical recipes in C*, Cambridge University Press, Cambridge, 2nd ed. **1992**; (b) Marquardt, D.W. *J. Soc. Ind. Appl. Math.* **1963**, *11*, 431-441; (c) Levenberg, K. *Q. Appl. Math.* **1944**, *2*, 164-168.
73. (a) Marko, J.F.; Siggia, E.D. *Macromolecules* **1995**, *28*, 8759-8770; (b) Bustamante, C.; Marko, J.F.; Siggia, E.D.; Smith, S. *Science* **1994**, *265*, 1599-1600; (c) Kratky, O.; Porod, G. *Recl. Trav. Chim.* **1949**, *68*, 1106-1122; (d) Flory, P.J. *Statistical mechanics of Chain Molecules*, Hanser, München, **1898**.
74. (a) Smith, S.B.; Finzi, L.; Bustamante, C. *Science* **1992**, *258*, 1122-1126; (b) Büche, F. *Physical Properties of Polymers*, Interscience, New York, **1962**.
75. Wang, M.D.; Yin, H.; Landick, R.; Gelles, J.; Block, S.M. *Biophys. J.* **1997**, *72*, 1335-1346.
76. Odijk, T. *Macromolecules* **1995**, *28*, 7016-7018.
77. Smith, S.B.; Cui, Y.; Bustamante, C. *Science* **1996**, *271*, 795-799.
78. Murphy, M.C.; Rasnik, I.; Cheng, W.; Lohman, T.M.; Ha, T. *Biophys. J.* **2004**, *86*, 2530-2537.
79. (a) Sharma, D.; Perisic, O.; Peng, Q.; Cao, Y.; Lam, C.; Lu, H.; Li, H. *Proc. Natl. Acad. Sci. U.S.A.* **2007**, *104*, 9278-9283; (b) Oroudjev, E.; Soares, J.; Arcidiacono, S.; Thompson, J.B.; Fossey, S.A. Hansma, H.G. *Proc. Natl. Acad. Sci. U.S.A.* **2002**, *99*,

- 6460-6465; (c) Rief, M.; Pascual, J.; Saraste, M.; Gaub, H.E. *J. Mol. Biol.* **1999**, 286, 553-561; (d) Rief, M.; Gautel, M.; Oesterhelt, F.; Fernandez, J.M.; Gaub, H.E. *Science* **1997**, 276, 1109-1112.
80. (a) Al-Maawali, S.; Bemis, J.E.; Akhremitchev, B.B.; Leecharoen, R.; Janesko, B.G.; Walker, G.C. *J. Adhes.* **2005**, 81, 999-1016; (b) Sakai, Y.; Ikehara, T.; Nishi, T. *Appl. Phys. Lett.* **2002**, 81, 724-726.
 81. Garnier, L.; Gauthier-Manuel, B.; Van der Vegte, E.W.; Snijders, J.; Hadziioannou, G. *J. Chem. Phys.* **2000**, 113, 2497-2503.
 82. (a) Al-Maawali, S.; Bemis, J.E.; Akhremitchev, B.B.; Liu, H.Y.; Walker, G.C. *J. Phys. Chem. B* **2001**, 105, 3965-3971; (b) Senden, T.J.; Di Meglio, J.-M.; Auroy, P. *Eur. Phys. J. B* **1998**, 3, 211-216.
 83. Haupt, B.J.; Senden, T.J.; Sevick, E.M. *Langmuir* **2002**, 18, 2174-2182.
 84. (a) Husale, S.; Grange, W.; Karle, M.; Bürgi, S.; Hegner, M. *Nucleic Acid Research* **2008**, 36, 1443-1449; (b) Punkkinen, O.; Hansen, P.L.; Miao, L.; Vattulainen, I. *Biophys. J.* **2005**, 89, 967-978; (c) Hugel, T.; Holland, N.B.; Cattani, A.; Moroder, L.; Seitz, M.; Gaub, H.E. *Science* **2002**, 296, 1103-1106; (c) Kienberger, F.; Pastushenko, V. Ph.; Kada, G.; Gruber, H.J.; Riener, C.; Schindler, H.; Hinterdorfer, P. *Single Mol.* **2000**, 1, 123-128; (d) Bouchiat, C.; Wang, M.D.; Allemand, J.-F.; Strick, T.; Block, S.M.; Croquette, V. *Biophys J.* **1999**, 76, 409-413.
 85. Lee, G.U.; Chrisey, L.A.; Colton, R.J. *Science* **1994**, 266, 771-773.
 86. Ortiz, C.; Hadziioannou, G. *Macromolecules* **1999**, 32, 780-787.
 87. (a) Cui, S.; Yu, Y.; Lin, Z. *Polymer* **2009**, 50, 930-935; (b) Schwaderer, P.; Funk, E.; Achenbach, F.; Weis, J.; Bräuchle, C.; Michaelis, J. *Langmuir* **2008**, 24, 1343-1349.
 88. (a) Zhang, W.K.; Zou, S.; Wang, C.; Zhang, X. *J. Phys. Chem. B* **2000**, 104, 10258-10264; (b) Oesterhelt, F.; Rief, M.; Gaub, H.E. *New. J. Phys.* **1999**, 1, 6; (c) Rief, M.; Oesterhelt, F.; Heymann, B.; Gaub, H.E. *Science* **1997**, 275, 1295-1297; (d) Marszalek, P.; Oberhauser, A.F.; Pang, Y.P.; Fernandez, J.M. *Nature* **1998**, 396, 661-664; (e) Kikuchi, H.; Yokoyama, N.; Kajiyama, T. *Chem Lett.* **1997**, 11, 1107-1108.
 89. Storm, C.; Nelson, P.C. *Phys. Rev. E* **2003**, 67, 051906.
 90. Chang, Z.; Wang, P.; Zheng, Y.-Y. *Commun. Theort. Phys.* **2008**, 49, 525-528.
 91. (a) Li, I.T.S.; Walker, G.C. *J. Am. Chem. Soc.* **2010**, 132, 6530-6540; (b) Zou, S.; Ma, Y.; Hempenius, M.; Schönherr, H.; Vancso, G.J. *Langmuir* **2004**, 20, 6278-6287; (c)

- Dessinges, M.-N.; Maier, B.; Zhang, Y.; Peliti, M.; Besimon, D.; Croquette, V. *Phys. Rev. Lett.* **2002**, *89*, 248102; (d) Bustamante, C.; Smith, S.B.; Liphardt, J.; Smith, D. *Curr. Opin. Struct. Biol.* **2000**, *10*, 279-285; (e) Li, H.; Zhang, W.; Zhang, X.; Shen, J.; Liu, B.; Gao, C.; Zou, G. *Macromol. Rapid Commun.* **1998**, *19*, 609-611.
92. Lo, Y.-S.; Hübner, N.D.; Chan, W.S.; Stevens, F.; Harris, J.M.; Beebe Jr., T.P. *Langmuir* **1999**, *15*, 1373-1882.
 93. (a) Lee, I.; Marchant, R.E. *Ultramicroscopy* **2003**, *97*, 341-352; (b) Lee, I.; Marchant, R.E. *Surf. Sci.* **2001**, 491, 433-443.
 94. (a) Dammer, U.; Hegner, M.; Anselmetti, D.; Wagner, P.; Dreier, M.; Huber, W.; Güntherodt, H.-J. *Biophys. J.* **1996**, *70*, 2437-244; (b) Van Oss, C.J. *In* Immunochemistry. (Eds. C.J. van Oss and M.H.V. van Regenmortel), **1994**, Marcel Dekker, New York, p. 581-614.
 95. Evans, E.; Ritchie, K. *Biophys. J.* **1997**, *72*, 1541-1555.
 96. Evans, E. *Annu. Rev. Biophys. Biomol. Struct.* **2001**, *30*, 105-128.
 97. Dudko, Hummer and Szabo, discuss the fact that the effective free energy profile may depend on the external force in a more complicated way as described by Evans. However a suitable model has to be chosen based on an often unknown energy potential profile. So this approach is not directly straightforward to use and often additional information is necessary (from for instance molecular dynamics simulations) next to single molecule data: Dudko, O.K.; Hummer, G.; Szabo, A. *Proc. Natl. Acad. Sci. U.S.A.* **2008**, *105*, 15755-15760.
 98. (a) Merkel, R. Nassoy, P.; Leung, A.; Ritchie K.; Evans, E. *Nature* **1999**, *397*, 50-53; (b) Wong, S.S.; Joselevich, E.; Woolley, A.T.; Cheung, C.L.; Lieber, C.M. *Nature* **1998**, *394*, 52-55.
 99. Evans, E. *Biophys. Chem.* **1999**, *82*, 83-97.
 100. Williams, P.; Evans, E. *Dynamic Force Spectroscopy in Physics of Bio-Molecules and Cells. Ecoles des Houches d'Été LXXV* (Eds: F. Julicher, P. Ormos, F. David, and H. Flyvbjerg) EDP Sciences, Springer Verlag, Berlin, **2002**, pp 147-203.
 101. Struntz, T.; Orozlan, K.; Shafer, R.; Guntherodt, H.-J. *Proc. Natl. Acad. Sci. U.S.A.* **1999**, *96*, 11277-11282.
 102. (a) Carrion-Vazquez, M.; Oberhauser, A.F.; Fischer, T.E.; Marszalek, P.E.; Li, H.; Fernandez, J.M. *Prog. Biophys. Mol. Bio.* **2000**, *74*, 63-91; (b) Kellermayer, M.S.Z.; Smith, S.B.; Granzier, H.L.; Bustamante, C. *Science* **1997**, *276*, 1112-1116.

CHAPTER 3

AFM-BASED SINGLE MOLECULE FORCE SPECTROSCOPY OF SUPRAMOLECULAR UREIDOPYRIMIDINONE DIMERS AND POLYMERS IN HEXADECANE

As for the forces, electromagnetism and gravity we experience in everyday life. But the weak and strong forces are beyond our ordinary experience. So in physics, lots of the basic building blocks take 20th- or perhaps 21st-century equipment to explore.

– Edward Witten

Abstract

Atomic Force Microscopy-based single molecule force spectroscopy (AFM-based SMFS) was used to study the bond strength of self-complementary hydrogen-bonded complexes based on 2-ureido-4[1H]-pyrimidinone (UPy) quadruple hydrogen-bonded polymers in hexadecane (HD). The unbinding force corresponding to single (UPy)₂ dimers was investigated at a fixed piezo retraction rate in the non-equilibrium loading rate regime. The rupture force of bridging supramolecular polymer chains formed between UPy functionalized substrates and AFM-tips in the presence of a bis-UPy derivative was found to decrease with increasing rupture length. The rupture length was identified as chain length of single, associating polymers, which allowed us to determine the number of supramolecular bonds (*N*) at rupture. The rupture force observed as a function of *N* was in quantitative agreement with the theory on uncooperative bond rupture for supramolecular linkages switched in a series. Hence the value of the dimer equilibrium constant $K_{eq} = (1.3 \pm 0.5) \times 10^9 \text{ M}^{-1}$, which is in good agreement with previously estimated values, was obtained by SMFS of supramolecular polymers at a single loading rate.

* the work described in this chapter was published in the following article: Embrechts, A.; Schönherr, H.; Vancso, G.J. *J. Phys. Chem. B* **2008**, 112, 7359-7362.

3.1 INTRODUCTION

The investigation of spontaneous self-assembly processes governed by supramolecular interactions on the molecular level has received growing attention^[1], as was already discussed in Chapter 2. Within the rapidly developing fields of nanotechnology and nanoscience, as well as molecular level biochemistry and biophysics, knowledge regarding molecular stability and bond strengths on a single-molecule level has become crucial^[2]. Using Atomic Force Microscopy-based single molecule force spectroscopy (AFM-based SMFS)^[3,4], optical tweezers^[5] or the biomembrane force probe (BFP)^[6], bond strengths can now be measured at a single molecule level^[7-9].

The important role of hydrogen-bonds in biological, as well as synthetic supramolecular systems^[10] has inspired us to focus our research on the investigation of hydrogen-bonded complexes on a single molecule level. Previously, we employed AFM-based SMFS to unravel the dimer bond strength of a self-complementary hydrogen-bonded system based on the 2-ureido-4[1H]-pyrimidinone (UPy) quadruple hydrogen-bond motif in hexadecane (HD)^[11]. Accordingly, single molecule recognition of UPy moieties on gold surfaces was characterized using X-ray photoelectron spectroscopy (XPS), differential pulse voltammetry (DPV), atomic force microscopy (AFM), and surface plasmon resonance (SPR) methods^[13]. The Bell-Evans model (equation 3-1)^[2,6] for the loading rate (r_f)-dependent most probable rupture force (f^*), provided the bond lifetime in the absence of any externally applied force, $t_{off}(f=0)$, of 5 - 7 seconds, which corresponds to a dimer equilibrium constant of $K_{eq} \sim 10^9 \text{ M}^{-1}$ (hexadecane, $T = 301 \text{ K}$)^[11,12a].

$$f^* = f_\beta \cdot \ln\left(\frac{r_f}{r_f^0}\right) = \left(\frac{k_B \cdot T}{x_\beta}\right) \cdot \ln\left(\frac{r_f}{f_\beta \cdot t_{off}(0)}\right) \quad \text{Equation 3-1}$$

Here f_β denotes the thermal force, r_f^0 is the loading rate at zero force, k_B is the Boltzmann constant and x_β is the distance of the energy barrier that needs to be overcome for unbinding along the direction of the applied force as was discussed in Chapter 2. So, using AFM-based SMFS the thermodynamic equilibrium parameters such as the Gibbs free energy of binding (ΔG), the bond lifetime (t_{off}) and the dimer binding constant of (UPy)₂ in hexadecane ($K_{eq} = K_{dim}$) could be determined for the first time. An overview of this study is presented in Figure 3- 1 and Figure 3- 2. The UPy-motif was previously also studied by Guan et al^[14].

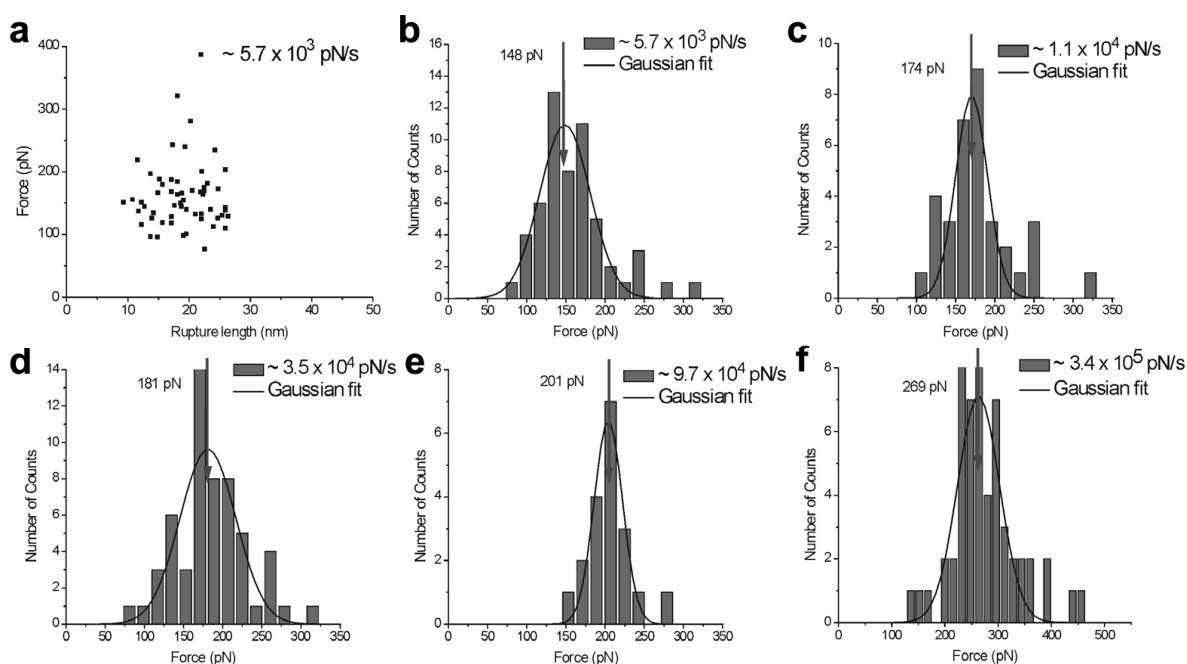


Figure 3- 1. (a) The rupture forces vs. the corresponding rupture lengths of $(UPy)_2$ measured under a loading rate of $(5.7 \pm 1.1) \times 10^3$ pN/s at 301 K in hexadecane. Histograms of pull-off forces of individual $(UPy)_2$ complexes at loading rates of (b) $(5.7 \pm 1.1) \times 10^3$ pN/s, (c) $(1.1 \pm 0.2) \times 10^4$ pN/s, (d) $(3.5 \pm 0.7) \times 10^4$ pN/s, (e) $(9.7 \pm 1.9) \times 10^4$ pN/s, and (f) $(3.4 \pm 0.7) \times 10^5$ pN/s at 301 K in hexadecane. Solid lines in (b) – (f) are Gaussian fits to the corresponding histograms. *Image was adapted from ref. 12.*

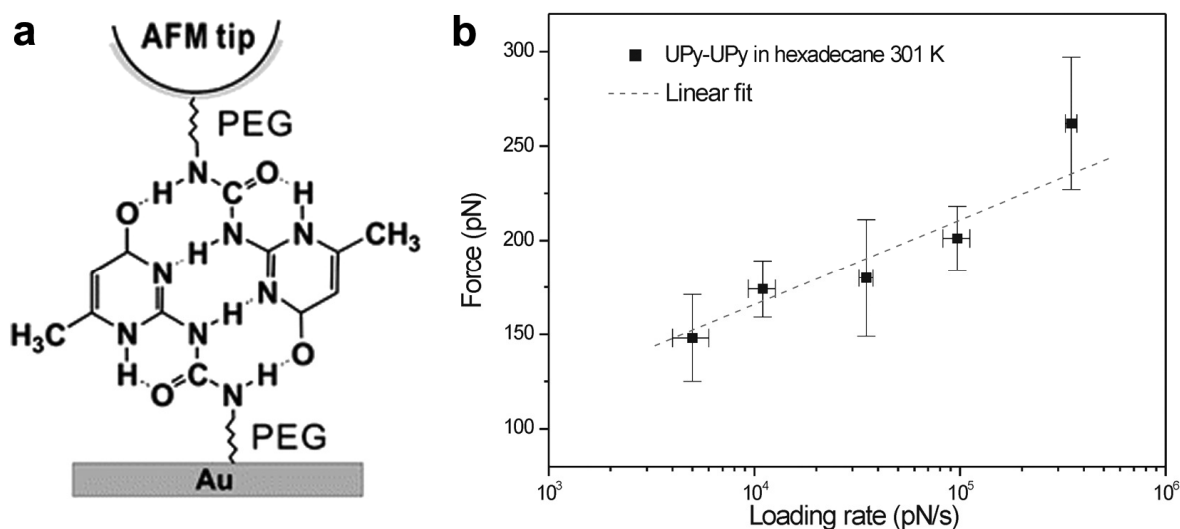
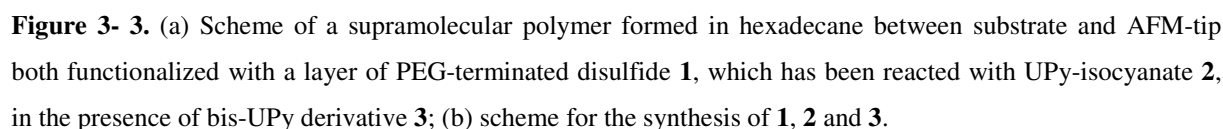


Figure 3- 2. (a) Scheme of $(UPy)_2$ dimer recognition event between a chemically modified gold-coated AFM tips and gold substrate; (b) plot of rupture force versus loading rate at 301 K in hexadecane. *Image was adapted from ref. 12.*

To obtain the thermal scale force f_β and thus the dimer equilibrium constant K_{eq} using this model, the most probable rupture force f^* is typically determined for various loading rates r_f

100

supramolecular polymer formation can now also be studied *in situ* (see also Figure 3- 3)^[15].



According to Evans and Williams^[16], uncooperative bond rupture in series leads to a decrease of the most probable rupture force f^* with the number of linkers N , as shown in equation 3-2, which provides direct access to f_β and all desired parameters to study the binding constant of the (UPy)₂ complex.

60

Thus, in our experiments the rupture forces of supramolecular, associative polymers^[10-12] formed between two UPy-motifs attached to gold-coated substrates and tips were studied in the presence of bis-UPy derivative **3** in hexadecane (Figure 3- 3)^[18]. The observed rupture forces were analyzed according to equation 3-2 to yield $t_{off}(f=0)$ and K_{eq} for (UPy)₂ for two data set at a single loading rate.

3.2 RESULTS AND DISCUSSION

(UPy)₂ bonds in series were probed in force-displacement measurements carried out in HD using UPy-functionalized AFM-tips and gold substrates in the presence of the bis-UPy derivative **3**. The force-distance (f-d) curves were obtained using the procedure described in Chapter 2 and Veeco offline software analysis. The f-d curves showed the typical stretching of the PEG-linker^[20,21] and the subsequent rupture of the polymeric chain formed between tip and sample (see Figure 3- 4a and Appendix)^[12].

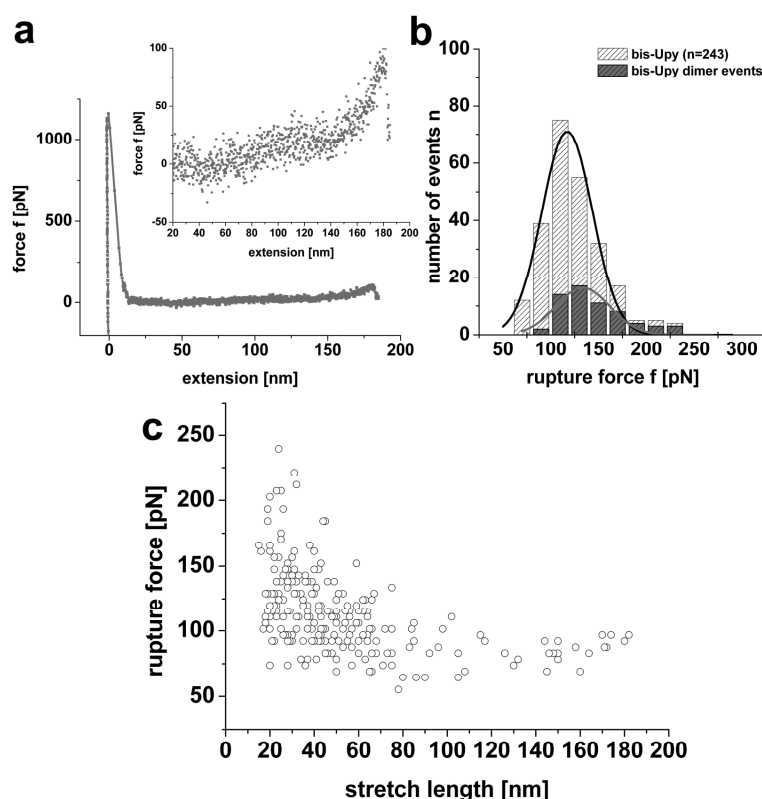


Figure 3- 4. (a) Force-extension curve of supramolecular polymer obtained in HD ($T = 303 \pm 2$ K, $r_f = 2.8 \times 10^3$ pN/s); inset: magnified section of f-d curve close to the rupture of the chain under load ($L = 182$ nm, $f = 97$ pN); (b) histogram of the rupture force f for dimer interactions (black) and all events (grey). The solid lines display Gaussian fits of the distributions of the dimer ($f^* = 119 \pm 30$ pN) and of all events ($f^* = 104 \pm 29$ pN), respectively; (c) rupture force f plotted vs. stretch length L for 243 f-d curves.

As the total length of one PEG-chain including the two UPy-moieties is 12 ± 3 nm, the supramolecular polymer probed consists of numerous $(UPy)_2$ bonds connected via PEG-linkers. For all f-d curves displaying single molecule events (number of events $n = 243$, probability of observing an event $p = 0.02$), the corresponding rupture forces and rupture lengths were determined (Figure 3- 4c). Figure 3- 4b shows two histograms in which the rupture forces for $(UPy)_2$ are compared with the rupture forces observed for all events, *i.e.* events attributed to the dimer and to supramolecular polymers. Dimer rupture events ($N = 1$) were defined as rupture events that occurred at a stretch (rupture) length L of 18 - 30 nm. The mean value of the rupture force obtained from the Gaussian fits indicates that the mean value of the dimer rupture force is larger than that of the polymer.

The stretch length L (in nm) in Figure 3- 4c is easily converted to the number of linkers N since each bis-UPy moiety **3** contributes 12 nm to the observed length, *i.e.* $N = (L/12 \text{ nm})-1$. For each integer value of N the most probable force f^* was estimated and plotted as a function of N (Figure 3- 5a). In the current data 82% of all single molecule events were observed for $N \leq 5$. As predicted by Evans and Williams, f^* was observed to decrease with increasing N .

The values of f_β and f_{single}^* were determined by fitting equation 3-2 to the data using the Marquardt-Levenberg algorithm^[22] (Figure 3- 5a). The parameter f_β correlates the most probable rupture force f^* with the loading rate r_f (equation 3-1). By plotting f^* obtained for the dimer versus the corresponding loading rate r_f and extrapolating f^* (in the plot versus the natural logarithm of the loading rate r_f) to zero force using the fitted values f_β , the thermal scale for the loading rate r_f^0 and consequently $t_{off}(f=0)$ and K_{eq} are obtained via equations 3-3 and 3-4.

$$r_f^0 = \left(\frac{f_\beta}{t_D} \right) \cdot e^{-\Delta G / k_B T} \quad \text{Equation 3-3}$$

$$\Delta G = -RT \ln K_{eq} \quad \text{Equation 3-4}$$

where t_D ($= 5 \times 10^{-9}$ s for viscous hexadecane, see below) is the diffusive relaxation time of the bound complex and R the molar gas constant.

The analysis described above provided the following parameters: $f_\beta = 21.3 \pm 2.0$ pN, $r_f^0 = 5.4 \pm 0.7$ pN/s, which leads to a value for the dimer binding constant of $K_{eq} = (1.3 \pm 0.5) \times 10^9 \text{ M}^{-1}$. Via $t_{off}(0) = f_\beta / r_f^0$ the bond lifetime at zero force was also determined: $t_{off}(f=0) = 3.9 \pm 0.9$ s. In general, a favourable agreement with approximate data available in the literature^[10,12] is observed; due to the improved statistics, more reliable values based on SMFS were obtained in our current study (Table 3- 1).

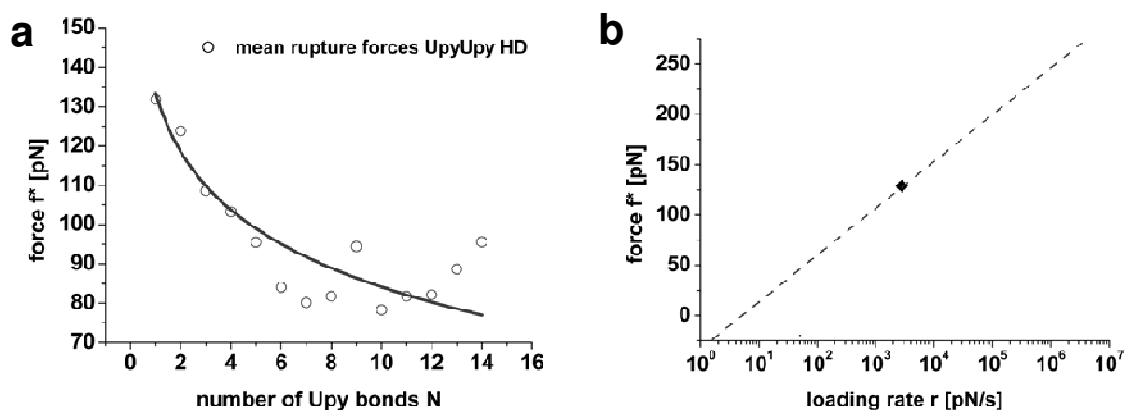


Figure 3- 5. (a) Plot of most probable rupture force f^* vs. number of UPy bonds N , $r_f = (2.8 \pm 0.5) \times 10^3$ pN/s. The uncooperative bond rupture model of weak bonds in series was fitted to yield the thermal force scale $f_\beta = 21.3 \pm 2.0$ pN ($R^2 = 0.92$); (b) extrapolation of the value of f^* determined for the dimer to zero force using f_β affords r_f^0 , which in turn is used to calculate $t_{off}(f=0)$ and K_{eq} .

	Bulk measurement ^[10]	SMFS (dimer, estimate) ^[11]	SMFS (dimer, $r_f = (5.7-340) \times 10^3$ pN/s) ^[12]	SMFS (polymer, $r_f = (2.8 \pm 0.5) \times 10^3$ pN/s)
f_β [pN]	-	~19	18.2 ± 2.0	21.3 ± 2.0
ΔG [kJ/mol]	~ 52	~ 49	51 ± 2	52 ± 2
K [M^{-1}]	~ 10^9	~ 10^9	$(6 \pm 5) \times 10^8$	$(1.3 \pm 0.5) \times 10^9$
$t_{off}(f=0)$ [s]	~ 5	~ 5 - 7	1.3-8.1	3.9 ± 0.9

Table 3- 1. Comparison of single molecule and ensemble thermodynamic parameters obtained using different single molecule approaches and bulk measurements.

A few remarks must be made regarding the approaches described above to determine the dimer equilibrium constant K for hydrogen-bonded species in solution. For both techniques

(dimer and polymer analysis) measurements are performed far-from equilibrium and hence only the kinetic off-rate ($t_{\text{off}}(0) = k_{\text{off}}^{-1}$) is determined. Although the kinetic on-rate can not be determined directly using this approach, an appropriate estimate for the diffusive relaxation ($t_D \leq \text{ns} \approx 10^{-9} - 10^{-10}$ s in water^[23]) will still lead to the dimer equilibrium constant K . Furthermore Hinterdorfer^[24a], Noy^[24b] and more recently Janshoff^[24d] and co-workers demonstrated that kinetic on-rates can also be determined by AFM-based techniques provided that suitable experimental conditions are used. In this case the probability of binding is probed^[24] and surface coverage has to be controlled profoundly. A combination of these two techniques would improve the accuracy of determined values for dimer binding constants and may reveal interesting phenomena on a single molecule level.

In the analysis of supramolecular polymers at a fixed loading rate minor errors are introduced by using a mean loading rate and by converting the measured extension length L at rupture to the number of UPy-bonds N employing the average length of **3** including the PEG-linker. Similar to the established approach of SMFS carried out at various loading rates, the first source of error is unavoidable. The error which is introduced in f^* due to polydispersity of the PEG-linker was estimated according to reference 25 to be on the order of 2%, assuming a symmetric distribution of the tether length.

A comparison of equations 3-1 and 3-2 shows that the error in f_β depends, both for the established SMFS and our new approach, linearly on the error in f^* , as long as N is small. Thus, by analyzing data from 100 or more single molecule events per N a reasonable basis is provided for determining f^* from the corresponding histogram. These boundary conditions are the main reason to use this approach in far-from-equilibrium conditions (at higher loading rates well above the cross-over regime). Although some rupture events for slightly higher N may still be observed close to the cross-over regime, it will take a substantial amount of time to collect a statistical large enough data set to obtain accurate results. Furthermore the distribution of stretch lengths that is obtained, may still lead to substantial error in dimer binding constant analysis if $N \leq 5$ (see also Appendix).

However, if unbinding of supramolecular polymer is studied in appropriate conditions, the application of the theory on uncooperative bond rupture in series provides direct access to the dimer equilibrium constant and related parameters of a ligand-receptor interaction. Furthermore, the value of the dimer equilibrium constant for (UPy)₂ in hexadecane agrees very well with the value of K_{eq} of $\sim 1 \times 10^9 \text{ M}^{-1}$ predicted by Sijbesma et al.^[10] based on an

extrapolation of the data obtained for (UPy)₂ interactions in different solvents (measurements in bulk).

3.3 CONCLUSIONS

The acquisition of single molecule rupture force parameters required to calculate off-rates and equilibrium complexation constants in the absence of force was shown to be feasible by studying the forced unbinding of single supramolecular polymers at one *fixed* piezo retraction rate in SMFS experiments. For the first time, access to the dimer bond lifetime at zero force $t_{off}(f=0)$ was achieved by exploiting the theory on uncooperative bond rupture in series, based on the rupture forces of supramolecular polymers of different length bridging between AFM-tip and surface and independent knowledge of the constituent segment length. Since this approach can also be applied to systems with a low degree of polymerization ($N \geq 5$) with the mere requirement of a large dataset (were the number of events n is high enough to obtain a reasonable fit of the data to equation 3-2), this new method can be applied to almost all self-complementary supramolecular polymer systems under suitable concentration and solvent conditions. In conclusion the data obtained in this study agree favourably with previously reported data acquired in loading rate-dependent measurements of (UPy)₂, as well as the value of $K_{eq} \sim 1 \times 10^9 \text{ M}^{-1}$ predicted by Sijbesma et al^[10]. Hence this new method is expected to facilitate the determination of bond lifetimes and dimer equilibrium constants by SMFS for complexes over a wide range of K_{eq} and different solution conditions.

3.4 MATERIALS AND METHODS

Materials. Anhydrous hexadecane (purity $\geq 99 \%$, water $< 0.005 \%$) and dibutyltindilaurate were purchased from Sigma-Aldrich (Steinheim, Germany) and used as received. Chloroform (stabilized with amylene) and dichloromethane were purchased from Biosolve (Valkenswaard, The Netherlands).

1,2-Dithiolane-3-pentyl-derivatized PEG **1**, (6-isocyanatohexylaminocarbonylamino)-6-methyl-4[1H]pyrimidinone **2** and PEG-linked bis-pyrimidinone **3** were synthesized according to published procedures^[12,19].

Sample preparation. Gold substrates ($11 \times 11 \text{ mm}^2$, 250 nm Au on 2 nm Cr on borosilicate glass) for SMFS measurements were purchased from Arrandee (Werther, Germany). Au(111)

samples were obtained by annealing these substrates in a high purity H₂ flame for 5 minutes^[13]. Prior to use, these substrates were cleaned in a piranha solution (2:1 H₂SO₄ conc: H₂O₂ (30%) by volume), then rinsed with Milli-Q water and ethanol and dried in a nitrogen stream. **Caution: Piranha solution should be handled with extreme caution: it has been reported to detonate unexpectedly.** On gold substrates, self-assembled monolayers (SAMs) of **1** were prepared from 1 mM CH₂Cl₂ solution and reacted with 2.5 mmol **2** in 10 ml CHCl₃ solution for 24 hours using one drop of dibutyltindilaurate as catalyst^[12b]. After rinsing with pure solvent and drying in an N₂ stream, measurements were performed with minimal delay. The same procedure was used for AFM-tip functionalization.

Atomic Force Microscopy. The AFM-based SMFS measurements were performed on a Picoforce AFM using a NanoScope IVa controller, a Picoforce vertical engage scanner and a liquid cell (Bruker/Veeco/Digital Instruments, Santa Barbara, CA). Gold-coated V-shaped Si₃N₄ cantilevers (Bruker/Veeco, NPG probes) were functionalized in two consecutive steps, as described above, with a self-assembled layer of **1** and subsequent reaction with **2**. Tips for SMFS were taken directly from solution followed by rinsing with pure solvent. The cantilever spring constant ($k = 0.187 \pm 0.02$ N/m) was determined in liquid via the thermal tune method^[26]. Loading rates were determined as the slope of the force versus time trace of the force-extension curves (~ 20 data points) close to the rupture event. All experiments were performed in a saturated solution of **3** in anhydrous hexadecane at $T = 303 \pm 2$ K (concentration $3.2 \pm 0.4 \times 10^{-5}$ M).

APPENDIX

In previous studies, based on temperature superposition, the cross-over regime from loading rate-dependent (far-from-equilibrium measurements) and loading rate-independent (near-equilibrium measurement) was estimated to occur at a loading rate of ~5nN/s^[11]. The measurements presented above are measured close to this loading rate regime. Below, the results of the unbinding events of supramolecular Upy-polymers at a loading rate even closer to the cross-over regime, than the previously discussed data set, is presented ($r = (2.3 \pm 0.8) \times 10^3$ pN/s). In this case measurements are starting to approach equilibrium conditions. Since the speed at which the rupture force is probed is slow, only supramolecular polymers with small N can be probed. As can be observed in Figure 3-6c, the majority of rupture events are dimer and trimer events and therefore the approach described above can no

longer be applied reliably (See also Figure 3- 6). Furthermore the dataset is substantially smaller than the dataset discussed above. Hence this dataset is statistically unsuitable for an accurate bond strength study.

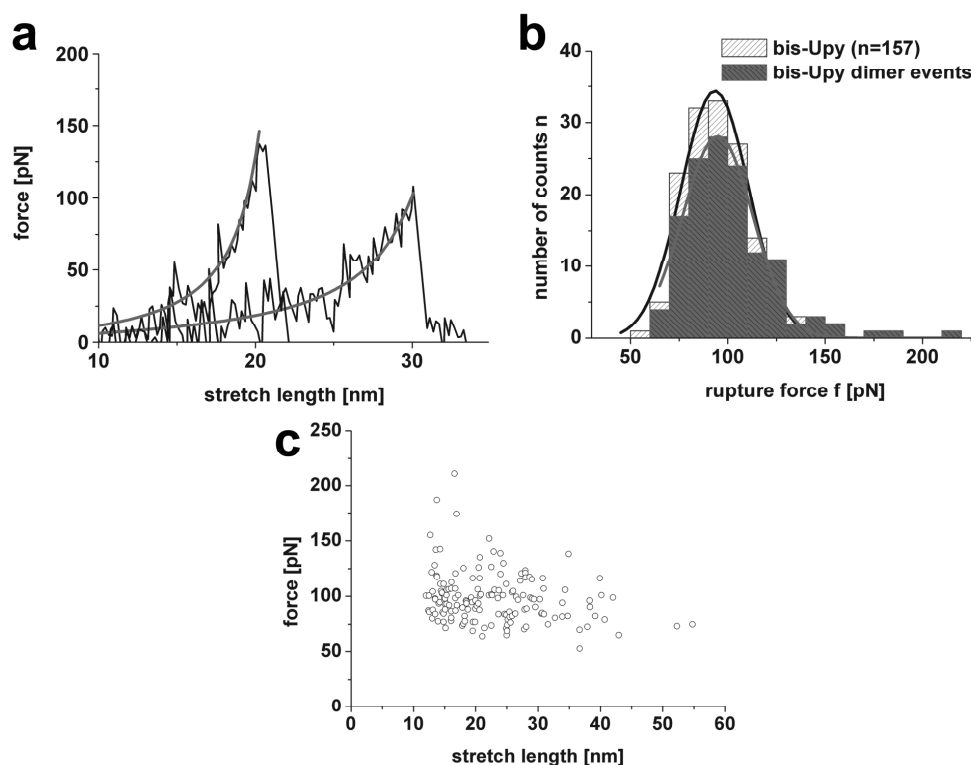


Figure 3- 6. (a) Part of the force-extension curves of supramolecular polymer in hexadecane close to the rupture event plus fit to the WLC model ($T = 303 \pm 2$ K, $r_f = (2.3 \pm 0.8) \times 10^3$ pN/s); (b) histogram of the rupture force f for dimer interactions (black) and all events (grey). The lines display Gaussian fits of the distributions of the dimer ($f^* = 95 \pm 35$ pN) and of all events ($f^* = 93 \pm 34$ pN), respectively; (c) rupture force f plotted vs. stretch length L for 157 f-d curves.

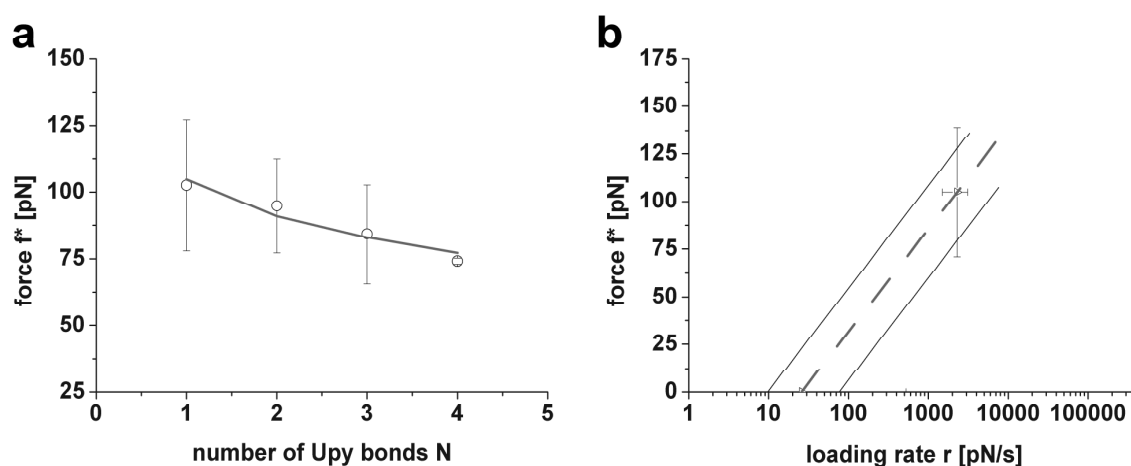


Figure 3- 7. (a) Plot of most probable rupture force f^* vs. number of UPy bonds N , $r_f = (2.3 \pm 0.8) \times 10^3$ pN/s. The uncooperative bond rupture model of weak bonds in series was fitted to yield the thermal force scale $f_\beta = 19.9 \pm 3.8$ pN ($R^2 = 0.93$); (b) extrapolation of the value of f^* determined for the dimer to zero force using f_β affords r_f^0 (error margins in grey lines), which in turn is used to calculate $t_{off}(f=0)$ and K_{eq} .

Thus, although this approach still provides a reasonable fit for the thermal scale force $f_{\beta} = 19.9 \pm 3.8$ pN (see Figure 3- 7), the errors that are introduced do lead to an underestimate of the bond life time and binding constant ($t_{off}(0) = 1.5 \pm 1.1$ s; $K_{dim} = (2 \pm 1) \times 10^8$ M⁻¹) of UPy moieties in hexadecane. Measurements at high loading rates in far-from-equilibrium conditions are therefore recommended since a larger data set (with larger number of N) can be obtained over a shorter period of time.

REFERENCES AND NOTES

1. (a) Samori, P. (Ed.) *Scanning Probe Microscopies Beyond Imaging: Manipulation of Molecules and Nanostructures*, Wiley-VCH, Weinheim, **2006**; (b) Serpe, M.J.; Craig, S.L. *Langmuir* **2007**, 23, 1626-1634; (c) Nie, Z.H.; Fava, D.; Kumacheva, E.; Zou, S.; Walker, G.C.; Rubinstein, M. *Nature Mater.* **2007**, 6, 609-614; (d) Cordier, P.; Tournilhac, F.; Soulié-Ziakovic, C.; Leibler, L. *Nature* **2008**, 451, 977-980.
2. Evans, E. *Annu. Rev. Biophys. Biomol. Struct.* **2001**, 30, 105-128.
3. (a) Florin, E.L.; Moy, V.T.; Gaub, H.E. *Science* **1994**, 264, 415-417; (b) Lee, G.U.; Kidwell, D.A.; Colton, R.J. *Langmuir* **1994**, 10, 354-357; (c) Rief, M.; Gautel, M.; Oesterhelt, F.; Fernandez, J.M.; Gaub, H.E. *Science* **1997**, 276, 1109-1112.
4. Vancso, G.J. *Angew. Chem. Int. Ed.* **2007**, 46, 3794-3796.
5. (a) Ashkin, A.; Dziedzic, J.; Bjorkholm, J.; Chu, S. *Opt. Lett.* **1986**, 11, 288-290; (b) Smith, S.B.; Cui, Y.; Bustamante, C. *Science* **1996**, 271, 795-799.
6. (a) Evans, E.; Ritchie, K.; Merkel, R. *Biophys. J.* **1995**, 68, 2580-2587; (b) Evans, E. *Biophys. Chem.* **1999**, 82, 83-97.
7. Bustamante, C.; Macosko, J.C.; Wuite, G.J.L. *Nat. Rev. Mol. Cell Biol.* **2000**, 1, 130-136.
8. Janshoff, A.; Neitzert, M.; Oberdörfer, Y.; Fuchs, H. *Angew. Chem. Int. Ed.* **2000**, 39, 3213-3237.
9. Zou, S.; Schönherr, H.; Vancso, G.J. in *Scanning Probe Microscopies Beyond Imaging: Manipulation of Molecules and Nanostructures*, (Ed. P. Samori), Wiley-VCH, Weinheim, **2006**, p. 315.
10. (a) Ten Cate, A.T.; Sijbesma, R.P. *Macromol. Rapid Commun.* **2002**, 23, 1094-1112; (b) Söntjens, S.H.M.; Sijbesma, R.P.; Van Genderen, M.H.P.; Meijer, E.W. *J. Am. Chem. Soc.* **2000**, 122, 7487-7493; (c) Sijbesma, R.P.; Beijer, F.H.; Brunsveld, L.; Folmer, B.J.

- B.; Hirschberg, J.H.K.K.; Lange, R.F.M.; Lowe, J.K.L.; Meijer, E.W. *Science* **1997**, 278, 1601-1604.
11. Zou, S. PhD thesis "Exploring individual supramolecular interactions and stimuli-responsive polymers by AFM-based force spectroscopy" **2005**, Enschede, The Netherlands, p 80-83.
 12. (a) Zou, S.; Schönherr, H.; Vancso, G.J. *J. Am. Chem. Soc.* **2005**, 127, 11230-11231; (b) Zou, S.; Schönherr, H.; Vancso, G.J. *Angew. Chem. Int. Ed.* **2005**, 44, 956-959.
 13. Zou, S.; Zhang, Z.H.; Förch, R.; Knoll, W.; Schönherr, H.; Vancso, G.J. *Langmuir* **2003**, 19, 8618-8621.
 14. Guan, Z.B.; Roland, J.T.; Bai, J.Z.; Ma, S.X.; McIntire, T.M.; Nguyen, M. *J. Am. Chem. Soc.* **2004**, 126, 2058-2065.
 15. Zou, S.; Schönherr, H.; Vancso, G.J. *Angew. Chem. Int. Ed.* **2005**, 44, 956-959.
 16. Williams, P.; Evans, E. *Dynamic Force Spectroscopy in Physics of Bio-Molecules and Cells. Ecoles des Houches d'Eté LXXV* (Eds: F. Julicher, P. Ormos, F. David, and H. Flyvbjerg) EDP Sciences, Springer Verlag, Berlin, **2002**, p. 147-203.
 17. (a) Chen, C.C.; Dormidontova, E.E. *Macromolecules* **2006**, 39, 9528-9538; (b) Hagy, M.C.; Chen, C.C.; Dormidontova, E.E. *Macromolecules* **2007**, 40, 3408-3421.
 18. Bridging chains of DNA have been reported before: Kersey, F.R.; Lee, G.; Marszalek, P.; Craig, S.L. *J. Am. Chem. Soc.* **2004**, 126, 3038-3039.
 19. Folmer, B.J.B.; Sijbesma, R.P.; Versteegen, R.M.; van der Rijt, J.A.J.; Meijer, E.W. *Adv. Mater.* **2000**, 12, 874-878.
 20. Oesterhelt, F.; Rief, M.; Gaub, H.E. *New J. Phys.* **1999**, 1, 6.1-6.11.
 21. Kienberger, F.; Pastushenko, V.P.; Kada, G.; Gruber, H.J.; Riener, C.; Schindler, H.; Hinterdorfer, P. *Single Mol.* **2000**, 1, 123-128.
 22. (a) Marquardt, D. *SIAM J. Appl. Math.* **1963**, 11, 431-441; (b) Gill, P.E.; Murray, W. *SIAM J. Num. Anal.* **1978**, 15, 977-992.
 23. (a) Grubmüller, H.; Heymann, B.; Tavan, P. *Science* **1996**, 271, 997-999; (b) Marrink, S.-J.; Berger, O.; Tieleman, P.; Jahnig, F. *Biophys. J.* **1998**, 74, 931-943; (c) Pope, L.H.; Davies, M.C.; Laughton, C.A.; Roberts, C.J.; Tendler, S.J.B.; Williams, P.M. *Eur. Biophys. J.* **2001**, 30, 53-62.
 24. (a) Hinterdorfer, P.; Baumgartner, W.; Gruber, H.J.; Schilcher, K.; Schindler, H. *Proc. Natl. Acad. Sci. U.S.A.* **1996**, 93, 3477-3481; (b) Friddle, R.W.; Podsiadlo, P.; Artyukhin, A.B.; Noy, A. *J. Phys. Chem. C* **2008**, 112, 4986-4990; (c) Guo, S.; Lad, N.; Ray, C.;

- Akhremitchev, B.B. *Biophys. J.* **2009**, *96*, 3412-3422; (d) Janke, M.; Rudzevich, Y.; Molokanova, O.; Metzroth, T.; Mey, I.; Diezemann, G.; Marszalek, P.E.; Gauss, J.; Böhmer, V.; Janshoff, A. *Nat. Nanotechnol.* **2009**, *4*, 225-229.
25. Ray, C.; Brown, J. R.; Akhremitchev, B.B. *J. Phys. Chem. B* **2007**, *111*, 1963-1974.
26. (a) Butt, H.J.; Cappella, B.; Kappl, M. *Surf. Sci. Rep.* **2005**, *59*, 1-152; (b) Hutter, J.L.; Bechhöfer, J. *Rev. Sci. Instrum.* **1993**, *64*, 1868-1873.

CHAPTER 4

AFM-BASED SINGLE MOLECULE FORCE SPECTROSCOPY OF SUPRAMOLECULAR UREA-AMINOTRIAZINE-BASED DIMERS

DADA... wants over and over again movement: it sees peace only in dynamism

– Raoul Hausmann

Abstract

Atomic Force Microscopy-based Single Molecule Force Spectroscopy (AFM-based SMFS) was used to determine the hydrogen-bond strength of a self-complementary quadruple urea-aminotriazine (UAT)-based hydrogen-bonded array in hexadecane. For this purpose, a UAT-based donor-acceptor-donor-acceptor (DADA)-array and complementary receptors were synthesized. The UAT receptor was immobilized on gold surfaces using an ultrathin layer of ethylene glycol terminated lipoic acid and isocyanate chemistry. The layers obtained were characterized with contact angle measurements, grazing angle Fourier transform infrared (FTIR) spectroscopy, X-ray photoelectron spectroscopy (XPS) and AFM. Reversible self-complementary recognition of surface-immobilized UAT moieties and solution borne UAT was confirmed by FTIR spectroscopy and AFM-based SMFS. Loading rate-dependent SMFS measurements yielded a value of the dimer binding of $K_{dim} = (2 \pm 1) \times 10^7 \text{ M}^{-1}$ of this DADA-array in hexadecane. This value is significantly higher than predicted on the basis of additive primary and secondary hydrogen-bond interactions. The remarkable difference is rationalized by additional intramolecular hydrogen-bond stabilization, confirmed by 2D proton nuclear magnetic resonance ($^1\text{H-NMR}$) measurements in CDCl_3 , which promotes a planar molecular geometry and significantly stabilizes the dimeric complex.

4.1 INTRODUCTION

As was discussed in Chapter 2 and demonstrated by several research groups over the past decades^[1,2], a new and exciting class of polymer materials can be ingeniously designed utilizing supramolecular hydrogen-bonding building blocks such as for instance widely available urea moieties. These polymers demonstrate exceptional self-healing properties and can be of interest for applications in a wide variety of fields, ranging from self-healing children's toys to molecular motors. The field of materials design will therefore greatly benefit from understanding the key contributions that determine hydrogen-bond strength and hence the resulting material properties. In Chapter 3 an AMF-based SMFS study of the binding strength and supramolecular polymer formation^[3] of the well-known ureidopyrimidinone (UPy, DDAA) array in hexadecane was already described^[4]. Single molecule and bulk studies on supramolecular polymer formation of ureidopyrimidinones were also performed by Guan and co-workers^[5].

To obtain insight in the key contributors that determine hydrogen-bond strength, a DADA urea-aminotriazine (UAT)-based hydrogen-bonded array was synthesized. The close resemblance of this UAT moiety with the well-studied ureidopyrimidinone (UPy) array provides the opportunity to investigate the influences of molecular structure, geometry and other contributions that might affect hydrogen-bond strength values. In this chapter the synthesis and characterization of this UAT-based hydrogen-bonded array are described. Additionally the surface chemistry and recognition of this hydrogen-bonded array on gold surfaces was investigated as a prerequisite for AFM-based SMFS. Although many triazine-based sensors have been reported in literature^[6] (often used to detect triazine-based herbicides), this urea-aminotriazine platform and the accompanying binding studies in hexadecane have not been reported. Ultimately the results of this binding study and theoretical calculations^[7] are compared for the two self-complementary quadruple UAT and UPy hydrogen-bonded systems in different solvents and the various contributions influencing the hydrogen-bond strength are discussed. The data obtained in Chapter 3 regarding the structure-property relationships associated with the bond strength of the UPy DDAA quadruple hydrogen-bonded array will be compared with the findings regarding the effect of structure-property relationships on the bond strength of the slightly different UAT-based DADA quadruple hydrogen-bonded array.

4.2 UAT-BASED DIMER CHARACTERIZATION IN BULK

Based on previously established platform chemistry^[8] for molecular recognition of UPy hydrogen-bonded arrays, a poly(ethylene glycol) (PEG)-terminated lipoic acid^[9] **1** and the UAT-based quadruple hydrogen-bonded array **2a** were synthesized (see Figure 4-1). Compound **2a** was synthesized following a slightly adapted procedure described previously by Sijbesma and Meijer^[11]. Complementary trifluoromethyl- **2b** and PEG-PPO-labeled **2c** UAT receptors were synthesized using isocyanate chemistry.

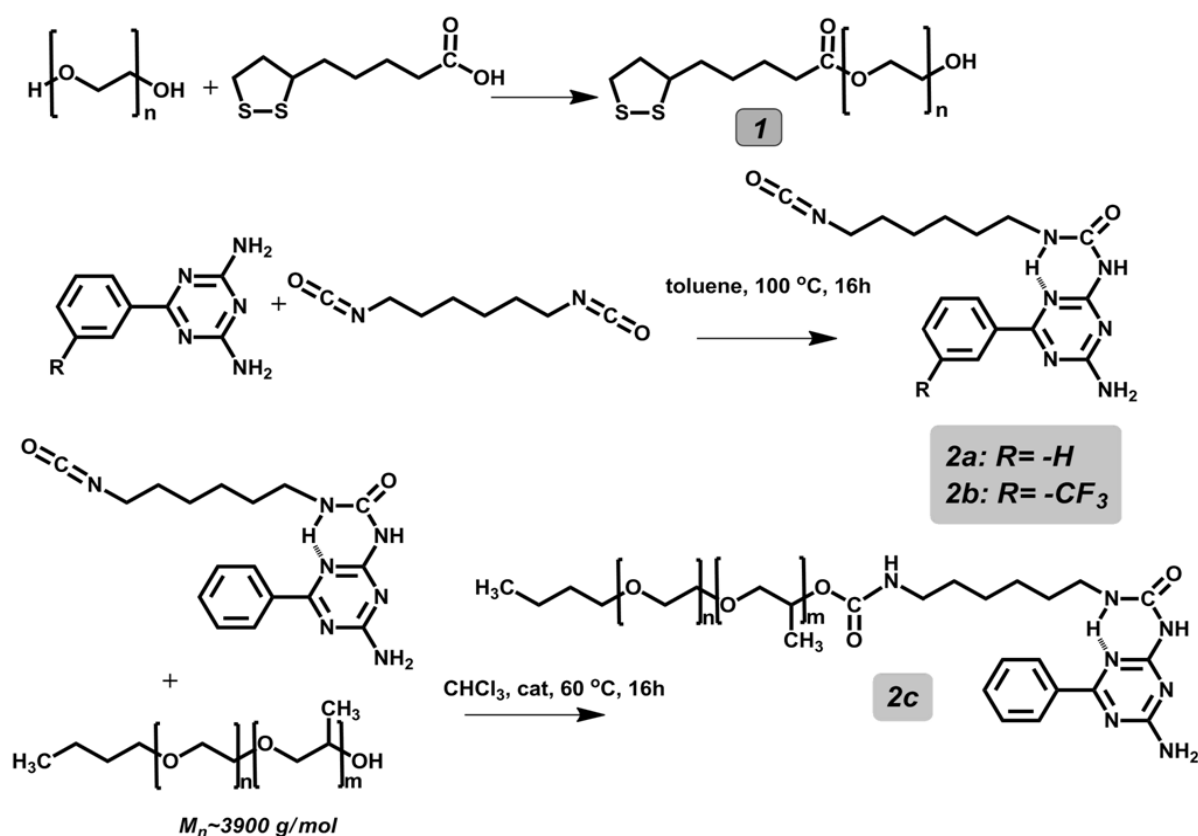


Figure 4-1. Synthesis of a PEG-terminated lipoic acid^[9] **1** and UAT-based hydrogen-bond moieties **2a-c** with a DADA recognition site for complementary hydrogen-bond formation and different substituents.

The UAT-based compounds were characterized using mass spectrometry, FTIR and NMR (1D and 2D) spectroscopy. 2D ¹H NMR provided additional information for the correct assignment of the hydrogen-bond interactions. ¹H NMR spectra of a saturated UAT solution were recorded in deuterated chloroform at two different temperatures (295 K and 265 K) and the signals were assigned using correlation spectroscopy (COSY, see Figure 4-2) and NOE data. The 1D ¹H spectrum of UAT shows the characteristic pattern for hydrogen-bonded dimers, with the two protons involved in the quadruple hydrogen-bonds being significantly

shifted downfield (see Figure 4- 3, 9.3 and 10.3 ppm for protons 'i', and 'h' respectively). The amine proton that is not involved in the hydrogen-bonding resonates at 5.5 ppm. Interestingly, the urea proton is observed at very low field (10.0 ppm). The corresponding signal is relatively sharp and does not change when the temperature is decreased. This indicates that this proton is involved in intramolecular hydrogen-bonding with the neighboring triazine nitrogen. Due to the dynamic behavior of the aliphatic chain and the fast rotation of the phenyl ring on the NMR time scale, as concluded from the single set of ortho and meta proton signals, NOE cross peaks are only weak at room temperature. Lowering the temperature, however, allows the recording of a Rotating-frame Overhauser Effect Spectroscopy (ROESY) spectrum with cross-peaks that further corroborate the intramolecular hydrogen-bond of the urea proton with the triazine.

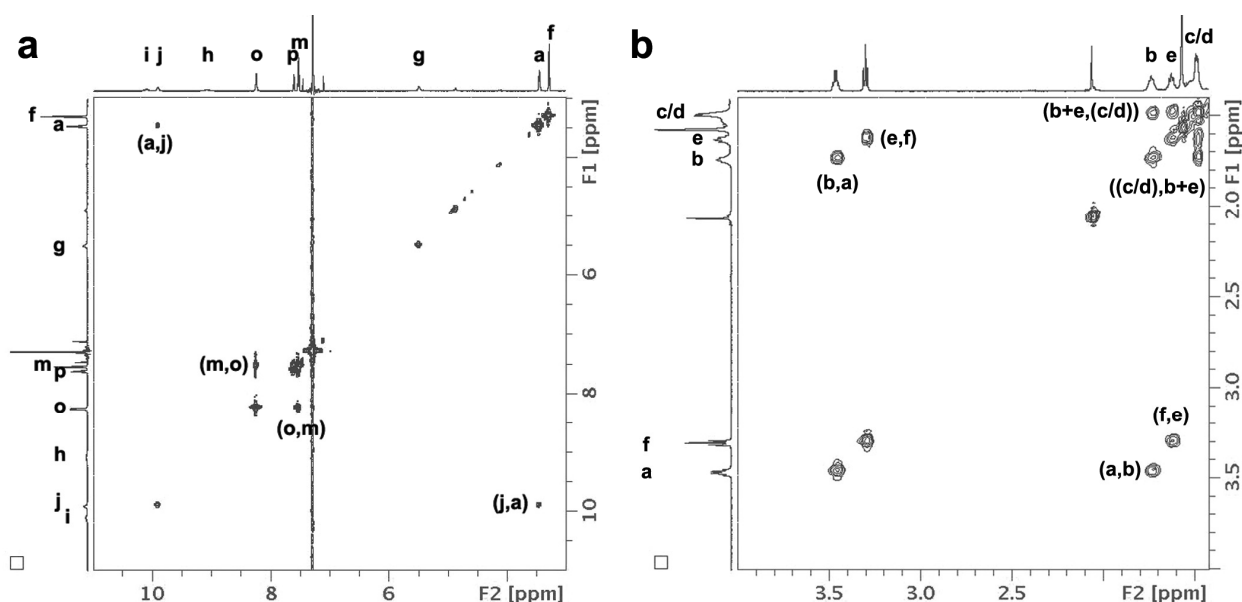


Figure 4- 2. 2D ^1H COSY spectrum of UAT-based hydrogen-bond dimerization in deuterated chloroform (a) lowfield, (b) highfield. COSY Interactions: intramolecular H-bond and $\text{CH}_2\text{-NH-(C=O)-NH}$ (3.5 ppm): (a,j); ortho (8.2 ppm) and meta (7.5 ppm) hydrogen phenyl ring: (o,m); CH_2 alkane chain (1.3 - 1.7 ppm) and $\text{CH}_2\text{-N}$ (3.5 ppm): (a,b); CH_2 alkane chain (1.3 - 1.7 ppm) and $\text{CH}_2\text{-N=C=O}$ (3.3 ppm): (f,e); CH_2 alkane chain (1.3 - 1.7 ppm): (b+e,(c/d)).

The ROESY spectrum shown in Figure 4- 3 shows characteristic NOE cross peaks for the ortho protons of the phenyl ring with the urea proton (Figure 4- 3a), and with the methylene protons of the aliphatic chain (Figure 4- 3b), respectively. The intramolecular hydrogen-bond is apparently strongly orienting the aliphatic chain which therefore lies parallel to the

triazine-phenyl ring system, explaining the NOE cross peaks. Interestingly, the NOE cross peak of the phenyl-ortho protons with the methylene 'b' and 'c/d' protons and urea-NH are stronger than the one with the methylene 'a' protons. This further confirms the strong intramolecular hydrogen-bond.

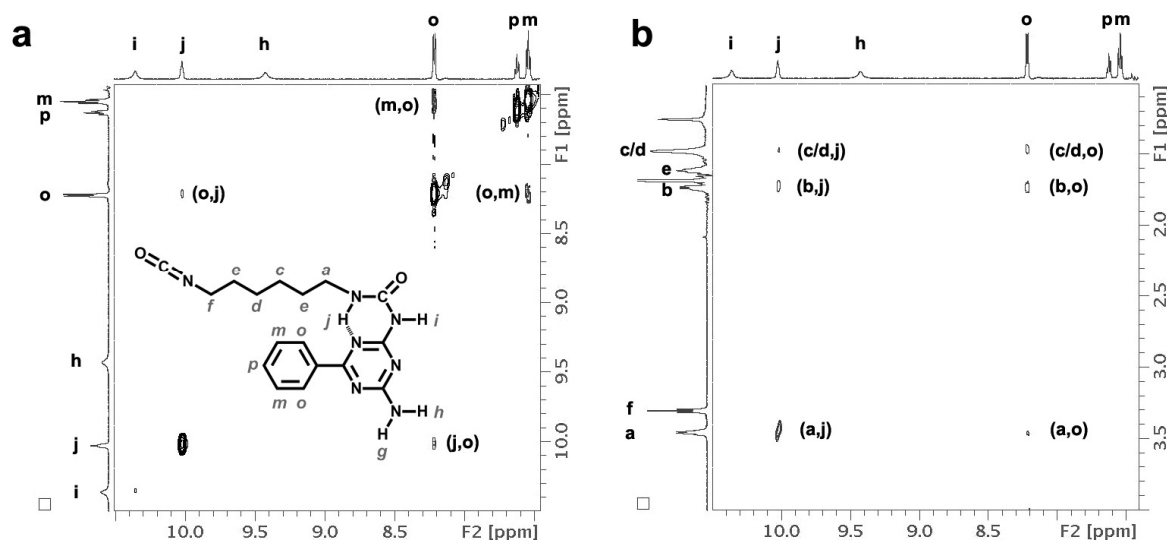


Figure 4- 3. 2D ¹H NMR spectrum of UAT recorded in deuterated chloroform using Rotating-frame Overhauser Effect Spectroscopy (ROESY) at 265 K. At low field (a) Nuclear Overhauser effects (NOE) between adjacent nuclei can be observed for the urea hydrogen involved in the intramolecular hydrogen-bond, at 10.0 ppm ('j'), with the ortho-hydrogens of the phenyl group, at 8.2 ppm ('o'); at high field (b), the urea ('j') and ortho ('o') protons show NOEs with the aliphatic CH₂-groups at 1.7 - 1.3 ppm ('b','c','d'). Inset: derived spatial arrangement of the self-complementary hydrogen-bonded array in solution.

Following molecular characterization, a recognition platform was prepared using a PEG self-assembled (mono)layer **1** on gold^[4,7], which was end-functionalized with a UAT-based hydrogen-bonded moiety **2a** (see Figure 4- 4). The established procedure provides low surface coverage UAT-based recognition platforms since this is a prerequisite for single molecule detection by AFM-based SMFS. The self-assembled layers on gold were characterized by contact angle measurements, grazing angle FTIR spectroscopy, X-ray photoelectron spectroscopy (XPS) and AFM. For the initial PEG-layer (**1**) advancing and receding contact angles of $38^\circ \pm 2^\circ$ and $23^\circ \pm 1^\circ$ were measured respectively, while the UAT-functionalized layers (**1+2a**) displayed advancing and receding contact angles of $61^\circ \pm 4^\circ$ and $24^\circ \pm 2^\circ$ for low surface coverage of the UAT-moiety and $76^\circ \pm 3^\circ$ and $56^\circ \pm 3^\circ$ for higher surface coverage. This substantial increase in contact angle is attributed to the phenyl-rings that now reside at the surface^[10].

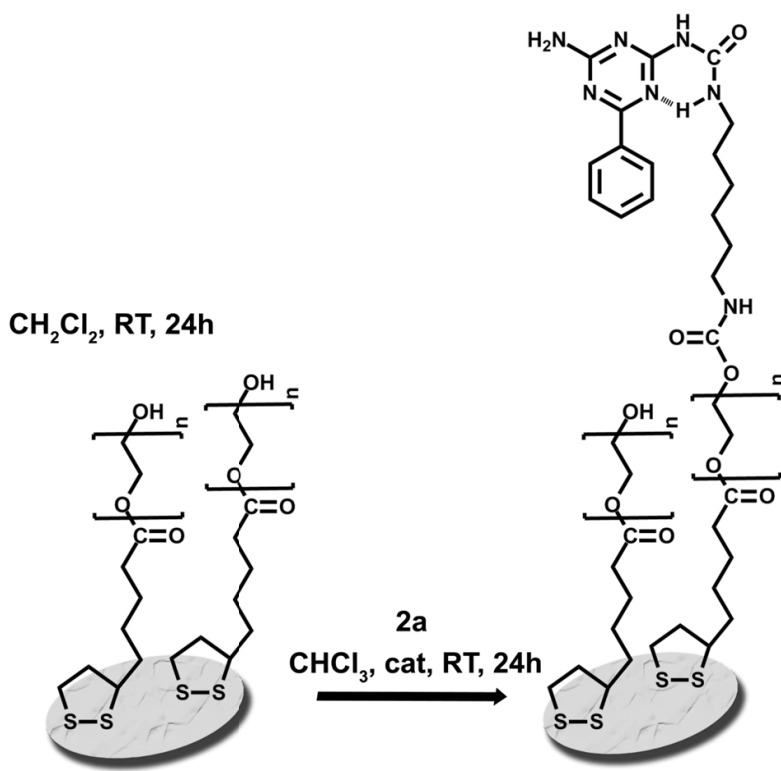


Figure 4- 4. Schematic of the immobilization of UAT-moieties on gold. A layer of PEG with exposed hydroxy-terminal groups is formed by adsorption of **1** from solution on gold, followed by reaction with **2a** to afford end-functionalized PEG-chains.

When this layer was immersed in the complementary PEGPPO-UAT **2c** solution (in CHCl_3) and rinsed afterwards, advancing and receding contact angles of $56^\circ \pm 2^\circ$ and $24^\circ \pm 2^\circ$ were measured. After thoroughly rinsing the sample with dimethylsulfoxide (DMSO) the advancing and receding contact angles were determined to be $71^\circ \pm 3^\circ$ and $49^\circ \pm 2^\circ$ respectively. These contact angle measurements already demonstrate the reversible character of the complexation, as the contact angle of the PEG-UAT layers is almost completely recovered after functionalization and subsequent rinsing with DMSO (which is known to break hydrogen-bonds).

FT-IR measurements in bulk and on the functionalized layer were performed to characterize the different layers as well (see Figure 4- 5). Reversible recognition could be controlled by rinsing with the proper choice of solvent (thorough DMSO or quick heptane/chloroform rinsing, data not shown).

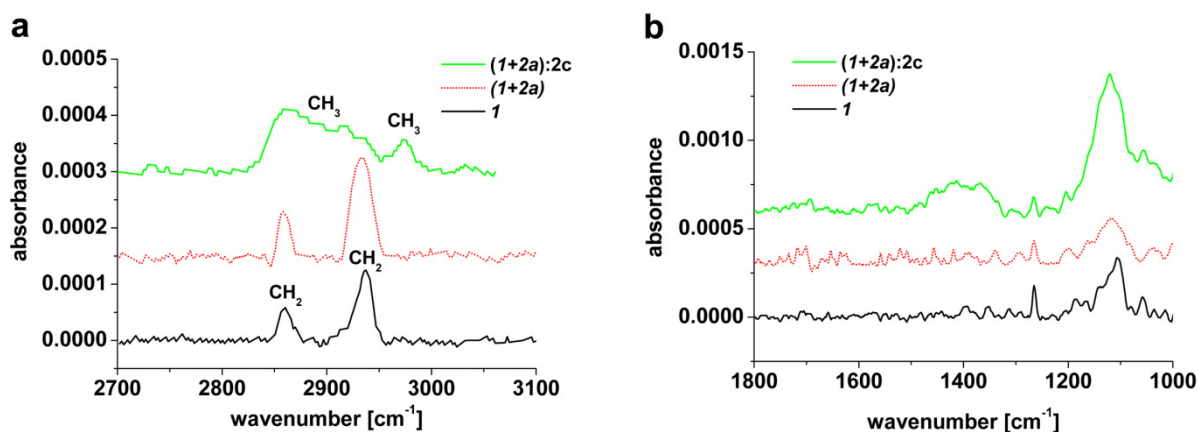


Figure 4- 5. (a,b) Grazing incidence reflection FT-IR spectra captured on gold of PEG **1** (bottom), PEG-UAT **1+2a** (middle) and after recognition of **1+2a** with the complementary PEGPPO-UAT **2c** (top), respectively. In the spectral region around 3000 cm^{-1} the CH_3 -groups of the PPO are clearly visible after reaction of **1+2a** with **2c**. The C-O-C stretching vibrations of the PEG-moieties are observed at wavenumbers of approximately 1100 cm^{-1} . The broad peaks at 1114 cm^{-1} and 1130 cm^{-1} indicate disordered PEG, *i.e.* PEG in a non-crystalline environment.

The PEG layer **1** on gold shows distinct but slightly shifted CH_2 stretching vibrations (compared to a rather crystalline octadecanethiol (ODT) layer), which can be attributed to a randomly coiled PEG-layer with additional CH_2 stretches from the liponic acid-ring^[11]. Since a sub-monolayer is obtained using this technique, PEG adopts different conformations on the surface which leads to peak broadening in the FT-IR spectrum. This is also apparent for the C-O-C stretches which broaden from a sharp peak at 1002 cm^{-1} (crystalline bulk) to a broad peak from 1002-1143 cm^{-1} . Although there is a small increase in the CH_2 intensity and small additional peaks from 1400-1600 cm^{-1} (CH_2 , urethane, phenyl and triazine stretches) the addition of UAT-moieties on top of the PEG-layer can only barely be detected.

As can be observed in Figure 4- 5, submersion of the UAT end-functionalized layer (**1+2a**) in a complementary PEGPPO-UAT solution (**2c**) and subsequent rinsing introduces CH_3 vibrations in the spectrum as well as a clear increase of the C-O-C stretches around 1100 cm^{-1} and 1325-1500 cm^{-1} (mostly additional CH_2 and CH_3 stretches). In addition, peak-broadening around 1100 cm^{-1} can also be observed due to PPO. The integral increase of the CH_2 - CH_3 region as well as the C-O-C region are both consistent with the interaction of the PEGPPO-tail.

XPS analysis^[12] of the PEG- (**1**) and PEG-UAT-layers (**1+2a**) provided evidence for the selective adsorption of the PEG-molecules to the gold surface, since the S(2p) binding energy was shifted to lower values (90% S-Au) compared to free sulfur bonds. Furthermore the C(1s) spectra in Figure 4- 6 displays a distinct C-O-C peak from the PEG-layer (286.8 eV) for both

samples. However some additional aliphatic carbon is detected which can be contributed to an adventitious carbon layer for PEG-substrates with low surface coverage^[12a].

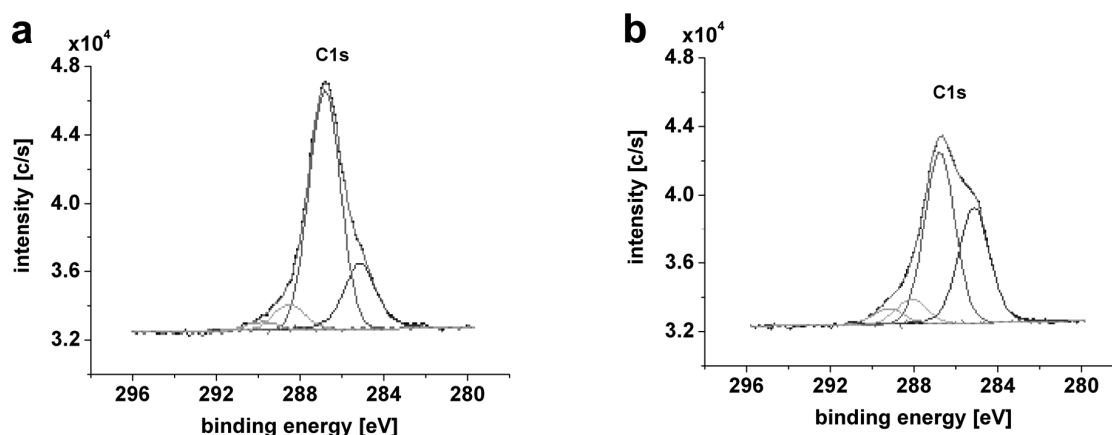


Figure 4- 6. C(1s) XPS spectra for the C1s peak for PEG- **1** (a) and PEG-UAT-substrates **1+2a** (b). The abundance of different carbon-bonds (aliphatic, C-O, C=O) was determined via spectral deconvolution. The C-O-C peaks from the PEG-layer located at 286.8 eV can be clearly discerned in both samples. *Note that the amount of aliphatic and aromatic carbon (285.0 eV) increases from a to b due to the reaction with the hydrogen-bonded moiety 2a in combination with adventitious carbon deposition^[12a].*

Using a correction for the added adventitious carbon, a surface coverage of the hydrogen-bonded moieties of 11 ± 6 % could be determined from the ratios of the atomic percentages of nitrogen with respect to sulfur determined from the corresponding N(1s) (binding energy, BE =400.5 eV) and S(2p) (binding energy, BE =162.5 eV) peaks^[12a] (see Appendix). So XPS measurements not only provided evidence for the correct assembly of the recognition platform, but also corroborated the low surface coverage of UAT-based recognition sites, which is essential for single molecule detection in an AFM-based SMFS experiment.

4.3 SINGLE MOLECULE CHARACTERIZATION OF UAT-BASED DIMERS

Reversible recognition was evident during the AFM-based SMFS experiments, where (UAT)₂ could be reversibly formed and broken, which is schematically displayed in Figure 4- 7. Reversible recognition AFM experiments^[13] were performed in hexadecane at different loading rates (see Figure 4- 8) and the rupture force of each single molecule rupture event was determined using the PEG-linker as a molecular extension length marker for single molecule

probing. This approach enabled us to determine various important parameters of the potential energy landscape along the unbinding axis, as was initially demonstrated by Bell^[14].

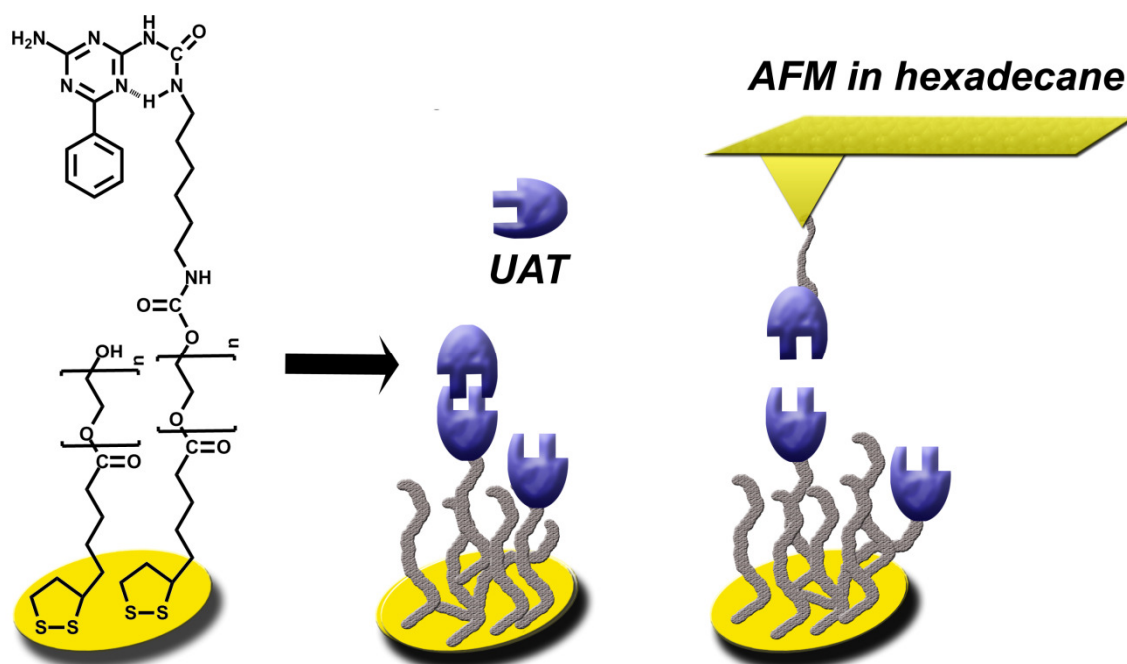


Figure 4- 7. Schematic of the modified gold surface. Reversible UAT-interactions can be studied by well-known bulk techniques like CA, FT-IR and XPS or AFM-based SMFS, which can be used *in situ*.

The single molecule rupture events were studied at different loading rates covering two orders of magnitude. For each loading rate the most probable rupture force f^* was determined using Gaussian fitting^[15]. A dimer-criterion was used where only rupture events corresponding to stretch lengths between 10 nm and 25 nm were considered based on the polydispersity of the PEG-linker and the attached UAT-moiety. According to ref 16 the polydispersity of the PEG-linker leads to an estimated error of 2% in f^* . The stretching of *individual* PEG chains was further confirmed by successfully fitting the force extension curves to the wormlike chain (WLC) model, which yielded loading rate-independent mean values for the persistence length (l_p) of 3.35 ± 0.49 Å, which agrees well with literature data. According to literature the helical state monomer length of PEG is 2.78 Å and a persistence length $l_p = 3.81 \pm 0.02$ Å (WLC) and Kuhn length $l_K = 7$ Å (from a fit to the freely joined chain (FJC) model) was previously reported^[17]. In our measurements the difference between the elasticity parameters obtained from fits to the WLC and FJC models is negligible since small extensions at low rupture forces were studied. In that case the following expressing for the relation of the persistence length and Kuhn length applies: $l_p = 1/2 \cdot l_K$. Hence the average persistence length of

$l_p = 3.35 \pm 0.49 \text{ \AA}$ is well in line with previously reported data and confirms that single chains were stretched and hence single molecule rupture events were probed.

The Bell-Evans approach of loading rate-dependent bond rupture analysis^[18] was applied to obtain a value for the thermal scale force f_β by fitting equation 4-1 via a Marquardt-Levenberg algorithm to the measured data (Figure 4- 8d). This approach is based on the fact that measurements are performed in far-from-equilibrium conditions where the chance of rebinding between receptor and ligand approaches zero, due to the flexible polymer linker. In this case the most probable rupture force of dissociation depends logarithmically on the applied loading rate. Therefore the kinetic off-time can be determined via these experiments. Although the kinetic on-time is not probed using the approach, the energy barrier between bound and unbound state can still be determined using an estimate for the diffusive relaxation time t_D ^[19]. According to the Bell-Evans theory the parameter f_β correlates the most probable rupture force f^* with the loading rate r_f (equation 4-1).

$$f^* = f_\beta \cdot \ln \frac{r_f}{r_f^0} \quad \text{Equation 4-1}$$

Using the fitted values of f_β and r_f^0 , the bond lifetime for the mechanical stress-free state $t_{off}(f=0)$ and consequently the dimer equilibrium constant K_{eq} are obtained via equations 4-2 until 4-5 (see also Chapter 2).

$$r_f^0 = \left(\frac{f_\beta}{t_D} \right) \cdot e^{-\Delta G/k_B T} \quad \text{Equation 4-2}$$

$$\frac{\Delta G}{k_B T} = -\ln(r_f^0) + \ln(f_\beta) - \ln(t_D) \quad \text{Equation 4-3}$$

$$\Delta G = -RT \ln K_{eq} \quad \text{Equation 4-4}$$

$$t_{off}(0) = \frac{f_\beta}{r_f^0} \quad \text{Equation 4-5}$$

where t_D is the diffusive relaxation time of the bound complex and R the molar gas constant.

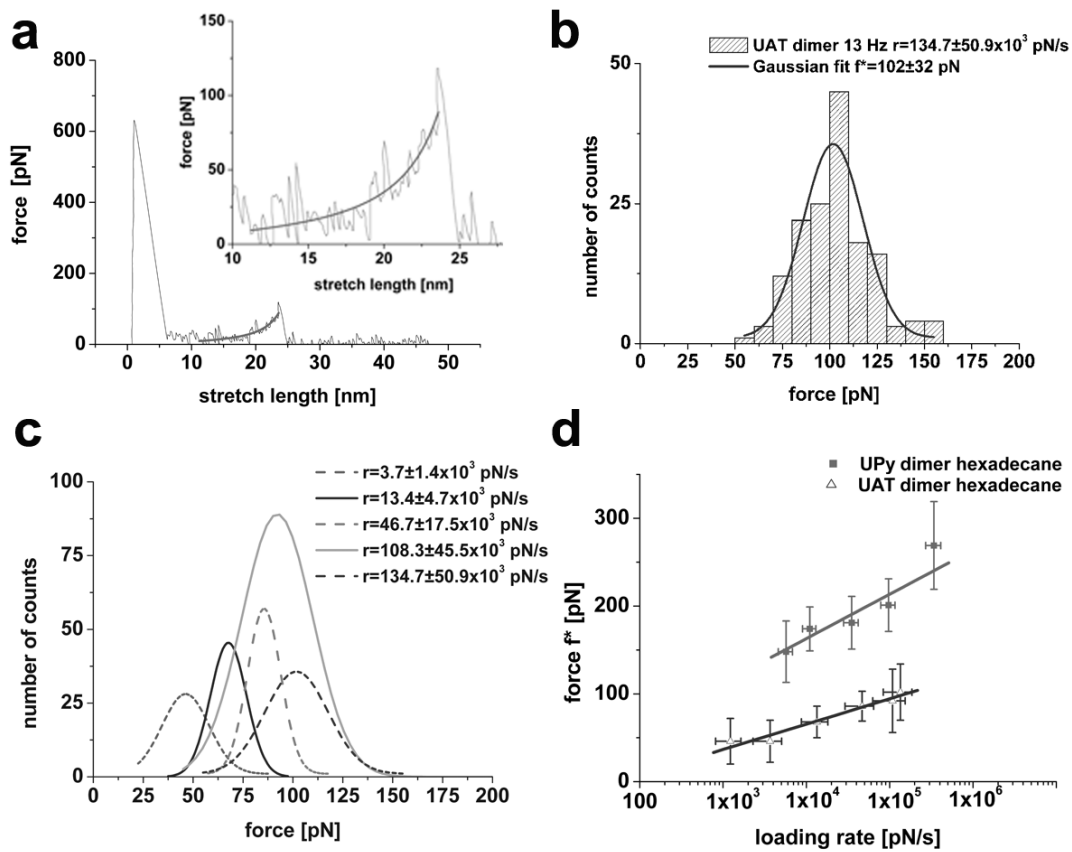


Figure 4- 8. SMFS data and analysis of reversible (UAT)₂ binding and bond rupture for different loading rates in hexadecane. (a) Force-extension curve showing a single molecule rupture event of (UAT)₂ at a loading rate r of $(134.7 \pm 50.9) \times 10^3$ pN/s; (b) histogram of bond rupture forces of (UAT)₂, most probable rupture force $f^* = 102 \pm 32$ pN; loading rate $r = (134.7 \pm 50.9) \times 10^3$ pN/s; (c) Gaussian fits of histograms of (UAT)₂ bond rupture for different loading rates ($r = (3.7 - 134.7) \times 10^3$ pN/s) in hexadecane; (d) loading rate-dependence of (UAT)₂ ($T = 303 \pm 2$ K, $f_\beta = 14.5 \pm 1.1$ pN; $t_{off}(0) = 100 \pm 80$ ms) in comparison to (UPy)₂ ($T = 303 \pm 2$ K; $f_\beta = 21.3 \pm 2.0$ pN; $t_{off}(0) = 3.9 \pm 0.9$ s).

The analysis described above provided the following parameters: $f_\beta = 14.5 \pm 1.1$ pN, $r_f^o = (1.5 \pm 0.9) \times 10^2$ pN/s. Based on these parameters the barrier width $x_\beta = 0.29 \pm 0.02$ nm, the bond lifetime at zero force $t_{off}(0) = 100 \pm 80$ ms and the dimer equilibrium constant $K_{eq} = (2 \pm 1) \times 10^7$ M⁻¹ were determined as well.

4.4 DISCUSSION AND CONCLUSION

The results obtained above regarding the binding constant of the UAT-based DADA array in hexadecane, clearly indicate that a substantial higher value for the binding constant was

measured $K_{dim} = (2 \pm 1) \times 10^7 \text{ M}^{-1}$ in comparison with the predicted values from currently available theoretical models^[7] ($K_{dim} = 310 \text{ M}^{-1}$ in chloroform; $K_{dim} \sim 3 \times 10^4 \text{ M}^{-1}$ in hexadecane). The data obtained here is however close in line with the measured binding constants for similar DADA arrays measured in chloroform by Sijbesma and Meijer^[20] by NMR binding studies ($K_{dim} = 2 \times 10^4 - 2 \times 10^5 \text{ M}^{-1}$) which would lead to extrapolated values of $K_{dim} \sim 2 \times 10^6 - 2 \times 10^7 \text{ M}^{-1}$ in hexadecane^[21]. This value can not be determined by any other technique currently available. The results could however be more closely evaluated using additional associating kinetics SMFS experiments which can provide complementary information on the kinetic on-rate as was for instance discussed by Hinterdorfer, Noy and more recently by Janshoff and co-workers^[22].

The substantially higher binding constant observed here for (UAT)₂ is attributed to the influence of the intermolecular hydrogen-bond which promotes a planar molecular geometry and significantly stabilizes the dimeric complex as was confirmed using 2D NMR (see Figure 4- 3). Since theoretical models are only based on primary and secondary hydrogen-bond interactions, the effect of the planarized molecular geometry is not covered in the currently available theoretical models. Furthermore the intramolecular hydrogen-bond stabilization effect is much more pronounced for this DADA array in comparison to the stronger DDAA quadruple hydrogen-bonded array. Recent literature also demonstrated the importance of geometric configuration^[23] and substituents^[24] in which a wide range of dimer equilibrium constants in chloroform could be obtained by fine-tuning the substituents attached to the same DDAA or DADA quadruple hydrogen-bonded array. Most notable is the dramatic 800-fold decrease of the dimer equilibrium constant of a UPy (DDAA) hydrogen-bonded array due to a directly attached oligomeric ethylene glycol chain^[24], which provides evidence for the major influence of substituents as (de)stabilizing factors on the dimer bond strength. The data presented here stress the need for direct measurements and more versatile models regarding hydrogen-bonding, since substituents and intramolecular/conformation hydrogen-bond stabilization can strengthen or weaken the hydrogen-bonded array over several orders of magnitude. Specifically when these systems are used for molecular motor applications^[25], small solvent effects could significantly influence the efficiency of these motors.

Nonetheless a major requirement for future application of AFM-based SMFS as a tool for automated bond strength analysis lies in a deeper understanding of the data analysis procedures as was recently discussed by Akhremitchev^[26]. Significant improvements of AFM-based SMFS measurements can still be made, such as easy access to a wide variety of

commercially available, smaller and softer cantilevers with precisely and accurately defined spring constants. The combination of established protocols for data analysis and low noise measurements will then enable small environmental fluctuations studies in close proximity of the single molecule rupture events and hence a new level of understanding of single molecule interactions. A combined approach of SMFS experiments in which kinetic on- and off-rates are determined would then become feasible and less time-consuming, which would lead to more accurate values for the dimer binding constant. This in turn can be of vital importance for future applications in areas like nanotechnology, biosensing and medicine.

4.5 MATERIALS AND METHODS

Materials. Anhydrous hexadecane (purity >99%, water <0.005%) and dibutyltindilaurate were purchased from Sigma-Aldrich (Steinheim, Germany) and used as received. Chloroform and dichloromethane (both stabilized with amylene) were purchased from Biosolve (Valkenswaard, The Netherlands). If not mentioned otherwise all other chemicals were purchased from Sigma-Aldrich.

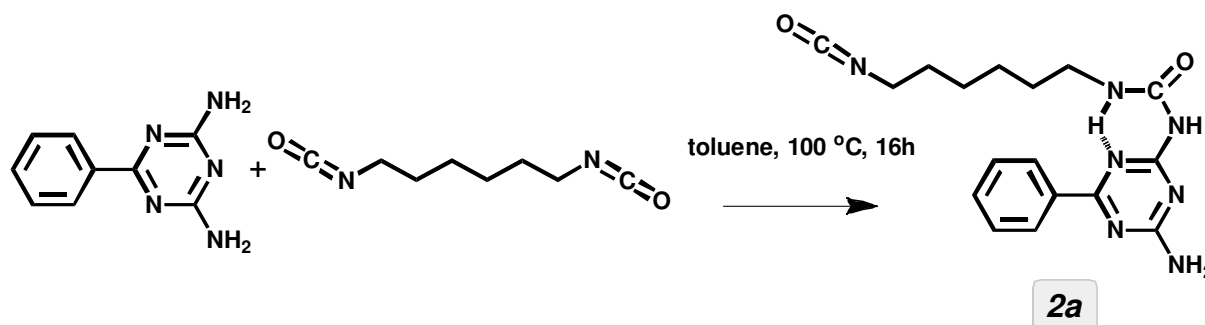
General characterization methods. The ^1H -NMR spectra were recorded on a Varian Unity 300. 300 MHz spectra were recorded in CDCl_3 and therefore chemical shifts are given relative to the residual CHCl_3 peak (7.26 ppm). 2D NMR and NMR on polymers were performed on a Bruker 600 MHz NMR. Electron spray mass spectrometry was performed on a Waters LCT (CV=15V). FT-IR bulk measurements were performed on a Bruker Alpha-P.

Synthesis.

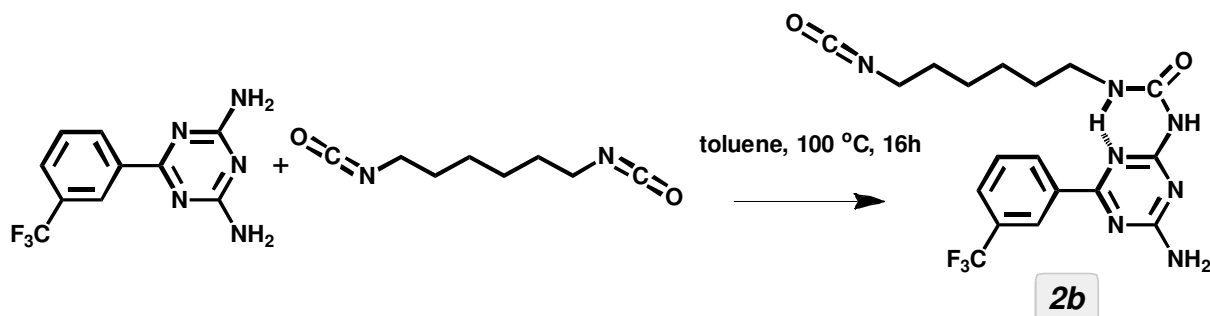


1. 1,2-Dithiolane-3-pentyl-derivatized PEG **1** was synthesized using published procedures^[9]. 1,2-Dithiolane-3-pentanoic acid (1.12 mmol) was added to a solution of PEG (3.46 mmol, $M_n = 1450$ g/mol, PDI = 1.1, as confirmed by independent GPC measurements), *N,N'*-dicyclohexylcarbodiimide (1.27 mmol), and 4-dimethylaminopyridine (1.6 mmol) in 50 ml anhydrous CH_2Cl_2 at 0°C . After 1 hour the solution was allowed to warm to room temperature and stirring was continued for 3 hours. After removal of the precipitated dicyclohexylurea by filtration and washing of the filtrate by 2 times 20 ml portions of 0.5 M NaCl and 2 times 20 ml portions NaHCO_3 , the product was dried overnight over anhydrous

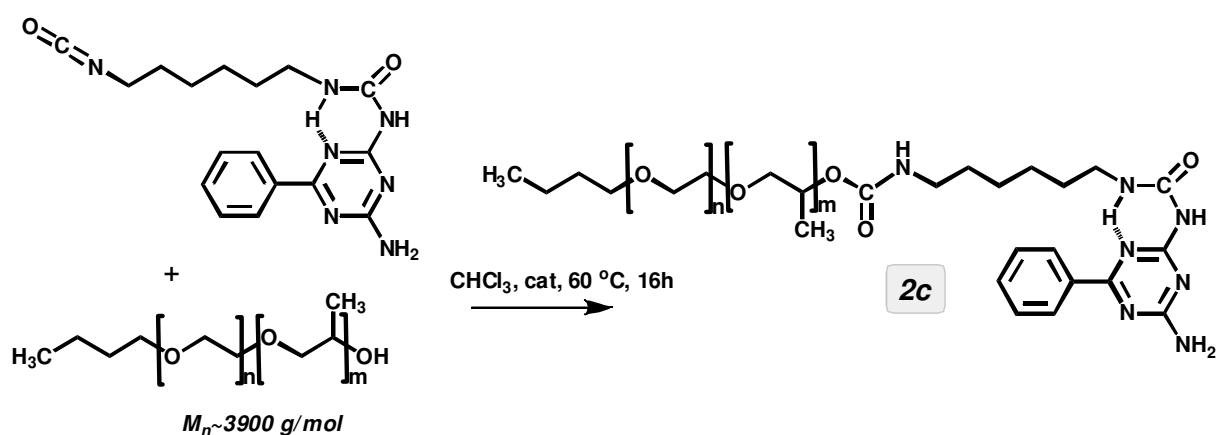
magnesium sulfate and concentrated using a rotary evaporator. The product was then dried under reduced pressure (yield 90%). $^1\text{H-NMR}$ (300 MHz, CDCl_3): δ 4.2 (t, 2H, $\text{CH}_2\text{-O-(C=O)}$), 3.7-3.5 (m, 130H, $\text{CH}_2\text{-CH}_2\text{-O}$, 1H, lipoic ring CH-S-S), 3.2-3.1 (m, 2H, lipoic ring $\text{CH}_2\text{-CH}_2\text{-S}$), 2.8 (br.s. 1H, $\text{CH}_2\text{-CH}_2\text{-OH}$), 2.5-2.4 (m, 2H, $\text{CH}_2\text{-(C=O)}$), 2.4, 1.9 (2H, lipoic ring $\text{CH}_2\text{-CH-S}$), 1.7-1.4 (m, 6H, $\text{CH}_2\text{-CH}_2\text{-CH}_2$). FT-IR: $3550\text{-}3300\text{ cm}^{-1}$ (ν_{OH} , br), $2940\text{-}2850\text{ cm}^{-1}$ (ν_{CH_2} , m), 1732 cm^{-1} ($\nu_{\text{C=O}}$, w), 1102 cm^{-1} ($\nu_{\text{C-O-C}}$, s), 946 cm^{-1} ($\nu_{\text{CH}_2}, \nu_{\text{OH}}$, m), 841 cm^{-1} ($\nu_{\text{C-O-C}}, \nu_{\text{CH}_2}$ m), 528 cm^{-1} ($\nu_{\text{CH}_2}, \nu_{\text{S-S}}$, w).



2. 1-(4-Amino-6-phenyl-1,3,5-triazin-2-yl)-3-(6-isocyanatohexyl)urea **2a** was synthesized using a slightly adapted published procedure¹. 2,4-diamino-phenyl-1,3,5-triazine 2.04 gram (0.11 mol) was reacted with 10 ml of 1,6-diisocyanatohexane as described by Sijbesma and Meijer, however excess dry toluene (40 ml) was added to improve mixing during the reaction. The system was heated to 100 °C and refluxed overnight. *The reactivity of phenyl-functionalized aminotriazine towards the isocyanate group is strongly reduced after monosubstitution which allows the monosubstituted 1-(4-amino-6-phenyl-1,3,5-triazin-2-yl)-3-(6-isocyanatohexyl)urea to be synthesized even with an excess of 1,6-diisocyanatohexane.* After cooling down the excess 1,6-diisocyanatohexane was removed by washing the reaction mixture with heptane over a glass filter. The resulting white powder was dried in vacuo. Isolated yield 2.34 gram (0.0065 mol) = 60 %. $^1\text{H-NMR}$ (300 MHz, CDCl_3), δ 10.22 (s, 1H, NH/N H-bond), 9.91 (s, 1H, NH/N intra H-bond), 9.31 (s, 1H, NH(from NH_2)/N H-bond), 8.20 (d, 2H, ortho), 7.60-7.48 (t, 3H, meta,para), 5.48 (s, 1H, HNH), 3.45 (q, 2H, $(\text{C=O})\text{-NH-CH}_2$), 3.25 (t, O=C=N-CH_2 , 2H), 1.7-1.3 (m, 8H, $\text{O=C=N-CH}_2\text{-(CH}_2\text{)}_4\text{-CH}_2\text{-NH}$), specific hydrogen interactions were determined by 2D NMR (^1H ROESY and COSY); mass (ESP), $m/z=356.2$ ($\text{M}+\text{H}$) and 711.4 (M_2+H), calculated for $\text{C}_{17}\text{H}_{21}\text{N}_7\text{O}_2 = 355.18\text{ g/mol}$; FT-IR: 3400 cm^{-1} ($\nu_{\text{NH},1\text{O}_{\text{amine}}}$, w), $3300\text{-}3200\text{ cm}^{-1}$ ($\nu_{\text{NH},2\text{O}_{\text{amine}}}$, w), $2930\text{-}2856\text{ cm}^{-1}$ (ν_{CH_2} , w), 2258 cm^{-1} ($\nu_{\text{N=C=O}}$, m), 1656 cm^{-1} (ν_{urethane} , m), 1596 cm^{-1} (ν_{phenyl} , m), 1557 cm^{-1} (ν_{amidIII} , m), 1511 cm^{-1} ($\nu_{\text{phenyl/as.triazine}}$, m), 1460 cm^{-1} (ν_{CH_2} , m).



3. 1-(4-Amino-6-(3-(trifluoromethyl)phenyl)-1,3,5-triazin-2-yl)-3-(6-isocyanatohexyl)urea **2b** was synthesized as described above using 1 gram (4 mmol) 6-(3-(trifluoromethyl)phenyl)-1,3,5-triazine-2,4-diamine as a starting material. Dry toluene (20 ml) and 10 ml of 1,6-diisocyanatohexane was added. The system was heated to 100 °C and refluxed overnight. After cooling down excess 1,6-diisocyanatohexane was removed by washing the reaction mixture with heptane over a glass filter. The resulting white powder was dried in vacuo. Isolated yield = 71.5 %. ¹H-NMR (300 MHz, CDCl₃): δ 10.23 ((s, 1H, NH/N H-bond), 9.72 (s, 1H, NH/N intra H-bond), 9.40 (s, 1H, NH(from NH₂)/N H-bond), 8.44 (s,d,2H, ortho), 7.82 (d, 1H, CF₃C-CH=CH (para)), 7.63 (t, 1H, HC=CH-CH(meta)), 5.53 (s, 1H, HNH), 3.45 (q, 2H, (C=O)-NH-CH₂), 3.28 (t, 2H, O=C=N-CH₂), 1.7-1.3 (m, 8H, O=C=N-CH₂-(CH₂)₄-CH₂-NH); mass (ESP), m/z=424.2 (M+H) and 847.5 (M₂+H), calculated for C₁₈H₂₀F₃N₇O₂ = 423.16 g/mol. FT-IR: 3396 cm⁻¹ (ν_{NH,1O}amine, w), 3300-3200 cm⁻¹ (ν_{NH,2O}amine, w), 2939-2862 cm⁻¹ (ν_{CH2},w), 2259 cm⁻¹ (ν_{N=C=O}, m), 1639 cm⁻¹ (ν_{urethane}, m), 1582cm⁻¹ (ν_{amidII}, m), 1520 cm⁻¹ (ν_{phenyl/as.triazine}, m), 1468cm⁻¹ (ν_{CH2}, m), 1321 cm⁻¹ (ν_{CF3}, w), 1164 cm⁻¹ (ν_{CF3}, w), 1126 cm⁻¹ (ν_{CF3}, w).



4. *N*-(6-(3-(4-amino-6-phenyl-1,3,5-triazin-2-yl)ureido)hexyl)acetamide-*ran*-PEGPPO was synthesized starting from 2.3287 gram of poly(ethylene glycol-*ran*-propylene glycol) monobutyl ether *M_n* ~3900 (PDI~1.1, 0.54 mmol) which was added to a roundbottom flask

and dried by 3 times azeotropic distillation over anhydrous toluene. Afterwards a slight excess of 1-(4-amino-6-phenyl-1,3,5-triazin-2-yl)-3-(6-isocyanatohexyl)urea **2a** 0.2107 gram (0.59 mmol), 2 drops of catalyst dibutyltin dilaurate and 40 ml of dry chloroform was added under nitrogen environment. The whole mixture was heated to 60 °C and the reaction was left stirring overnight under argon atmosphere. Afterwards 1 gram of silica (Kieselgel 60) and 2 drops of catalyst were added to remove unreacted isocyanate-endfunctionalized urea-aminotriazine and the reaction was left to take place over 4 hours after which no residual isocyanate peak could be detected via FT-IR. After cooling down, the silica-bound material was removed by washing the reaction mixture with chloroform over a glass filter. The resulting liquid like white product was dried in vacuo (yield = 83 %). ¹H-NMR (600 MHz, CDCl₃), 9.91 ppm (s, 1H, NH/N intra H-bond), 8.10 (d, 2H, ortho), 7.60-7.48 (t, 3H, meta,para), 3.7-3.6(m, CH₂-O PEGPPO) 1.7-1.3 (m, O=C-NH-CH₂-(CH₂)₄-CH₂-NH and PEGPPO-endgroup), 1.16 (m, CH₃, [PPO]m), 0.9 ppm (m,CH₃ PEGPPO-endgroup); *some PEGPPO peaks overlap with UAT and can not be accurately assigned*; FT-IR 2973-2867 cm⁻¹ (ν_{CH3},ν_{CH2},w), 1656 cm⁻¹ (ν_{urethane}, w), 1603 cm⁻¹ (ν_{phenyl}, w), 1523 cm⁻¹ (ν_{phenyl/as.triazine}, w), 1457cm⁻¹ (ν_{CH2}, w), 1373cm⁻¹ (ν_{alkane}, m), 1247 cm⁻¹ (ν_{alkane}, w), 1094 cm⁻¹ (ν_{C-O-Csym}, s), 748 cm⁻¹ (ν_{aromatic}, s).

Preparation of Substrates. Gold substrates (200 nm gold on top of 3.5 nm Ti deposited onto glass substrates) were purchased from Ssens BV (Hengelo, The Netherlands). Prior to use, these substrates were cleaned in piranha solution [2:1 H₂SO₄ (Sigma-Aldrich)/H₂O₂ (30 %, Fluka) by volume], then rinsed three times with Milli-Q water and ethanol, and subsequently rinsed with the pure solvent. The samples were directly transferred to the monolayer solution preventing any direct contact with air. *Caution: Piranha solution should be handled with extreme caution. It has been reported to detonate unexpectedly.*

Preparation and Characterization of Monolayers. Monolayers were prepared by immersing (annealed) gold substrates into a dilute solution of the corresponding compound for at least 16 hours (typical concentration: 1 mM). See Figure 4- 4 for a reaction scheme for the preparation of the different layers. After rinsing in pure solvent and drying in a nitrogen stream, the measurements were performed with minimum delay. The layers were characterized by contact angle measurements, XPS, FT-IR spectroscopy and AFM.

Grazing incidence FT-IR spectra were recorded at room temperature on a Bruker Vertex 70v vacuum FT-IR spectrometer equipped with a MCT detector (angle of incidence 80

degrees). Background spectra were recorded on deuterated octadecanethiol (ODT) functionalized gold surfaces.

Dynamic contact angle measurements were performed at room temperature on a OCA-20 contact angle analyzer using the dynamic sessile drop method. The advancing and receding contact angles were determined using video based analysis and build-in software. The specified contact angles provide average values determined at several spots on the functionalized gold surfaces.

X-ray Photoelectron Spectroscopy. XPS spectra were recorded using a PHI Quantera SXM (scanning XPS microprobe) from Physical Electronics. Spectra were acquired using a monochromated X-ray beam (Al K α , monochromatic at 1486.6 eV) with the following beam specification: 100- μ m-diameter; 25 W; 45° take-off angle. Atomic concentrations were determined by numerical integration of the relative peak areas in the detailed element scans using the following sensitivity factors: Au(4f) [6.805], C(1s) [0.314], N(1s) [0.499], O(1s) [0.733], S(2p) [0.717].

Atomic Force Microscopy. The measurements were carried out with a Veeco/Bruker Multimode with a NanoScope V controller (Veeco/Bruker, Santa Barbara, CA). The calibration of the AFM scanner in the z direction was carried out using a set of three vertical calibration standards (TGZ 01-03) with step heights of 25.5, 104, and 512 nm, respectively (Silicon-MDT, Moscow, Russia). A double-sided gold coated MikroMasch rectangular beam cantilever (CSC38) was used (the spring constant was determined by the thermal noise method^[27] to be $k = 0.133 \pm 0.014$ N/m).

APPENDIX

Additional bulk characterization data of the synthesized products (FTIR, XPS) and AFM-based SMFS data is presented below.

FTIR analysis

FTIR bulk characterization of the in Figure 4- 1 displayed dithiolane-derivatized PEG **1** and the self-complementary receptor molecules **2a-c** is displayed here.

Peak assignment of the FT-IR spectra can be found in the experimental section (paragraph 4.5).

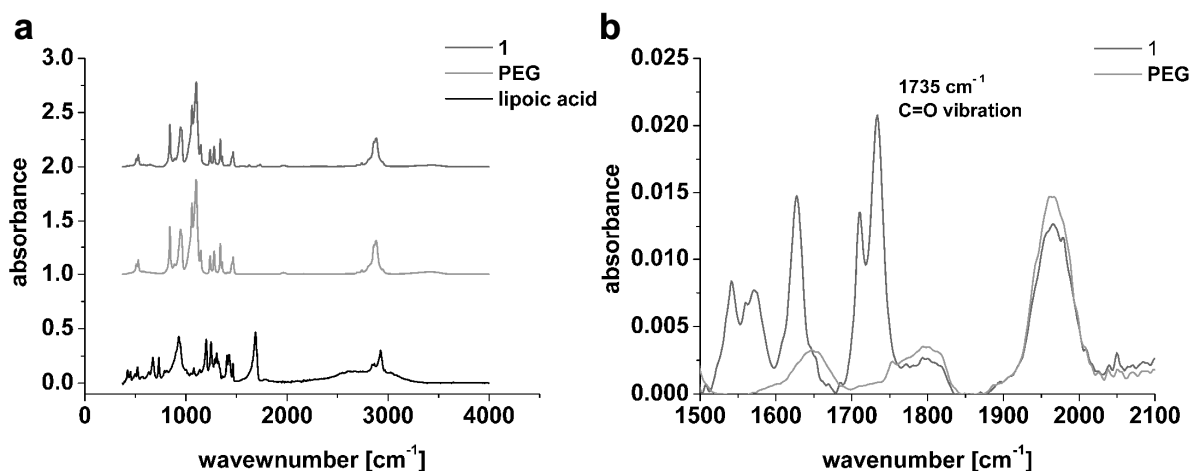


Figure 4- 9. (a) Bulk FT-IR spectra of synthesized product **1** from the starting materials (lipoic acid and PEG) and a zoom (b) in the region for the carboxylic acid vibrations to provide evidence for the coupling reaction. *For peak identifications see previous experimental section.*

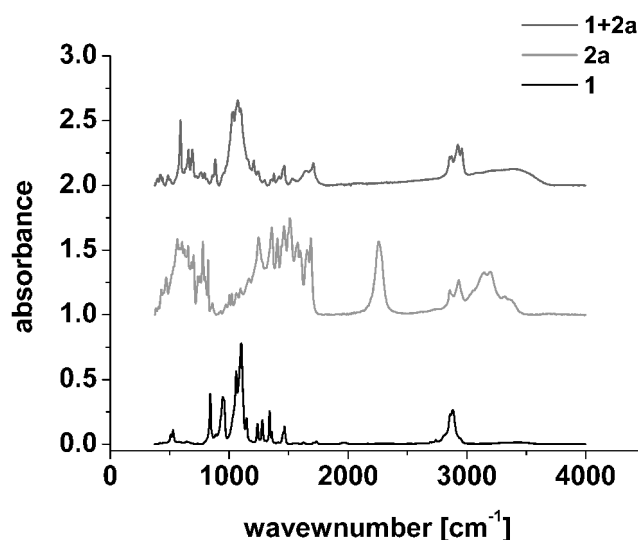


Figure 4- 10. Bulk FT-IR spectra of synthesized product **1+2a** via isocyanate chemistry. The isocyanate peak around 2256 cm^{-1} clearly disappears after the reaction and peak broadening of the PEG C-O-C vibration around 1100 cm^{-1} can be observed as well, due to the loss of crystallinity. *For peak identifications see previous experimental section.*

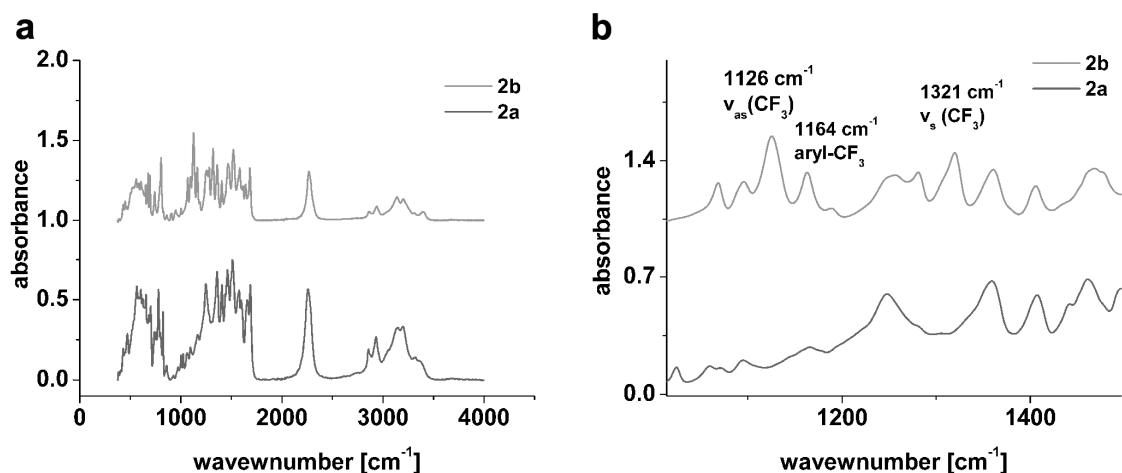


Figure 4- 11. (a) Bulk FT-IR spectra of synthesized product **2a** (UAT) and **2b** (UAT- CF_3); (b) zoom in the region for the CF_3 vibrations which can clearly be identified from the spectrum. *For peak identifications see previous experimental section.*

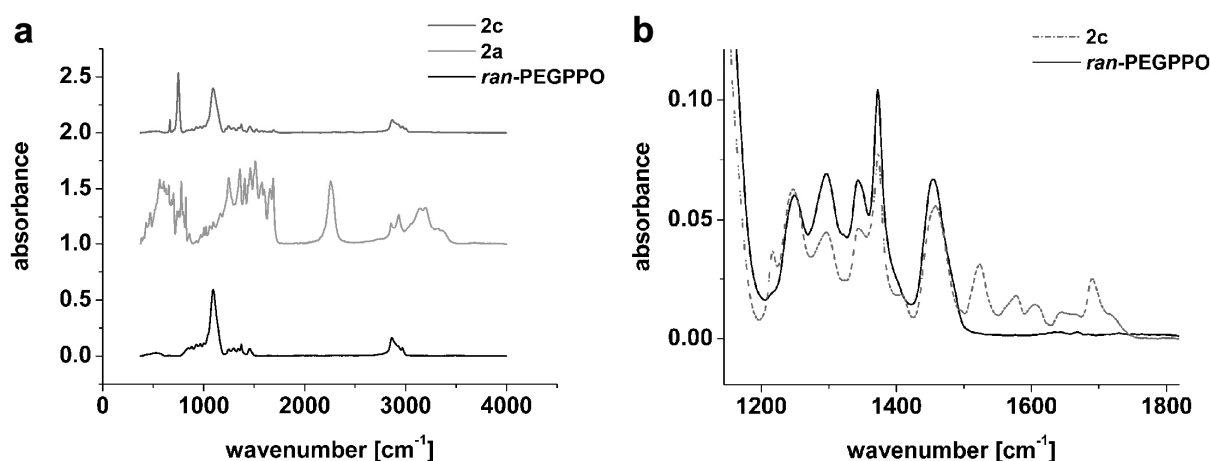


Figure 4- 12. (a) Bulk FT-IR spectra of ran-PEGPPO and the synthesized products **2a** (UAT) and **2c** (UAT-PEGPPO); (b) zoom in the region for the phenyl, triazine, urethane, and $\text{C}=\text{O}$ vibrations of the UAT-moiety. *For peak identifications see previous experimental section.*

X-ray photoelectron spectroscopy

XPS was used to determine the composition of the self-assembled layers. $\text{Au}(4f)$, $\text{C}(1s)$, $\text{N}(1s)$, $\text{O}(1s)$, $\text{S}(2p)$ signals were studied in detail. Peak positions were aligned using the binding energy peaks of $\text{Au}(4f_{7/2})$ electrons at 84.5 eV. Effective coupling of the PEG-chains to the gold surface could be observed (Au-S in $\text{S}(2p)$ spectrum) and the abundances of the different atoms were analyzed (see Tables below and Figure 4- 14). To be able to obtain reasonably dense PEG-layers and detect the added UAT-hydrogen-bonded moieties the

reaction times were substantially prolonged in several cases in comparison to samples prepared for single molecule detection. Within error margins the abundances detected on the surface are as expected from theoretical calculations (see Table 4- 1 until 4- 6), although slightly more sulfur is detected for all samples. In the PEG-UAT **1+2a** sample additional nitrogen is clearly present (see Figure 4- 14).

Since a small nitrogen contamination can be observed on a blank and the PEG sample as well, this will be taken into account for the surface coverage calculations on the PEG-UAT-layer. Taking into account the polydispersity of the PEG-chains, the distribution of C1s peaks should be as follows:

aliphatic C	8.6 - 10.1 %
C-O	88.4 - 90.1 %
C=O	remaining % (only 1 bond)

The actual distribution for the PEG-layer **1** is:

aliphatic C	22.4 %
C-O	70.1 %

	%	error	theoretical
C1s [0.314]	0.63	0.04	0.66
O1s [0.733]	0.33	0.01	0.32
S2p [0.717]	0.04	0.01	0.02

Table 4- 1. Surface composition of PEG layer **1** on gold. Only C, O and S signals are taken into account and a comparison with theoretical values is presented.

	%	error	theoretical
C1s [0.314]	0.62	0.03	0.66
O1s [0.733]	0.32	0.01	0.32
S2p [0.717]	0.04	0.01	0.02
N1s [0.499]	0.02	0.01	0

Table 4- 2. Surface composition of PEG layer **1** on gold. C, O, N and S signals are taken into account and a comparison with theoretical values is presented.

So at least 12 % of aliphatic carbon is detected that can not be contributed to the molecules on the surface. This is well-known phenomenon and often reported in literature^[12a] as an

“adventitious carbon layer”. Depending on the thickness of the layer under investigation the influence of this “adventitious carbon layer” is more or less pronounced.

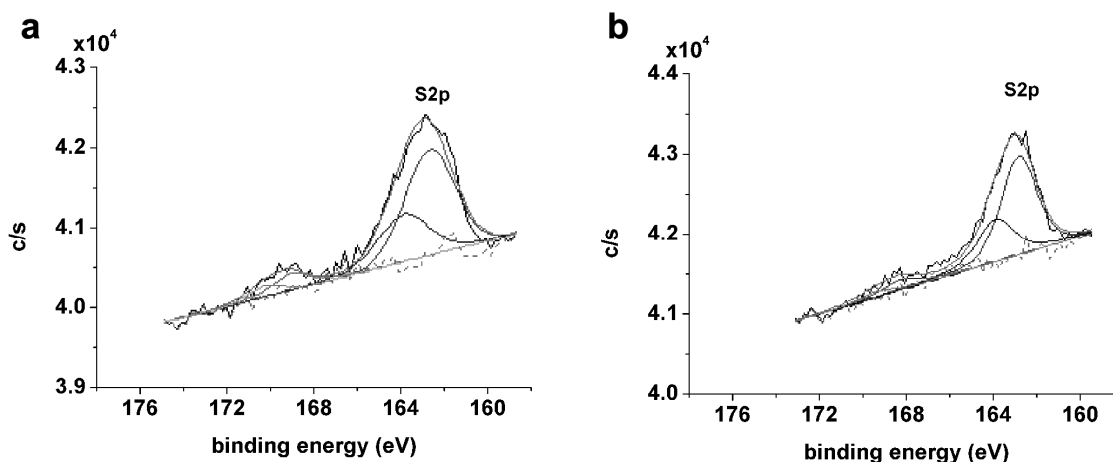


Figure 4- 13. XPS data for S_{2p} signals of (a) PEG **1** and (b) PEG-UAT **1+2a** covered gold surfaces. *The large abundance of thiol-gold bonds (S-Au, relative shift to free S) provides evidence for the adsorption of the thiol end-functionalized PEG.*

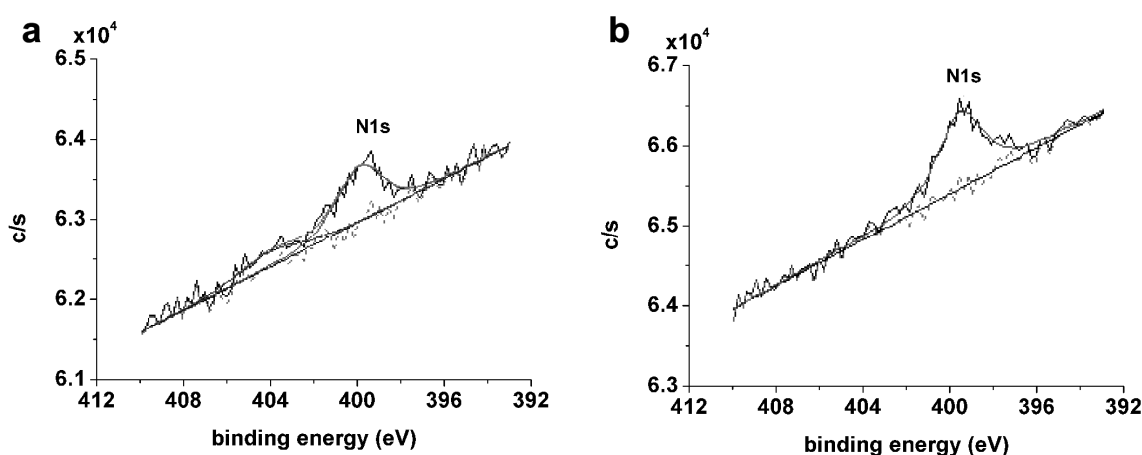


Figure 4- 14. XPS data for N_{1s} signals of (a) PEG **1** and (b) PEG-UAT **1+2a** covered gold surfaces.

Using a correction for the adventitious carbon layer (determined via a blank measurement and the relative layer thickness) gives the following numbers for the C_{1s} distribution.

	PEG 1	PEG 1 theory	PEG 1 error (%)
Aliphatic carbon	11.4	10.0	12.2
C-O	88.6	89.0	0.4

Table 4- 3. Corrected distribution of the C_{1s} signal for aliphatic and C-O bonds for the PEG **1**. Using the data for the adventitious carbon layer the aliphatic carbon and C-O distributions can be calculated.

The XPS analysis for the PEG-UAT-layer **1+2a** gives the following results. First the analysis of a gold surface with short reaction time is presented (which can be used for single molecule detection).

	%	error	theoretical
C1s [0.314]	0.67	0.01	0.66-0.67
O1s [0.733]	0.28	0.02	0.26-0.32
S2p [0.717]	0.05	0.00	0.02
N1s [0.499]	0.02	0.02	0-0.06

Table 4- 4. Surface composition of PEG-UAT-layer **1+2a** on gold short reaction times (for single molecule experiments). C, O, N and S signals are taken into account and a comparison with theoretical values is presented depending on the surface coverage. *Note that the nitrogen signal lies within the measured error margin.*

Since the nitrogen signal lies within the error margins of the detection sensitivity of the XPS, a second sample was prepared with substantially prolonged reaction times. Now the amount of nitrogen on the surface clearly exceeds the detection limit.

	%	error	theoretical
C1s [0.314]	0.69	0.03	0.66-0.67
O1s [0.733]	0.26	0.01	0.26-0.32
S2p [0.717]	0.05	0.01	0.02
N1s [0.499]	0.04	0.01	0-0.06

Table 4- 5. Surface composition of PEG-UAT-layer **1+2a** on gold with substantially prolonged reaction times. C, O, N and S signals are taken into account and a comparison with theoretical values is presented depending on the surface coverage.

From the data in Table 4- 5 a surface coverage of $11 \pm 6\%$ can be determined for this sample. The “adventitious carbon effect” is even more obvious in the C1s spectrum of the PEG-UAT **1+2a** sample where a surface coverage of $11 \pm 6\%$ would lead to an aliphatic/aromatic carbon contribution of $10 \pm 2\%$. However an actual percentage aliphatic/aromatic carbon of 37% is determined. Using the data for the adventitious carbon layer the aliphatic carbon and C-O distributions can be calculated again, although errors get larger due to the fact that this layer was thinner than the PEG-layer **1**. Corrections for a thinner layer logically introduce more errors as is demonstrated in Table 4- 6.

	PEG-UAT 1+2a	PEG-UAT 1+2a theory	PEG-UAT 1+2a error (%)
Aliphatic carbon	25.1	9.6	61.6
C-O	74.9	79.8	6.5

Table 4- 6. Corrected distribution of the C1s signal for aliphatic/aromatic and C-O bonds for the PEG-UAT **1+2a**.

AFM force spectroscopy data

Single molecule dimer rupture events were selected using a dimer criterium, based on the most probable monomer length of the PEG-UAT-moiety (10.3 - 12.2 nm, PDI of 1.1; $n = 30$ -36 monomer units).

Rupture events between 10 and 25 nm were processed and wormlike chain fitting was performed to confirm a single molecule rupture event.

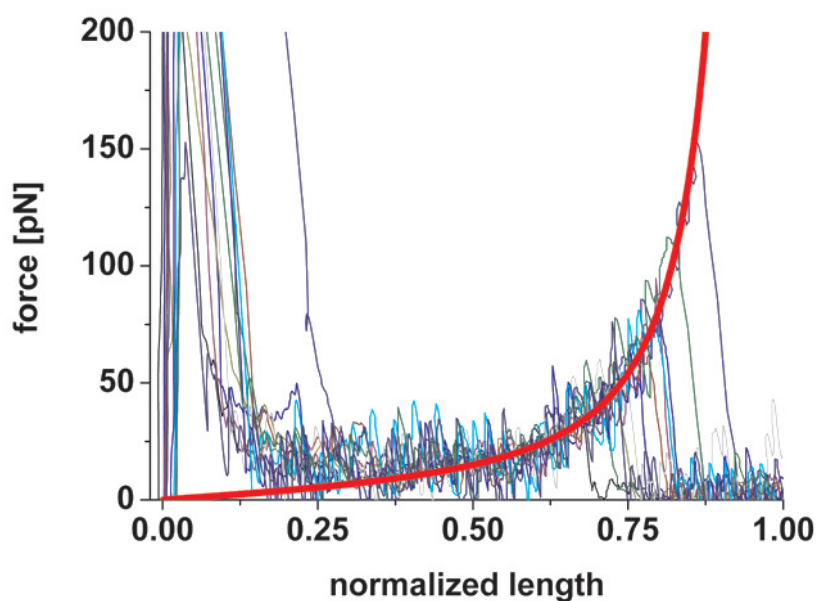


Figure 4- 15. Normalized force curves of $(\text{UAT})_2$ rupture events for different loading rates. The fitted persistence length matches the reported values for the persistence length for PEG in literature (overlay curve)^[17]. The average persistence length for all loading rates is $3.35 \pm 0.49 \text{ \AA}$. Reported values in literature: for wormlike chain fitting persistence length $l_p = 3.81 \pm 0.02 \text{ \AA}$ ^[17a] and freely jointed chain fitting Kuhn's length $l_K = 2 \cdot l_p = 7 \text{ \AA}$ ^[17b].

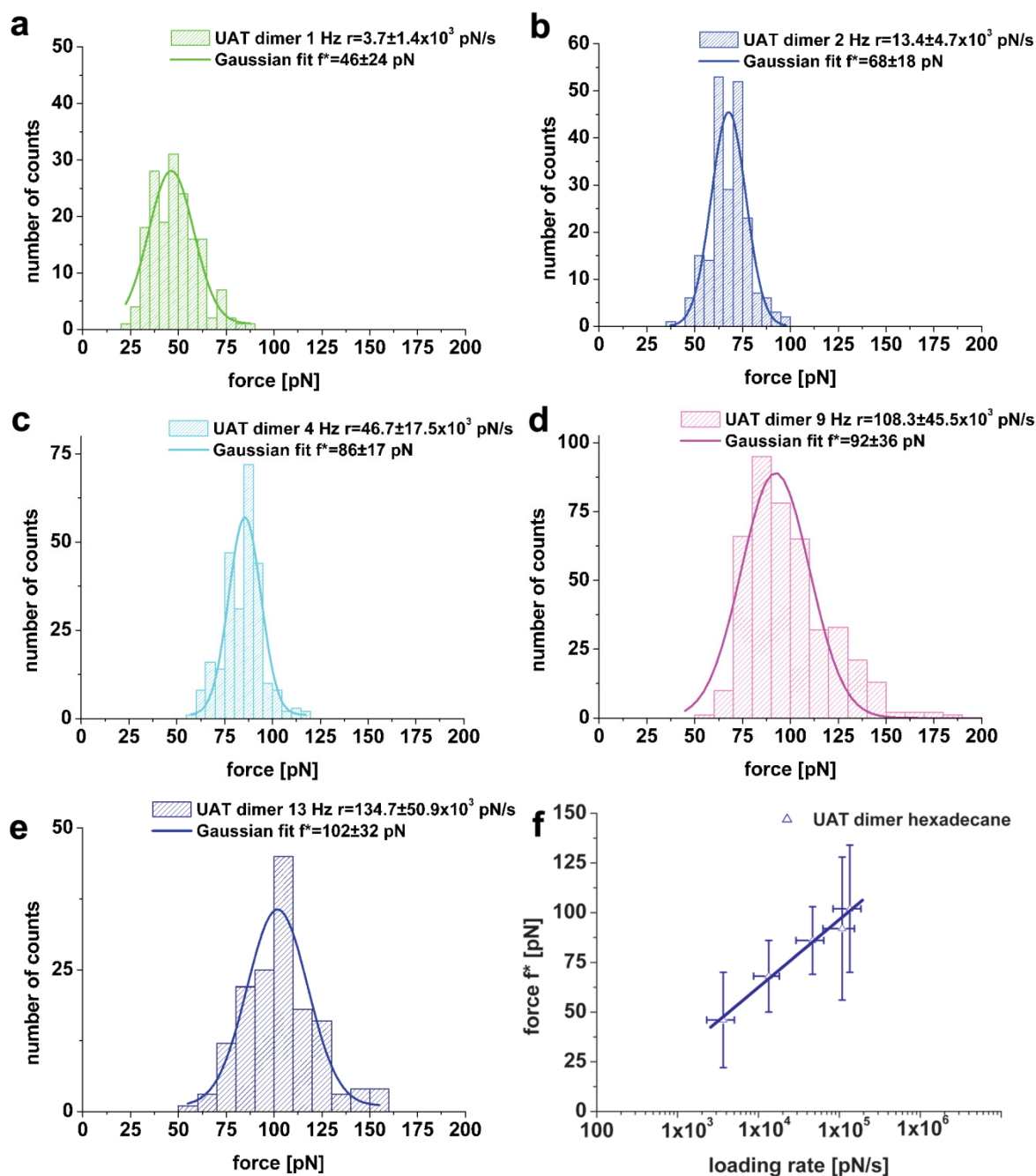


Figure 4- 16. (a-e) Histograms of DADA hydrogen-bond rupture events for different loading rates at $T = 303 \pm 2$ K. (a) $r = (3.7 \pm 1.4) \times 10^3$ pN/s, $f^* = 46 \pm 24$ pN; (b) $r = (13.4 \pm 4.7) \times 10^3$ pN/s, $f^* = 68 \pm 18$ pN; (c) $r = (46.7 \pm 17.5) \times 10^3$ pN/s, $f^* = 86 \pm 17$ pN; (d) $r = (108.3 \pm 45.5) \times 10^3$ pN/s, $f^* = 92 \pm 36$ pN; (e) $r = (134.7 \pm 50.9) \times 10^3$ pN/s, $f^* = 102 \pm 32$ pN; (f) loading rate-dependent rupture force for (UAT)₂ in hexadecane.

REFERENCES AND NOTES

1. Folmer, B.J.B.; Sijbesma, R.P.; Versteegen, R.M.; Van der Rijt, J.A.J.; Meijer, E.W. *Adv. Mater.* **2000**, *12*, 874-878.

2. Montarnal, D.; Tournilhac, F.; Hidalgo, M.; Couturier, J.-L.; Leibler, L. *J. Am. Chem. Soc.* **2009**, *131*, 7966-7968.
3. Vancso, G.J.; *Angew. Chem., Int. Ed.* **2007**, *46*, 3794-2796.
4. (a) Zou, S.; Schönherr, H.; Vancso, G.J. *J. Am. Chem. Soc.* **2005**, *127*, 11230-11231; (b) Zou, S.; Schönherr, H.; Vancso, G.J. *Angew. Chem. Int. Ed.* **2005**, *44*, 956-959; (c) Embrechts, A.; Schönherr, H.; Vancso, G.J. *J. Phys. Chem B* **2008**, *112*, 7359-7362.
5. Guan, Z.; Roland, Z.T.; Bai, J.Z.; Ma, S.H.; McIntire, T.M.; Nguyen, M. *J. Am. Chem. Soc.* **2004**, *126*, 2058-2065.
6. (a) Schipper, E.F.; Rauchalles, S.; Kooyman, R.P.H.; Hock, B.; Greve, J. *Anal. Chem.* **1998**, *70*, 1192-1197; (b) Nakamura, C.; Hasegawa, M.; Shimada, K.; Shirai, M.; Miyake. *J. Biotechnol. Bioprocess Eng.* **2000**, *5*, 413-417; (c) Fuchiwaki, Y.; Shimizu, A.; Kubo, I. *Anal. Sci.* **2007**, *23*, 49-53.
7. Sartorius, J.; Schneider, H.-J. *Chem-Eur. J.* **1996**, *2*, 1446-1452.
8. Zou, S.; Zhang, Z.; Förch, R.; Knoll, W.; Schönherr, H.; Vancso, G.J. *Langmuir* **2003**, *19*, 8618-8621.
9. Neises, B.; Steglich, W. *Organic Syntheses Vol. 7*; **1990**, p. 93-94.
10. Kang, J.F.; Liao, S.; Jordan, R. Ulman, A. *J. Am. Chem. Soc.* **1998**, *120*, 9662-9667.
11. (a) Miyazawa, T.; Fukushima, K.; Ideguchi, Y. *J. Chem. Phys.* **1962**, *37*, 2764-2776; (b) Valiokas, R.; Svedhem, S.; Svensson, S.C.T.; Liedberg, B. *Langmuir* **1999**, *15*, 3390-3394; (c) Naumann, R.; Schiller, S.M.; Giess, F.; Grohe, B.; Hartman, K.B.; Kärcher, I.; Lübben, J.; Vasilev, V.; Knoll, W. *Langmuir* **2003**, *19*, 5435-5443; (d) Vanderah, D.J.; Pham, C.P.; Springer, S.K.; Silin, V.; Meuse, C.W. *Langmuir* **2000**, *16*, 6527-6532; (e) Kim, C.-H.; Kim, D.-W.; Cho, K.Y. *Polym. Bull.* **2009**, *63*, 91-99; (f) Buchbinder, A.M.; Weitz, E.; Geiger, F.M. *J. Phys. Chem. C* **2010**, *114*, 554-566.
12. (a) Sharma, S.; Johnson, R.W.; Desai, T.A. *Biosens. Bioelectron.* **2004**, *20*, 227-239; (b) Moulder, J.F.; Stickle, W.F.; Sobol, P.E.; Bomben, K.D. *Handbook of X-ray Photoelectron Spectroscopy*, Perkin-Elmer Corporation: Eden Prairie, **1992**; (c) Beamson, G.; Briggs, D. *High Resolution XPS of Organic Polymers: The Scienta ESCA300 Database*; John Wiley & Sons: Chichester, **1992**.
13. (a) Raible, M.; Evstigneev, M.; Bartels, F.W.; Eckel, R.; Nguyen-Duong, M.; Merkel, R.; Ros, R.; Anselmetti, D.; Reimann, P. *Biophys. J.* **2006**, *90*, 3851-3864; (b) Auletta, T.; De Jong, M.R.; Mulder, A.; Van Veggel, F.C.J.M.; Huskens, J.; Reinhoudt, D.N.; Zou, S.;

- Zapotoczny, S.; Schönherr, H.; Vancso, G.J.; Kuipers, L. *J. Am. Chem. Soc.* **2004**, *126*, 1577-1584.
14. Bell, G.I. *Science* **1978**, *200*, 618-627.
 15. High loading rates and a flexible polymer linker are used in these experiments. Furthermore the loading rate is determined as the slope of the force vs. time trace close to the actual rupture event. Therefore Gaussian fitting can directly be applied to determine the most probable rupture force f^* and subsequently the thermal scale force f_β without the need of for instance Monte Carlo simulations which take into account the linker parameters: L_b (contour length) and l_p (persistence length).
 16. Ray, C.; Brown, J.R.; Akhremitchev, B.B. *J. Phys. Chem. B* **2007**, *111*, 1963-1974.
 17. (a) Oesterhelt, F.; Rief, M.; Gaub, H.E. *New J. Phys.* **1999**, *1*, 6.1–6.11; (b) Kienberger, F.; Pastushenko, V.P.; Kada, G.; Gruber, H.J.; Riener, C.; Schindler, H.; Hinterdorfer, P. *Single Mol.* **2000**, *1*, 123-128.
 18. (a) Merkel, R.; Nassoy, P.; Leung, A.; Ritchie, K.; Evans, E. *Nature* **1999**, *397*, 50-53; (b) Evans, E. *Annu. Rev. Biophys. Biomol. Struct.* **2001**, *30*, 105-128.
 19. The diffusion relaxation time t_D - or rather the microscopic attempt frequency $1/t_D$ - was previously estimated based on damping factors from molecular dynamics simulations for the biotin/streptavidin system and lipid extraction from a bilayer in water: $t_D \sim 1$ ns ($1/t_D \sim 10^9 - 10^{10} \text{ s}^{-1}$). Since t_D is governed by viscous damping, and hexadecane is much more viscous than water an estimate for $t_D = 5 \times 10^{-9}$ s in HD was used here. If a broad range of $t_D = (1-10) \times 10^{-9}$ s is used, equation 3 can be written as: $\frac{\Delta G}{k_B T} = -\ln(r_f^0) + \ln(f_\beta) + (\approx 19.5 \pm 1)$. The error that is now introduced lies in the same range as those that are already present by the applied method ($\ln(r_f^0) = -22.7 \pm 0.6$; $\Delta \ln(r_f^0) = 3\%$ vs $\Delta \ln(t_D) = 5\%$), however it opens up the possibility to determine the dimer binding constant of the hydrogen-bonded UAT system. Over this whole t_D -range the calculated values for K_{dim} range from $1 \times 10^7 - 3 \times 10^8 \text{ M}^{-1}$ which is still at least three orders of magnitude above the predicted values based on theoretical approaches^[7].
 20. Beijer, F.H.; Kooijman, H.; Spek, A.L.; Sijbesma, R.P.; Meijer, E.W. *Angew. Chem. Int. Ed.* **1998**, *37*, 75-78.
 21. Furthermore the calculated characteristic transition state length $x_\beta = 0.29 \pm 0.02$ nm correlates well to the crystallographic data for the intermolecular UAT hydrogen-bond length (0.275 - 0.325 nm) determined by Sijbesma and Meijer.

22. (a) Hinterdorfer, P.; Baumgartner, W.; Gruber, H.J.; Schilcher, K.; Schindler, H. *Proc. Natl. Acad. Sci. U.S.A.* **1996**, *93*, 3477-3481; (b) Friddle, R.W.; Podsiadlo, P.; Artyukhin, A.B.; Noy, A. *J. Phys. Chem. C* **2008**, *112*, 4986-4990; (c) Guo, S.; Lad, N.; Ray, C.; Akhremitchev, B.B. *Biophys. J.* **2009**, *96*, 3412-3422; (d) Janke, M.; Rudzevich, Y.; Molokanova, O.; Metzroth, T.; Mey, I.; Diezemann, G.; Marszalek, P.E.; Gauss, J.; Böhmer, V.; Janshoff, A. *Nat. Nanotechnol.* **2009**, *4*, 225-229.
23. Ligthart, G.B.W.L.; Guo, D.; Spek, A.L.; Kooijman, H.; Zuilhof, H.; Sijbesma, R.P. *J. Org. Chem.* **2008**, *73*, 111-117.
24. (a) De Greef, T.F.A.; Nieuwenhuizen, M.M.L.; Stals, P.J.M.; Fité, C.F.C.; Palmans, A.R.A.; Sijbesma, R.P.; Meijer, E.W. *Chem. Commun.* **2008**, 4306-4308; (b) De Greef, T.F.A.; Nieuwenhuizen, M.M.L.; Sijbesma, R.P.; Meijer, E.W. *J. Org. Chem.* **2010**, *75*, 598-610.
25. Leigh, D.A.; Wong, J.K.Y.; Dehez, F.; Zerbetto, F. *Nature* **2003**, *424*, 174-179.
26. Li, N.; Guo, S.; Akhremitchev, B.B. *ChemPhysChem* **2010**, *11*, 2096-2098.
27. Hutter, J.L.; Bechhöfer, J.; *Rev. Sci. Instrum.* **1993**, *64*, 1868-1873.



CHAPTER 5

AFM-BASED SINGLE MOLECULE FORCE SPECTROSCOPY OF SUPRAMOLECULAR UREA-AMINOTRIAZINE-BASED POLYMERS

Abstract

Atomic Force Microscopy-based single molecule force spectroscopy (AFM-based SMFS) was used to study the bond strength of self-complementary hydrogen-bonded complexes based on supramolecular urea-aminotriazine (UAT) quadruple hydrogen-bonded polymers in hexadecane (HD). The unbinding forces were investigated at different fixed piezo retraction rates in far-from-equilibrium conditions. The rupture events observed were identified as the unbinding of single bonds of an associating polymer. Based on the independent knowledge of the linker length, the number of supramolecular bonds (N) at rupture was determined. The rupture force of supramolecular UAT polymer chains was found to decrease with increasing rupture length and its dependence on N was in quantitative agreement with the theory on uncooperative bond rupture for supramolecular linkages switched in series. In experiments with three different fixed loading rates, identical values for the characteristic bond length x_β to within the experimental error, were obtained. Thus a mean dimer equilibrium constant K_{dim} of $(1.1 \pm 0.3) \times 10^7 \text{ M}^{-1}$ was estimated. This value is in good agreement with the previously measured value for the binding constant of $(\text{UAT})_2$ (Chapter 4). Hence the new approach to estimate the relevant parameters for the rupture of dimers in experiments on supramolecular linkages switched in series at one fixed loading rate, presented in Chapter 3 for the UPy system, was validated.

5.1 INTRODUCTION

In this Chapter we apply the new approach, presented in Chapter 3 for the UPy-system^[1], of estimating all relevant parameters for the rupture of supramolecular dimeric complexes in experiments on supramolecular linkages switched in series at *one fixed* loading rate, to the ureido-amino-triazine (UAT) system introduced in Chapter 4. Thereby we aim at a validation and independent check of this approach. For this purpose a bifunctional UAT-PEG-linker was synthesized (Figure 5- 1) and rupture forces of supramolecular UAT-polymers were studied in hexadecane using Atomic Force Microscopy (AFM)-based Single Molecule Force Spectroscopy (SMFS) (Figure 5- 2).

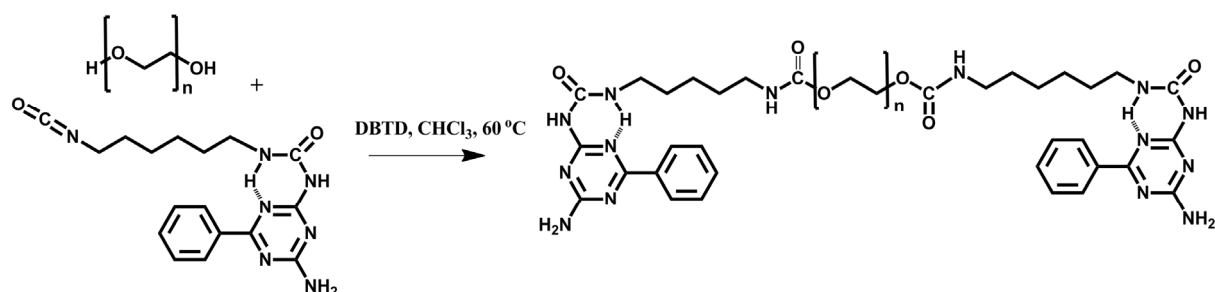


Figure 5- 1. Synthesis of the bifunctional UAT-PEG-linker (monomer) for supramolecular polymer formation.

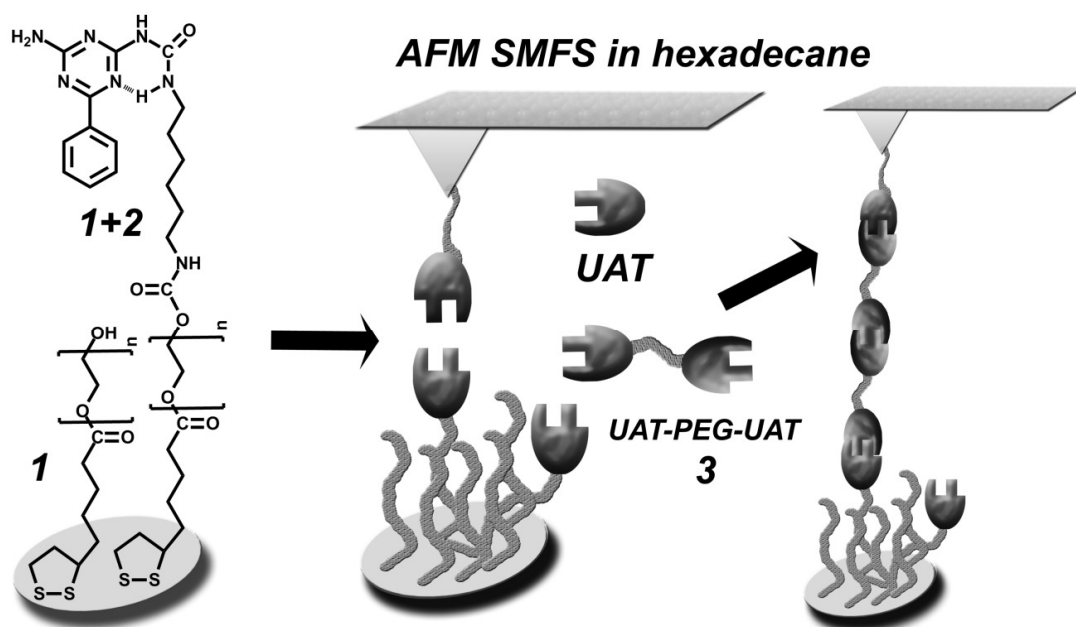


Figure 5- 2. Schematic of AFM-based SMFS of supramolecular UAT-polymers in hexadecane. A gold coated surface and AFM-probe are functionalized with PEG **1** and PEG-UAT **1+2** moieties. The bifunctional UAT-PEG-linker **3** is added to form supramolecular polymers in hexadecane for *in situ* AFM-based SMFS studies.

The dependence of the bond strength on supramolecular polymer length was studied in the same manner as was discussed in Chapter 3 for the UPy supramolecular polymers.

5.2 RESULTS AND DISCUSSION

To determine the rupture forces of supramolecular UAT-polymers in hexadecane a PEG-UAT-functionalized gold surface and gold-coated AFM-probe were used as described in Chapter 4. However, the bis-UAT-PEG-linker **3** was added to the system in a concentration of 2.5×10^{-5} M to result in the formation of supramolecular UAT-polymers *in situ*. Using AFM-based SMFS, bridging supramolecular polymer chains were stretched and broken at three different, but *fixed* loading rates. The loading rates used ensure far-from-equilibrium conditions: $r = (32.0 \pm 7.0) \times 10^3$ pN/s, $r = (68.4 \pm 20.5) \times 10^3$ pN/s and $r = (121.3 \pm 28.1) \times 10^3$ pN/s.

As can be seen in Figure 5- 3, the rupture lengths observed exceeded those expected for the dimer (Chapter 4) significantly. Since these rupture lengths were only observed in the presence of **3** the formation of supramolecular polymer chains bridging between the substrate surface and the tip can be concluded.

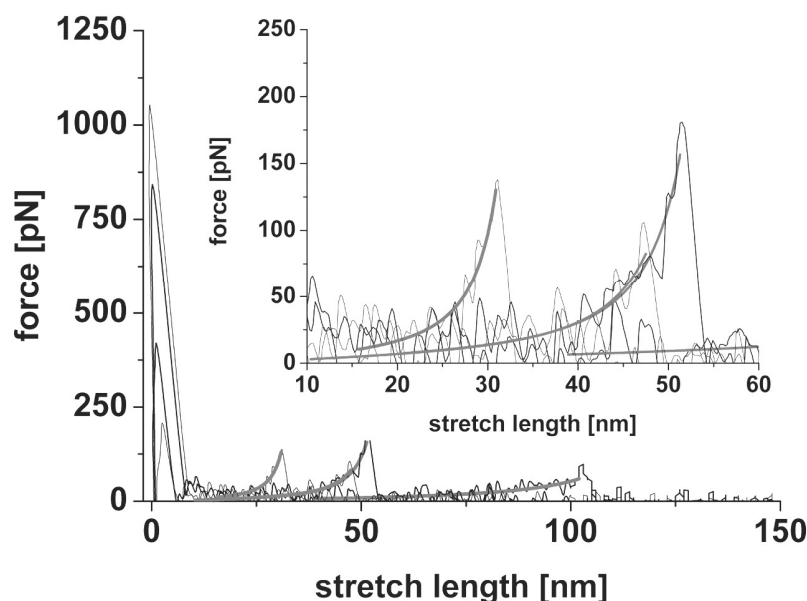


Figure 5- 3. Unbinding events of UAT-moieties in the presence of bis-UAT **3**. The force-extension curves were fitted to the wormlike chain (WLC) model which provided the persistence length $l_p = 3.63 \pm 0.40$ Å.

After the data was converted to force-extension curves (see Chapter 2), such as those shown in Figure 5- 3, the rupture length and rupture force were determined^[2]. The corresponding

data is plotted in histograms for the three different, but *fixed* loading rates used (Figure 5- 4). Fitting the force-extension curves to the wormlike chain (WLC) model confirmed that single molecule supramolecular polymers were stretched^[3,4]. The wormlike chain fits provided the following value for the persistence length $l_p = 3.63 \pm 0.40$ Å, which is in good agreement with literature data^[3].

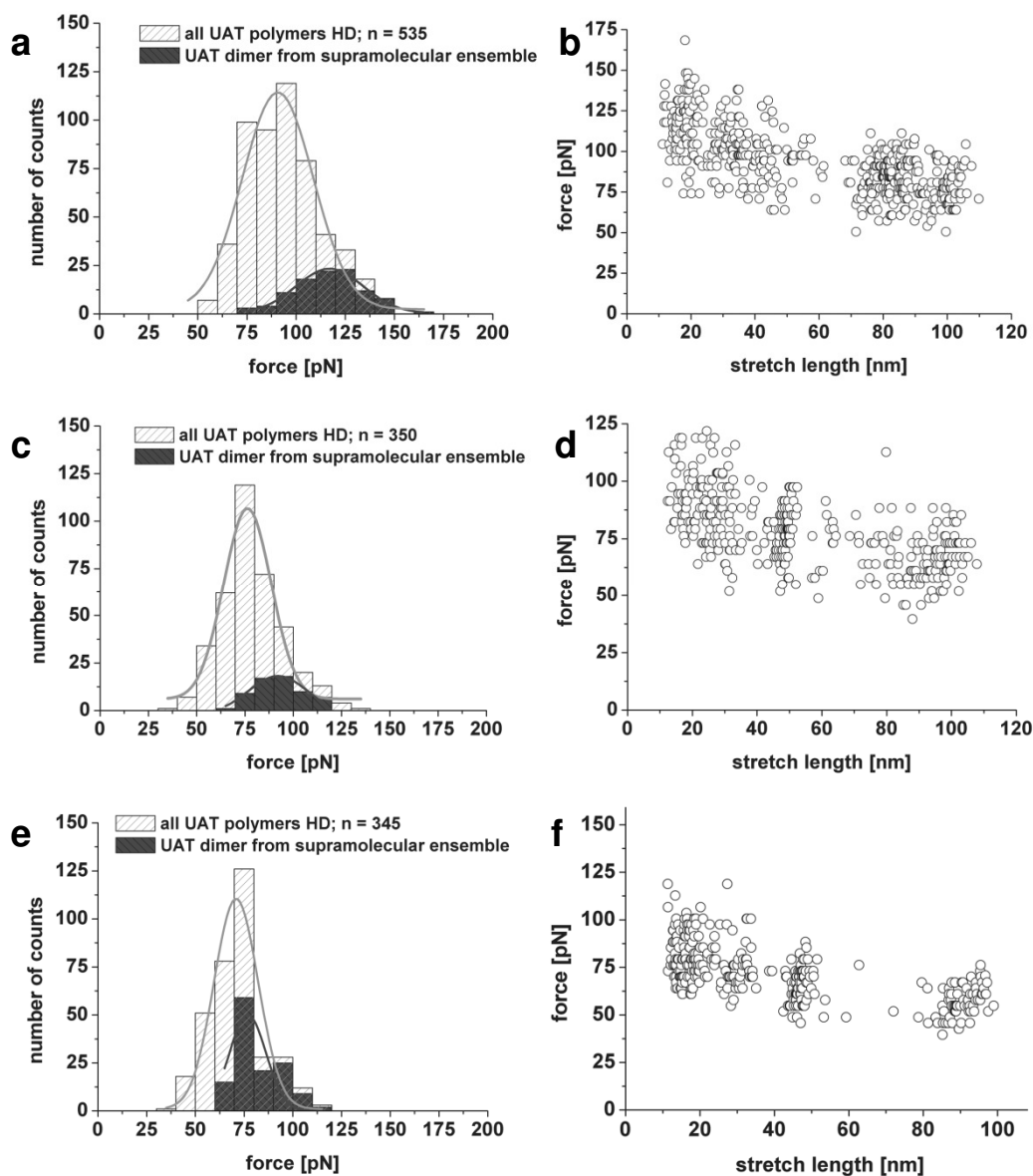


Figure 5- 4. Histograms of rupture forces (left, a,c,e) and plots of rupture force vs length for unbinding in hexadecane (right, b,d,f) at the following loading rates: (a,b) $r = (121.3 \pm 28.1) \times 10^3$ pN/s; (c,d) $r = (68.4 \pm 20.5) \times 10^3$ pN/s; (e,f) $r = (32.0 \pm 7.0) \times 10^3$ pN/s. Note that the dimer rupture events (qualified as unbinding events with stretch lengths between 11 and 25 nm, black) in all histograms display a substantially higher most probable unbinding force in comparison with the ensemble of all supramolecular polymer unbinding events (grey) for a specific loading rate.

Based on the length of the PEG-linker and the attached UAT-moieties of the bis-UAT-linker, the stretch length of every single supramolecular UAT polymer was converted to the number of linkers N : $N = (L/11 \text{ nm}) \cdot I^{[5]}$. Hence the most probable force f^* was estimated and plotted as a function of N and a decrease of the most probable rupture force f^* with the number of linkers N was observed for all data sets. Subsequently the data was fitted in the same manner as described in Chapter 3, using a fast-converging Marquart-Levenberg algorithm and equation 5-1 for uncooperative bond rupture in series described by Evans and Williams^[6]:

$$f^* = f_\beta \cdot \left[\ln(r_f) - \ln(N) \right] = f_{\text{single}}^* - f_\beta \cdot \ln(N) \quad \text{Equation 5-1}$$

The fitted data for the three data sets obtained at different, but *fixed* loading rates, provided the most probable rupture force of the dimer f_{single}^* as well as the thermal scale force f_β . Subsequently the value for the dimer equilibrium constant was determined. An overview of the obtained data is presented in Figure 5- 5, where the error bars denote the standard deviation of the distribution. The analysis of the three different data sets provided the data presented in Table 5- 1.

Parameter	polymer $r = (32.0 \pm 7.0)$ $\times 10^3 \text{ pN/s}$	polymer $r = (68.4 \pm 20.5)$ $\times 10^3 \text{ pN/s}$	polymer $r = (121.3 \pm 28.1)$ $\times 10^3 \text{ pN/s}$	dimer study Chapter 4
$f_\beta [\text{pN}]$	13.5 ± 2.7	14.6 ± 1.4	15.3 ± 1.6	14.5 ± 1.1
$f_{\text{single}}^* [\text{pN}]^{[8]}$	82.2 ± 2.1	96.2 ± 2.1	105.6 ± 2.4	$r_f\text{-dependent}$
$r_f^0 [\text{pN/s}]$	$(2.4 \pm 1.9) \times 10^2$	$(2.8 \pm 1.4) \times 10^2$	$(3.9 \pm 2.1) \times 10^2$	$(1.5 \pm 0.9) \times 10^2$
$t_{\text{off}}(0) [\text{ms}]$	130 ± 90	70 ± 30	50 ± 30	100 ± 80
$x_\beta [\text{nm}]$	0.31 ± 0.08	0.29 ± 0.03	0.27 ± 0.04	0.29 ± 0.02
$\Delta G [\text{kJ/mol}]$	42 ± 2	41 ± 1	40 ± 2	44 ± 2
$K_{\text{dim}} [\text{M}^{-1}]$	$(3 \pm 2) \times 10^7$	$(1 \pm 1) \times 10^7$	$(9 \pm 6) \times 10^6$	$(2 \pm 1) \times 10^7$

Table 5- 1. Overview of parameters determined via AFM-based SMFS of UAT supramolecular polymers in hexadecane for three different, but *fixed* loading rates $r = (32.0 \pm 7.0) \times 10^3 \text{ pN/s}$; $r = (68.4 \pm 20.5) \times 10^3 \text{ pN/s}$ and $r = (121.3 \pm 28.1) \times 10^3 \text{ pN/s}$ in comparison with loading rate-dependent dimer bond rupture studies.

In Figure 5- 5 (panel d) a comparison of the fitted most probable rupture force of the dimers f_{single}^* (as part of the supramolecular ensemble, $N=1$) at the three different, but *fixed* loading

rates and the loading rate-dependent dimer studies in Chapter 4 is presented as well. As can be observed in Figure 5- 5 (panel d) and Table 5- 1 the fitted values obtained for the three different data sets - at a single *fixed* loading rate - and the corresponding parameters of the potential energy landscape are in close agreement with each other. The characteristic transition state length x_β also corresponds to approximate values estimated on the basis of crystallographic data of the hydrogen-bond lengths of DADA arrays by Sijbesma and Meijer^[10]. These hydrogen-bond lengths were obtained by Sijbesma and Meijer using crystallographic data for colourless crystals of different DADA arrays of which the structure was solved by automated direct methods (SHELXS-96). For a more detailed description see ref. 10.

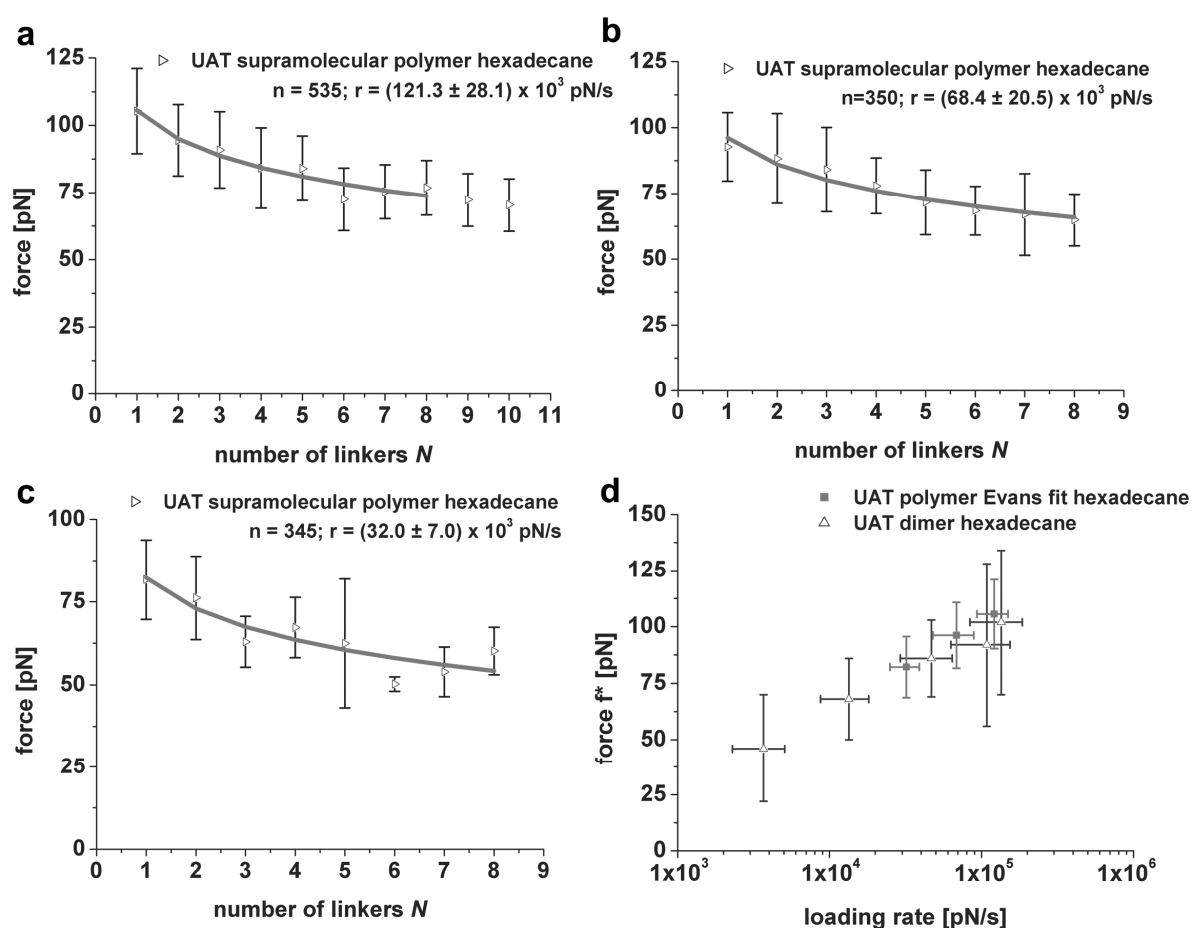


Figure 5- 5. (a-c) Plots of fitted data using the model for uncooperative bond failure in series for supramolecular polymers in hexadecane at fixed loading rates: (a) $r = (121.3 \pm 28.1) \times 10^3$ pN/s; $f_\beta = 15.3 \pm 1.6$ pN; $f_{single}^* = 105.6 \pm 2.4$ pN; (b) $r = (68.4 \pm 20.5) \times 10^3$ pN/s; $f_\beta = 14.6 \pm 1.4$ pN; $f_{single}^* = 96.2 \pm 2.1$ pN; (c) $r = (32.0 \pm 7.0) \times 10^3$ pN/s; $f_\beta = 13.5 \pm 2.7$ pN; $f_{single}^* = 82.2 \pm 2.1$ pN; (d) comparison of the dimer rupture study (Chapter 4) and the fits obtained in this chapter of the most probable dimer rupture force f_{single}^* based on the uncooperative bond failure model.

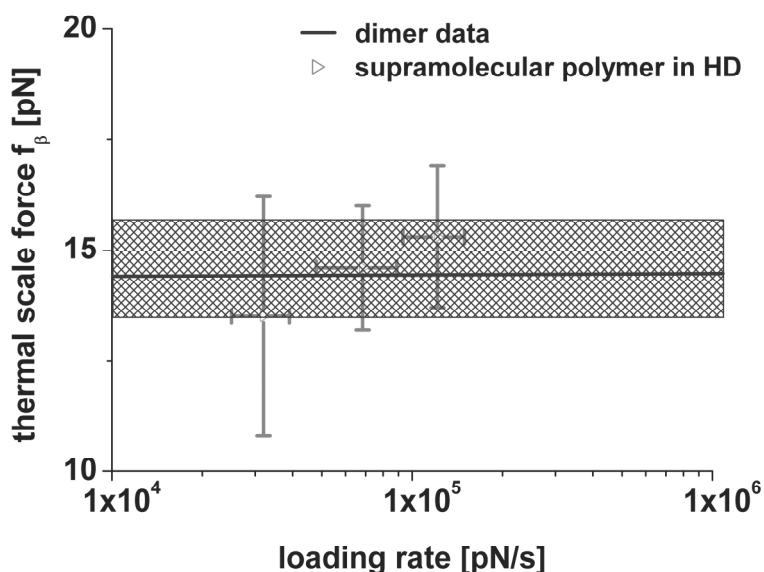


Figure 5- 6. Plot of the thermal scale force f_β data obtained by unbinding studies of dimers (Chapter 4, long band) and supramolecular polymers (this chapter, datapoints) in hexadecane including their error margins. *Since a range of loading rates was used in Chapter 4 to determine the thermal scale force f_β this is represented with a line and the corresponding error bar over the full range of loading rates.*

The value for the dimer binding constant of $(\text{UAT})_2$ was then calculated exactly as discussed in Chapter 3. The main advantage of this procedure lies in the fact that only one single measured data set at one *fixed* loading rate is required. Since the same procedure and equations are used to determine the dimer binding constant and the parameters of the potential energy landscape, also similar errors are introduced^[7]. An additional error, which is only introduced by this approach, lies in the conversion of stretch length to number of linkers N . From equation 5- 1 it can be concluded that the error in f_β depends linearly on the error in f^* for small N and hence reasonable accuracy is obtained when large data sets with a substantial polymer length such as those presented here are used to determine f_β .

The average value of the dimer equilibrium constant – based on the three data sets – $K_{eq} = K_{dim} = (1.1 \pm 0.3) \times 10^7 \text{ M}^{-1}$ for $(\text{UAT})_2$ in hexadecane agrees well with the value obtained for the loading rate-dependent studies presented in Chapter 4^[9]. This central result fully validates our new approach and shows that the choice of the loading rate possesses only negligible influence on the parameters estimated, as long as the unbinding events occurs under far-from-equilibrium conditions.

5.3 CONCLUSIONS

The combined results from Chapter 3 and Chapter 5 demonstrate that studying the forced unbinding of single supramolecular polymers at one *fixed* piezo retraction rate at far-from-equilibrium conditions by AFM-based SMFS can provide single molecule rupture force parameters required to calculate kinetic off-rates and (assuming a t_D) equilibrium complexation constants. The measured rupture forces of supramolecular polymers of different length and independent knowledge of the constituent segment length provided access to the dimer bond lifetime at zero force $t_{off}(f=0)$. For both supramolecular polymers (UPy and UAT) the results agree with previously obtained data for loading rate-dependent dimer interaction studies. Furthermore, the results are well in line with actual measurements by Sijbesma and Meijer^[10,11] of the dimer binding constant of the same or similar systems in chloroform and other organic solvents based on NMR binding studies (DADA) or fluorescence spectroscopy studies of pyrene-labeled UPy-moieties (DDAA). Finally, these results demonstrate that the uncooperative bond failure model can be applied for strongly interacting systems as long as far-from-equilibrium conditions are applied.

5.4 MATERIALS AND METHODS

Materials. Anhydrous hexadecane (purity ≥ 99 %, water < 0.005 %) and dibutyltindilaurate were purchased from Sigma-Aldrich (Steinheim, Germany) and used as received. Chloroform (stabilized with amylene) and dichloromethane were purchased from Biosolve (Valkenswaard, The Netherlands).

1,2-Dithiolane-3-pentyl-derivatized PEG **1**, 1-(4-amino-6-phenyl-1,3,5-triazin-2-yl)-3-(6-isocyanatohexyl)urea (UAT) **2** and PEG-linked bis-urea-aminotriazine **3** were synthesized according to published procedures^[12]. See also Chapter 3 and 5 for a more detailed description of the synthesis procedures.

PEG-linked bis-urea-aminotriazine was synthesized using 1.0525 gram of PEG₂₈ (Polypure 95% pure PEG₂₈ $M_w = 1251.5$ g/mol; 0.8 mmol), which was previously dried by three times azeotropic distillation over anhydrous toluene. Excess 1-(4-amino-6-phenyl-1,3,5-triazin-2-yl)-3-(6-isocyanato-hexyl)urea **2** 1.2330 gram (3.5 mmol), 2 drops of catalyst dibutyltindilaurate and 40 ml of dry chloroform were added under nitrogen environment. The clear solvent mixture was heated to 60 °C and the reaction was left stirring overnight under argon atmosphere. After 20 hours of reaction time 2.5 gram silica (Kieselgel 60) and 2 drops

of catalyst were added to remove unreacted isocyanate-endfunctionalized urea-aminotriazine and the reaction was left to take place over 6 hours, after which no residual isocyanate peak could be detected via FT-IR. After cooling down, the silica-bound material was removed by washing the reaction mixture with chloroform over a glass filter. Chloroform was removed by rotation evaporation and the residue was further dried under vacuum for several hours and stored under argon atmosphere. Isolated yield: 66.4 % (1.40 gram). $^1\text{H-NMR}$ (300 MHz, CDCl_3), δ 10.29 (s, 2H, NH/N H-bond), 9.90 (s, 2H, NH/N intra H-bond), 9.33 (s, 2H, NH(from NH_2)/N H-bond), 8.20 (d, 4H, ortho), 7.60-7.47 (t, 6H, meta,para), 5.63 (s, 2H, HNH), 4.21 (t, 4H, $(\text{C}=\text{O})\text{-O-CH}_2$), 3.69-3.58 (m, CH_2 PEG), 3.42 (t, $(\text{C}=\text{O})\text{-NH-CH}_2$ PEG, 4H), 3.13 (t, $(\text{C}=\text{O})\text{-NH-CH}_2$ UAT, 4H), 1.7-1.3 (m, 16H, $\text{O}=\text{C}=\text{N-CH}_2\text{-(CH}_2\text{)}_4\text{-CH}_2\text{-NH}$). *From the integrals an estimate of the PEG units is obtained which is very close to the actual number of 28*; mass (MALDI-TOF MS), $m/z=1961.9$ (M, PEG $M_w = 1251.5$ g/mol, UAT $M_w = 355$ g/mol (2x), PEG-(UAT) $_2$ $M_w = 1961.5$), FT-IR 3500 cm^{-1} (ν_{OH} H-bond, w), 3400 cm^{-1} ($\nu_{\text{NH},1\text{O}_{\text{amine}}}$, w), $3300\text{-}3200\text{ cm}^{-1}$ ($\nu_{\text{NH},2\text{O}_{\text{amine}}}$, w), $2959\text{-}2882\text{ cm}^{-1}$ (ν_{CH_2} , w), 1739 cm^{-1} ($\nu_{\text{C}=\text{O}}$ ester, w), 1711 cm^{-1} ($\nu_{\text{C}=\text{O}}$, w), 1630 cm^{-1} ($\nu_{\text{C}=\text{O}}$ amide, w), 1543 cm^{-1} (ν_{NH} , amidII, w), $1454\text{-}1466\text{ cm}^{-1}$ (ν_{CH_2} , m), 1280 cm^{-1} ($\nu_{\text{C-O/C-N}}$, w), 1240 cm^{-1} ($\nu_{\text{C-O}}$, w), 1239 cm^{-1} ($\nu_{\text{C-O-C}}$, w), 1101 cm^{-1} ($\nu_{\text{C-O-C}}$, s), 1060 cm^{-1} ($\nu_{\text{C-O-C}}$, s), 952 cm^{-1} (ν_{CH_2} , m), 841 cm^{-1} ($\nu_{\text{C-O-C}}$, ν_{CH_2} m), 528 cm^{-1} (ν_{CH_2} , w).

Sample preparation. Gold substrates (200 nm gold on top of 3.5 nm Ti deposited onto glass substrates) were purchased from Ssens BV (Hengelo, The Netherlands). Prior to use, these substrates were cleaned in piranha solution [2:1 H_2SO_4 (Sigma-Aldrich)/ H_2O_2 (30 %, Fluka) by volume], then rinsed three times with Milli-Q water and ethanol, and subsequently rinsed with the pure solvent. The samples were directly transferred to the monolayer solution preventing any direct contact with air. *Caution: Piranha solution should be handled with extreme caution. It has been reported to detonate unexpectedly.* On gold substrates, self-assembled monolayers (SAMs) of **1** were prepared from 1 mM CH_2Cl_2 solution and reacted with 2.5 mmol **2** in 10 ml CHCl_3 solution for 24 hours using one drop of dibutyltindilaurate as catalyst. After rinsing with pure solvent and drying in an N_2 stream, measurements were performed with minimal delay. The same procedure was used for AFM-tip functionalization.

General characterization methods. The $^1\text{H-NMR}$ spectra were recorded on a Varian Unity 300. 300 MHz spectra were recorded in CDCl_3 and therefore chemical shifts are given relative to the residual CHCl_3 peak (7.26 ppm). $^1\text{H-NMR}$ on polymers was performed on a Bruker

600 MHz. FT-IR bulk measurements were performed on a Bruker Alpha-P. The mass of the bifunctional PEG-(UAT)₂ linker was analyzed with MALDI-TOF spectrometry on a Applied Biosystems Voyager DE-RP.

Atomic Force Microscopy. The AFM-based SMFS measurements were performed on a Veeco/Bruker Multimode (NanoScope V controller (Veeco/Bruker, Santa Barbara, CA)) with a Picoforce vertical engage scanner and a liquid cell (Bruker/Veeco, Santa Barbara, CA). A double-sided gold coated MikroMasch rectangular beam cantilever (CSC38) was functionalized in two consecutive steps, as described above, with a self-assembled layer of **1** and subsequent reaction with **2**. Tips for SMFS were taken directly from solution followed by rinsing with pure solvent. The cantilever spring constant ($k = 0.133 \pm 0.014$ N/m) was determined in liquid via the thermal tune method^[13]. Loading rates were determined as the slope of the force versus time trace of the force-extension curves (~ 20 data points) close to the rupture event. All experiments were performed in a saturated solution of **3** in anhydrous hexadecane at $T = 303 \pm 2$ K. conc. = 2.5×10^{-5} M.

REFERENCES AND NOTES

1. Embrechts, A.; Schönherr, H.; Vancso, G.J. *J. Phys. Chem. B* **2008**, 112, 7359-7362.
2. The conversion from deflection vs. piezo-position to force-distance curves was carried out using Veeco offline analysis software v730r1sr2 and V810r1sr1. Baseline correction and WLC fitting was subsequently achieved using Origin version 6.1. Stretch lengths and unbinding forces were determined using PUNIAS 3D. Loading rates were determined as the slope of the force versus time trace of the force-extension curves (~ 20 data points) close to the rupture event (Origin 6.1).
3. (a) Oesterhelt, F.; Rief, M.; Gaub, H.E. *New J. Phys.* **1999**, 1, 6.1–6.11; (b) Kienberger, F.; Pastushenko, V.P.; Kada, G.; Gruber, H.J.; Riener, C.; Schindler, H.; Hinterdorfer, P. *Single Mol.* **2000**, 1, 123-128.
4. According to literature the helical state monomer length of PEG is 2.78 Å and a persistence length $l_p = 3.81 \pm 0.02$ Å (WLC) and Kuhn length $l_K = 7$ Å (from a fit to the freely joined chain (FJC) model) were previously reported^[3]. So, the fitted persistence length agrees very well with literature which confirms that *single supramolecular polymers* were probed. In our measurements the difference between the elasticity parameters obtained from fits to the WLC and FJC models is negligible since small

extensions at low rupture forces were studied. In that case the following expression for the relation of the persistence length and Kuhn length applies: $l_p = \frac{1}{2} \cdot l_K$. Hence the average persistence length of $l_p = 3.63 \pm 0.40 \text{ \AA}$ is well in line with previously reported data and confirms that single chains were stretched and hence single molecule rupture events were probed.

5. An almost monodisperse PEG/linker was used with $n = 28$. The monodispersity of the final bifunctional linker was confirmed using Maldi-TOF (see experimental section). So based on the bond length between atoms of the complete structure and the number of PEG-units the total length of the bifunctional UAT-linker can be determined as 11 nm. The error in the stretch length is very small in this case due to the low polydispersity ($\pm 0.3 \text{ nm}$ for a difference in the PEG linker by a PEG unit).
6. Williams, P.; Evans, E. *Dynamic Force Spectroscopy in Physics of Bio-Molecules and Cells. Ecoles des Houches d'Eté LXXV* (Eds: F. Julicher, P. Ormos, F. David, and H. Flyvbjerg) EDP Sciences, Springer Verlag, Berlin, **2002**, p. 147-203.
7. In the analysis of supramolecular dimer and polymers minor errors are introduced by using a mean loading rate. Furthermore - as discussed extensively in Chapter 4 - an estimate for the diffusive relaxation time t_D ($t_D = 5 \times 10^{-9} \text{ s}$) was used here as well, based on data from MD simulations for receptor-ligand interactions in water and the fact that measurements were performed in highly viscous hexadecane. In case SMFS association measurements are also performed an estimate for t_D is no longer necessary since k_{off} and k_{on} are both known, which could lead to more accurate values for the dimer binding constant. See also Chapter 4 for a more detailed discussion.
8. Although the mathematical fitting provides errors in the order of 2 pN for the most probable rupture force of the dimer, this can not be regarded as the standard deviation of the force distribution of a thermally activated unbinding event, since thermal fluctuations already broaden the distribution and the standard deviation Δf scales with f_β ($\Delta f = f_\beta$), even without any experimental uncertainty. Therefore the fitted value for f_β is used to get a more accurate value for Δf^* .
9. Embrechts, A.; Velders, A.H.; Schönherr, H.; Vancso, G.J. unpublished data.
10. Beijer, F.H.; Kooijman, H.; Spek, A.L.; Sijbesma, R.P.; Meijer, E.W. *Angew. Chem. Int. Ed.* **1998**, *37*, 75-78.

11. (a) Söntjens, S.H.M.; Sijbesma, R.P.; Van Genderen, M.H.P.; Meijer, E.W. *J. Am. Chem. Soc.* **2000**, *122*, 7487-7493; (b) De Greef, T.F.A.; Nieuwenhuizen, M.M.L.; Sijbesma, R.P.; Meijer, E.W. *J. Org. Chem.* **2010**, *75*, 598-610.
12. (a) Neises, B.; Steglich, W. *Org. Synth.* **1990**, *7*, 93-94; (b) Folmer, B.J.B.; Sijbesma, R.P.; Versteegen, R.M.; van der Rijt, J.A.J.; Meijer, E.W. *Adv. Mater.* **2000**, *12*, 874-878; (c) Zou, S.; Schönherr, H.; Vancso, G.J. *J. Am. Chem. Soc.* **2005**, *127*, 11230-11231; (d) Zou, S.; Schönherr, H.; Vancso, G.J. *Angew. Chem. Int. Ed.* **2005**, *44*, 956-959.
13. Hutter, J.L.; Bechhöfer, J. *Rev. Sci. Instrum.* **1993**, *64*, 1868-1873.

CHAPTER 6

AFM-BASED SMFS OF UPY DIMERS AND POLYMERS IN DIFFERENT SOLVENTS

Abstract

The influence of solvent polarity on the bond strength of ureidopyrimidinone (UPy) supramolecular dimers was investigated in 2-propanol, 1-nonanol and hexadecane as well as in binary mixtures of 2-propanol and hexadecane. The bond strength appears to scale with solvent polarity, which is consistent when solvent “competition” is assumed for hydrogen-bond formation. Based on the literature we infer that the more polar solvent molecules compete with the hydrogen-bond formation in supramolecular dimer and polymers and hence reduce the hydrogen-bond strength. Using single molecule force spectroscopy measurements it was observed that the unbinding forces shift to lower values for increasingly polar solvents. The corresponding distributions of the rupture forces were shown to deviate from a normal distribution. Whereas in pure hexadecane the rupture force distributions can be described with a Gaussian function, the distributions of rupture forces in polar 2-propanol and to a lesser extent in 1-nonanol deviate markedly from a Gaussian distribution, as confirmed e.g. by the Shapiro-Wilks test. The distributions in polar solvents are tentatively attributed to bond rupture in different local environments that may be related to molecular clustering, observed by others, in these solvents. In binary mixtures of 2-propanol and hexadecane similar bond strengths and bond strength distributions as in 2-propanol were observed.

6.1 INTRODUCTION

The bond strength between hydrogen-bonded moieties in various solvents is among others affected by the polarity of the solvent (classified by the dielectric constant) as was pointed out in Chapter 2. Abrahams^[1] and Hunter^[2] described the interactions between solvent and solute, which can both consist of hydrogen-bond donors and acceptors, using a rather straightforward electrostatic approach. This leads to a general scheme for the hydrogen-bond interactions between two neutral functional groups in an arbitrary solvent (Figure 6- 1).

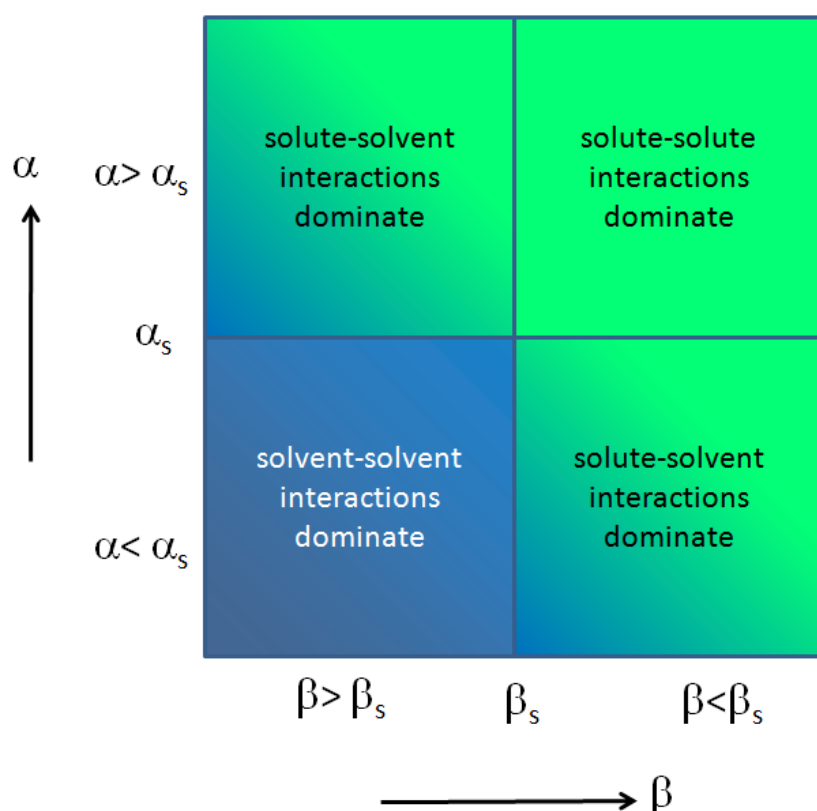


Figure 6- 1. General scheme for the hydrogen-bond interactions between two neutral functional groups in any solvent. Based on the competition between solvent-solute, solute-solute and solvent-solvent an estimate for the free-energy of binding ΔG of the hydrogen-bond interaction can be obtained using the hydrogen-bond donor and acceptor constants for the solute (α and β , respectively) and the hydrogen-bond donor and acceptor constant for the solvent (α_s and β_s , respectively). *Image adapted from ref. 2.*

In case of the hydrogen-bond interactions in hexadecane, as discussed in Chapter 3, the observed high dimer binding constant values can be explained by the fact that the highly apolar solvent drives dimer and polymer formation to reduce the interaction of hexadecane

with the hydrogen-bond monomers (solvophobic zone; in Figure 6- 1 bottom-left quadrant; see Chapter 2). Due to the absence of a dipole moment in the solvent molecules, no additional preferential solvation exists, as a result of the dipole moment of solvent molecules. However, when the hydrogen-bond strength in different alcohols - with a significant dipole moment - is studied, the solvent-solute interaction is expected to compete with the formation of hydrogen-bonds in supramolecular dimers and polymers. Based on polarity the hydrogen-bond strength of supramolecular dimers and polymers should increase from top-to-bottom along the polarity range presented in Table 6- 1.

	Dipole moment* [D] *in the gas phase	Dielectric constant ϵ_r
H ₂ O	1.85	80 (300 K)
methanol	1.70	32.6 (298 K)
1-butanol	1.66	17.8 (293 K)
toluene	0.4	2.4 (293 K)
hexane, heptane, octadecane, hexadecane, etc.	-	~2 (293 K)

Table 6- 1. Dipole moments and dielectric constants for various solvents^[3].

Although a quantitative relationship between hydrogen-bond strength and solvent polarity was never fully established, a trend as presented above is clearly observed in NMR and fluorescence spectroscopy studies of the dimer binding constant K_D and bond lifetime of (UPy)₂ in various solvents^[4].

solvent	Dimer binding constant K_D [M ⁻¹]	Bond lifetime [ms]
CHCl ₃ +H ₂ O	1 x 10 ⁷	80
CHCl ₃	6 x 10 ⁷	120
toluene	6 x 10 ⁸	1700

Table 6- 2. UPy-dimer bond strength and bond lifetimes in various solvents (bulk studies) determined via fluorescence spectroscopy of pyrene-labeled UPy^[4].

Depending on the solvent however, different contributions influence the formation of hydrogen-bonds. For hydrogen-bonded moieties in a solvent with multiple hydrogen-bond donors or acceptors, such as a range of alcohols, these interactions become more complex. According to the simplified approach by Hunter^[2], such multiple hydrogen-bonded interactions can be considered as sums of the individual donor-acceptor contributions. For example, a 1:1 mixture of water and dimethylether would behave similar to methanol (see Appendix). However, this coarse approach has clear limitations (see discussion in section 2.4, Chapter 2 and Figure 2- 9).

In addition to relevance for physical chemistry of solutions, single molecule studies provide new insights for the growing field of chemistry at the nanoscale. For example, recent studies on hydrogen-bond-based single molecular motors demonstrated the influence of solvent composition on the rotary speed of molecular rings in catenanes^[5]. In this chapter various experiments are described to study the structure-property relationships and the influence of solvent polarity on the hydrogen-bond formation on a single molecule level in different solvents and solvent mixtures, including:

1. 2-propanol
2. 1-nonanol
3. 50:50 (v/v) mixture of 2-propanol and hexadecane
4. 80:20 (v/v) mixture of 2-propanol and hexadecane

2-Propanol was chosen due to its high polarity and the low solubility of UPy supramolecular dimers and polymers. This low solubility renders the determination of the bond strength by standard approaches such as nuclear magnetic resonance (NMR), isothermal titration calorimetry (ITC) or fluorescence spectroscopy not feasible. In addition to the otherwise not attainable access to bond strengths in this solvent, the already reported effect of solvent on the rotary speed of molecular motors in solution motivates this study^[6]: when a few percent of a poor solvent is added to a solution of molecular motors, this might change the rotary speed of several single molecular motors in solution. Hence, the following paragraphs will discuss single molecule studies of supramolecular dimers and polymers in polar and mixtures of polar and apolar solvents.

6.2 UPY DIMERS IN 2-PROPANOL AND 1-NONANOL

Atomic Force Microscopy-based Single Molecule Force Spectroscopy (AFM-based SMFS) of ureidopyrimidinone (UPy) was used to study dimers in two different alcohols with a distinct difference in solvent polarity. Unlike highly polar 2-propanol the polarity of 1-nonanol is greatly reduced due to the long alkane chain (Table 6- 3).

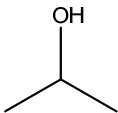
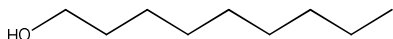
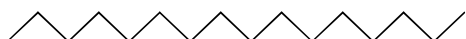
	Dipole moment [D]	Dielectric constant [-]
2-propanol 	1.66	20
1-nonanol 	1.7	9
hexadecane 	-	~2

Table 6- 3. Dipole moments and dielectric constants of the chosen polarity range: 2-propanol, 1-nonanol and hexadecane.

The effect of a long alkane chain in alcohols on the dielectric constant is the most striking indication for the shift from a rather polar to apolar solvent (methanol (33), 1-butanol (17), 1-nonanol (9), dodecan-1-ol (6))^[3]. Therefore 2-propanol and 1-nonanol with a rather large difference in dielectric constant were chosen as candidates for single molecule bond strength analysis of (UPy)₂. The results of this study are presented below.

6.2.1 UPy dimers in 2-propanol

Using AFM-based SMFS, the unbinding force of (UPy)₂ in 2-propanol was studied at four different loading rates. Force-extension curves were obtained using the procedure described in Chapter 2. Based on the polydispersity of the polyethylene glycol (PEG)-linker and the attached UPy-moiety (total stretch length of $UPy-PEG = 12 \pm 3 \text{ nm}$) only rupture events with a stretch length between 12 and 25 nm were considered. The force-extension curves were fitted to the wormlike chain (WLC) model to provide evidence for the stretching of individual PEG-linkers and hence of measuring single molecule UPy interactions. The observed

persistence length l_p of 3.24 ± 0.20 Å is consistent with previously reported literature values (see also Chapters 3, 4 and 5 for discussion)^[7]. The rupture events were probed at four different loading rates to investigate the loading rate dependence of the most probable rupture force of UPy dimers in 2-propanol. Figure 6- 2 shows the rupture force-stretch length data of (UPy)₂ in 2-propanol for two different loading rates (r).

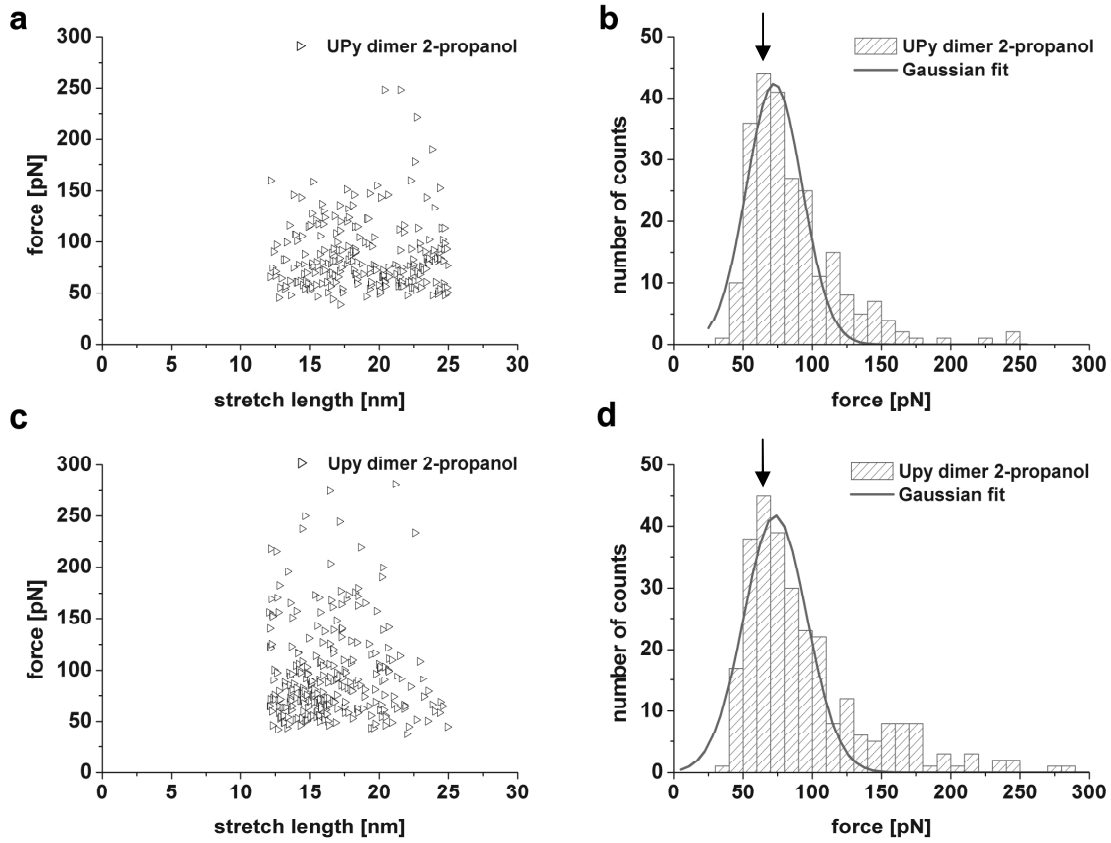


Figure 6- 2. Plots of force vs. rupture length (a,c) and histograms of unbinding forces (b,d) of (UPy)₂ in 2-propanol at two different loading rates, $r = (4.4 \pm 2.4) \times 10^3$ pN/s (top); $r = (14.5 \pm 4.1) \times 10^3$ pN/s (bottom). Note that 1. the Gaussian (normal) distribution does not fit the data very well; 2. the location of the maximum of the rupture force distributions (indicated by the arrows) is not loading rate-dependent.

Since AFM-based SMFS experiments of (UPy)₂ in 2-propanol are expected to be carried out at near-equilibrium conditions at room temperature the rupture force f can be estimated via^[8]:

$$f \cong [2 \cdot \kappa_s k_B T \ln(K_{eq})]^{1/2} \quad \text{Equation 6-1}$$

with κ_s the stiffness of the spring, k_B the Boltzmann constant, T the temperature and K_{eq} the dimer association constant (estimated as $\kappa_s = 0.1$ N/m and $K_{eq} = 55$ M⁻¹)^[9]. Hence the most probable rupture force is estimated to lie around $f \cong 65$ pN.

As can be observed in Figure 6- 2, the maxima of both distributions are located at $f \sim 70$ pN. Data acquired for two additional loading rates confirmed that the maximum is loading rate-independent (see below). The asymmetric form of the distributions appears to deviate from a symmetric Gaussian distribution. This type of unbinding force distribution was generally *not* observed for single molecule force measurements of ureidopyrimidone (UPy)₂ and urea-aminotriazine dimers (UAT)₂ in hexadecane (Chapter 3 and 4). To quantify these differences, the distributions were examined in more detail. Based on the moments of distribution (mean, variance, skewness and kurtosis) the ‘normality’ of the distribution of a set of data points in comparison with a Gaussian distribution is expressed^[10]. The arithmetic mean \bar{x} for a set of N datapoints with values $x_1 \dots x_N$ is defined as:

$$\bar{x} = \frac{1}{N} \sum_{j=1}^N x_j \quad \text{Equation 6-2}$$

The variance and standard deviation provide a measure for the width of the distribution around the arithmetic mean. The variance (Var) and standard deviation (σ) are defined as:

$$Var(x_1 \dots x_N) = \frac{1}{N-1} \sum_{j=1}^N (x_j - \bar{x})^2 \quad \text{Equation 6-3}$$

$$\sigma(x_1 \dots x_N) = \sqrt{Var(x_1 \dots x_N)} \quad \text{Equation 6-4}$$

Finally, the shape of the distribution can be characterized based on the values for the skewness ($Skew$) and kurtosis ($Kurt$):

$$Skew(x_1 \dots x_N) = \frac{1}{N} \sum_{j=1}^N \left[\frac{x_j - \bar{x}}{\sigma} \right]^3 \quad \text{Equation 6-5}$$

$$Kurt(x_1 \dots x_N) = \left\{ \frac{1}{N} \sum_{j=1}^N \left[\frac{x_j - \bar{x}}{\sigma} \right]^4 \right\} - 3 \quad \text{Equation 6-6}$$

The definition for kurtosis is based on a convention that values for the skewness and kurtosis equal zero for a normal (Gaussian) distribution. Thus, based on the skewness and kurtosis of the distribution, the ‘normality’ of a distribution can be assessed. In Figure 6- 3 a schematic of different distributions and their skewness and kurtosis is presented.

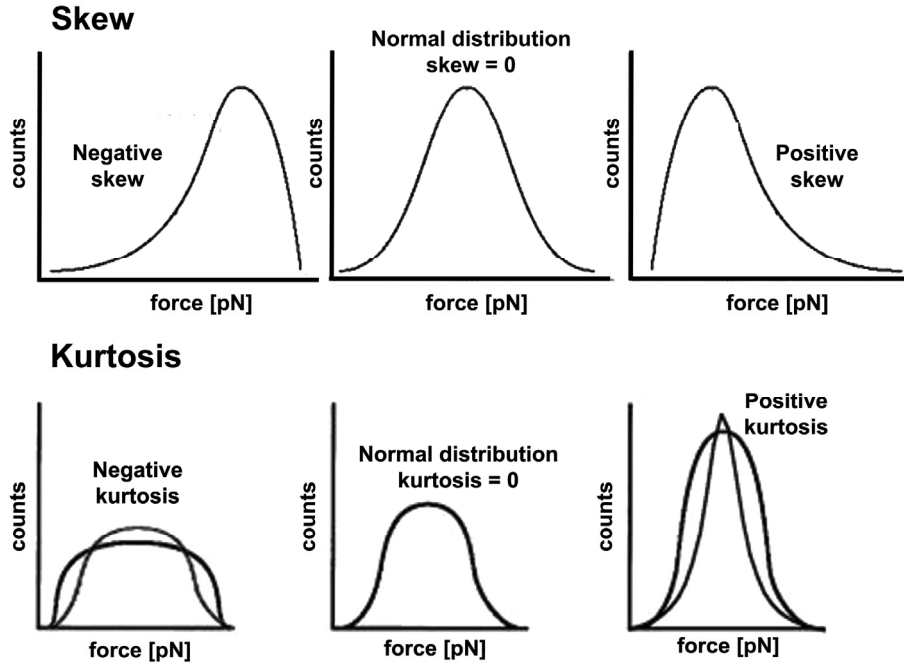


Figure 6- 3. Various distributions and their skewness and kurtosis. For a complete Gaussian (normal) distribution the skewness and kurtosis parameters are equal to zero.

Another tool to investigate the ‘normality’ of a distribution was described by Shapiro and Wilk in 1965^[11]. For small data sets (below 2000 data points)^[12] the Shapiro-Wilks test is considered to be a well-established and powerful test to estimate deviations from Gaussian distributions. For data sets with more than 2000 datapoints the Kolmogorov-Smirnov^[13] test can be applied. Since datasets for unbinding events almost never exceed 500 datapoints the Shapiro-Wilks test can be used here. For a set of N data points with samples x_1, \dots, x_N the W -statistics of the Shapiro-Wilks test is defined as:

$$W = \frac{\left(\sum_{j=1}^N a_j x_j\right)^2}{\sum_{j=1}^N (x_j - \bar{x})^2} \quad \text{Equation 6-7}$$

with a_j defined as:

$$(a_1 \dots a_N) = \frac{m'V^{-1}}{(m'V^{-1}V^{-1}m)^{1/2}} \quad \text{Equation 6-8}$$

and $m' = (m_1 \dots m_N)$ the vector of expected values of standard order statistics and V the corresponding covariance matrix. Covariance (Cov) is an estimator for the magnitude to which elements from two ordered data sets evolve in the same way.

$$Cov(X, Y) = \frac{\sum (X_i - \bar{X})(Y_i - \bar{Y})}{N} = \frac{\sum x_i y_i}{N} \quad \text{Equation 6-9}$$

with N the number of data points, \bar{X} the mean of all data points for the first set of $X_1 \dots X_N$ and \bar{Y} the mean of all data points for the second set of $Y_1 \dots Y_N$, x_i and y_i are the i^{th} deviation scores in the first and second set respectively. The covariance can be displayed in a covariance matrix:

$$\mathbf{V} = \begin{pmatrix} \sum x_1^2 / N & \sum x_1 x_2 / N & \dots & \sum x_1 x_c / N \\ \sum x_2 x_1 / N & \sum x_2^2 / N & \dots & \sum x_2 x_c / N \\ \dots & \dots & \dots & \dots \\ \sum x_c x_1 / N & \sum x_c x_2 / N & \dots & \sum x_c^2 / N \end{pmatrix} \quad \text{Equation 6-10}$$

A confidence level interval provides an estimate of the possible range of a parameter of a distribution. The confidence level and hence the value α is determined *a priori* and often used as an input parameter. Given the confidence level $(1-\alpha)$, the Shapiro-Wilks test defines the boundary value of W at which a given set of N samples can no longer be considered as a normal distribution. Based on the sample set it is now possible to numerically determine the value of α (which is based on the output parameter p in the Shapiro-Wilks test) at which the hypothesis for normality still stands. So a p -value of 0.08 would justify a rejection of the normality hypothesis with a 90% confidence level, but not with a 95% confidence level.

Statistical analyses for skewness and kurtosis were therefore performed for the unbinding force distributions of $(UPy)_2$ in 2-propanol for the four different loading rates (see Figure 6- 4). These statistical parameters were compared to the unbinding force distributions of dimers of urea-aminotriazines $(UAT)_2$ in hexadecane (Chapter 4), since these data sets possess similar numbers of unbinding events per loading rate.

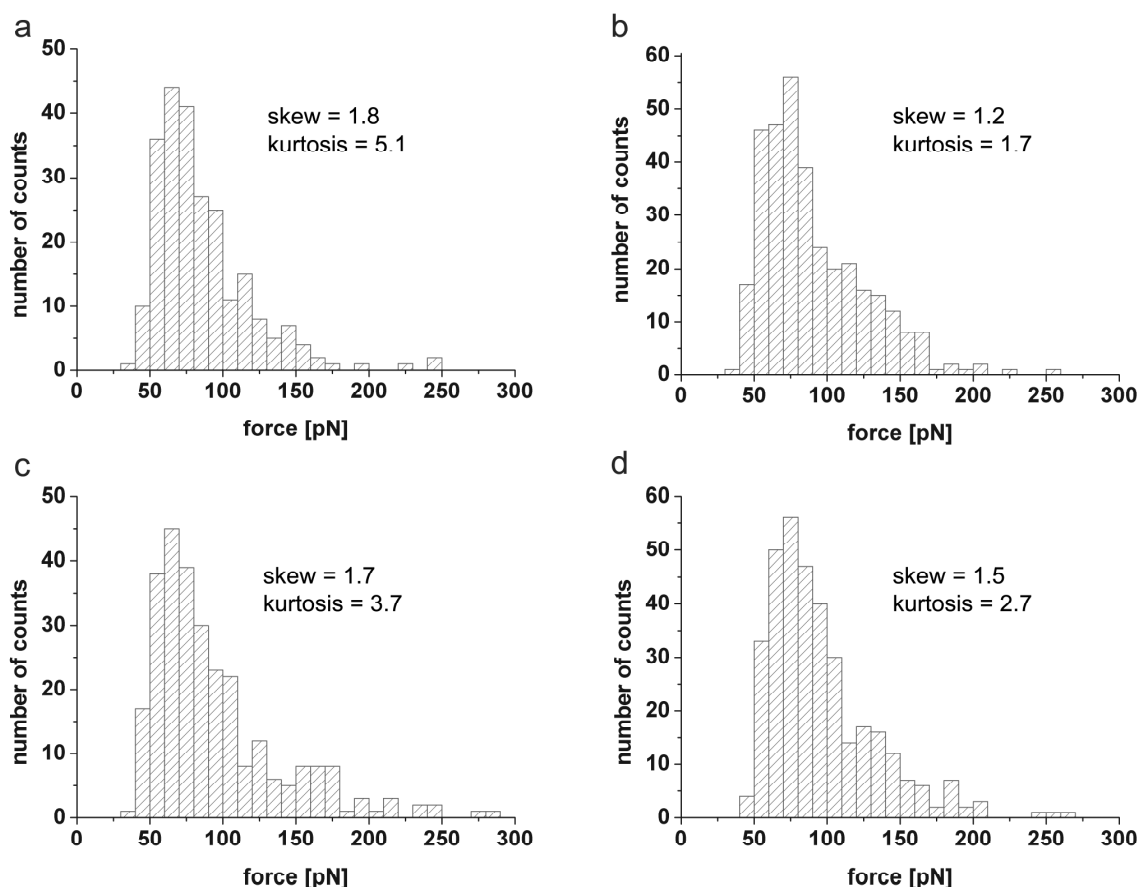


Figure 6- 4. Unbinding force histograms for (UPy)₂ in 2-propanol for (a) $r = (4.4 \pm 2.4) \times 10^3$ pN/s; (b) $r = (7.5 \pm 3.7) \times 10^3$ pN/s; (c) $r = (14.5 \pm 4.1) \times 10^3$ pN/s and (d) $r = (40.3 \pm 11.6) \times 10^3$ pN/s. The values for the skewness and kurtosis of every distribution are provided. *Note that all distributions apparently deviate significantly from a normal distribution for which skewness and kurtosis parameters of nearly zero must be expected.*

Based on the skewness and kurtosis values for the rupture force distributions in 2-propanol, a clear deviation from values for a Gaussian (normal) distributions is observed. By contrast, the distributions of rupture events of (UAT)₂ in hexadecane do *not* display these large deviations (see Figure 6- 5 below). Thus we conclude that the distribution of rupture forces of (UPy)₂ in 2-propanol deviates much more significantly from a Gaussian (normal) distribution than the distribution of rupture forces of (UAT)₂ in hexadecane. To investigate this deviation from ‘normality’ in 2-propanol more closely, the Shapiro-Wilks test was used. The Shapiro-Wilks test was performed for unbinding events of (UAT)₂ in hexadecane and (UPy)₂ in 2-propanol based on random-number generated data sets of $N = 100$ events. The results are shown in Table 6- 4 and Table 6- 5, respectively.

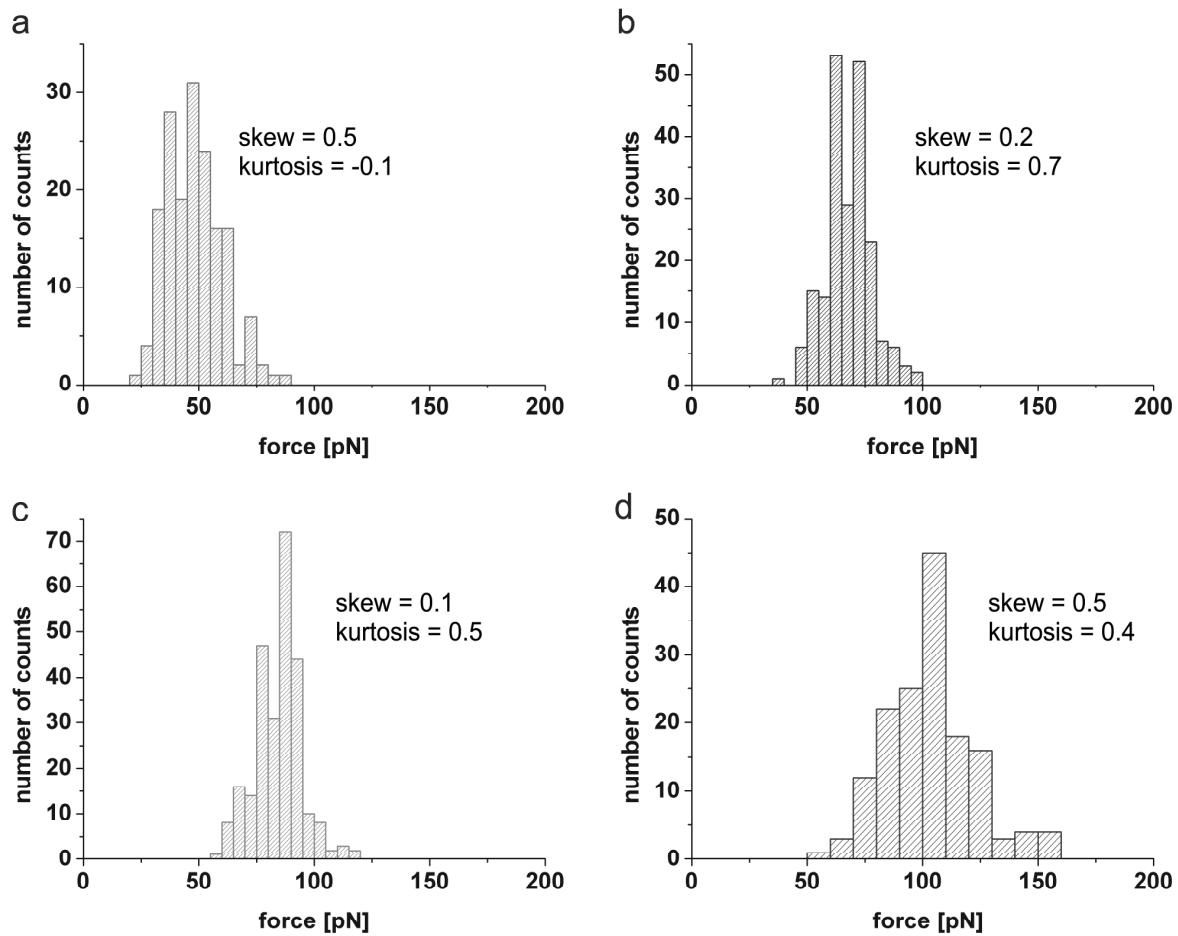


Figure 6- 5. Unbinding force histograms for (UAT)₂ in hexadecane for (a) $r = (3.7 \pm 1.4) \times 10^3$ pN/s; (b) $r = (13.4 \pm 4.7) \times 10^3$ pN/s; (c) $r = (46.7 \pm 17.5) \times 10^3$ pN/s and (d) $r = (134.7 \pm 50.9) \times 10^3$ pN/s. The values for the skewness and kurtosis of every distribution are provided. *Note that for all distributions skewness and kurtosis parameters are close to zero as expected for a normal distribution.*

If a confidence level of 99% is chosen ($\alpha = 0.01$) the normal distribution must be rejected for all distributions of (UPy)₂ in 2-propanol, whereas the hypothesis of a normal distribution for all dataset of (UAT)₂ in hexadecane holds.

	hexadecane $r = (3.7 \pm 1.4) \times 10^3$ pN/s	hexadecane $r = (13.4 \pm 4.7) \times 10^3$ pN/s	hexadecane $r = (46.7 \pm 17.5) \times 10^3$ pN/s	hexadecane $r = (134.7 \pm 50.9) \times 10^3$ pN/s
W	0.97	0.98	0.87	0.99
p	0.02	0.24	0.02	0.45

Table 6- 4. Shapiro-Wilks statistics of the unbinding force distributions of (UAT)₂ in hexadecane for various loading rates. *The hypothesis of a normal distribution holds for $\alpha = 0.01$ (99%) for all loading rates.*

	2-propanol $r = (4.4 \pm 2.4) \times 10^3$ pN/s	2-propanol $r = (7.5 \pm 3.7) \times 10^3$ pN/s	2-propanol $r = (14.5 \pm 4.1) \times 10^3$ pN/s	2-propanol $r = (40.3 \pm 11.6) \times 10^3$ pN/s
W	0.87	0.87	0.82	0.88
p	6.2×10^{-8}	1.3×10^{-7}	1.0×10^{-9}	2.5×10^{-7}

Table 6- 5. Shapiro-Wilks statistics of the unbinding force distributions of (UPy)₂ in 2-propanol for various loading rates. *The hypothesis of a normal distribution must be rejected for $\alpha = 0.01$ (99%) for all loading rates.*

The combined statistical analysis with the large differences in skewness, kurtosis and W - and p -parameters for the distribution of unbinding events of (UPy)₂ in 2-propanol clearly indicate that the data sets can not be considered as normal distributions.

Various reports confirm the presence of solvent clusters in alcohols, including 2-propanol, which was used in our studies. Molecular aggregates, or solvent clusters, in alcohols have for instance been predicted by a.o. Jorgensen and co-workers^[14b] using experimental studies and Monte Carlo simulations. Furthermore the formation of (solvent) clusters in H₂O and alcohols with the polyelectrolyte C₁₂EO₂₃ (which resembles the PEG-linker in our experiments) was studied by dynamic light scattering (DLS) and small angle X-ray scattering (SAXS)^[15].

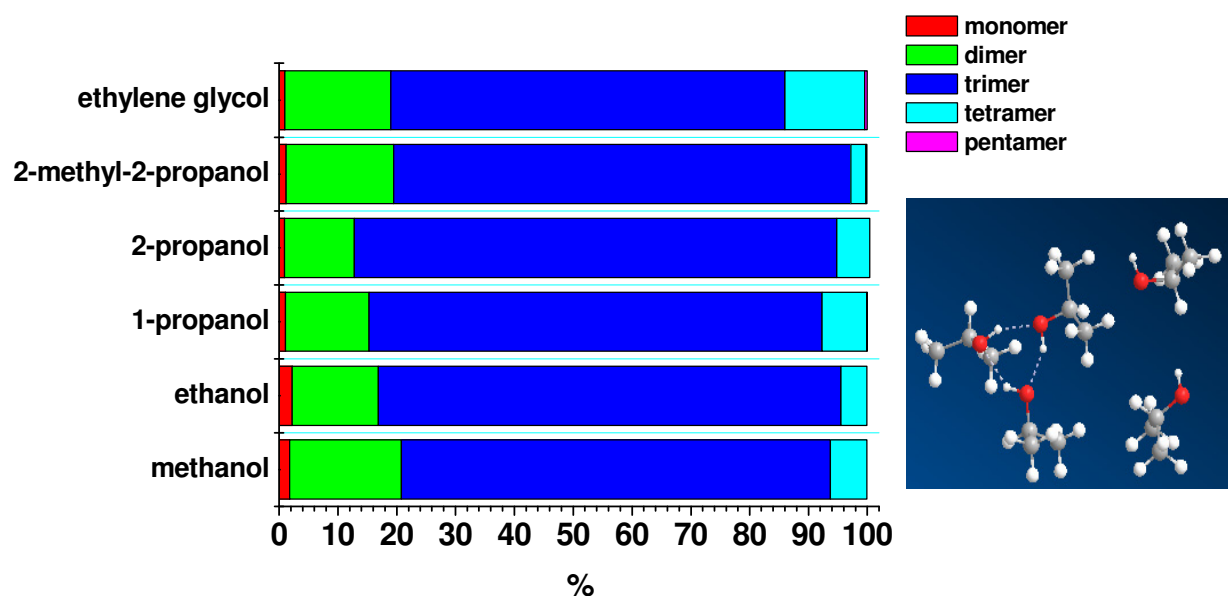


Figure 6- 6. Chart of the distribution of molecular aggregates (solvent clusters) in alcohols and ethylene glycol determined via molecular simulations^[14]. Inset: 3D representation of cluster formation of 2-propanol molecules in pure solvent. *Chart constructed based on data from ref. 14.*

In addition, literature reports provide evidence for the presence of a slow dynamics component for solvent molecules which are bound via hydrogen-bonding to supramolecular aggregates (such as H₂O around proteins and DNA) or if local viscosity effects play a role^[16].

We speculate that the unusual skewed rupture force distributions observed may be indirectly related to solvent clustering. While the data discussed in this chapter precludes any definite statement, we would like to put this tentative interpretation forward as a working hypothesis.

For thermally activated rupture processes, such as the rupture of ligand-receptor interactions, a normal Gaussian distribution is expected, for which the width of the rupture force distribution is governed by the temperature T and the characteristic length of the ligand-receptor bond x_β ($=k_B T/f_\beta$). As shown above (and also for other scenarios below), the estimated values for skew, kurtosis and the Shapiro-Wilks parameters showed that the data deviated markedly from single Gaussian distributions. This can be attributed to different contributions, *i.e.* populations of different rupture forces.

To rationalize this result we speculate that the bond rupture in a locally different environment is different as the potential energy surface of the unbinding reaction is different and that these different environments are defined by the intermolecular interaction in solvent clusters of different compositions. Following this hypothesis the influence of solvent clustering effects on the rupture forces of (UPy)₂ in 2-propanol is not present, *i.e.* this explanation must be rejected if among others the width (indicated by σ) of a single unimodal distribution is consistent with the expected width for a single thermally activated ligand-receptor interaction (See Chapters 3 and 4 for σ -values of (UPy)₂ and (UAT)₂ in hexadecane). To test this hypothesis and assign plausible contributions to the force distributions an overlay plot of unbinding events for (UPy)₂ in hexadecane and 2-propanol was created for various loading rates. The results of this comparison are displayed in Figure 6- 7.

The comparison indicates that the high force tail of the distribution of rupture forces of (UPy)₂ in 2-propanol coincides with the force distribution measured in hexadecane at similar loading rates. Furthermore the maximum of the total rupture force distributions was loading rate-independent, as mentioned above. Hence, we may further speculate that this data is consistent with the assumption of contributions from rupture forces of (UPy)₂ in a predominantly polar (-OH like) and a predominantly apolar (hexadecane-like) environment which results in a possible bimodal distribution.

Such an interpretation would be in strong contrast to data obtained in ensemble averaged measurements for a water-saturated chloroform mixture, where consequently an ensemble averaged association constant was obtained^[4].

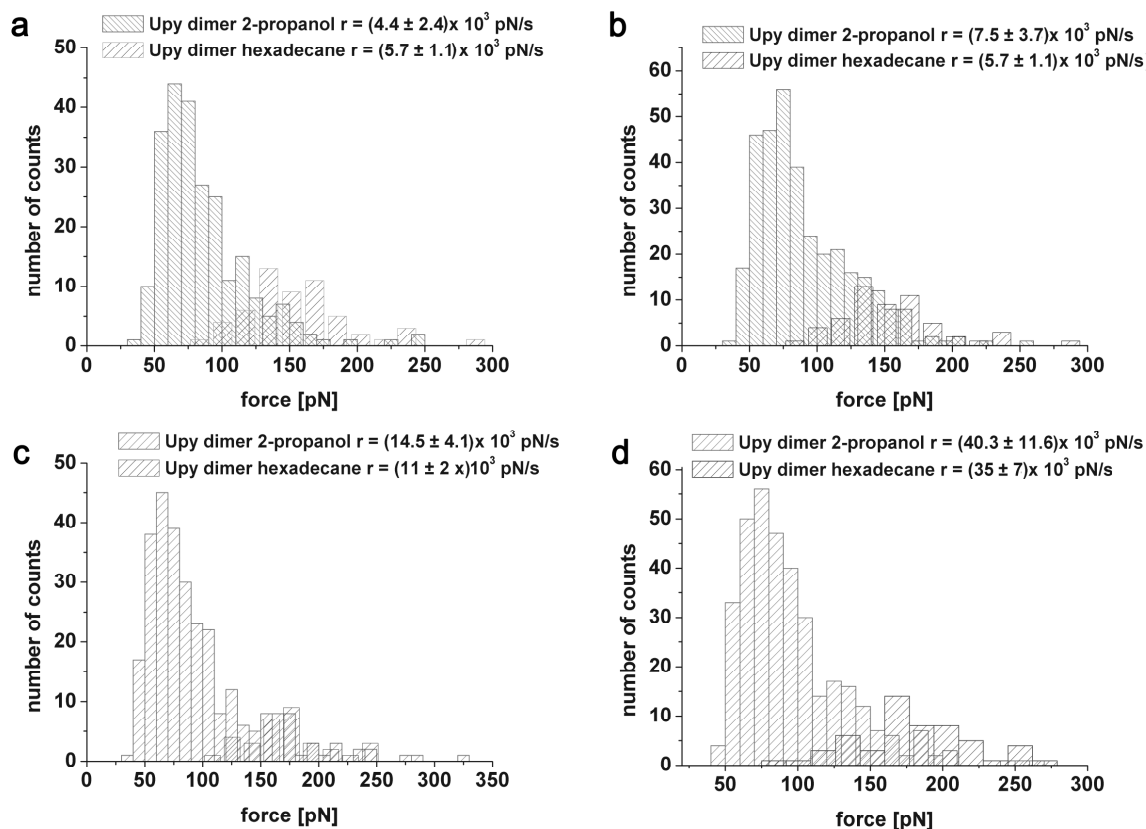


Figure 6- 7. Comparison of unbinding distributions of $(UPy)_2$ in 2-propanol and hexadecane for similar loading rates. *Note that the high force tail in the distributions for 2-propanol overlap closely with the rupture forces for $(UPy)_2$ unbinding events in hexadecane for similar loading rates.*

In case a bimodal distribution is assumed, the low force peak has a most probable rupture force of $f^* \sim 70 \pm 30$ pN for the four different data sets and hence the following plot for the loading rate-(in)dependence on the rupture force is obtained (see Figure 6- 8). The most probable rupture force f^* does not scale logarithmically with the loading rate over almost two orders of loading rate. Thus at least over the range of loading rates investigated here, equilibrium conditions are likely. Furthermore these measurements indicate that the dimer binding constant is significantly higher than $K_{eq} = 50 \text{ M}^{-1}$, since a higher average rupture force is measured with a more flexible spring. This result does not come as a complete surprise since Sijbesma and Meijer reported a dimer binding constant of $K_{eq} = 1 \times 10^7 \text{ M}^{-1}$ for completely water-saturated chloroform^[4].

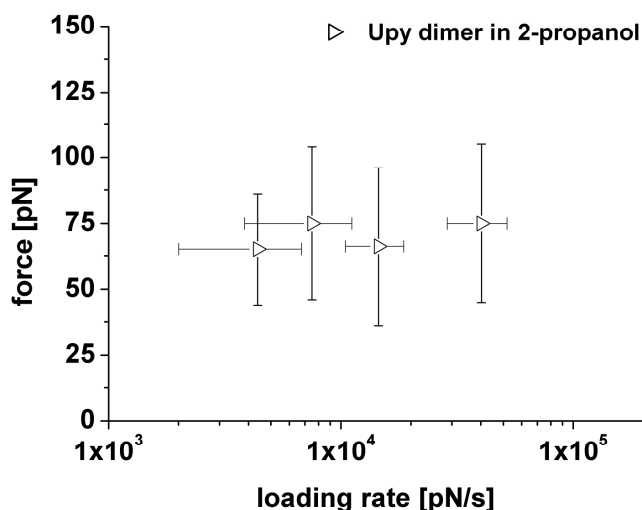


Figure 6- 8. Most probable rupture force as a function of loading rate for UPy dimers in 2-propanol, based on a Gaussian fit of the low force region. *The data shown here leads to the conclusion that the unbinding of (UPy)₂ in 2-propanol was mostly likely performed in near-equilibrium conditions over the loading rate range probed here: $r = (4.4 \pm 2.4) - (40.3 \pm 11.6) \times 10^3$ pN/s.*

6.2.2 UPy dimers in 1-nonanol

The rupture forces of (UPy)₂ were also studied in 1-nonanol as described previously. Unlike 2-propanol, 1-nonanol has a long aliphatic tail and based on the molecular structure and the dielectric constant, the rupture forces are expected to shift towards higher values. The results of this study are presented in Figure 6- 9 and Figure 6- 10.

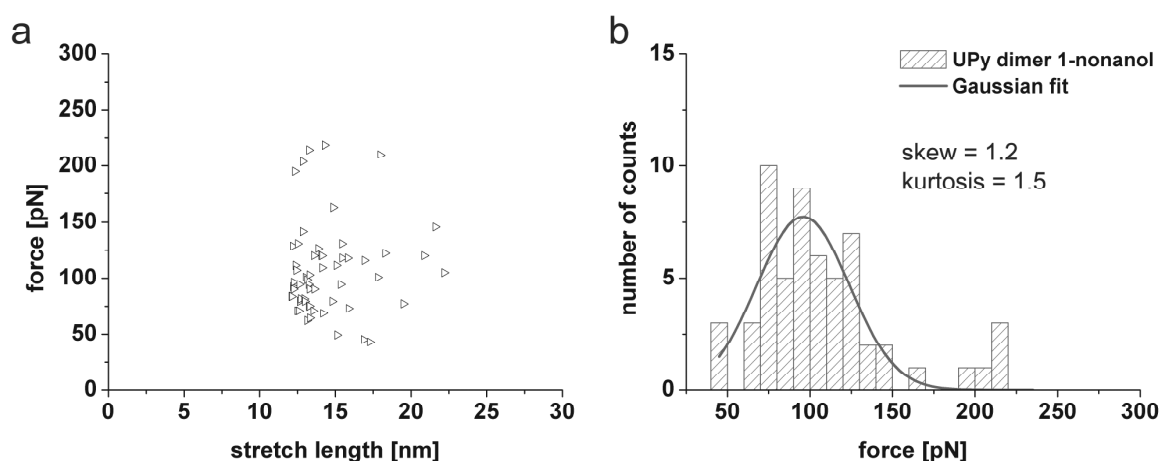


Figure 6- 9. (a) Distribution of stretch lengths and rupture forces for UPy dimers in 1-nonanol for $r = (2.1 \pm 0.7) \times 10^3$ pN/s; (b) Histogram of rupture forces, $f^* = 95 \pm 51$ pN.

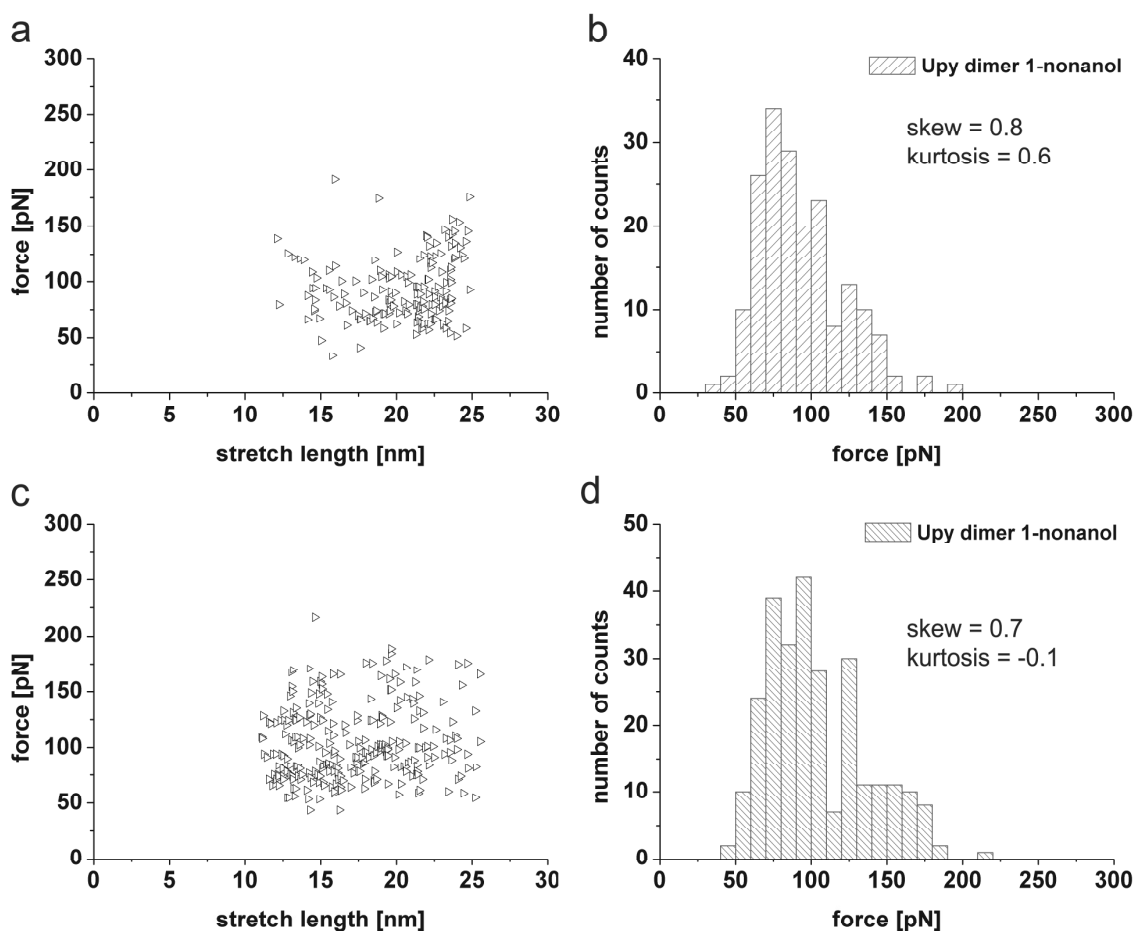


Figure 6- 10. (a,c) Distribution of stretch lengths and rupture forces for Upy dimers in 1-nonanol for $r = (4.7 \pm 2.5) \times 10^3$ pN/s and $r = (7.6 \pm 2.7) \times 10^3$ pN/s respectively; (b,d) histogram of rupture forces for $r = (4.7 \pm 2.5) \times 10^3$ pN/s and $r = (7.6 \pm 2.7) \times 10^3$ pN/s respectively, including the statistical parameters skewness and kurtosis.

The force-extension curves were fitted to the WLC model which provided the following value for the persistence length of $l_p = 3.52 \pm 0.32$ Å. Only a small data set was collected for the lowest loading rate presented in Figure 6- 9 which is not very suitable for statistical analysis. However the data presented in Figure 6- 10 can be analyzed with the statistical approaches (skewness, kurtosis and Shapiro-Wilks test) described above. The values for the skewness and kurtosis indicate that the distributions of unbinding forces for (UPy)₂ in 1-nonanol deviate from a normal distribution, however not as much as those in 2-propanol. This conclusion is supported by the Shapiro-Wilks test for the data sets in 1-nonanol (see Table 6- 6).

The deviations from a Gaussian distribution are less pronounced in 1-nonanol as compared to those in 2-propanol, presumably since 1-nonanol with its long alkane tail resembles hexadecane more closely. The rupture force distributions were also compared to the rupture force distributions of (UPy)₂ in hexadecane (see Figure 6- 11).

	1-nonanol $r = (2.1 \pm 0.7) \times 10^3$ pN/s	1-nonanol $r = (4.7 \pm 2.5) \times 10^3$ pN/s	1-nonanol $r = (7.6 \pm 2.7) \times 10^3$ pN/s
W	0.88	0.96	0.94
p	5.2×10^{-5}	4.0×10^{-3}	2.0×10^{-4}

Table 6- 6. Shapiro-Wilks statistics of the unbinding force distributions of (UPy)₂ in 1-nonanol for various loading rates. *The hypothesis of a normal distribution still has to be rejected for $\alpha = 0.01$ (99%).*

Similar to the data obtained in 2-propanol the high force tail of the unbinding force distributions of (UPy)₂ in 1-nonanol coincides with the data obtained for the unbinding force of (UPy)₂ in hexadecane. Furthermore the standard deviation in Figure 6- 10 demonstrates that the width σ of a unimodal Gaussian distribution is substantially larger than those obtained for measurements in hexadecane. Hence the distribution of unbinding forces in 1-nonanol again appears to be consistent with a bimodal distribution consisting of two overlapping Gaussian distributions.

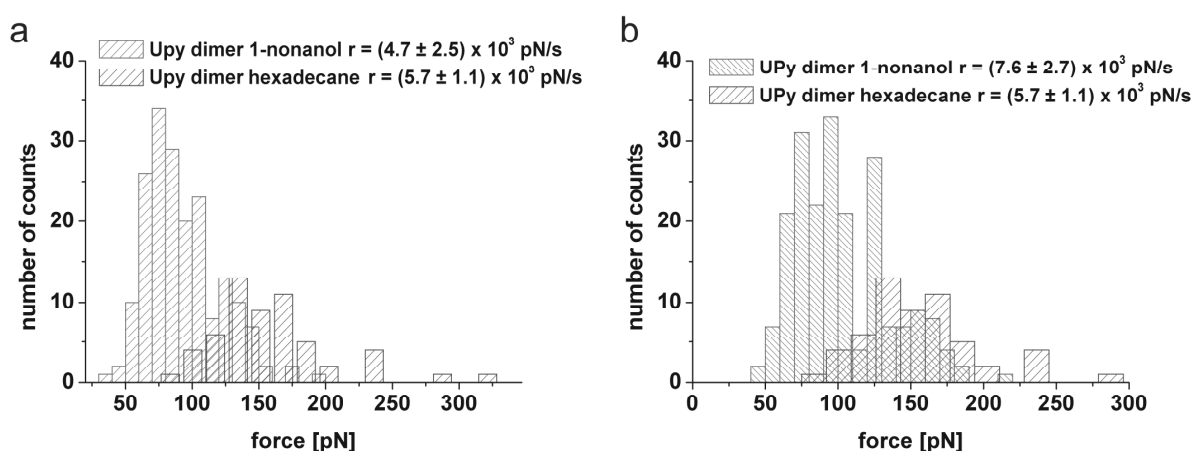


Figure 6- 11. Comparison of unbinding distributions of (UPy)₂ in 1-nonanol and hexadecane for similar loading rates. *Note that the high force tail in the distributions for 1-nonanol seems to overlap closely with the rupture forces for (UPy)₂ unbinding events in hexadecane for similar loading rates.*

If the “low-force maximum” of the unbinding distributions of (UPy)₂ in 1-nonanol, determined by fitting the distribution to a Gaussian function, is plotted against the loading rate, no marked dependence can be observed (see Figure 6- 12). Hence we can conclude that the measurements were most likely performed in near-equilibrium conditions in this loading rate regime.

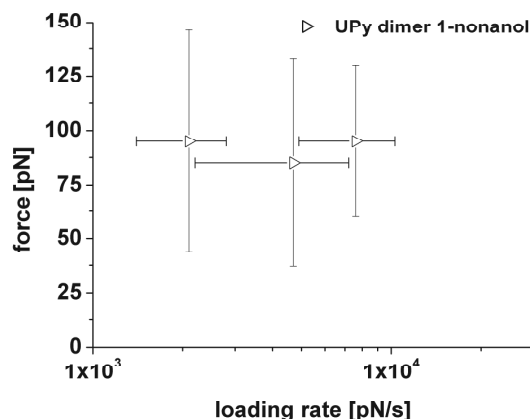


Figure 6- 12. Rupture force vs. loading rate of (UPy)₂ in 1-nonanol $r = (2.1 \pm 0.7) \times 10^3 - (7.6 \pm 2.7) \times 10^3$ pN/s.

It should be mentioned that only a small data set was available for the lowest loading rate, hence the conclusions are provisional. More data at higher loading rates has to be collected to substantiate or reject the conclusions of loading rate-dependence of the rupture forces of (UPy)₂ in 1-nonanol. Thus no direct value for the hydrogen-bond strength of (UPy)₂ in 1-nonanol can be provided, but the values of the most probable rupture forces $f^* \sim 95 \pm 30$ pN may indicate a higher bond strength in a less polar solvent (1-nonanol versus 2-propanol). Finally the obtained rupture force distributions also appear to be consistent with the hypothesis of the influence of solvent clustering in this single molecule study in 1-nonanol.

6.2.3 Discussion and conclusion

A clear trend was observed based on the data presented above for the unbinding events of (UPy)₂ in pure solvents in the decreasing polarity range from 2-propanol, 1-nonanol and hexadecane (Chapter 3). The rupture forces likely scale with the polarity of the solvent, but a dependable value for the bond strength for (UPy)₂ in the polar solvents could not be determined since the experimental loading rate range used was too narrow. The data were consistent with the assumption of a bimodal distribution, composed of the contribution of bond rupture in predominantly polar and predominantly apolar environments, for rupture forces of (UPy)₂ in 2-propanol and 1-nonanol. To study these effects in more detail the unbinding events of supramolecular UPy polymers in mixed solvents of 2-propanol and hexadecane were investigated. The volume ratio of the solvents and the loading rate were varied to study the force distributions under these conditions.

6.3 SUPRAMOLECULAR UPY POLYMERS IN MIXED SOLVENTS

The rupture forces of UPy-polymers in a binary mixture of polar and apolar solvent was probed for two different compositions. These rupture forces were studied as described previously in Chapter 3, where the number of linkers in a single supramolecular polymer is defined as $N = (L/12 \text{ nm}) - 1$ based on the polydispersity of the PEG linker and the attached UPy-moieties. Furthermore the distributions were analyzed statistically based on skewness, kurtosis and the Shapiro-Wilks test.

6.3.1 UPy polymers in a 50:50 mixture of 2-propanol and hexadecane

The unbinding events of UPy-polymers in a 50:50 (v/v) mixture of 2-propanol and hexadecane (named 5050 HDIsop) were studied at two *fixed* loading rates: $r = (3.8 \pm 1.3) \times 10^3 \text{ pN/s}$ and $r = (9.4 \pm 3.5) \times 10^3 \text{ pN/s}$. When the bis-UPy linker was added, the rupture lengths observed exceeded those expected for the dimer, indicating the formation of supramolecular polymer chains bridging between the substrate surface and the AFM-tip (see Figure 6- 13). The force distance curves were fitted to the WLC model and a persistence length of $l_p = 3.60 \pm 0.32 \text{ \AA}$ was obtained, which corresponds well with values for PEG-linkers reported in literature^[6]. This supports the notion that single molecule supramolecular polymers were studied in a 50:50 (v/v) ratio of 2-propanol and hexadecane. The distribution of rupture forces is presented in Figure 6- 14. From the distribution of forces and stretch lengths (Figure 6- 14a,c) it is obvious that the unbinding force decreases with increasing stretch length.

The rupture of $(\text{UPy})_2$ in these mixed solvents was studied in the same fashion and the force data was then compared to the unbinding events of $(\text{UPy})_2$ in pure hexadecane (for similar loading rates). Figure 6- 15 shows an overlay plot of UPy dimer rupture events obtained in a 50:50 (v/v) mixture of 2-propanol and hexadecane in comparison with rupture events in pure hexadecane. The same stretch lengths L for the rupture forces of $(\text{UPy})_2$ in the mixed solvent as well as for those in purely apolar hexadecane are considered here (12 nm until 25 nm based on the polydispersity of the PEG-linker and the attached UPy-moiety, as discussed in Chapter 3).

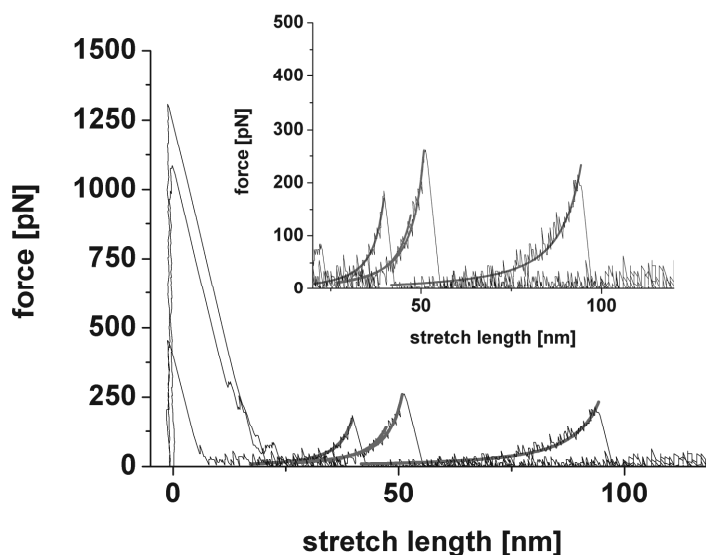


Figure 6- 13. Force-extension curves of unbinding events of UPy supramolecular polymers in a 50:50 (v/v) ratio of 2-propanol and hexadecane. Inset: zoom of unbinding events. Solid lines represent wormlike chain (WLC) fits.

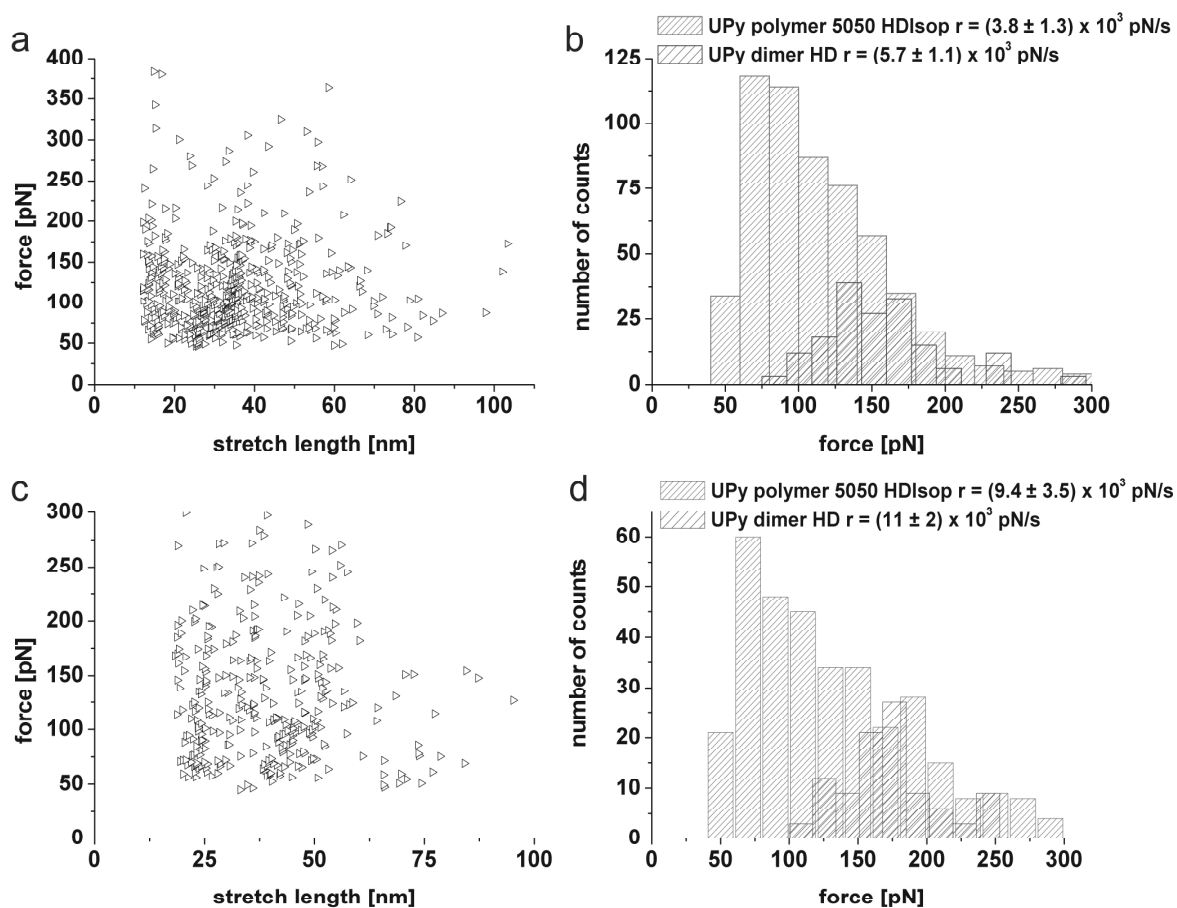


Figure 6- 14. Plots of force versus stretch length (a,c) and histograms (b,d) of rupture force of UPy polymers in a 50:50 (v/v) mixture of 2-propanol and hexadecane (5050 HDIsop): (a,b) $r = (3.8 \pm 1.3) \times 10^3$ pN/s; (c,d) $r = (9.4 \pm 3.5) \times 10^3$ pN/s. Note that the overlay plot of the unbinding force of $(UPy)_2$ in pure hexadecane overlaps rather well with the high force tail in (b,d).

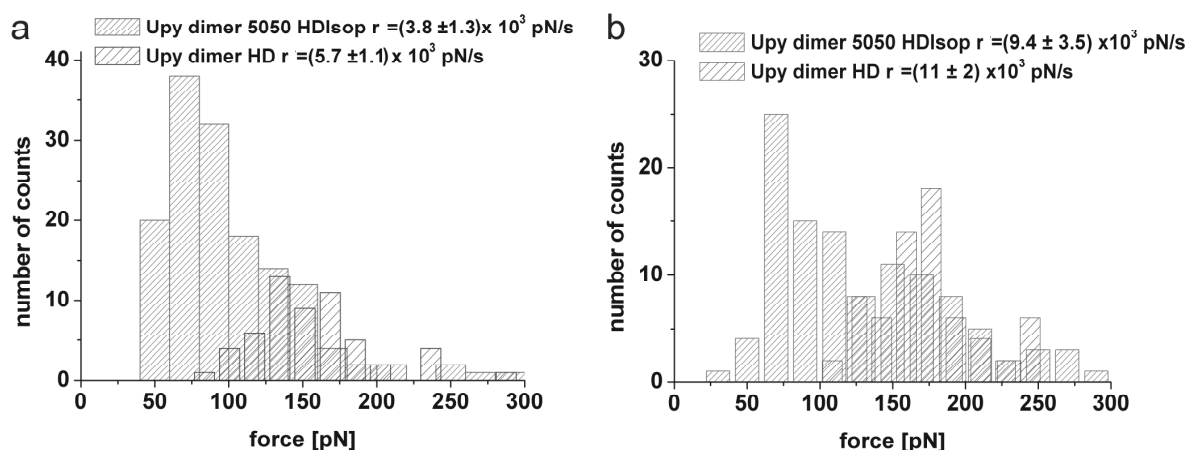


Figure 6- 15. Comparison of distributions of (UPy)₂ rupture events in a 50:50 (v/v) mixture of 2-propanol and hexadecane (5050 HDIsop) and pure hexadecane (HD) for similar loading rates: (a) $r = (3.8 \pm 1.3) \times 10^3$ pN/s and (b) $r = (9.4 \pm 3.5) \times 10^3$ pN/s.

Based on the dimer interactions, present in the total ensemble of supramolecular polymer rupture events in the 50:50 (v/v) solvent mixture of hexadecane and 2-propanol, statistical analysis of the skew and kurtosis was performed. Furthermore a random-number-generated data set of $N = 100$ was again used to obtain values for the W -statistics and p -values of the Shapiro-Wilks test.

	UPy dimer 50-50 HDIsop $r = (3.8 \pm 1.3) \times 10^3$ pN/s	UPy dimer 5050 HDIsop $r = (9.4 \pm 3.5) \times 10^3$ pN/s
<i>skewness</i>	1.6	0.7
<i>kurtosis</i>	3.4	-0.1
<i>W statistics</i>	0.85	0.95
<i>p-value</i>	7.1×10^{-9}	4.5×10^{-4}

Table 6- 7. Statistical analysis of a subset of the unbinding events of supramolecular polymers in a 50:50 (v/v) 2-propanol/hexadecane for two loading rates $r = (3.8 \pm 1.3) \times 10^3$ pN/s and (b) $r = (9.4 \pm 3.5) \times 10^3$ pN/s.

Based on the data presented above a deviation from a Gaussian distribution was observed for the obtained distributions of unbinding of UPy-based supramolecular polymers in a 50:50 (v/v) mixed solvent of 2-propanol and hexadecane. Furthermore the low force peak of the unbinding of (UPy)₂ in this mixture was located at approximately the same force $f^* \sim 70$ pN as for pure 2-propanol. Finally the high force tail coincides with the results of the unbinding experiments of (UPy)₂ in pure apolar hexadecane.

If the high force tail is assumed to be caused by rupture events of (UPy)₂ in a predominantly apolar environment, the most probable rupture force should be loading rate-dependent. Since only quite narrow loading rate regimes were investigated no direct conclusions can be drawn. However one would also expect a decrease in the rupture force for longer supramolecular polymers, based on the uncooperative bond failure for ligand-receptor interactions switched in series as discussed in Chapter 3. Therefore the rupture force distribution of dimers, trimers, etc. (with $N = 1..4$) was also determined using $N = (L/12 \text{ nm}) - 1$. The resulting rupture force distributions of the supramolecular UPy dimer, trimers, etc. in the 50:50 (v/v) solvent mixture of hexadecane and 2-propanol is compared to the distribution of UPy dimers in hexadecane for the two different loading rates (see Figure 6- 16 and Appendix Figure 6- 19 and 6- 20 for a complete overview).

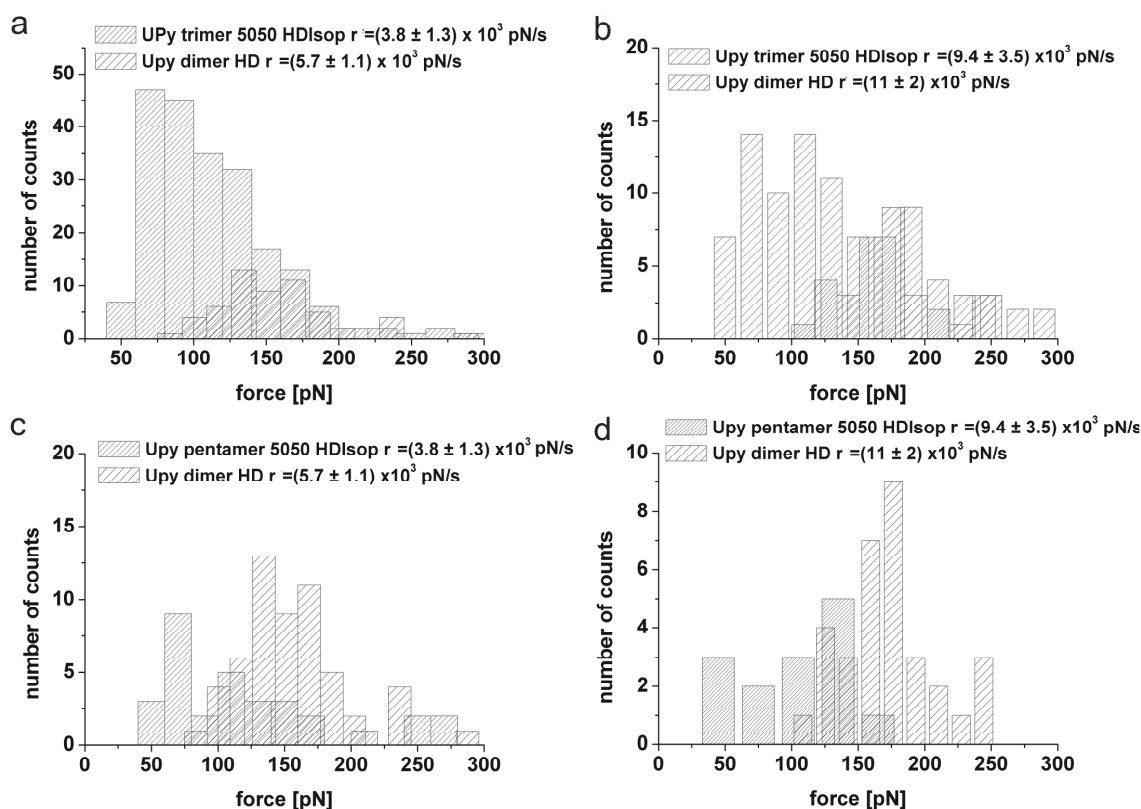


Figure 6- 16. Comparison of supramolecular UPy-trimer and pentamer polymer rupture events of a 50:50 (v/v) mixture of hexadecane and 2-propanol (5050 HDIsop) and (UPy)₂ in pure hexadecane (HD) (a,c) $r = (3.8 \pm 1.3) \times 10^3 \text{ pN/s}$ and (b,d) $r = (9.4 \pm 3.5) \times 10^3 \text{ pN/s}$. Note that a clear shift to lower forces is present in comparison with the dimer rupture events at a similar loading rate.

The rupture forces of (UPy)₂ in the 50:50 mixture of hexadecane and 2-propanol indeed seem to move towards lower rupture forces for larger N . Hence the high force tail in the rupture distribution seems to be consistent with unbinding of UPy moieties in an apolar environment. This supports the hypothesis that solvent clustering might play a role in the rupture force distribution of these supramolecular dimers and polymers in these polar solvents.

6.3.2 UPy polymers in a 80:20 mixture of 2-propanol and hexadecane

The distribution of unbinding events of (UPy)₂ in a 80:20 (v/v) mixture of 2-propanol and hexadecane (named HDIsop 20/80) was studied at a *fixed* loading rate of $r = (7.2 \pm 3.6) \times 10^3$ pN/s. Again the same procedure was followed as described above. Rupture lengths were observed that exceeded those expected for the dimer after the bis-UPy linker was added. The distribution of rupture events is presented in Figure 6- 17.

The force-distance curves were fitted to the WLC model. A value for the a fitted persistence length of $l_p = 3.54 \pm 0.31$ Å was obtained. Therefore the formation of supramolecular polymer chains can be confirmed.

From the distribution of forces and stretch lengths (Figure 6- 17a) it can be concluded that the unbinding forces decreased with increasing stretch length.

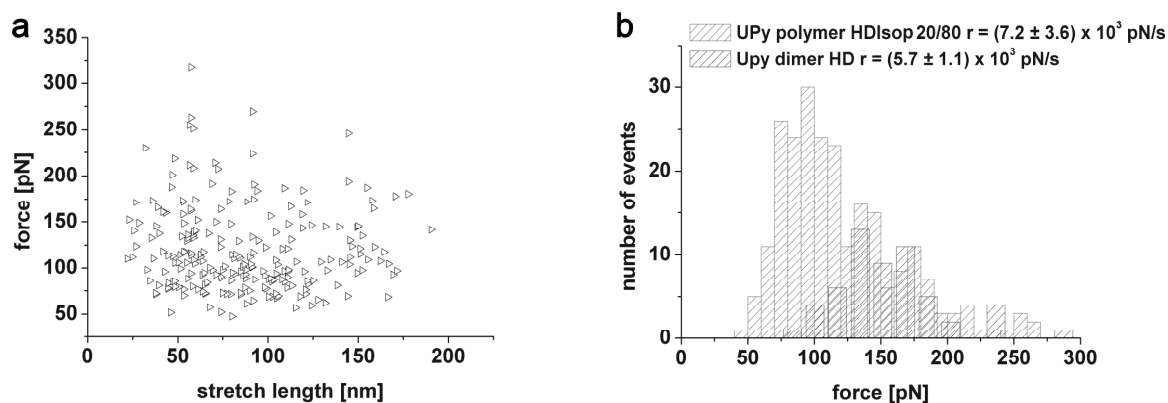


Figure 6- 17. (a) Supramolecular UPy polymer rupture events in a 80:20 (v/v) mixture of 2-propanol and hexadecane; (b) comparison of distributions of supramolecular UPy polymer rupture events in a 80:20 (v/v) mixture of 2-propanol and hexadecane (HDIsop 20/80) and (UPy)₂ rupture in pure hexadecane (HD) for similar loading rates: $r = (7.2 \pm 3.6) \times 10^3$ pN/s and $r = (5.7 \pm 1.1) \times 10^3$ pN/s. *The effect of uncooperative unbinding of supramolecular UPy polymers can be observed since the rupture force decreases for polymers with longer stretch lengths.*

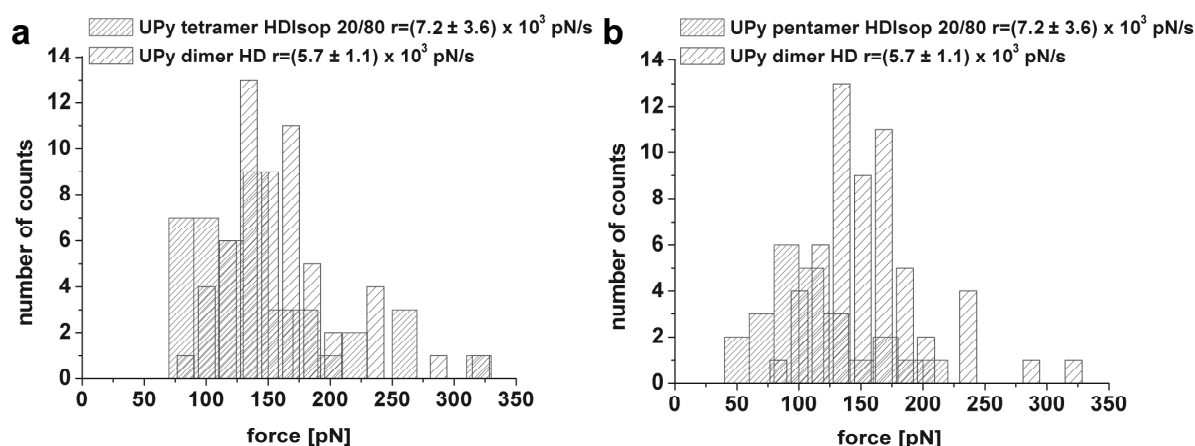


Figure 6- 18. Comparison of distributions of supramolecular UPy polymer rupture events in a 80:20 (v/v) mixture of 2-propanol and hexadecane (HDIsop 20/80) and (UPy)₂ rupture in pure hexadecane (HD) for similar loading rates: $r = (7.2 \pm 3.6) \times 10^3$ pN/s and $r = (5.7 \pm 1.1) \times 10^3$ pN/s. *Note that indeed the rupture forces shift to lower values for longer supramolecular polymers.*

Once more the high force tail in the histogram seems to be consistent with the rupture forces that were measured for (UPy)₂ in pure hexadecane. A low force tail with $f^* \sim 75$ pN is observed as well. The hypothesis of the possible influence of solvent clusters on the rupture force distribution is again examined. Hence the rupture events of supramolecular tetra- and pentamers in this mixed solvent are compared to the unbinding events of (UPy)₂ in pure hexadecane for a similar loading rate (see Figure 6- 18): the rupture forces shift towards lower values in comparison to the rupture forces in apolar hexadecane.

The data discussed here are not in conflict with the possible influence of solvent clustering on the rupture force distribution. However further research must be performed to support or reject the hypothesis presented here.

6.4 DISCUSSION AND CONCLUSION

The rupture events of supramolecular UPy-dimers and polymers were studied in a variety of solvents (2-propanol, 1-nonanol and hexadecane) and solvent mixtures (of 2-propanol and hexadecane). In all cases, except for pure apolar hexadecane, a distribution of rupture forces was found which can not be classified as a single Gaussian (normal) distribution. Deviations of this Gaussian (normal) distribution were studied using the skewness and kurtosis parameters, as well as a Shapiro-Wilks test. From this analysis it was concluded that the distribution of unbinding events in 1-nonanol approaches a Gaussian distribution more closely

than in 2-propanol, which is rationalized by the fact that 1-nonanol, with its long alkane chain, and hexadecane are more alike. Furthermore the rupture forces scale with polarity: more polar solvents weaken the hydrogen-bond strength, since the dipoles of the solvent influence solute-solute and solvent-solute interactions. Unfortunately no clear conclusions about the hydrogen-bond strength in 2-propanol and 1-nonanol can be provided since the range of loading rates that was utilized, was too small. However the statistical analysis of the unbinding force distributions clearly hint at different contributors to the rupture forces and possibly the role of molecular solvent clusters during bond rupture. In particular the high force tail observed in the rupture force distributions coincides with previous results for the unbinding events of (UPy)₂ in pure hexadecane. Investigating the unbinding effects at higher loading rates is therefore strongly recommended since a loading rate dependency of the high force peak would be expected if this high force tail was indeed caused by apolar solvent clusters in these alcohols.

The unbinding of supramolecular polymers in a mixture of solvents was studied as well, to obtain more insight in the influence of polar and apolar components in solution. A 50:50 (v/v) an 80:20 (v/v) ratio of 2-propanol and hexadecane was chosen. In both cases a distribution of rupture forces was observed, which deviated from a Gaussian (normal) distribution. Furthermore the apparent trend of uncooperative bond failure in series (a decrease in f^* when more linkers are involved) indicates that the high force tail in these measurements is consistent with unbinding events of (UPy)₂ in a predominantly apolar environment.

6.5 MATERIALS AND METHODS

Materials. Anhydrous hexadecane (purity ≥ 99 %, water < 0.005 %), anhydrous 2-propanol (purity ≥ 99.5 %, water < 0.005 %) and dibutyltindilaurate were purchased from Sigma-Aldrich (Steinheim, Germany) and used as received. 1-nonanol (purity ≥ 99.5 %) was also bought from Sigma-Aldrich and dried over mol sieves for several weeks. Chloroform (stabilized with amylene) and dichloromethane were purchased from Biosolve (Valkenswaard, The Netherlands).

1,2-Dithiolane-3-pentyl-derivatized PEG **1**, (6-isocyanatohexylaminocarbonylamino)-6-methyl-4[1H]pyrimidinone **2** and PEG-linked bis-pyrimidinone **3** were synthesized according to published procedures^[18,20].

Sample preparation. Gold substrates ($11 \times 11 \text{ mm}^2$, 250 nm Au on 2 nm Cr on borosilicate glass) for SMFS measurements were purchased from Arrandee (Werther, Germany). Au(111) samples were obtained by annealing these substrates in a high purity H_2 flame for 5 minutes^[19]. Prior to use, these substrates were cleaned in a piranha solution (2:1 H_2SO_4 conc: H_2O_2 (30%) by volume), then rinsed with Milli-Q water and ethanol followed by drying in a nitrogen stream. **Caution: Piranha solution should be handled with extreme caution: it has been reported to detonate unexpectedly.** On gold substrates, self-assembled monolayers (SAMs) of **1** were prepared from 1 mM CH_2Cl_2 solution and reacted with 2.5 mmol **2** in 10 ml CHCl_3 solution for 24 hours using one drop of dibutyltindilaurate as catalyst^[20b]. After rinsing with pure solvent and drying under an N_2 stream, measurements were performed with minimal delay. The same procedure was used for AFM-tip functionalization.

Atomic Force Microscopy. The AFM-based SMFS measurements were performed on a Nanoscope V and Picoforce AFM using a NanoScope V or IVa controller respectively, a (Picoforce) vertical engage scanner and a liquid cell (Bruker/Veeco, Santa Barbara, CA). Gold-coated V-shaped Si_3N_4 cantilevers (Bruker/Veeco, NPG probes) were functionalized in two consecutive steps, as described above, with a self-assembled layer of **1** and subsequent reaction with **2**. Tips for SMFS were taken directly from solution followed by rinsing with pure solvent. The cantilever spring constants ($k = 0.056 \pm 0.001 \text{ N/m}$; $k = 0.065 \pm 0.005 \text{ N/m}$ and $k = 0.070 \pm 0.002 \text{ N/m}$) were determined in liquid via the thermal tune method^[21]. Loading rates were determined as the slope of the force versus time trace of the force-extension curves (~ 20 data points) close to the rupture event. All supramolecular experiments were performed in a saturated solution of **3** in anhydrous hexadecane at $T = 303 \pm 2 \text{ K}$.

APPENDIX

Hunter^[2] discusses the influence of multiple hydrogen-bond donor and acceptors in a mixed solvent, based on the individual contribution. According to a simplified approach by Hunter^[2] the interaction in a solvent with multiple hydrogen-bond donors and acceptors can be determined from the contributions of solvents which possess only one of these hydrogen-bond donors and acceptors: a 1:1 mixture of water and dimethylether would behave in a similar fashion as methanol (see Figure 6- 19 and Table 6- 8).

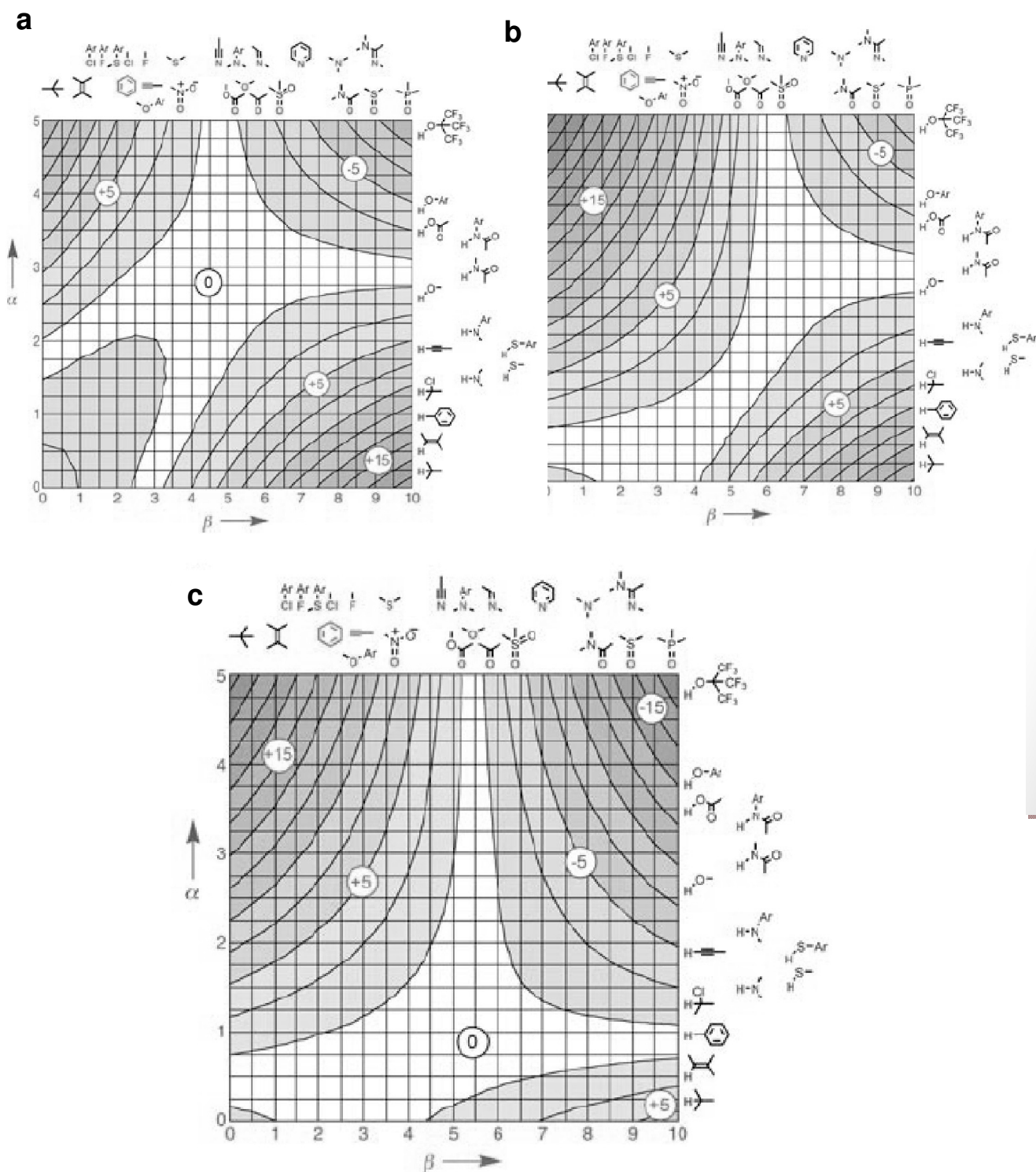


Figure 6-19. General profile of hydrogen-bond interactions in (a) water, (b) diethylether and (c) methanol. An estimate for the free energy of binding ΔG can be obtained using the hydrogen-bond donor and acceptor constants for the solute (α and β , respectively) and the hydrogen-bond donor and acceptor constant for the solvent (α_s and β_s , respectively). *Reproduced from ref. 2.*

	H ₂ O	Dimethylether (CH ₃ -O-CH ₃)	Methanol (CH ₃ -OH)
H-bond donor	OH	C-H	O-H C-H
H-bond acceptor	O	O	O

Table 6- 8. Overview of hydrogen-bond donors and acceptors of water, diethylether and methanol.

Supramolecular polymer distributions

Below an overview is presented of the rupture force distribution of dimers until pentamers of supramolecular UPy-polymers in a 50:50 (v/v) ratio of hexadecane and 2-propanol in comparison with the rupture distribution of UPy dimers in purely apolar hexadecane.

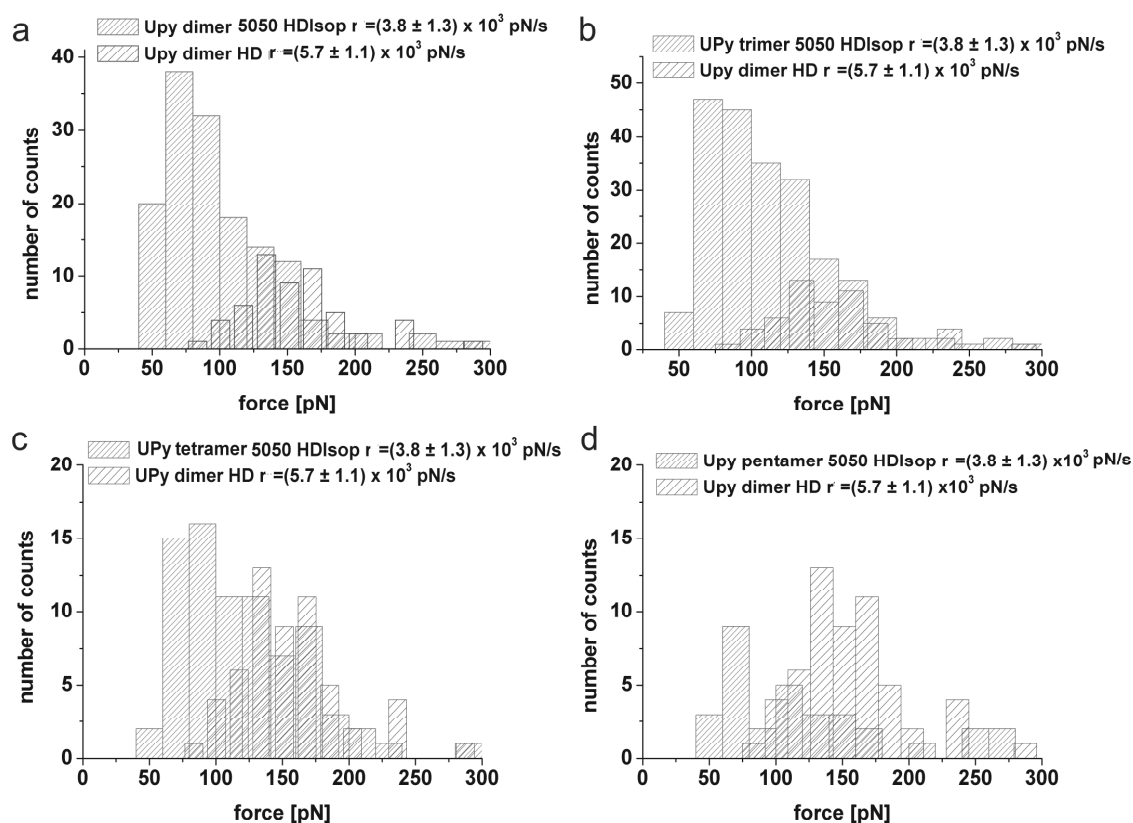


Figure 6- 20. Comparison of supramolecular UPy-dimer until pentamer polymer rupture events of a 50:50 (v/v) mixture of hexadecane and 2-propanol (5050 HDIsop) and (UPy)₂ in pure hexadecane (HD): $r = (3.8 \pm 1.3) \times 10^3$ pN/s. Note that a clear shift to lower forces is present in comparison with the dimer rupture events at a similar loading rate.

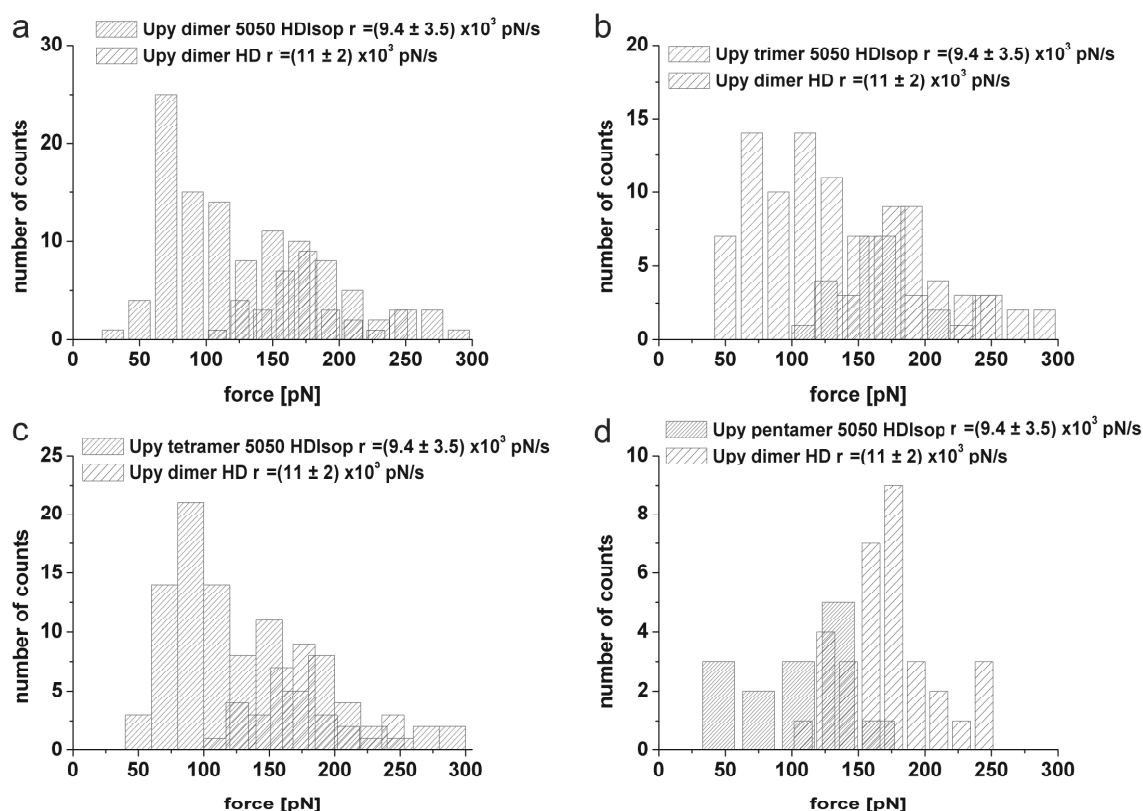


Figure 6- 21. Comparison of supramolecular UPy dimer until pentamer polymer rupture events of a 50:50 (v/v) mixture of hexadecane and 2-propanol (5050 HDIsop) and $(UPy)_2$ in pure hexadecane (HD): $r = (9.4 \pm 3.5) \times 10^3$ pN/s. Note that a clear shift to lower forces is present in comparison with the dimer rupture events at a similar loading rate.

REFERENCES

1. Abrahams, M.H.; Platts, J.A. *J. Org. Chem.* **2001**, *66*, 3484-3491.
2. Hunter, C.A. *Angew. Chem. Int. Ed.* **2004**, *43*, 5310-5324.
3. <http://www.asiinstr.com/technical/Dielectric%20Constants.htm#Section%20B>, last viewed 20-04-2011.
4. (a) Söntjens, S.H.M.; Sijbesma, R.P.; Van Genderen, M.H.P.; Meijer, E.W. *J. Am. Chem. Soc.* **2000**, *122*, 7487-7493; (b) Söntjens, S.H.M. PhD thesis “Dynamics of Quadruple Hydrogen-bonded Systems”, **2002**, Eindhoven, The Netherlands, p. 23-43.

5. (a) Leigh, D.A.; Wong, J.K.Y.; Dehez, F.; Zerbetto, F. *Nature* **2003**, *424*, 174-179; (b) Leigh, D.A.; Murphy, A.; Smart, J.P.; Deleuze, M.S.; Zerbetto, F. *J. Am. Chem. Soc.* **1998**, *120*, 6458-6467.
6. (a) Kay, A.R.; Leigh, D.A.; Zerbetto, F. *Angew. Chem. Int. Ed.* **2007**, *46*, 72-191; (b) Ghosh, P.; Federwisch, G.; Kogej, M.; Schalley, C.A.; Haase, D.; Saak, W.; Lützen, A.; Gschwind, R.M. *Org. Biomol. Chem.* **2005**, *3*, 2691-2700.
7. (a) Oesterhelt, F.; Rief, M.; Gaub, H.E. *New J. Phys.* **1999**, *1*, 6.1–6.11; (b) Kienberger, F.; Pastushenko, V.P.; Kada, G.; Gruber, H.J.; Riener, C.; Schindler, H.; Hinterdorfer, P. *Single Mol.* **2000**, *1*, 123-128.
8. Evans, E. *Annu. Rev. Biophys. Bio.* **2001**, *30*, 105-128.
9. Zou, S. PhD. Thesis. “Exploring individual supramolecular interactions and stimuli-responsive polymers by AFM-based force spectroscopy”, **2005**, Enschede, The Netherlands, p. 87-88.
10. Press, W.H.; Flannery, B.P.; Teukolsky, S.A.; Vetterling, W.T. *Numerical recipes*. Cambridge University Press, New York, USA, **1986**, p. 455-458.
11. Shapiro, S.S.; Wilk, M.B. *Biometrika* **1965**, *52*, 591-611.
12. (a) Royston, J.P. *Appl. Statist.* **1995**, *44*, 547-551. (b) Royston, J.P. *Appl. Statist.* **1982**, *31*, 115-124.
13. (a) Smirnov, N.V. *Ann. Mat. Statist.* **1948**, *19*, 279-281; (b) Kolmogorov, A. *G. Inst. Ital. Attuari* **1933**, *4*, 83-91.
14. (a) Padro, J.A.; Saiz, L.; Guardia, E. *J. Mol. Struct.* **1997**, *416*, 243-248; (b) Jorgensen, W.L. *J. Phys. Chem.* **1986**, *90*, 1276-1284.
15. (a) Vrhovsek, A.; Gereben, O.; Pothoczki, S.; Tomsic, M.; Jamnik, A.; Kohara, S.; Pusztai, L. *J. Phys. Condens. Matter* **2010**, *22*, 404214; (b) Tomsic, M.; Jamnik, M.; Fritz-Popovski, G.; Glatter, O.; Vlcek, L. *J. Phys. Chem. B* **2007**, *111*, 1738-1751; (c) Tomsic, M.; Bester-Rogac, M.; Jamnik, A.; Kunz, W.; Touraud, D.; Bergmann, A.; Glatter, O. *J. Phys. Chem. B* **2004**, *108*, 7021-7032; (d) Misaka, M. *J. Phys. Soc. Jpn.* **2003**, *72*, 185-188.
16. (a) Bhattacharyya, K. *Accounts Chem. Res.* **2003**, *36*, 95-101; (b) Fillingim, T.G.; Luo, N.; Lee, J.; Robinson, G.W. *J. Phys. Chem.* **1990**, *94*, 6368-6371.
17. Gohres, J.L.; Shukla, C.L.; Popov, A.V.; Hernandez, R.; Liotta, C.L.; Eckert, C.A. *J. Phys. Chem. B* **2008**, *112*, 14993-14998.

18. (a) Zou, S.; Schönherr, H.; Vancso, G.J. *J. Am. Chem. Soc.* **2005**, *127*, 11230-11231; (b) Zou, S.; Schönherr, H.; Vancso, G.J. *Angew. Chem. Int. Ed.* **2005**, *44*, 956-959.
19. Zou, S.; Zhang, Z.H.; Förch, R.; Knoll, W.; Schönherr, H.; Vancso, G.J. *Langmuir* **2003**, *19*, 8618-8621.
20. Folmer, B.J.B.; Sijbesma, R.P.; Versteegen, R.M.; van der Rijt, J.A.J.; Meijer, E.W. *Adv. Mater.* **2000**, *12*, 874-878.
21. (a) Butt, H.J.; Cappella, B.; Kappl, M. *Surf. Sci. Rep.* **2005**, *59*, 1-152; (b) Hutter, J.L.; Bechhöfer, J. *Rev. Sci. Instrum.* **1993**, *64*, 1868-1873.



CHAPTER 7

OUTLOOK AND FUTURE EXPERIMENTS

And above all, watch with glittering eyes the whole world around you because the greatest secrets are always hidden in the most unlikely places....

– Roald Dahl

7.1 OUTLOOK

Utilizing AFM-based SMFS as an approach for (single molecule) binding studies has revealed interesting phenomena and quantitative estimates for hydrogen-bond strength in a highly apolar solvent which could not be obtained with the standard techniques currently available. Using this technique a comparison of the hydrogen-bond strength of complementary quadruple hydrogen-bonded arrays hexadecane^[1] becomes feasible due to the loading rate-dependent energy landscape of the bond. Since AFM-based SMFS is performed at very low concentrations ($\sim\mu\text{M}$ and nM) and far-from-equilibrium conditions, possible solubility and aggregation problems are circumvented. So AFM-based SMFS enables one to study hydrogen-bond stability where common methods like isothermal titration calorimetry (ITC), nuclear magnetic resonance (NMR) or even fluorescence microscopy tend to fail due their detection limit. In addition, single molecule data and ensemble averaged bulk data are obtained simultaneously. Hence also the influence of molecular aggregates, *c.q.* molecular clusters, in solvents can directly be studied using this technique, which can among others be used for future design and development of molecular machines, such as the catenanes^[2].

Nevertheless, AFM-based SMFS is still an emerging technique which can be substantially refined and improved over the next decade. One of the current drawbacks of using AFM-based SMFS for binding studies lies in the fact that it is still more tedious and time-consuming compared to other bulk analysis techniques. However ongoing developments towards automated force spectroscopy have made considerable progress in the past few years^[3] which might drive this rather exotic analysis technique in the direction of a more common analysis tool like NMR and fluorescence spectroscopy. Automated force spectroscopy would substantially enhance the possibilities to investigate statistical binding of ligand-receptor interactions, which allows us to determine also k_{on} values. These k_{on} values will contribute to a more detailed insight in the measurements that have been discussed in this thesis. In addition, linker chemistry for functionalized AFM-tips has significantly advanced and standard recipes are readily available^[4]. Moreover smaller cantilevers reduce thermal noise in AFM measurements^[5,6] and hence a new range of small cantilevers with properties like the currently available Olympus Bio-lever, would significantly enhance the accuracy and precision of SMFS. However the interpretation of low-noise data also requires a deeper understanding of the data analysis procedures as was recently discussed by Akhremitchev^[7] and others^[8]. The combination of established protocols for data analysis and low noise measurements will then enable small environmental fluctuations studies in close proximity of

the single molecule binding events and hence a new level of understanding of single molecule interactions can be obtained.

So there is still plenty of room for fascinating future experiments which may either focus on an even more elaborate single molecule study of the quadruple hydrogen-bonded UPy and UAT-moieties in different and mixed solvents or on the more accurate detection of the influence of confinement and environmental effects in close proximity of a supramolecular bond. Since UPy quadruple hydrogen-bonds are known to be able to tautomerize^[9] into pyrimidin-4-ol monomer - which has a DADA hydrogen-bond configuration (see Figure 7- 1) - binding studies between various UPy and UAT moieties could enhance the existing understanding of structure-property relationships of mixed hydrogen-bonded dimers and polymers in solution.

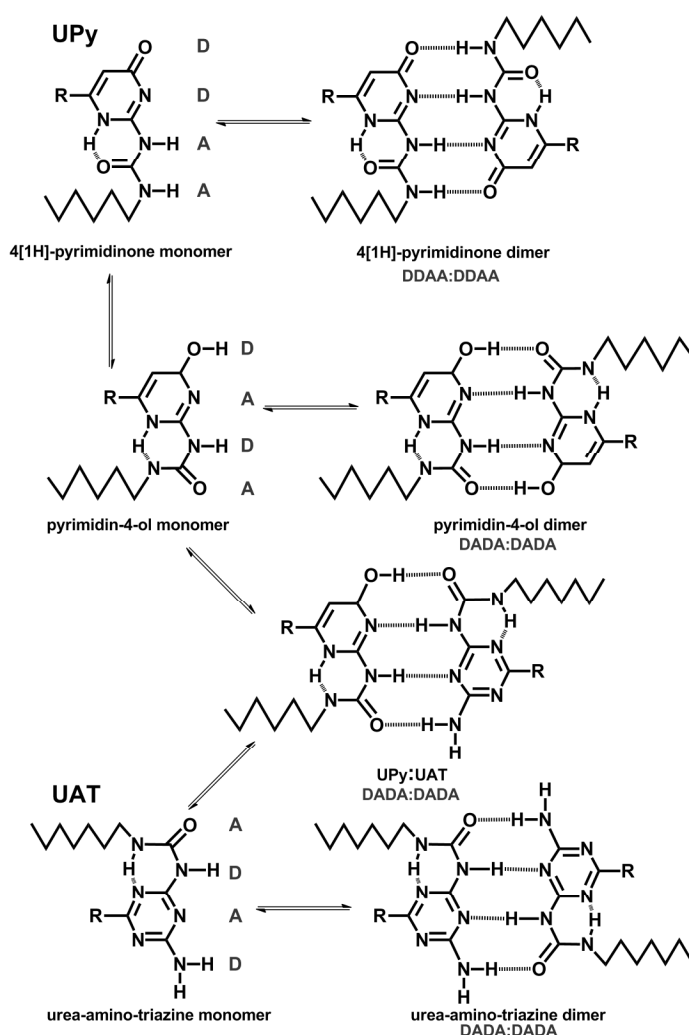


Figure 7- 1. Possible equilibria for UPy and UAT hydrogen-bonded arrays due to the tautomerization of 4[1H]-pyrimidinone to pyrimidin-4-ol. The equilibria between the different species depend on concentration, the solvent and the substituents R. If the conditions are well-controlled a solution of UPy and UAT monomers could contain four different dimeric species based on only two hydrogen-bonded monomers.

The tautomerized form is also able to form an intramolecular hydrogen-bond and hence a planar 3D geometry which should substantially stabilize the hydrogen-bonded array according to our previous observations in Chapters 3 and 4. Based on the substituents of the UPy-moieties DADA dimerization can even be promoted as is demonstrated in Table 7- 1. Electron withdrawing substituents such as CF₃ (on the R₁ position, see also Figure 7- 2) seem to promote the dimerization of UPy in the tautomeric pyrimidin-4-ol form in chloroform as well as toluene^[9]. Based on this information the UPy-moieties with the right substituents for DADA binding could be used as receptors for UAT moieties.

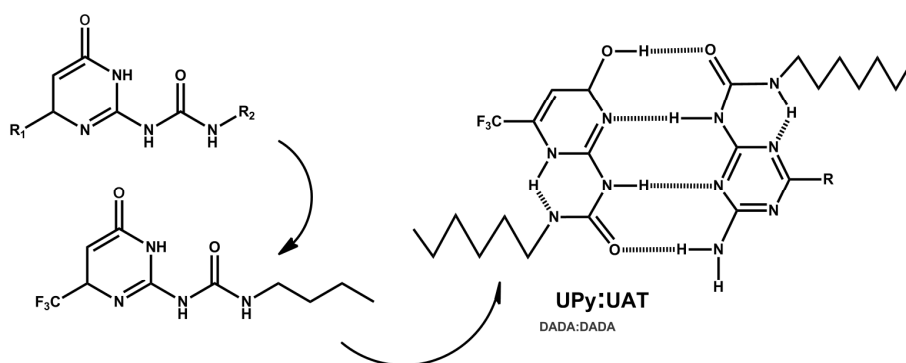


Figure 7- 2. Example of DADA dimerization of CF₃-UPy and UAT via the tautomeric pyrimidin-4-ol form.

		¹ H			
UPy dimers incl. substituents	influence	NH/OH	NH	NH	C ₅ -H
R ₁ = CH ₃ , R ₂ = C ₄ H ₉	e-donor	13.14	11.86	10.14	5.82
R ₁ = Cl, R ₂ = C ₁₂ H ₂₅	e-withdraw	13.84	11.15	9.21	6.36
R ₁ = C ₂ Si(CH ₃) ₃ , R ₂ = C ₁₂ H ₂₅ keto enol		13.10	11.65	9.95	6.11
		13.76	11.08	9.65	6.41
R ₁ = N(C ₄ H ₉) ₂ , R ₂ = C ₁₂ H ₂₅		12.60	11.22	9.58	5.33
R ₁ = CF ₃ , R ₂ = C ₄ H ₉	e-withdraw	14.30	11.14	9.30	6.64
R ₁ = Ph, R ₂ = C ₄ H ₉ keto enol	e-donor	13.92	12.04	10.21	6.35
		13.60	11.30	10.0	6.70

Table 7- 1. ¹H chemical shifts (in ppm) of UPy-dimers with various substituents measured in CDCl₃ at 10 mM and T = 25 °C. Electron withdrawing substituents such as CF₃ seem to promote dimerization via the pyrimidin-4-ol tautomeric form (in CDCl₃ and also toluene-d₈). Data taken from ref. 9b.

Furthermore it would be interesting to study the effect of the pulling direction on the bond strength and energy landscape of the bond in more detail. A different synthetic approach can yield molecular shear- or zipper-pulling^[10-12] geometries which could reveal additional information on the energy landscape of the bond as well as novel material properties as was demonstrated by Guan and co-workers for supramolecular UPy-interactions (see Figure 7- 3). The single molecule investigation of supramolecular (hydrogen-bond-based) mechano-chemistry could be approached in a similar manner^[13].

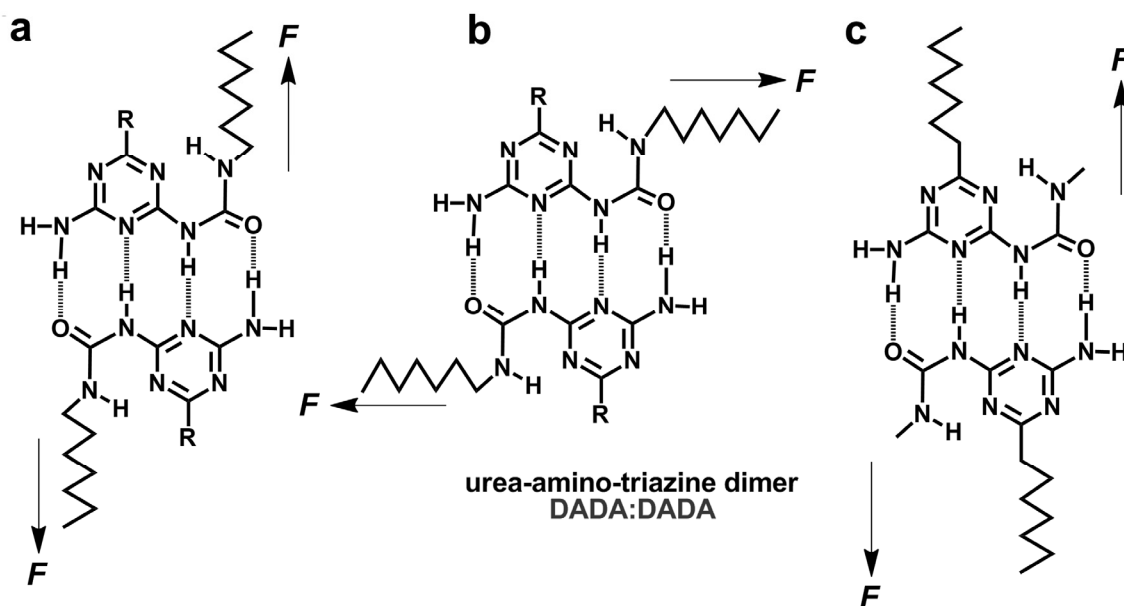


Figure 7- 3. Three possible geometries for pulling experiments for a UAT-based hydrogen-bonded dimer or polymer.

More challenging future experiments can be designed to study local environmental effects in close proximity of the bond of interest. As was previously demonstrated, confinement, geometry and the hydrophilicity of enzymatic pockets are of major influence on the specific catalytic effect in (biological) enzymatic systems^[14]. Studying the energy landscape in a confined environment of biomolecules such as enzymes^[15], may not only shed light on the enzymatic pathway but might also generate valuable information regarding future materials design. This was for instance demonstrated by Gaub and co-workers^[10a,15c] who studied the energy landscape of induced DNA slippage as well as the influence of ATP binding to titin kinase by controlling the protein conformation using a mechanical pump and probe protocol in combination with AFM-based SMFS (see Figure 7- 4a). The technique described above could be a valuable tool for studying other mechano-enzymatic proteins as well as synthetic mechano-enzymatic systems based on for instance supramolecular interactions.

Completely new insight in the complexity of nature can furthermore be achieved by combining single molecule techniques with other (single molecule) detection techniques such as optical/magnetic tweezers combined with fluorescent spectroscopy^[16], AFM-TIR (Total Internal Reflection) spectroscopy^[17,18], AFM-SNOM (Scanning Near-Field Optical Microscopy)^[19], AFM-NMR (Nuclear Magnetic Resonance)^[20], AFM-QCM (Quartz Crystal Microbalance)^[21] and AFM combined with fluorescence spectroscopy^[18,22]. These techniques lead to new developments in materials design and controlled nanofabrication. Using AFM-TIRF in combination with a new technique called blink microscopy^[23] nanometer control (~ 50 - 60 nm) could be achieved which is demonstrated in Figure 7- 4d.

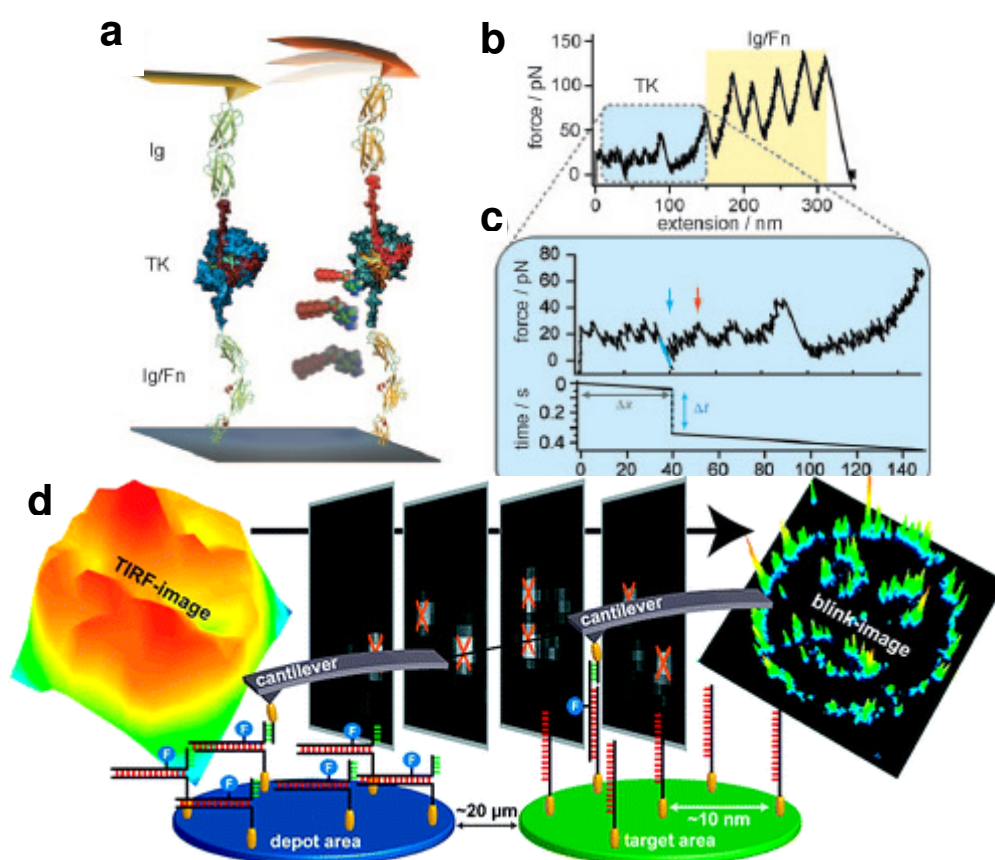


Figure 7- 4. (a) AFM-based SMFS is combined with probe and pump experiments to study the influence of adenosine triphosphate (ATP) binding on the conformations of titin kinase (TK); (b,c) a certain pump-and-probe cycle is used to study the influence of the applied force on the conformation of TK which unfolds below 50 pN. *Image adapted from ref 15c*; (d) a combined single-molecule-cut-and-paste AFM-TIRF and blink microscopy experiment. DNA recognition is used to create a nanometer scale fluorescent image which is resolved using blink microscopy. *Image adapted from ref 23*.

As is demonstrated in Figure 7- 4, emerging combinatory single molecule techniques considerably enhance the amount and type of data that can be obtained on a single molecule level. Thus well-designed experiments using a combination of available single molecule techniques will eventually provide more insight in the complex processes that exist in nature and will guide materials scientist to develop novel and energy efficient products. One example of new insight that was recently obtained using existing techniques in a creative way is the assessment of binding thermodynamics of cosolutes when a single molecule is pulled from a surface. So, in line with the fast-developing area of single molecule techniques over the past decades, a smart combination of currently existing techniques might open up a whole new realm of approaches which provide us with a more detailed knowledge on phenomena that occur on the single molecule level.

REFERENCES

1. (a) Zou, S.; Schönherr, H.; Vancso, G.J. *J. Am. Chem. Soc.* **2005**, *127*, 11230–11231; (b) Zou, S.; Schönherr, H.; Vancso, G.J. *Angew. Chem. Int. Ed.* **2005**, *44*, 956-959; (c) Embrechts, A.; Schönherr, H.; Vancso, G.J. *J. Phys. Chem B* **2008**, *112*, 7359-7362; (d) Embrechts, A.; Velders, A.H.; Schönherr, H.; Vancso, G.J. *unpublished data*.
2. Leigh, D.A.; Wong, J.K.Y.; Dehez, F.; Zerbetto, F. *Nature* **2003**, *424*, 174-179.
3. (a) Kuhn, M.; Janovjak, H.; Hubain, M.; Müller, D.J. *J. Microsc.* **2005**, *218*, 125-132; (b) Struckmeier, J.; Wahl, R.; Leuschner, M.; Nunes, J.; Janovjak, H.; Geisler, U.; Hoffman, G.; Jähnke, T.; Müller, D.J. *Nanotechnology* **2008**, *19*, 384020.
4. (a) Hinterdorfer, P.; Baumgartner, W.; Gruber, H.J.; Schilcher, K.; Schindler, H. *Proc. Natl. Acad. Sci. U.S.A.* **1996**, *93*, 3477-3481; (b) Ebner, A.; Wildling, L.; Zhu, R.; Rankl, C.; Haselgrübler, T.; Hinterdorfer, P.; Gruber, H.J. *Top. Curr. Chem.* **2008**, *285*, 29-76.
5. Viani, M.B.; Schäffer, T.E.; Chand, A.; Rief, M.; Gaub, H.E.; Hansma, P.K. *J. Appl. Phys.* **1999**, *86*, 2258-2262.
6. Katan, A.J. *Measuring interactions in fluids with small-cantilever AFM*. PhD Thesis **2007**, Leiden, The Netherlands.
7. (a) Li, N.; Guo, S.; Akhremitchev, B.B. *ChemPhysChem* **2010**, *11*, 2096-2098; (b) Guo, S.; Li, N.; Lad, N.; Ray, C.; Akhremitchev, B.B. *J. Am. Chem. Soc.* **2010**, *132*, 9681-9687; (c) Guo, S.; Li, N.; Lad, N.; Desai, S.; Akhremitchev, B.B. *J. Phys. Chem. C*

- 2010**, *114*, 8755-8765; (d) Ray, C.; Brown, J.R.; Akhremitchev, B.B. *J. Phys. Chem. B* **2007**, *111*, 1963-1974.
8. Raible, M.; Evstigneev, M.; Bartels, F.W.; Eckel, R.; Nguyen-Duong, M.; Merker, R.; Ros, R.; Anselmetti, D.; Reimann, P. *Biophys. J.* **2006**, *90*, 3851-3864.
 9. (a) Beijer, F.H.; Sijbesma, R.P.; Kooijman, H.; Spek, A.L.; Meijer, E.W. *J. Am. Chem. Soc.* **1998**, *120*, 6761-6769; (b) De Greef, T.F.A. *Mechanistic studies on Quadruple Hydrogen Bonding Systems*. PhD Thesis **2009**, Eindhoven, The Netherlands, p. 37.
 10. (a) Kühner, F.; Morfill, J.; Neher, R.A.; Blank, K.; Gaub, H.E. *Biophys. J.* **2007**, *92*, 2491-2497; (b) Krautbauer, R.; Rief, M.; Gaub, H.E. *Nano Lett.* **2003**, *3*, 493-496; (c) Struntz, T.; Oroszlan, K.; Schumakovitch, I.; Güntherodt, H.-J.; Hegner, M. *Biophys. J.* **2000**, *79*, 1206-1212; (d) Struntz, T.; Orozlan, K.; Schäfer, R.; Güntherodt, H.-J. *Proc. Natl. Acad. Sci. U.S.A.* **1999**, *96*, 11277-11282.
 11. (a) Guan, Z.; Roland J.T.; Bai, J.Z.; Ma, S.X.; McIntire, T.M.; Nguyen, M. *J. Am. Chem. Soc.* **2004**, *126*, 2058-2065; (b) Roland, J.T.; Guan, Z. *J. Am. Chem. Soc.* **2004**, *126*, 14328-14329.
 12. (a) Beke-Somfai, T.; Perczel, A.; *J. Phys. Chem. Lett.* **2010**, *1*, 1341-1345; (b) Bornschlögl, T.; Woehlke, G.; Rief, M. *Proc. Natl. Acad. Sci. U.S.A.* **2009**, *106*, 6992-6997.
 13. Liang, J.; Fernandez, J.M.; *ACS Nano* **2009**, *3*, 1628-1645.
 14. (a) Chi, Y.C.; Scroggins, S.T.; Fréchet, J.M.J. *J. Am. Chem. Soc.* **2008**, *130*, 6322-6323; (b) Vriezema, D.M.; Garcia, P.M.L.; Oltra, N.S.; Hatzakis, N.S.; Kuiper, S.M.; Nolte, R.J.M.; Rowan, A.E.; Van Hest J.C.M. *Angew. Chem. Int. Ed.* **2007**, *46*, 7378-7382 (c) Commellas-Aragones, M.; Engelkamp, H.; Claessen, V.I.; Sommerdijk, N.A.J.M.; Rowan, A.E.; Christianen, P.C.M.; Maan, J.C.; Verduin, B.J.M.; Cornelissen, J.J.L.M.; Nolte, R.J.M. *Nat. Nanotechnol.* **2007**, *2*, 635-639; (d) Helms, B.; Guillaudeu, S.J. Xie, Y, McMurdo, M.; Hawker, C.J.; Fréchet, J.M.J. *Angew. Chem. Int. Ed.* **2005**, *44*, 6384-6387; (e) Hecht, S.; Fréchet, J.M.J. *Angew. Chem. Int. Ed.* **2001**, *40*, 74-91; (f) Kim, C.U.; Lew, W.; Williams, M.A.; Liu, H.; Zhang, L.; Swaminathan, S.; Bischofberger, N.; Chen M.S.; Mendel, D.B.; Tai, C.Y.; Laver, G.; Stevens, R.C. *J. Am. Chem. Soc.* **1997**, *119*, 681-690.
 15. (a) Alegre-Cebollada, J.; Perez-Jimenez, R.; Kosuri, P.; Fernandez, J.M. *J. Biol. Chem.* **2010**, *285*, 18961-18966; (b) Puchner, E.M.; Gaub, H.E. *Angew. Chem. Int. Ed.* **2010**, *49*, 1147-1150; (c) Puchner, E.M.; Alexandrovich, A.; Kho, A.L.; Hensen, U.; Schäfer, L.V.;

- Brandmeier, B.; Gräter, F.; Grubmüller, H.; Gaub, H.E.; Gautel, M. *Proc. Natl. Acad. Sci. U.S.A.* **2008**, *105*, 13385-13390.
16. (a) Gross, P.; Farge, G.; Peterman, E.J.G.; Luite, G.J.L. *Method. Enzymol.* **2010**, *475*, 427-453; (b) Yodh, J.G.; Schlierf, M.; Ha, T. *Q. Rev. Biophys.* **2010**, *43*, 185-217; (c) Tarsa, B.P.; Brau, R.R.; Ferrer, J.M.; Freyzon, Y.; Matsudaira, P.; Lang, M.J. *Angew. Chem. Int. Ed.* **2007**, *46*, 1999-2001; (c) Van Dijk, M.A.; Kapitein, L.C.; Van Mameren, J.; Schmidt, C.F.; Peterman, E.J.G. *J. Phys. Chem. B* **2004**, *108*, 6479-6484; (d) Bianco, P.R.; Brewer, L.R.; Corzett, M.; Balhorn, R.; Yeh, Y.; Kowalczykowski, S.C.; Baskin, R.J. *Nature* **2001**, *409*, 374-378; (e) Ishijima, A.; Kojima, H.; Funatsu, T.; Tokunaga, M.; Higuchi, H.; Tanaka, H.; Yanagida, T. *Cell* **1998**, *92*, 161-171.
17. Hugel, T.; Holland, N.B.; Cattani, A.; Moroder, L.; Seitz, M.; Gaub, H.E. *Science* **2002**, *296*, 1103-1106.
18. (a) Gump, H.; Stahl, S.W.; Strackharn, M.; Puchner, E.M.; Gaub, H.E. *Rev. Sci. Instrum.* **2009**, *80*, 063704; (b) Shaw, J.E.; Oreopoulos, J.; Wong, D.; Hsu, J.C.; Yip, C.M. *Surf. Interface Anal.* **2006**, *38*, 1459-1471.
19. (a) Meyer, K.A.; Ng, K.C.; Gu, Z.; Pan, Z.; Whitten, W.B.; Shaw, R.W. *Appl. Spectrosc.* **2010**, *64*, 1-7; (b) Hu, M.; Chen, J.; Wang, J.; Wang, X.; Ma, S.; Cai, J.; Chen, C.Y.; Chen, Z.W. *J. Mol. Recognit.* **2009**, *22*, 516-520; (c) Kim, J.; Song, K.-B. *Micron* **2007**, *38*, 409-426.
20. (a) Mamin, H.J.; Oosterkamp, T.J.; Poggio, M.; Degen, C.L.; Rettner, C.T.; Rugar, D. *Nano. Lett.* **2009**, *9*, 3020-3024; (b) Rugar, D.; Budakian, R.; Mamin, H.J.; Chui, B.W. *Nature* **2004**, *430*, 329-332.
21. (a) Johannsmann, D.; Reviakine, I.; Rojas, E.; Gallego, M. *Anal. Chem.* **2008**, *80*, 8891-8899; (b) Iwata, F.; Saruta, K.; Sasaki, A. *Appl. Phys. A* **1998**, *66*, S463-S466.
22. (a) Tisler, J.; Balasubramanian, G.; Naydenov, B.; Koselov, R.; Grotz, B.; Reuter, R.; Boudou, J.-P.; Curmi, P.A.; Sennour, M.; Thorel, A.; Börsch, M.; Aulenbacher, K.; Erdmann, R.; Hemmer, P.R.; Jelezko, F.; Wrachtrup, J. *ACS Nano* **2009**, *3*, 1959-1965; (b) Schütz, G.J.; Hinterdorfer, P. *Exp. Gerontol.* **2002**, *37*, 1493-1509; (c) Ha, T. *Single Mol.* **2001**, *4*, 283-284.
23. Cordes, T.; Strackharn, M.; Stahl, S.W.; Summeren, W.; Steinhauer, C.; Forthmann, C.; Puchner, E.M.; Vogelsang, J.; Gaub, H.E.; Tinnefeld, P. *Nano Lett.* **2010**, *10*, 645-651.
24. Geisler, M.; Netz, R.R.; Hugel, T. *Angew. Chem. Int. Ed.* **2010**, *39*, 4739-4733.



SUMMARY

Atomic Force Microscopy (AFM)-based techniques were used to control, manipulate and study supramolecular hydrogen-bonded dimers and polymers in organic solvents on a single molecule level. Hydrogen-bonded dimers and polymer units were synthesized and self-assembled monolayer (SAMs) techniques were exploited to study the forces in supramolecular hydrogen-bonded host-guest interactions by single molecule AFM. Furthermore the mechanical properties of single supramolecular polymers were investigated and the relation of bond strength as a function of the number of polymer linkers N was established for supramolecular polymer units linked in series.

In Chapter 2 the influence of non-covalent interactions and self-assembly in nature is discussed. Synthetic supramolecular systems and polymers are introduced as well as methods to study supramolecular hydrogen-bonded host-guest interactions on a single molecule level. Since examples from nature demonstrated its well-controlled and energy efficient use of non-covalent interactions and self-assembly, a higher level of understanding is anticipated from the detailed investigation of these molecular forces. This in turn will lead to completely new approaches in the investigation, manipulation and design of nanostructures and self-assembling systems.

Chapter 3 describes the single molecule investigation of self-complementary host-guest interactions of ureidopyrimidinone (UPy) dimers and polymers in hexadecane. AFM-based Single Molecule Force Spectroscopy (SMFS) was used to investigate the energy landscape of the hydrogen-bonds and mechanical properties of supramolecular UPy-polymers on a single molecule level. The rupture forces *at one fixed loading rate* were observed as a function of the number of linkers N and were in quantitative agreement with the theory on uncooperative bond rupture for supramolecular linkages switched in series. Based on these results, an estimate for the value of the dimer equilibrium constant $K_{dim} = (1.3 \pm 0.5) \times 10^9 \text{ M}^{-1}$ was obtained, which is in good agreement with previously estimated values based on loading rate-dependent SMFS in hexadecane.

In Chapter 4 an urea-aminotriazine (UAT)-based donor-acceptor-donor-acceptor (DADA)-array and complementary receptors were synthesized. The UAT-receptor was

immobilized on gold surfaces using an ultrathin layer of ethylene glycol terminated lipoic acid and isocyanate chemistry. The surface chemistry and recognition of this hydrogen-bonded array was investigated as a prerequisite for AFM-based SMFS, using contact angle measurements, grazing angle Fourier transform infrared (FTIR) spectroscopy, X-ray photoelectron spectroscopy (XPS) and AFM. Reversible self-complementary recognition of surface-immobilized UAT-moieties and solution borne UAT was confirmed by FTIR spectroscopy and AFM-based SMFS. Exploiting the Kramers-Bell-Evans approach, loading rate-dependent SMFS measurements yielded a value of the dimer binding constant of $K_{dim} = (2 \pm 1) \times 10^7 \text{ M}^{-1}$ of this DADA-array in hexadecane. This value is significantly higher than predicted on the basis of additive primary and secondary hydrogen-bond interactions. The remarkable difference is rationalized by additional intramolecular hydrogen-bond stabilization, confirmed by 2D proton nuclear magnetic resonance (^1H -NMR) measurements in CDCl_3 , which promotes a planar molecular geometry and stabilizes the dimeric complex.

In Chapter 5 the mechanical properties of UAT-based supramolecular polymers were studied. The unbinding forces of UAT complexes were investigated at different *fixed piezo retraction rates* in far-from-equilibrium conditions. The rupture forces of supramolecular UAT-polymer chains were found to decrease with increasing rupture lengths and their dependence on the number of linkers N was in quantitative agreement with the theory on uncooperative bond rupture for supramolecular linkages switched in series. In experiments with three different *fixed* loading rates, identical values for the characteristic bond length x_β , to within the experimental error, were obtained. Thus a mean dimer equilibrium constant K_{dim} of $(1.1 \pm 0.3) \times 10^7 \text{ M}^{-1}$ was estimated. This value is in good agreement with the previously measured value for $(\text{UAT})_2$ (Chapter 4). Hence the new approach to estimate the relevant parameters for the rupture of dimers in experiments on supramolecular linkages switched in series at one fixed loading rate, presented in Chapter 3 for the UPy-system, was validated.

In Chapter 6 the influence of solvent polarity on the bond strength of UPy dimers was analyzed in 2-propanol, 1-nonanol and hexadecane as well as in binary mixtures of 2-propanol and hexadecane. The bond strength appears to scale with solvent polarity, which is consistent when solvent “competition” is assumed for hydrogen-bond formation. The corresponding distributions of the rupture forces were shown to deviate from a normal

distribution. Whereas in pure hexadecane the rupture force distributions can be described with a Gaussian function, the distributions of rupture forces in polar 2-propanol, and to a lesser extent in 1-nonanol, deviate markedly from a Gaussian distribution, as confirmed *e.g.* by the Shapiro-Wilks test. The distributions in polar solvents are tentatively attributed to bond rupture in different local environments that may be related to molecular clustering observed by others in these solvents. In binary mixtures of 2-propanol and hexadecane similar bond strengths and bond strength distributions as in 2-propanol were observed.

In Chapter 7 an outlook is presented on future developments which may create opportunities to enhance our understanding of the key contributors to hydrogen-bond stability and their influence on the stability and function of higher architectures or even bulk materials. Furthermore the feasibility of AFM-based SMFS as a tool for (single molecule) bond strength analyses is discussed. Ultimately AFM-based SMFS will contribute to a better understanding of the structure-property relationships that determine the bond strength and resulting bulk properties of these supramolecular systems.



SAMENVATTING

In dit onderzoek zijn atoomkrachtmicroscopie (Atomic Force Microscopy of AFM)-gebaseerde technieken gebruikt om afzonderlijke supramoleculaire waterstofbruggebonden dimeren en polymeren in organische oplosmiddelen te manipuleren en bestuderen. Voor dit onderzoek zijn verschillende supramoleculaire eenheden gesynthetiseerd, die via vier waterstofbruggen zelf-complementaire dimeren en polymeren kunnen vormen. Vervolgens zijn self-assembled monolayer (SAM)-technieken toegepast om de bindingssterkte van deze afzonderlijke supramoleculaire waterstofbrugvormende complexen en polymeren te bestuderen. Bovendien is er onderzoek verricht naar de mechanische eigenschappen van afzonderlijke supramoleculaire polymeren. Met behulp van AFM-metingen is zo de relatie van de bindingssterkte als functie van het aantal polymeereenheden N vastgesteld voor supramoleculaire polymeereenheden in serie.

In Hoofdstuk 2 wordt een overzicht gegeven van de invloed van niet-covalente interacties en zelf-organisatie in de natuur. Bovendien worden synthetische supramoleculaire systemen en tevens verschillende methoden voor het bestuderen van waterstofbruginteracties op het niveau van één enkel molecuul besproken. Voorbeelden uit de natuur hebben namelijk laten zien dat het mogelijk is om deze niet-covalente interacties te gebruiken voor gecontroleerde en energiezuinige processen. Een gedetailleerde studie naar deze niet-covalente interacties en moleculaire krachten zou dan niet alleen moeten leiden tot nieuwe theoretische inzichten, maar ook tot nieuwe ontwikkelingen op het gebied van het manipuleren en ontwerpen van deze nanostructuren.

Hoofdstuk 3 geeft een overzicht van het onderzoek naar zelf-complementaire waterstofbruginteracties van ureidopyrimidinone (UPy) dimeren en polymeren in hexadecaan. Door middel van AFM-metingen aan afzonderlijke polymeren zijn het energielandschap van het waterstofbruggencomplex en de mechanische eigenschappen van supramoleculaire UPy moleculen in kaart gebracht. De kracht die nodig is om een enkel supramoleculair UPy-polymeer te breken (voor één specifieke belastingssnelheid of loading rate) blijkt dan af te nemen naarmate het polymeer langer wordt. Dit is in overeenstemming met de theorie die het niet-coöperatief falen van niet-covalente bindingen in serie beschrijft. Met behulp van deze resultaten is vervolgens de bindingsconstante van UPy-complexen in hexadecaan

benaderd: $K_{dim} = (1.3 \pm 0.5) \times 10^9 \text{ M}^{-1}$. Deze waarde blijkt goed overeen te komen met eerdere belastingssnelheid-afhankelijke AFM Single Molecule Force Spectroscopy (SMFS)-metingen en voorspellingen gebaseerd op bulkmetingen in andere organische oplosmiddelen.

In Hoofdstuk 4 wordt de synthese beschreven van een op urea-aminotriazine (UAT)-gebaseerd donor-acceptor-donor-acceptor (DADA) waterstofbruggensysteem en de daarbijbehorende complementaire receptoren. De UAT-receptor is vervolgens via een isocyanaatreactie gekoppeld aan een goudoppervlak met een dunne laag ethyleenglycol. De oppervlaktechemie en herkenning van dit waterstofbruggensysteem werd vervolgens onderzocht met behulp van contacthoekmetingen, grazing angle Fourier Transform infraroodspectroscopie (FTIR), X-ray photoelectron spectroscopy (XPS) en AFM. Zelf-complementaire reversibele interacties van geïmmobiliseerde UAT moleculen aan het goudoppervlak en in oplossing werden gedetecteerd via FTIR spectroscopie en AFM. Met behulp van belastingssnelheid-afhankelijke AFM-gebaseerde SMFS metingen en de Kramers-Bell-Evans benadering is vervolgens de waarde van de dimerisatieconstante van het UAT-complex in hexadecaan benaderd: $K_{dim} = (2 \pm 1) \times 10^7 \text{ M}^{-1}$. Deze waarde van de bindingsconstante is substantieel hoger dan de waarde die voorspeld wordt door middel van een theoretische benadering uitgaande van additieve primaire en secundaire waterstofbruginteracties. Dit opmerkelijke verschil wordt verklaard door de aanwezigheid van een extra intramoleculaire waterstofbrug die ervoor zorgt dat het systeem moleculair vlak is en het complex stabiliseert. Dit werd bevestigd door middel van 2D proton kernspinresonantie ($^1\text{H-NMR}$)-metingen in chloroform.

In Hoofdstuk 5 worden de mechanische eigenschappen van UAT-gebaseerde supramoleculaire polymeren bestudeerd. De kracht die nodig is om een UAT-interactie te verbreken werd bestudeerd bij verschillende, vaststaande piëzo terugtrekkingssnelheid en omstandigheden die ver verwijderd waren van het thermodynamische evenwicht. Ook voor UAT-gebaseerde supramoleculaire polymeren bleek de benodigde kracht voor het verbreken van een UAT-complex af te nemen naarmate het polymeer langer was. De relatie voor het niet-coöperatief falen van N niet-covalente eenheden in serie komt kwantitatief goed overeen met de gemeten resultaten. Verder blijkt voor experimenten met drie verschillende belastingssnelheden de berekende karakteristieke bindingslengte x_β gelijk te zijn, binnen de aanwezige foutenmarges. Met behulp van deze resultaten is vervolgens weer de gemiddelde

dimerisatieconstante voor het UAT complex in hexadecaan benaderd: $K_{dim} = (1.1 \pm 0.3) \times 10^7 \text{ M}^{-1}$. Deze waarde komt goed overeen met de eerder via belastingssnelheid-afhankelijke AFM-metingen bepaalde waarde voor de bindingsconstante van het UAT-complex in hexadecaan (Hoofdstuk 4). Deze metingen maken dan ook de validatie mogelijk van de nieuwe, in Hoofdstuk 3 beschreven, benadering voor het bepalen van de relevante parameters van het energielandschap.

In Hoofdstuk 6 wordt de invloed van de polariteit van organische oplosmiddelen op de bindingssterke van UPy-complexen bestudeerd in 2-propanol, 1-nonanol en hexadecaan maar ook in binaire mengsels van 2-propanol en hexadecaan. De invloed van de polariteit van het oplosmiddel op de bindingssterkte lijkt duidelijk gecorreleerd, wat in overeenstemming is met de aanname van oplosmiddel-competitie tijdens de vorming van de waterstofbruginteracties. De verdeling van de kracht die nodig is om het UPy-complex te verbreken wijkt echter af van een normale verdeling. Terwijl de distributie van krachten in hexadecaan beschreven kan worden met een Gaussische functie, wijken de distributies in polair 2-propanol, en in wat minder mate in 1-nonanol, duidelijk af van deze Gaussische distributie. Dit werd onder andere bevestigd met behulp van de Shapiro-Wilks toets. De afwijkende distributies in polaire oplosmiddelen worden toegeschreven aan een veranderende lokale omgeving die kan ontstaan indien clustering van moleculen in oplossing plaatsvindt. In binaire mengsels van 2-propanol en hexadecaan werden vergelijkbare distributies als in zuiver 2-propanol waargenomen.

In Hoofdstuk 7 worden mogelijke scenario's beschreven die zouden kunnen leiden tot een dieper inzicht en begrip met betrekking tot de belangrijkste effecten die bijdragen aan de stabiliteit van waterstofbrugsystemen, hogere orde nanostructuren en misschien zelfs bulk materialen. Verder wordt de haalbaarheid van AFM-gebaseerde SMFS technieken als een nieuwe methode voor de analyse van bindingssterkte van non-covalente complexen besproken. In de (nabije) toekomst zouden AFM-gebaseerde SMFS technieken kunnen bijdragen aan een beter begrip van de factoren die bepalend zijn voor de bindingssterkte en daaruit voortvloeiende materiaaleigenschappen van supramoleculaire systemen.



ACKNOWLEDGEMENTS

Finally we arrive at the last and especially rewarding part of this thesis in which I would like to thank all the people who contributed to this piece of work in so many different ways.

First of all I would like to thank my daily supervisor, professor Holger Schönherr for showing me how decent science is done. Your scientific ways and knowledge were the reason I decided to continue research in MTP knowing I would be able to learn so much more during the four years of a PhD. I have even been more lucky since it turned out to be more than five years in the end :D. And although your well-earned professorship in Siegen came as a surprise in the middle of the PhD it opened up new opportunities and insights. In one of our first discussions during my PhD you reminded me that “Der Weg ist das Ziel” and it has indeed been a challenging and bumpy road. The road is still long, but I am grateful that you were there to guide me along this part of my way....

Of course I also would like to thank professor Julius Vancso for giving me the opportunity to travel the globe and present my work in a great field of scientific researchers. Although your duties all over the world created a challenge for all of us, I am happy that we succeeded in writing this little book. And of course I will always have fond memories of the many Christmas dinners we spend at your place, together with your wife Klara, the kids and all old and new MTP-members.

Special thanks also go out to Dr. Mark Hempenius who kept on believing in my “synthesis-qualities” necessary to create the molecules I so desperately needed for my research. With your help I nowadays manage to feel quite comfortable doing chemical synthesis (even simultaneously). Also Clemens Padberg, our technician deserves special thanks for all the effort he puts in keeping all our equipment up and running, but even more for the constant happy face moving around the corridors! And of course I would also like to thank Genevieve for her constant support and for sharing her view on life. The chats and the many trips, conferences and courses we organized together were a nice bonus next to the scientific work.

I also would like to thank my current supervisor Eduardo Mendes for the stimulating (scientific) environment he creates in “our” lab. A constant buzz of creative energy has made my life a lot easier since I joined Nanostructured Materials in Delft, especially due to your

firm believe in your group and constant support. Long will I remember our first joint “days-at-the-office” in Cork and the work meeting in Tel Aviv together with you wife Paula as well as our (ongoing) discussion about the “important things in life”. Muito obrigada!

Furthermore I would like to thank Edit Kutnyánszky, Joost Duvigneau and Sissi de Beer for all the challenging scientific discussions we had during the past couple of years. I enjoyed our coffee and tea breaks, when there was time to share our thoughts on so many different topics. I would also like to thank Aldrik Velders and Gerard Kip for their help with NMR and XPS measurements. And of course Davide, Ekram, Marc and all the rest of the Siegen-family for their support and nice discussions while I was visiting! Special thanks go out to my paranymphs Edit and Veronika, who will hopefully create a little confusion during the PhD defense :D.

Doing my PhD would not have been much fun without the contribution of many people who came and went over the years, like Eddy, In Yee, Szczepan, Nikodem, Monique, Ewa, Nina, Henrik, Dorota, Cindy, Alex, Maria, Leon&Leon, Yujie, Jing, ChuanLiang, Hong Jing, Marina, Melba, Cynthia, Ketty, Weiqing, Kanjanee, Qi, Martin, Ramon&Ramon, Eugenia, Janet, Denis, Oya, Xiaofeng, Mathijs, Wilma, Peter, Mine, Gabriella, Kristin, Johannes, Emilia, Jolante, Carlos, Wenbin, Gerwin, Anna, Michel, Lennard, Yuan-Yuan, Bas, Fons, Bart, Bram and many more... I will cherish the good memories of the crazy parties, BBQs and conferences we enjoyed together.

I thank all my friends @ P-NUT (Marije, Michel, Nicolas, Maryana, Sergio, Shashank, Giovane, Josine, Amy and Björn) for letting me be one of your gossip queens... It is good to hear that P-NUT is doing better every year and will become a recognized PhD association as of September 2011! Continue the good work, we'll keep in touch!

Als laatste wil ik natuurlijk mijn vrienden en “geliefden” bedanken die ondanks mijn drukke leventje van de afgelopen tijd nog steeds een bijzonder deel uitmaken van mijn leven en voor de nodige afwisseling hebben gezorgd gedurende deze jaren. Iris & Leon, ook al hebben we elkaar de laatste jaren minder gezien, ik voel me altijd thuis bij jullie. Bedankt, ik ben supertrots op jullie (nu nog) kleine gezinnetje!

Ciska en Sander, het was geweldig om vorig jaar even alle drukte te ontvluchten en getuige te mogen zijn bij jullie bruiloft!

Kommer en Jannie, hopelijk is er na de verhuizingen, het klussen, de kraamvisites, het afstuderen en promoveren weer meer tijd voor een gezellig avondje bridge ;-).

Niels, bedankt dat je als voorbeeld en spiegel hebt willen dienen bij het schrijven van mijn thesis, maar vooral voor 'the moral support' tijdens de laatste fase van de PhD.

Oma Annie, Ferry, Astrid, Monique en Jonas, jullie zijn ondertussen een soort tweede familie voor me geworden. Wat zouden de afgelopen jaren toch saai geweest zijn zonder jullie geweldige gevoel voor humor!

Paps en mams, natuurlijk wil ik ook jullie bedanken voor het onvoorwaardelijke vertrouwen in de studiekeuzes die ik gemaakt heb. Ondanks dat niet iedereen ervan overtuigd was dat scheikunde studeren een goede beslissing was, weten wij zoveel jaar later wel beter.

Mijn broer Arjan verdient een speciale plaats in dit boekje omdat hij mij altijd weer laat zien, dat het heel bijzonder is om zelf in staat te zijn je eigen dromen te realiseren. Als het onderzoek weer eens muurvast zat, sleepte die gedachte me er doorheen en leverde weer nieuwe energie.

Gelukkig was ook Paul er altijd als het onderzoek muurvast leek te zitten of plannings weer eens compleet omgegooid moesten worden. Nachtenlang hebben we gediscussieerd over statistische benaderingen, foutenanalyses, computerprogramma's voor data-analyse en wat ik nog niet meer op mijn pad tegenkwam en je kwam telkens weer met interessante inzichten die me dan iets verder hielpen in de speurtocht naar antwoorden. Het is van onschatbare waarde om na een lange dag echt "thuis te komen", de gebeurtenissen van de dag te kunnen bespreken en je zo af en toe even nergens druk om hoeven te maken.

Heel veel liefs,

Anika

CURRICULUM VITAE

Anika Embrechts was born on January the 15th of 1980 in Rotterdam (The Netherlands). After her master degree in Chemical Technology in 2006 in the group of Julius Vancso, she decided to continue her research at the University of Twente as a PhD. Her master project was a joint research project in cooperation with the University of Münster and Barcelona and embedded in the Nano2Life European Network of Excellence for Nanobiotechnology. Her Master thesis entitled “*Inverted microcontact printing on thin reactive polymer films*” was one of the nine nominees for the KIVI-NIRIA Afstudeerprijs 2007.

On the 15th of April 2006 she started her work as a PhD investigating single molecule interactions of hydrogen-bonded dimers and polymers. In 2009 she received the lecture prize in Physics & Theory at the Dutch Polymer Days for her lecture: “*In-situ single molecule studies of hydrogen-bonded supramolecular polymers by AFM*”. Her poster entitled “*AFM-based single molecule force spectroscopy of complementary quadruple hydrogen-bonded systems*” was awarded the poster prize in Physics & Theory during the Dutch Polymer Days 2010 in Veldhoven. This thesis presents an overview of the research that was performed during her PhD.

From the 15th of October 2010 she works as a Postdoc in the Nanostructured Materials group of professor Steven Picken at the Technical University of Delft. Under supervision of Eduardo Mendes she will study microrheology of stimulus-responsive polymer gels for biomedical applications as part of the 7th EU framework program *Heart-e-Gel*.

PUBLICATIONS

Reviewed Papers

Embrechts, A.; Schönherr, H.; Vancso, G.J. Rupture Force of Single Supramolecular Bonds in Associative Polymers by AFM at Fixed Loading Rates. *J. Phys. Chem. B* **2008**, *112*, 7359-7362.

Embrechts, A.; Feng, C.L.; Mills, C.; Lee, M.; Bredebusch, I.; Schnekenburger, J.; Domschke, W.; Vancso, G.J.; Schönherr, H. Inverted Microcontact Printing on Polystyrene-block-Poly(tert-butyl acrylate) Films: A Versatile Approach to Fabricate Structured Biointerfaces Across the Length Scales. *Langmuir* **2008**, *24*, 8841-8849.

Feng, C.L.; Embrechts, A.; Bredebusch, I.; Schnekenburger, J.; Domschke, W.; Vancso, G. J.; Schönherr, H. Reactive Microcontact Printing on Block Copolymer Films: Exploiting Chemistry in Microcontacts for Sub- μm Patterning of Biomolecules. *Adv. Mater.* **2007**, *19*, 286-290.

Feng, C.L.; Embrechts, A.E.; Bredebusch, I.; Bouma, A.; Schnekenburger, J.; García-Parajó, M.; Domschke, W.; Vancso, G.J.; Schönherr, H. Tailored Interfaces for Biosensors and Cell-Surface Interaction Studies via Activation and Derivatization of Polystyrene-block-poly(tert-butyl acrylate) Thin Films. *Eur. Polym. J.* **2007**, *43*, 2177-2190.

Feng, C. L.; Embrechts, A.; Vancso, G. J.; Schönherr H. Reactive μCP on Ultrathin Block Copolymer Films: Localized Chemistry for Micro- and Nano-Scale Biomolecular Patterning. *Eur. Polym. J.* **2006**, *42*, 1954-1965.

Book Chapters

Embrechts, A., Feng, C.L., Bredebusch, I., Rommel, C.E., Schnekenburger, J., Vancso, G.J.; Schönherr, H. Interaction of Structured and Fuctionalized Polymers with Cancer Cells. *In R. Förch, H. Schönherr & A.T.A. Jenkins (Eds.), Surface Design; Applications in Bioscience and Nanotechnology*, Wiley-VHC Verlag GmbH & Co. KGaA, Weinheim, Germany **2009**, p. 233-250.

Schönherr, H., Feng, C.L., Embrechts, A.; Vancso, G.J. Structured and Functionalized Polymer Thin-Film Architectures. *In R. Förch, H. Schönherr & A.T.A. Jenkins (Eds.), Surface Design; Applications in Bioscience and Nanotechnology*, Wiley-VHC Verlag GmbH & Co. KGaA, Weinheim, Germany **2009**, p. 165-180.